



National Library
of Canada

Bibliothèque nationale
du Canada

Canadian Theses Service

Services des thèses canadiennes

Ottawa, Canada
K1A 0N4

CANADIAN THESES

THÈSES CANADIENNES

NOTICE

The quality of this microfiche is heavily dependent upon the quality of the original thesis submitted for microfilming. Every effort has been made to ensure the highest quality of reproduction possible.

If pages are missing, contact the university which granted the degree.

Some pages may have indistinct print especially if the original pages were typed with a poor typewriter ribbon or if the university sent us an inferior photocopy.

Previously copyrighted materials (journal articles, published tests, etc.) are not filmed.

Reproduction in full or in part of this film is governed by the Canadian Copyright Act, R.S.C. 1970, c. C-30.

**THIS DISSERTATION
HAS BEEN MICROFILMED
EXACTLY AS RECEIVED**

AVIS

La qualité de cette microfiche dépend grandement de la qualité de la thèse soumise au microfilmage. Nous avons tout fait pour assurer une qualité supérieure de reproduction.

S'il manque des pages, veuillez communiquer avec l'université qui a conféré le grade.

La qualité d'impression de certaines pages peut laisser à désirer, surtout si les pages originales ont été dactylographiées à l'aide d'un ruban usé ou si l'université nous a fait parvenir une photocopie de qualité inférieure.

Les documents qui font déjà l'objet d'un droit d'auteur (articles de revue, examens publiés, etc.) ne sont pas microfilmés.

La reproduction, même partielle, de ce microfilm est soumise à la loi canadienne sur le droit d'auteur, SRC 1970, c. C-30.

**LA THÈSE A ÉTÉ
MICROFILMÉE TELLE QUE
NOUS L'AVONS REÇUE**

**STUDIES OF ELECTRIC CONDUCTION AND CONVECTION
IN ORGANIC SOLUTIONS OF LOW DIELECTRIC CONSTANT**

by

Anita Margarit McBride

B.Sc. (Hons.), Simon Fraser University 1980

**A THESIS SUBMITTED IN PARTIAL FULFILLMENT
OF THE REQUIREMENTS FOR THE DEGREE OF
MASTER OF SCIENCE
in Chemical Physics
under Special Arrangements**

© **Anita Margarit McBride 1985**

SIMON FRASER UNIVERSITY

July 1985

**All rights reserved. This thesis may not be
reproduced in whole or in part, by photocopy
or other means, without permission of the author.**

Permission has been granted to the National Library of Canada to microfilm this thesis and to lend or sell copies of the film.

The author (copyright owner) has reserved other publication rights, and neither the thesis nor extensive extracts from it may be printed or otherwise reproduced without his/her written permission.

L'autorisation a été accordée à la Bibliothèque nationale du Canada de microfilmer cette thèse et de prêter ou de vendre des exemplaires du film.

L'auteur (titulaire du droit d'auteur) se réserve les autres droits de publication; ni la thèse ni de longs extraits de celle-ci ne doivent être imprimés ou autrement reproduits sans son autorisation écrite.

ISBN 0-315-30857-5

APPROVAL

Name: Anita Margarit McBride

Degree: Master of Science

Title of Thesis: Studies of Electric Conduction and Convection
in Organic Solutions of Low Dielectric Constant

Examining Committee:

Chairman: J.M. Webster

K.E. Rieckhoff
Senior Supervisor

E.M. Voigt
Senior Supervisor

E.D. Crozier

G.B. Porter
External Examiner
Honorary Professor
University of British Columbia, Vancouver, B.C.

Date Approved: August 12th, 1985

PARTIAL COPYRIGHT LICENSE

I hereby grant to Simon Fraser University the right to lend my thesis, project or extended essay (the title of which is shown below) to users of the Simon Fraser University Library, and to make partial or single copies only for such users or in response to a request from the library of any other university, or other educational institution, on its own behalf or for one of its users. I further agree that permission for multiple copying of this work for scholarly purposes may be granted by me or the Dean of Graduate Studies. It is understood that copying or publication of this work for financial gain shall not be allowed without my written permission.

Title of Thesis/Project/Extended Essay

STUDIES OF ELECTRIC CONDUCTION AND CONVECTION
IN ORGANIC SOLUTIONS OF
LOW DIELECTRIC CONSTANT

Author:

(signature)

Anita Margarit McFonle

(name)

Aug 13 1985

(date)

ABSTRACT

Studies of conduction, photoconduction and convection processes in organic solutions of intermediate conductivity ($K \approx 10^{-6} \Omega^{-1} \text{m}^{-1}$) are reported. Specifically, solutions of tetracyanoethylene (TCNE) in dichloroethane (DCE) and tetraethylammonium 1,1,2,3,3 pentacyanopropenide ($\text{TEA}^+ \text{PCP}^-$) in DCE were investigated. The dielectric constant of DCE is about ten ($\epsilon \approx 10$). Current characteristics of solutions with ion concentrations of $10^{-7} - 10^{-6}$ M. are qualitatively interpreted by considering the effects of electrical boundary layers, electrohydrodynamic behaviour, and ion concentration variation (temporal and spatial). A variety of cell geometries (electrode spacing, $d = 1$ to 9 mm.) and electrode materials (platinum, indium and aluminum) were used in the experiments.

The dominant negative charge carriers in solutions of TCNE in DCE are the 1,1,2,3,3 pentacyanopropenide anion (PCP^-) and tricyanovinylalcoholate anion (TCV^-). The measured effective mobility of ions in TCNE/DCE and $\text{TEA}^+ \text{PCP}^-$ /DCE solutions is $(3-4) \times 10^{-8} \text{m}^2 \text{V}^{-1} \text{s}^{-1}$. The visible/ultraviolet spectra of these anions are used to interpret the current characteristics of TCNE/DCE solutions. Some information is presented on the chemical generation of charge carriers in TCNE/DCE. In particular, the equilibria involving water, TCNE and pentacyanopropenide in DCE and in acetonitrile are considered.

Concentration gradients in solution accompany transient current behaviour and are related to hydrodynamic instabilities in the liquid. Concentration gradients of $6 \times 10^{-7} \text{ M/mm}$ are sufficient to generate turbulence in DCE. Ion density gradients of this magnitude are not sufficient to bring about gravitationally driven convection. Diffusion drag forces on the liquid are proposed as a mechanism for the generation of fluid flow in electrolyte solutions with concentration gradients.

A model is presented which considers the contributions of diffusion and space charge to convective flow in electrolyte solutions with an applied electric field (E). The ratio between space charge and diffusive drag forces is shown to vary as E^2/c where c is the ion concentration in the solution. The general applicability of this model to conduction studies of electrolyte solutions of low and high conductivity is discussed.

ACKNOWLEDGEMENTS

Many people contributed their help in the course of my research and the preparation of this dissertation. I am grateful to Dr. Rieckhoff and Dr. Voigt for their assistance in completing this project (particularly in the preparation of the thesis). Vern Moen helped with the experimental work and contributed many ideas to the research. Dr. Wen Chen gave me assistance with laser work. Dr. Pomeroy, Dr. Pinto, and Joyce Schachter provided information on chemical preparation. The glass and machine shops assisted with the construction and design of conductivity cells.

The diagrams in this thesis were prepared with the help of the Instructional Media Centre. Vern Moen and Brian Charlesworth sacrificed one night of sleep to photocopy and put page numbers on the thesis.

A special word of thanks goes to my husband, Randy, who always encouraged me and believed that things would work out for the best. I acknowledge the help of God who provided me with the strength and purpose to finish this work.

TABLE OF CONTENTS	Page
Approval	ii
Abstract	iii
Acknowledgements	v
List of Tables	ix
List of Figures	xi
Chapter 1. INTRODUCTION	1
REFERENCES	7
Chapter 2. PHOTOCURRENT MEASUREMENTS IN TCNE	
CHARGE TRANSFER COMPLEXES	9
2.0 Experimental	14
2.1 Discussion	19
REFERENCES	28
Chapter 3. REINTERPRETING THE PHOTOSIGNAL	29
3.1.1 Photocurrent, Dependence on Light Exposure Time	29
3.1.2 Photosignal, Geometry Dependence	38
3.2.1 Evidence for Convection as a Charge Transport	
Process in Charge Transfer Solutions	41
3.2.2 Evidence for Convection in an Analogous System:	
Indigo(dye)/DCE	42
REFERENCES	52

	Page
Chapter 4. CURRENT CHARACTERISTICS OF TCNE/DCE	53
4.0 Materials and Methods for Sections 4.1, 4.2, and 4.3	53
4.1 Concentration Dependence of Conductivity	59
4.2 Current/Time Response: Electrical Boundary Layers and Resistivity Changes	70
4.2.1 Current Response to Square Wave Voltage over many Cycles	88
4.3 Temperature and Mechanical Vibration	88
4.4 Current Voltage Characteristics	92
4.4.0 Experimental	93
4.4.1 I/V Response (Voltage Steps)	96
4.4.2 I/V Response (Continuous Voltage Scanning)	104
REFERENCES	126
 Chapter 5. ION CONCENTRATION BEHAVIOUR WITH APPLIED VOLTAGE	 129
5.0 Experimental	129
5.1.1 Concentration vs. Time Behaviour	134
5.1.2 Ion Drift Velocity Estimates in TCNE/DCE	143
5.1.3 Electric and Optical Response of TEA ⁺ PCP ⁻ /DCE	148
5.1.4 PCP ⁻ and TCY ⁻ Contributions to Conduction	155

	Page
5.1.5 Relaxation of Concentration with $V=0$ in TCNE/DCE	158
5.1.6 Concentration Gradients in Solution	161
5.2.1 Spatial concentration Behaviour in Time	166
5.2.2 Concentration Gradients and Hydrodynamic Instabilities	183
5.3 Electrohydrodynamic Instabilities in Low Conductivity Electrolyte Solutions	188
REFERENCES	202
Chapter 6. SOME CYANOCARBON CHEMISTRY	203
6.0 Experimental	203
6.1 Results and Discussion	204
6.1.1 Reactions of Water and TCNE in Solution	214
6.1.2 TCNE ⁻ Injection in TCNE/CH ₃ CN	225
6.1.3 Ions in Conductivity Studies	234
REFERENCES	237
Chapter 7. CONCLUSIONS	238
7.1 Summary of Thesis Research	238
7.2 Suggestions for Further Work	240
REFERENCES	241

LIST OF TABLES		Page
2.1	Efficiencies for Photocurrent Generation	25
3.1	DC Current Photoresponse	39
3.2	Geometry Dependence of Photocurrent Signal	40
3.3	Indigo/DCE Electroconvective Patterns	50
4.1	DCE Current Response with different Cleaning Methods	58
4.2	Voltage Dependence of Current Peak Time	79
4.3	Temperature Dependence of Conductivity	90
5.1	Drift Velocity Estimates from Changes in Current and Concentration (TCNE/DCE)	142
5.2	Drift Velocity Estimates from Current and Concentration Data (TEA⁺PCP⁻/DCE)	153
5.3	Drift Velocity Estimates from Current and Concentration Changes (TEA⁺PCP⁻/DCE)	154

	Page
5.4 Concentration Gradients and Diffusion-Induced Drag Forces	187
5.5 Typical F_e/F_D Values for Experimental Conditions	199
5.6 Conditions for $F_e/F_D = 1$	201
6.1 PCP ⁻ Peaks in Different Solvents	209
6.2 Spectrum of TCNE ⁻ in CH ₃ CN	211
6.3 Formation of PCP ⁻ from TCNE and H ₂ O in DCE and CH ₃ CN.	221
6.4 Slow formation of PCP in TCNE/Solvent (independent of water concentration)	221
6.5 [TCNE ⁻] injected into CH ₃ CN	229

LIST OF FIGURES		Page
2.1	Structure of Tetracyanoethylene	10
2.2	Charge Transfer Complex of TCNE/Mesitylene	10
2.3	CT Complex Absorption Spectrum TCNE/Mesitylene in DCE	12
2.4	Simplified Potential Energy Curves for the Ground and Excited Charge Transfer States	15
2.5	Calculated Absorption, Fluorescence and Raman Resonance Excitation Profiles for Charge Transfer Complexes	15
2.6	Experimental Apparatus for Photoconductivity Measurements	17
2.7	Photosignal vs. Incident Laser Power	20
2.8	Photosignal vs. Incident Laser Power	21
2.9	Photosignal vs. Voltage	23
2.10	Quantum Efficiency vs. Excitation Wavelength	27
3.1	Photosignal vs. Chopper Frequency	30
3.2	Photosignal vs. Half Cycle Time	31
3.3	Signal Averaging Apparatus	33
3.4	Photosignal Shape	34

	Page	
3.5	Photosignal Shape	35
3.6	DC Photocurrent reponse	37
3.7	DC Current Acoustic Effect	43
3.8	Signal Averaging Apparatus, Acoustic Effect	44
3.9	DC Current Response of TCNE/DCE	46
3.10	DC Current Response of Indigo/DCE	46
3.11	Photocurrent Response of Indigo/DCE at Different Voltages	48
3.12	Dye Particle Patterns in Indigo/DCE at Different Voltages	49
4.1	Platinum Electrode Cell	54
4.2	Current Measurement	56
4.3	Steady State Current vs. [TCNE] (Single Step Applied Voltage)	61
4.4	Peak and Steady State Current vs. [TCNE] (Square Wave Voltage, $f=0.0005$ Hz.)	62
4.5	Current vs. Mesitylene Content	63
4.6	Current Response to a Step Voltage	65
4.7	Square Wave Current Response	66

	Page
4.8 Peak and Steady State Currents vs. Number of Square Wave Cycles	67
4.9 Current vs. Time Following Voltage Reversal	71
4.10 Current Response for ADT/Xylene	72
4.11 Electrical Boundary Layers	74
4.12 Electrical Boundary Layers and Associated Potentials	75
4.13 Current vs. Time (Square Wave Voltage, $f = 0.005$ Hz.)	82
4.14 Current Response to Voltage Reversal after Mixing	87
4.15 Thin Indium Cells	94
4.16 Current vs. Time for Voltage Steps	97
4.17 Peak Current (after discharge) vs. Voltage	100
4.18 Discharge Current vs. Time	101
4.19 (Q Discharged in 150 seconds) vs. Voltage	102
4.20 Current vs. Voltage, Above and Below the Critical Frequency (Triangular Wave Voltage)	105
4.21 Current vs. Voltage, Above and Below the Critical Frequency (Sine Wave Voltage)	106
4.22 Current vs. Voltage Response at Different Frequencies (Triangular Wave Voltage)	107

	Page
4.23.1 Current vs. Voltage ($f=0.002 \text{ Hz} < f_c$, Triangular Wave Voltage)	109
4.23.2 Current vs. Voltage ($f=0.007 \text{ Hz} < f_c$, Triangular Wave Voltage)	110
4.24 Current vs. Voltage, with Mixing ($f=0.007 \text{ Hz} < f_c$, Triangular Wave Voltage)	112
4.25 I/V Response with Changing Frequency (Sine Wave Voltage)	114
4.26 I/V Response with Changing Frequency (Triangular Wave Voltage)	115
4.27 Critical Frequency vs. Voltage Amplitude (Triangular Wave Voltage)	116
4.28 ⁸⁰ Critical Time vs. Voltage Amplitude (Triangular Wave Voltage)	117
4.29 Critical Frequency vs. Voltage Amplitude (Triangular Wave Voltage)	118
4.30 Critical Time vs. Voltage Amplitude (Triangular Wave Voltage)	119
4.31 Discharge Current vs. Voltage	120
5.1 Sample Cells and Electrodes	130
5.2 Apparatus, Spatially Asymmetric Concentration Response	133

	Page
5.3 Apparatus, Transmission Profiles	135
5.4 $\text{Log } I_0/I$ vs. Time, Current vs. Time (1a,1b)	137
5.5 $\text{Log } I_0/I$ vs. Time, Current vs. Time (2a)	138
5.6 $\text{Log } I_0/I$ vs. Time, Current vs. Time (1d)	139
5.7 Absorption Spectrum of TCNE/DCE at Different Times after Voltage Application	140
5.8 Current (i_0) vs. $[\text{TEA}^+\text{PCP}^-]$ in DCE	149
5.9 $\text{Log } I_0/I$ vs. Time, Current vs. Time for TEA^+PCP^-	150
5.10 $\text{Log } I_0/I$ vs. Time, Current vs. Time for TEA^+PCP^-	151
5.11 Spectrum of TCNE-H ₂ O/DCE	156
5.12 $\Delta(\text{Log } I_0/I)$ vs Time, Voltage set to zero after 20V treatment	159
5.13 $(\text{Log } I_0/I)$ vs. Time, Voltage set to zero before steady state	160
5.14 Solution Resistance	163
5.15 $(\text{Log } I_0/I)$ vs. Time, beam positioned closer to one electrode	167
5.16 Absorption vs. Time	168

	Page
5.17	Transmission Profile (Al) 170
5.18	Transmission Profile (Al) 171
5.19	Transmission Profile (Al) 172
5.20	Transmission Profile (Al) 173
5.21	Transmission Profile (Al) 174
5.22	Transmission Profile (In) 176
5.23	Transmission Profile (In) 177
5.24	Transmission Profile (Pt) 179
5.25	Transmission Profile (Pt) 180
5.26	Transmission Profile (Pt) 181
5.27	Log I_0/I Fluctuations at different Voltages 182
5.28	Space Charge Associated with Ion Concentration Gradients to maintain a Constant Current Flux 194
5.29	Formation of a Space Charge Layer on a Concentration Gradient 195
6.1	Cell for Preparation of TCNE ⁻ from TCNE/CH ₃ CN 205

	Page
6.2 Absorption Spectrum of TCNE, TCNE ⁻ in Methyltetrahydrofuran	206
6.3 PCP ⁻ ,TCV ⁻ Absorption Spectra in Water	207
6.4 PCP ⁻ Absorption Spectrum in DCE	210
6.5 PCP ⁻ ,TCV ⁻ Structures	212
6.6 Protonated forms of TCV ⁻ and PCP ⁻	213
6.7 TCNE/CH ₃ CN Spectra after addition of water	216
6.8 Log I ₀ /I vs. Time after water addition	217
6.9 [PCP ⁻] vs. [H ₂ O]	219
6.10 [PCP ⁻] vs. [H ₂ O]	220
6.11 Log I ₀ /I vs. Time (332 nm)	223
6.12 TCNE/DCE Spectra with and without distilled solvent	224
6.13 Log I ₀ /I (420 nm) vs. *TCNE Sublimations	226
6.14 TCNE/CH ₃ CN before and after voltage treatment	228
6.15 Conversion of TCNE ⁻ to PCP ⁻	230
6.16 ln ((TCNE ⁻ , I ₀ /I) vs. Time	232
6.17 Conversion of TCNE ⁻ to PCP ⁻ and another species with λ=320nm	233

6.18 Spectrum of $\text{Na}^+(\text{TCNE}^-)$ in MTHF at 77 K

235

CHAPTER 1 - INTRODUCTION:

The present thesis is concerned with the problem of DC conduction in organic solutions of low dielectric constant with conductivities in the neighbourhood of $10^{-6} \Omega^{-1} \text{m}^{-1}$. Samples are prepared with the cyanocarbon anions pentacyanopropenide (PCP^-) and tricyanovinylalcoholate (TCV^-) present in dichloroethane (DCE) ($\epsilon \approx 10$) at concentrations of about 10^{-7}M . The contribution of convection to ion transport and the source of hydrodynamic instabilities in these systems are considered in detail.

A model is presented for the generation of fluid flow in the systems investigated here. This model applies to electrolyte solutions of a wide range of conductivities. Concentration gradients in solution are related to unbalanced drag forces generating fluid flow. This is demonstrated experimentally and concentration gradients of the order of (10^{-7}M/mm) are found to be sufficient to initiate hydrodynamic instabilities. To my knowledge, this is the first study of convection driven by concentration gradients too small to result in mass density gradients.

Conduction processes in dielectric liquids have been studied by a number of workers and have been reviewed by Gallagher¹. Electrohydrodynamic phenomena are characteristic of low conductivity liquids and have been extensively studied for the cases of unipolar or bipolar injection^{2,3,4}. The more general problem of electrohydrodynamic behaviour in weakly

conducting electrolyte solutions with dissociated ions is not well understood⁵ and this thesis makes a significant contribution in that area.

Unipolar and bipolar injection studies cannot be easily extended to describe the properties of industrial liquids of interest (i.e. fuel, mineral oil) which have more in common with weakly conducting electrolyte solutions. The electrostatic hazards associated with the transfer of fuels are related to their relatively low conductivity⁶. A better knowledge of conduction processes in low conductivity liquids is considered a key issue in reducing the considerable hazards associated with the fuel industry. Charge separation that occurs during fuel flow through pipes may result in voltages of sufficient magnitude to generate sparks and initiate an explosion of the fuel.

The results of this study are applicable to electrolyte solutions over a wide range of conductivities although measurements were performed on solutions of intermediate conductivity. Conduction studies have been carried out in very low conductivity solutions ($K < 10^{-9} \Omega^{-1} \text{m}^{-1}$) by physicists interested in the intrinsic conductivity of dielectric liquids. However, the chemical identity and mobility of charge carriers is generally unknown⁷.

Electrochemical measurements are routinely carried out by chemists in solutions of relatively high conductivity ($K \geq 10^{-2} \Omega^{-1} \text{m}^{-1}$). In electrochemical studies the applied electric potential is dropped largely at the electrode/solution interface and the current response is governed by electrode processes. In this study, a significant portion of the electric

potential is dropped across the bulk of the sample. Therefore ion conduction through the bulk of the liquid plays a much more important role in the interpretation of sample current characteristics. For the samples considered in this study it is possible to observe some of the electrohydrodynamic phenomena characteristic of low conductivity liquids, yet ion concentrations are sufficiently high to be monitored directly via absorption spectroscopy. The ion concentration behaviour in space and time is used to interpret conduction processes in the samples.

The role of electrode/liquid interface properties in the observed conduction of dielectric liquids is also of interest. Many of the data in the literature on solvent conduction are poorly reproducible and extremely sensitive to electrode material and preparation⁸. In this thesis the effect of different electrode materials on ion concentration behaviour near the metal/liquid interface is clearly demonstrated and is shown to be related to hydrodynamic phenomena in the liquids.

This study arose out of an attempt to obtain evidence substantiating a model proposed by Michaelian et.al.⁹ on the spectroscopic and photoconduction properties of charge transfer (CT) solutions of tetracyanoethylene (TCNE). CT interactions are of general interest in many chemical and biological systems. The proposed model explains qualitatively the observed red shifts in the Resonance Raman spectra of CT complexes with respect to the absorption profiles¹⁰. The existence of highly damped vibrational levels is an important assumption in the model. Photoionic

dissociation of CT complexes was one of the suggested relaxation mechanisms for CT complexes in their excited state. In conjunction with the spectroscopic studies, Michaelian et. al. observed that the conductivity of CT solutions was photodependent¹¹. The photoconduction effect was interpreted in terms of photoionic dissociation of the TCNE CT complexes and according to the model this process was expected to be dependent on the excitation wavelength.

The starting point for this research were the data of Michaelian et. al. on photoconduction in CT solutions¹¹. The results were repeated for TCNE/mesitylene/dichloroethane solutions and extended to include the wavelength dependence of photoconduction. These data and a brief introduction to TCNE CT complexes are included in Chapter 1.

In order to obtain unambiguous, reproducible data, further experimental work was carried out investigation in detail the variables affecting the system. The results of these experiments are discussed in Chapter 2. They showed that the photoconductivity of CT solutions could no longer be interpreted in terms of the original model.

By considering convection as a possible charge transport process in TCNE CT solutions, the photoconductivity could be interpreted qualitatively. In Chapter 3 photodependent current response of a system displaying convection visibly (Indigo/DCE) will be compared with the behaviour of CT solutions.

Further experimental work on conduction in CT solutions and TCNE/DCE solutions is discussed in Chapter 4. An interpretation of the current response in terms of electrical boundary layer space charge and ion concentration is suggested. Both current versus time and current vs. voltage behaviour are considered. The current versus voltage behaviour provides evidence for transitions in convective flow in the sample as voltage is increased.

Conduction in TCNE/DCE solutions is analyzed in terms of the temporal and spatial behaviour of ion concentration in Chapter 5. This chapter is divided into three sections. In the first section (5.1) correlations of the current and concentration response in time are discussed. Current and mobility measurements in TCNE/DCE are compared to those in pentacyanopropenide salt solutions and pentacyanopropenide is shown to be the dominant negative charge carrier in TCNE/DCE. In Section 5.2, measurements of the spatial behaviour of ion concentration in TCNE/DCE solutions demonstrate the presence of hydrodynamic instabilities for concentration gradients greater than about 10^{-7} M/mm. A drag force exerted on the liquid by diffusion of ions is suggested as a mechanism for generating fluid flow. In Section 5.3 a model explaining the origin of fluid flow in electrolyte solutions is presented. The contributions of space charge and concentration gradients to unbalanced forces in a liquid are considered.

Chemistry related to the study of conduction in solutions with TCNE and TCV^- and PCP^- respectively, as well as electrochemical generation of TCNE^- in solution are discussed in Chapter 6. Some of the properties of TCNE/DCE solutions are compared with acetonitrile solutions of TCNE.

A final summary of the thesis includes a discussion of the implications of this work and suggestions for further work.

REFERENCES:

1. T.J. Gallagher, "Simple Dielectric Liquids"; Clarendon Press: Oxford 1975.
2. R.W.L. Snaddon, R. Poulter, "Mass transfer and Dissipation in Unipolar Electrophoretic Flows", Journal of Physics, D: Applied Physics 1980, 13, 2263-2274.
3. B. Malraison, P. Atten, "Chaotic Behaviour of Instability Due to Unipolar Ion Injection in a Dielectric Liquid", Physical Review Letters 1982, 49, 723-726.
4. Y. Aikawa, H. Shimoda, K. Kobayashi, A. Takahashi, S. Takeda, T. Sakata, M. Sukigara, "Electrohydrodynamic Dissipative Structure in Unipolar and Bipolar Injection Cases", The Bulletin of the Chemical Society of Japan 1982, 55, 654-659.
5. P. Atten, B. Malraison, S. Ali Kani, "Electrohydrodynamic Stability of Dielectric Liquids Subjected to A.C. Fields", Journal of Electrostatics 1982, 12, 477-488.
6. J. Lowell, Electrostatics 1979, Institute of Physics Conference Series No.48; J. Lowell, Editor; v (preface).
7. T.J. Gallagher, "Simple Dielectric Liquids"; Clarendon Press: Oxford 1975, Chapter 1.
8. J.C.Gibbings, "Interaction of Electrostatics and Fluid Motion", Electrostatics 1979, Institute of Physics Conference Series No.48; J. Lowell, Editor; 145.
9. K.H. Michaelian, K.E. Rieckhoff, E.M.Voigt, "Model Theory of Resonance Raman Excitation Profiles in Electron Donor/Acceptor Complexes", Chemical Physics Letters 1977, 45, 250-254.
10. K.H. Michaelian, K.E. Rieckhoff, E.M.Voigt, "Raman Resonance of Electron

Donor/Acceptor Complexes", Proceedings of the National Academy of Sciences 1975, 72, 4196-4199.

11. **K.H. Michaelian, K.E. Rieckhoff, E.M.Voigt, "Photoionic Dissociation of Electron Donor/Acceptor Complexes of Tetracyanoethylene in Solution", Chemical Physics Letters 1976, 44, 482-483.**

CHAPTER 2 - PHOTOCURRENT MEASUREMENTS IN TCNE CHARGE TRANSFER COMPLEXES

This chapter covers the initial experiments that were carried out to corroborate and investigate further K.H. Michaelian et. al.'s work on the photoconduction effect observed in solutions of tetracyanoethylene (TCNE) charge-transfer (CT) complexes¹. The observations include the dependence of the photoinduced current change on incident laser power, applied voltage, and excitation wavelength. Before discussing these results, a brief introduction to the structure and spectra of CT complexes or electron donor/acceptor (EDA) complexes will be given.

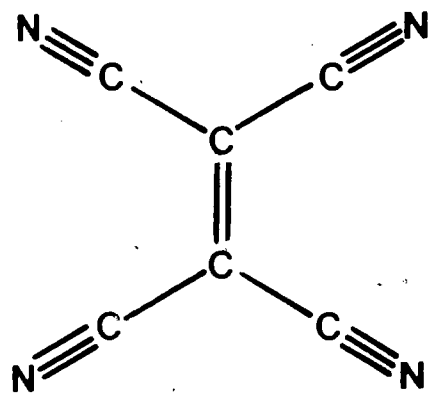
TCNE is a strong electron acceptor and its structure is shown in Figure 2.1. The four cyano groups decrease the electron density in the π cloud of the ethene bond. TCNE forms π - π^* complexes with a number of electron donating molecules. Complexes of TCNE with aromatic compounds have a sandwich-like structure allowing maximum interaction between the empty π^* orbital of TCNE and the filled π orbital of the donor molecule (Figure 2.2). According to Mulliken's valence band model of weak CT complexes², wave functions of the ground and excited states of the complex can be written as follows:

$$\Psi_N(DA) = a \Psi_0(D...A) + b \Psi_1(D^+...A^-) \quad a \gg b$$

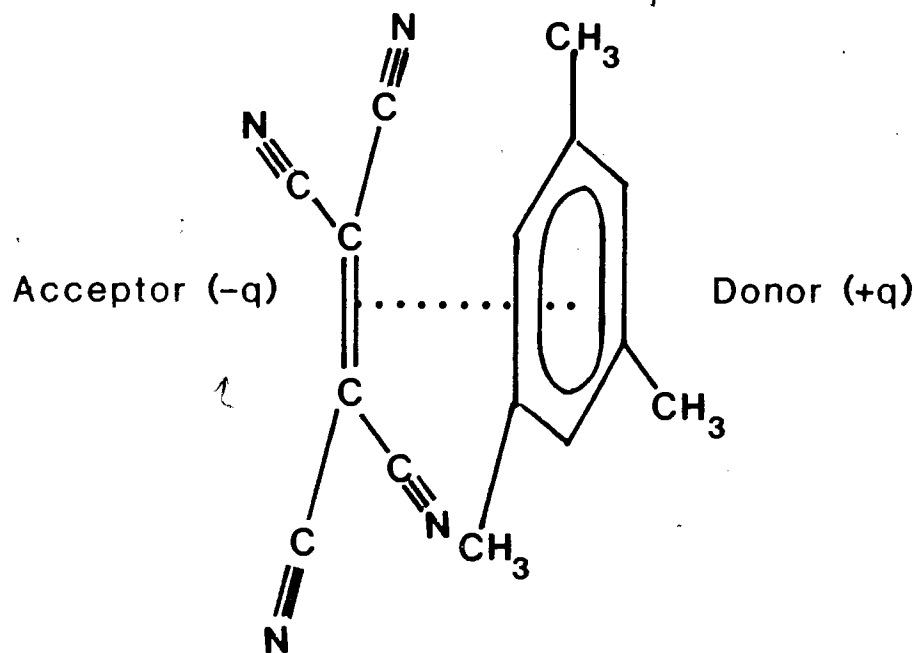
$$\Psi_E(DA) = a^* \Psi_1(D^+...A^-) + b^* \Psi_0(D...A) \quad a^* \gg b^*$$

FIGURE 2.1 - STRUCTURE OF TETRACYANOETHYLENE

FIGURE 2.2 - CHARGE TRANSFER COMPLEX OF TCNE/MESITYLENE



Tetracyanoethylene



where D = donor

A = acceptor

Ψ_N (DA) = ground state wave function of CT complex

Ψ_E (DA) = excited state wave function of CT complex

(orthogonal to Ψ_N (DA))

Ψ_0 (D...A) = 'no bond' wave function (dipole-dipole and London dispersion forces only)

Ψ_1 (D⁺...A⁻) = dative or charge transfer wave function

The electronic transition from the ground CT state to the excited CT state is responsible for the CT absorption band. On excitation within the absorption band, an electron is partially transferred from the donor to the acceptor molecule and the excited state has predominantly ionic character. The optical absorption spectrum is typically a broad structureless band in the visible region as is shown in Figure 1.3 for the TCNE/mesitylene complex in a solvent (but this also applies to the gas phase).

The characteristic absence of vibronic structure in CT spectra is an indication that the excited state of the complex is short-lived because of relaxation pathways available to it. One of the radiationless relaxation processes proposed by Michaelian et. al.¹ was the dissociation of the excited state into ions which is referred to as photoionic dissociation. An outline

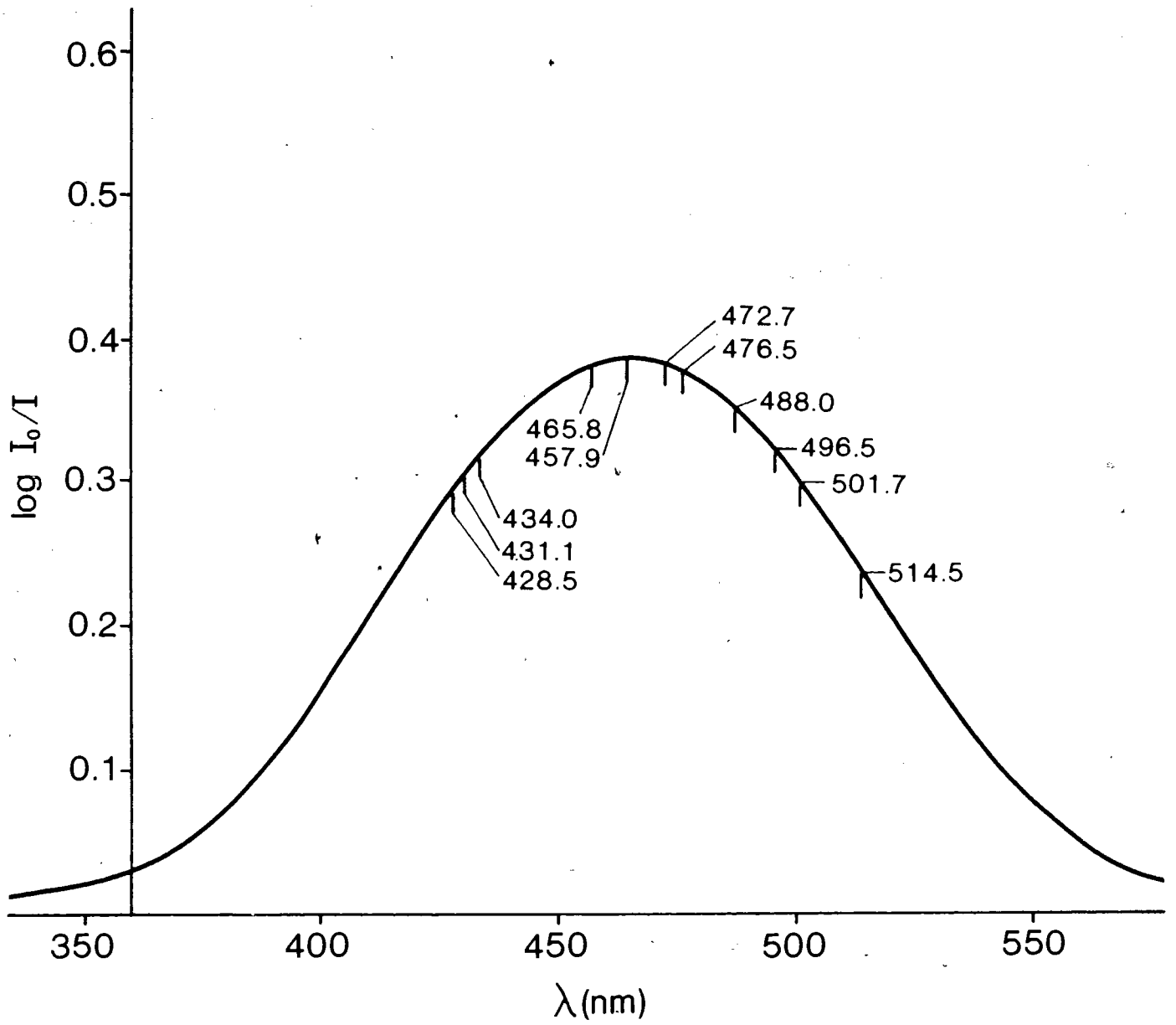
FIGURE 2.3 - CT COMPLEX ABSORPTION SPECTRUM**TCNE/mesitylene in DCE**

Sample: [TCNE] = 0.005 M.

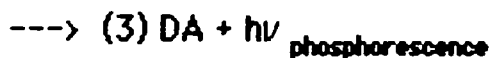
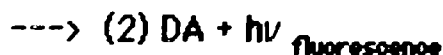
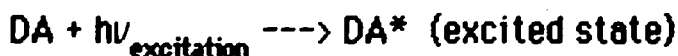
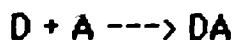
[mesitylene] = 0.025 M.

[Complex] $\approx 7 \times 10^{-5}$ M.

Excitation wavelengths are marked.



of the excitation and relaxation processes for donor/acceptor complexes is shown below.



The scheme outlined above does not include the effects of solvent interactions on the complex or the dissociated ions. The dissociation of the complex into ions in step (1) is favoured in solvents with a high dielectric constant. Thus, it is logical to study photoionic dissociation of CT complexes in a solvent with sufficiently high dielectric constant to stabilize free ions generated with light absorption.

The initial observations of photoconduction in CT solutions can be interpreted legitimately by a model of photoionic dissociation of charge transfer complexes. These observations included the dependence of the photoinduced current change on incident laser power, applied voltage and excitation wavelength. The dependence of photocurrent on the excitation energy was of particular interest since this would shed light on a model of

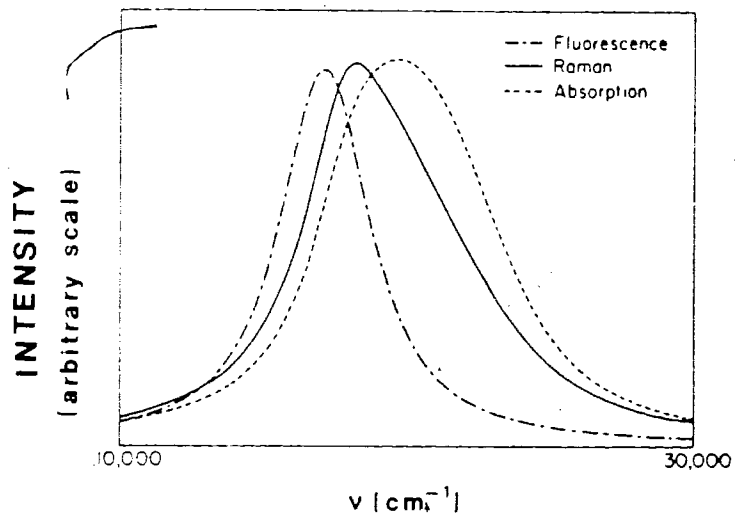
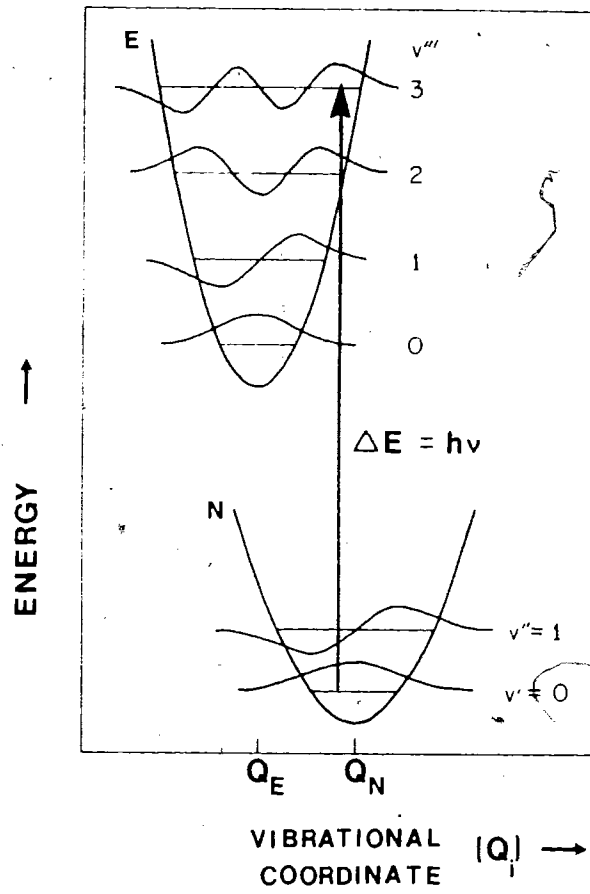
the resonance Raman, absorption, and fluorescence profiles of electron donor-acceptor complexes proposed by Michaelian et. al.³

The following spectroscopic properties of EDA complexes could be accounted for qualitatively by introducing large damping terms representing non-radiative relaxation processes in the excited electronic state of the complex: [1] the red shift of resonance Raman (RR) excitation profiles with respect to the absorption band and [2] the broad, asymmetric structureless shape of absorption and fluorescence spectra and RR excitation profiles. Figure 2.4 shows simplified potential energy wells for a single vibrational coordinate (Q_1) and the ground and excited states of an EDA complex in the gas phase (vibrational quantum numbers are indicated by v' and v'' in the ground state, and v''' in the excited state). The spectral profiles calculated using these curves and the corresponding wave functions of the vibrational states are shown in Figure 2.5 for a frequency dependent damping term ($E_{\text{excitation}} = h\nu$ where ν is the frequency)³. An experimental study of one damping mechanism, namely photoionic-dissociation, was possible via photocurrent measurements. The dependence of the photocurrent on the excitation frequency or wavelength was expected to yield information on the excited state of EDA complexes which could then be related to EDA spectra.

1.0 - EXPERIMENTAL

**FIGURE 2.4 - SIMPLIFIED POTENTIAL ENERGY CURVES FOR THE
GROUND AND EXCITED CHARGE TRANSFER STATES³
(in the gas phase)**

**FIGURE 2.5 - CALCULATED ABSORPTION, FLUORESCENCE AND
RAMAN RESONANCE EXCITATION PROFILES FOR CHARGE
TRANSFER COMPLEXES³ (in the gas phase)**



Absorption and fluorescence spectra and RR excitation profile calculated for frequency dependent damping using the potential energy curves shown above.

$$Q_N - Q_E = 0.19$$

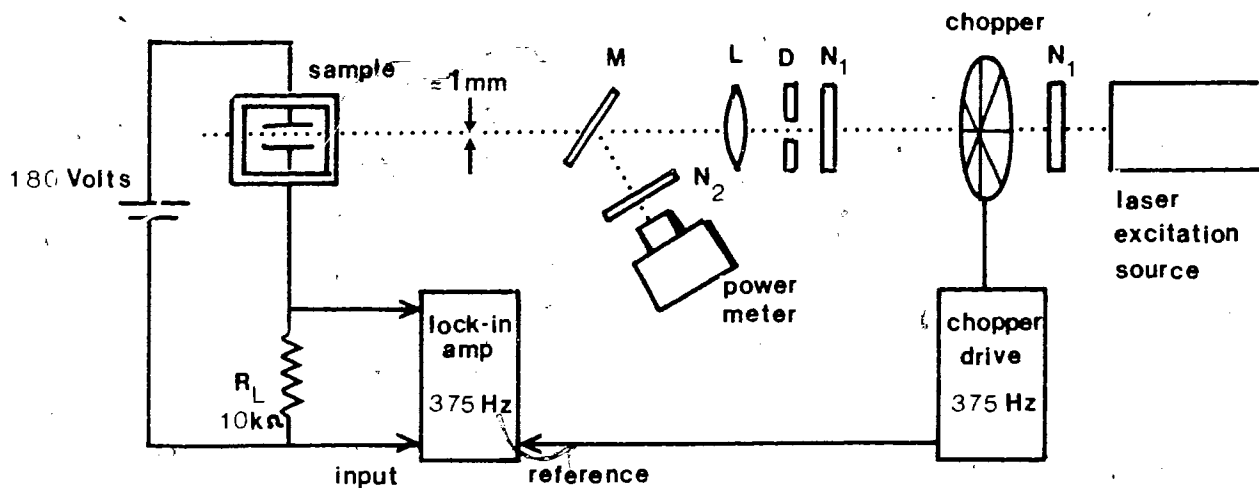
$$E_{v''=1} - E_{v'=0} = 500 \text{ cm}^{-1}$$

TCNE (Kodak Eastman) was sublimed 3 times under vacuum. Mesitylene was fractionally distilled. The solvents dichloroethane (DCE) (Fisher Scientific) and dichloromethane (DCM) (Fisher Scientific) were distilled over P_2O_5 under N_2 and stored over molecular sieve. Stock solutions of TCNE in DCE took about 3 days to prepare using a solution shaker. Typically the concentrations ranged from 0.01 - 0.1M. Any prepared solutions of TCNE were kept in the refrigerator between experiments. Mesitylene was added to samples directly before any measurements.

A schematic of the experimental apparatus used in the photoconductivity measurements is shown in Figure 2.6. A sample TCNE/donor solution was contained in a glass cell with two platinum electrodes (spacing, $x = 2\text{mm}$) to which variable voltage could be applied. A laser beam ($d \approx 1\text{mm}$) was positioned midway between the electrodes so that no light shone directly on the platinum. Coherent® Krypton and Argon ion lasers (Coherent® CR 2000K and Model 52 respectively) and a dye laser (Coherent® Model 590) were used as excitation sources. The beam geometry was approximately constant throughout the sample length. In order to normalize the power density of the incident laser light at different excitation wavelengths, the beam width was kept at a constant diameter using a diaphragm. A Photodyne power meter (66XLA) was used to monitor a given fraction of the beam intensity.

Ion pairs produced in solution after excitation were swept toward respective electrodes, and a signal in phase with the chopped incident light

**FIGURE 2.6 - EXPERIMENTAL APPARATUS FOR
PHOTOCONDUCTIVITY MEASUREMENTS**



M = beam splitter

$86 \pm 1\%$ transmitted $14 \pm 1\%$ reflected

L = convex lens

D = diaphragm

N = neutral density filter

N_1 : variable transmission N_2 : $11.7 \pm 0.2\%$ transmitted

was monitored using a lock-in amplifier (PAR Model 124 or HR-8). A signal of about 0.05 nanoamperes was observed for one milliwatt of incident light. This was equivalent to generating one charge at the electrodes for every 10^7 incident photons. The resulting AC photocurrent signal was superimposed on a relatively large DC current offset from the sample's intrinsic conductivity. The transformer mode of the lock-in amplifier was used to measure the current photosignal despite the large offset, and even though phase information was lost in the process. The signal to noise ratio was optimized using a chopping frequency of 375 Hz. Photocurrents were measured one to two hours after voltage application to ensure sample stabilization

DCE was chosen as solvent because it had a sufficiently high dielectric constant ($\epsilon \approx 10$) to support ions and did not interact appreciably with the electron acceptor TCNE. Mesitylene was chosen as a donor since its charge transfer band with TCNE was in a wavelength region sufficiently well covered by the ion lasers available. The laser lines used are indicated on the CT band of TCNE/Mesitylene in Figure 2.3. Mesitylene mixes readily with DCE for all concentrations.

A CARY 17 spectrophotometer was used to measure the absorbances of CT solutions. The concentration of CT complexes could then be determined, as well as the fraction of light absorbed at different wavelengths.

1.1 - DISCUSSION

The initial data on the photo-current response of solutions with CT complexes were consistent with a model of wavelength dependent photo-ionic dissociation of the complex as suggested by Michaelian et. al.^{1,3}

Three properties of the photosignal were expected from this model:

1. Photocurrent \approx incident laser power
(\bullet ion pairs produced \approx \bullet CT complexes excited)

2. Photosignal \approx voltage applied
(current \approx drift velocity)

note: It was assumed that the lifetimes of ions in solution were much shorter than the chopper cycle time ($t_{ions} \ll t_{chopper}$)

3. Quantum efficiency ($\bullet e^- / \bullet$ photons absorbed) increases with excitation energy.

(non-radiative relaxation via dissociation is a function of the excitation energy)

The photosignal was found to increase linearly with incident laser power (Figure 2.7). A saturation effect was observed in a few samples at lower voltages (i.e. 150V vs. 180V) (Figure 2.8).

FIGURE 2.7 - PHOTOSIGNAL VS. INCIDENT LASER POWER

Sample: [TCNE] = 0.005 M.

[Mesitylene] = 0.025 M. in DCE

$\lambda = 457.9$ nm.

V = 180 Volts

slope = 0.055 nA/mW

Trial 1 and Trial 2 were carried out on two consecutive days.

- trial 1
- trial 2

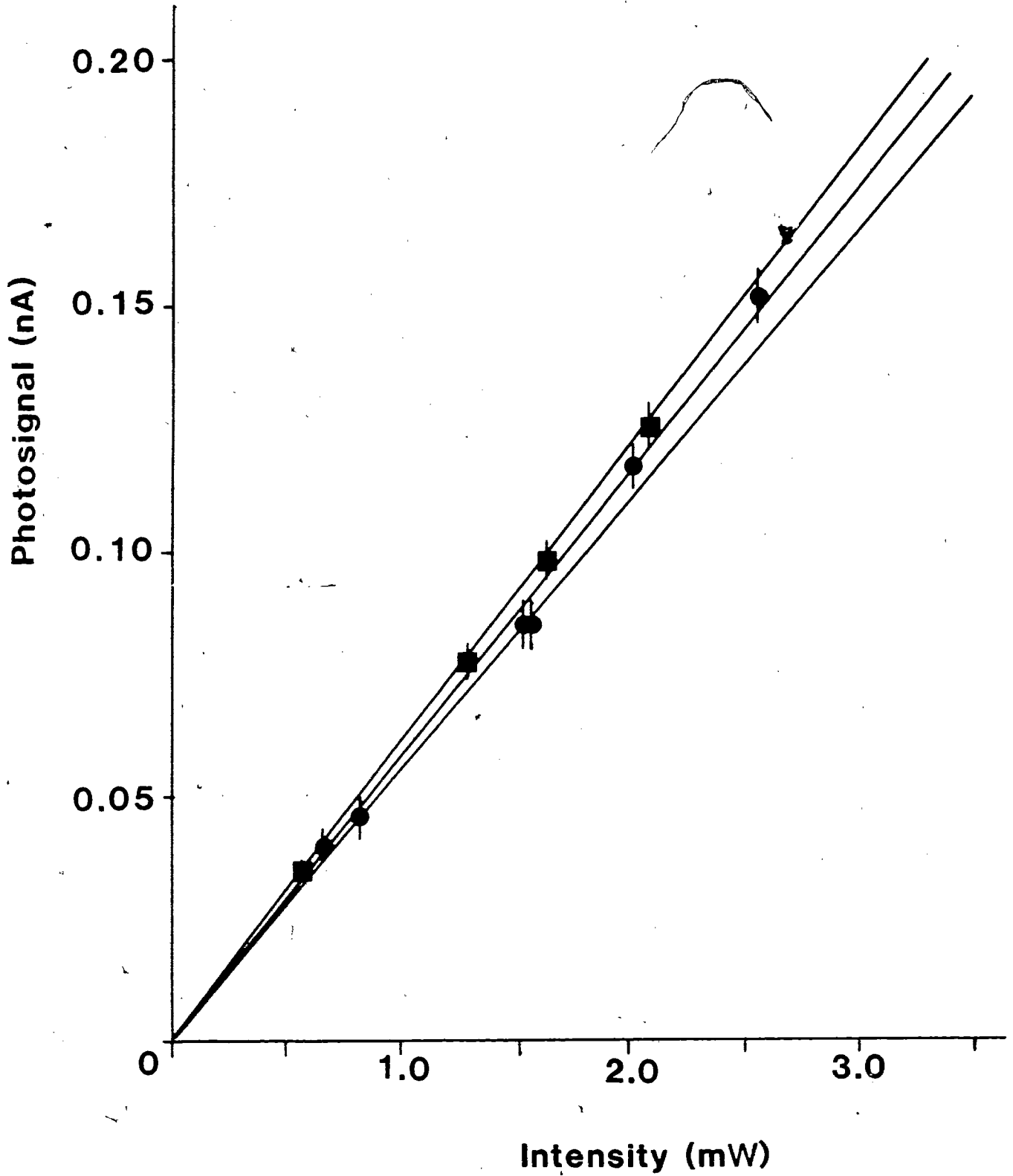


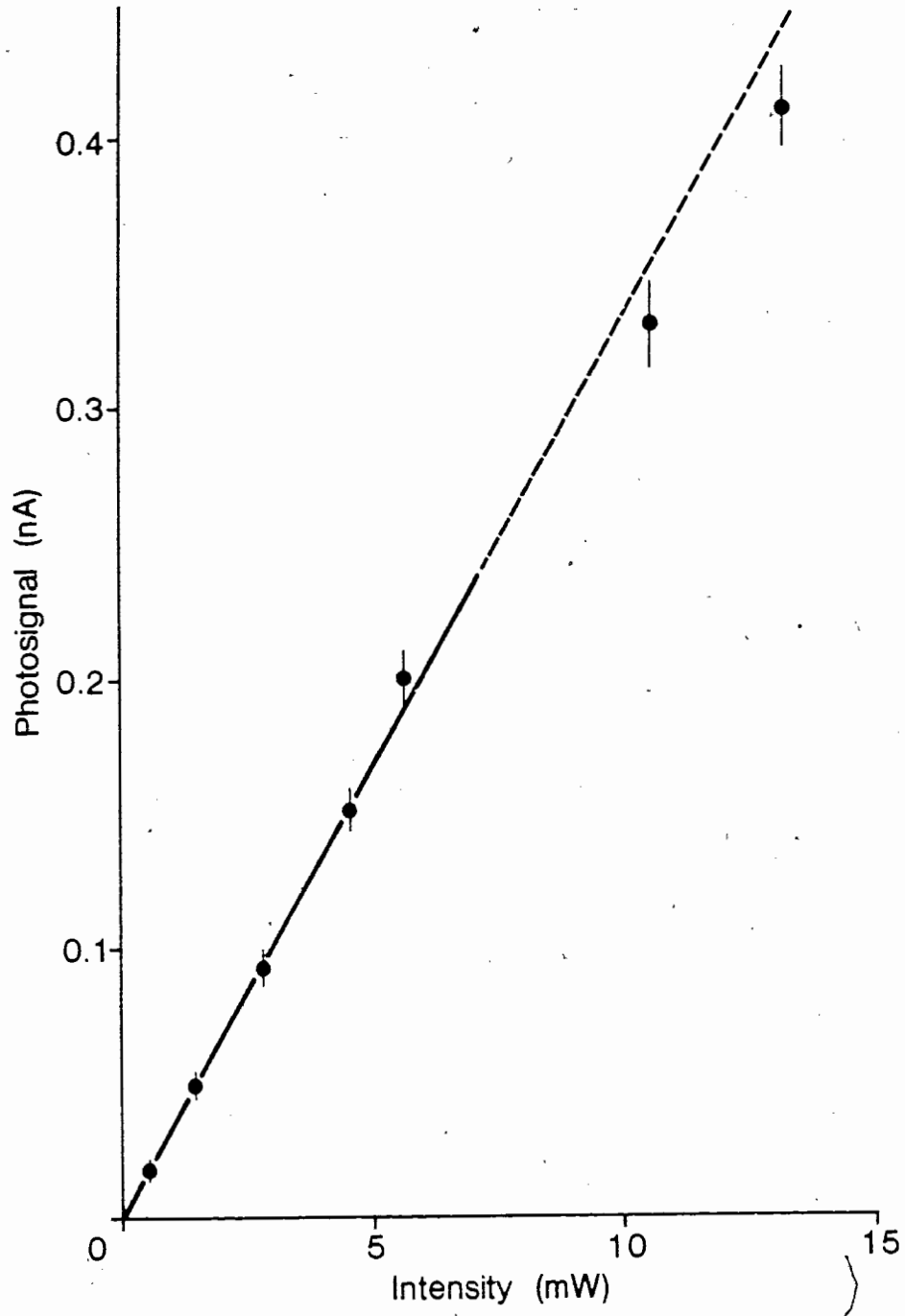
FIGURE 2.8 - PHOTOSIGNAL VS. INCIDENT LASER POWER

Sample: [TCNE] = 0.005 M.

[Mesitylene] = 0.025 M. in DCE

$\lambda = 476.0$ nm.

V = 150 Volts



The linear dependence of the photosignal on the applied voltage is shown in Figure 2.9. Two sets of measurements are shown which were performed on consecutive days. The results were reproducible within the error limits. Such linear dependence of photosignal on voltage and incident laser power had been demonstrated previously¹.

In order to assess the effect of excitation frequency on the photocurrent, the measurements of laser power were corrected to give the amount of light actually absorbed in the region between the electrodes.

$$I_A = I_0 \times T \times A$$

where

I_A = light absorbed between electrodes

I_0 = light incident on cell

T = % transmittance up to electrodes

A = % absorbance between electrodes

The effective transmittance through the air-glass interface changes by only 0.1% over the green to violet wavelength range.

The photosignal ($V_L = i_L R$ where i_L = photocurrent) was measured as a function of incident laser power (I_0) for a number of different wavelengths

FIGURE 2.9 - PHOTOSIGNAL VS. VOLTAGE

Sample: [TCNE] = 0.005 M.

[Mesitylene] = 0.025 M. in DCE

$\lambda = 488 \text{ nm.}$

$I_0 = 46 \text{ mW.}$

Trial 1 and Trial 2 were carried out on two consecutive days.

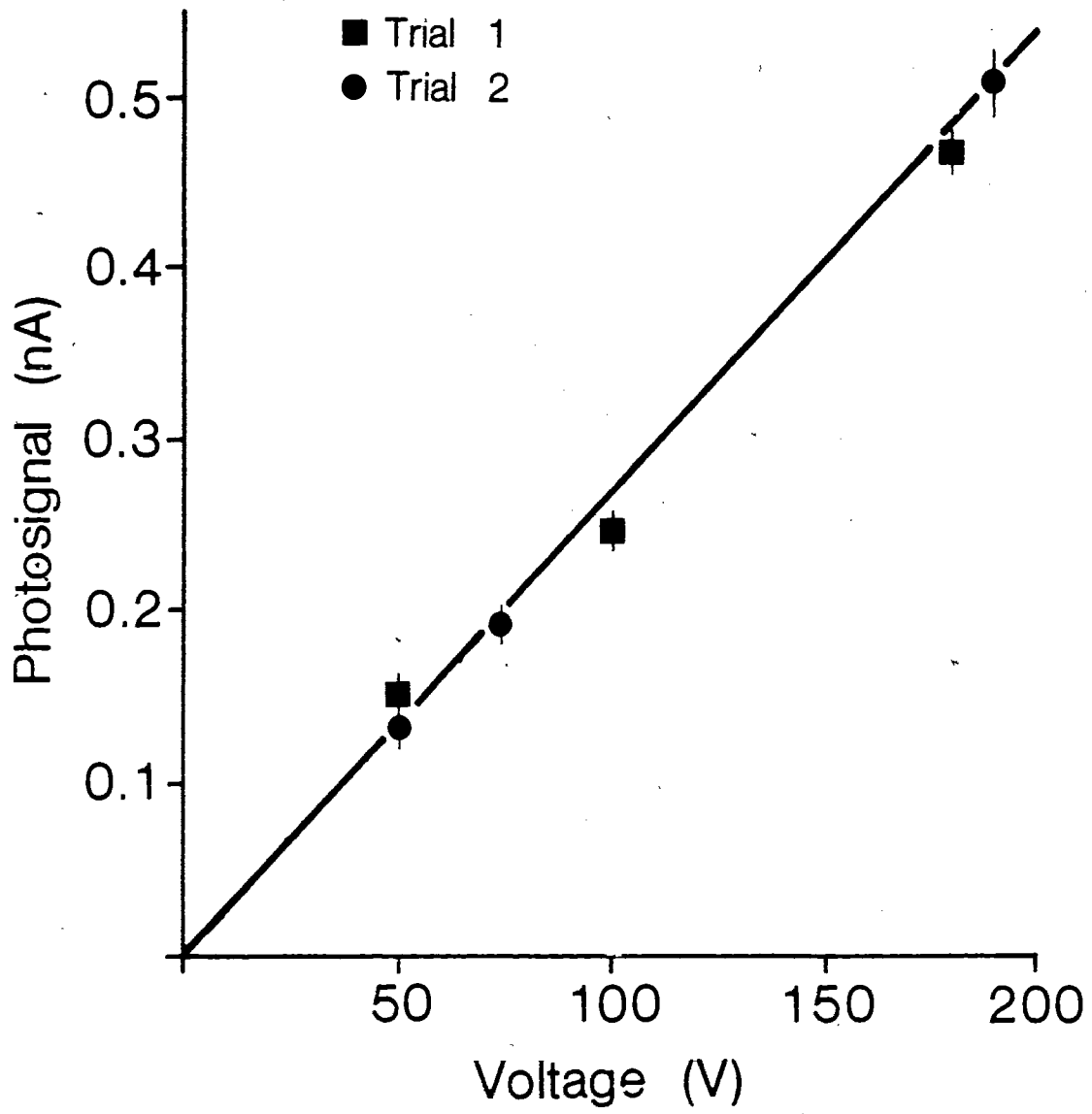


(Figure 2.6). 180 volts were applied across the cell. A typical graph of photosignal versus incident laser power is shown in Figure 2.7. The amount of photocurrent (nA) generated per milliwatt of incident power was calculated from the slope of i_L vs. I_0 . This measurement was then corrected to give the photocurrent generated per milliwatt of absorbed light.

$$i_L/I_A = i_L/I_0 \times (1/T_A)$$

where

i_L = photocurrent signal

I_0 = incident laser power

I_A = absorbed laser power

T = % transmittance up to electrodes

A = % absorbance between electrodes

Values for i_L/I_A are shown in Table 2.1 along with values for the quantum efficiency at different excitation wavelengths. The quantum efficiency (R) was calculated as shown below and represents the number of electronic charges produced at the electrode per absorbed photon.

TABLE 2.1
EFFICIENCIES FOR PHOTOCURRENT GENERATION

λ (nm)	i_L / I_0 (nA/mW)	i_L / I_A (nA/mW)	R ($\bullet e^-$ /photons)
428.5	$0.064 \pm .006$	$0.15 \pm .01$	$0.45 \pm .04 \times 10^{-6}$
431.0	$0.064 \pm .006$	$0.15 \pm .01$	$0.43 \pm .04 \times 10^{-6}$
434.0	$0.064 \pm .006$	$0.15 \pm .01$	$0.41 \pm .04 \times 10^{-6}$
457.9	$0.055 \pm .003$	$0.115 \pm .008$	$0.32 \pm .02 \times 10^{-6}$
465.8	$0.056 \pm .002$	$0.119 \pm .004$	$0.32 \pm .01 \times 10^{-6}$
472.7	$0.055 \pm .002$	$0.115 \pm .004$	$0.30 \pm .01 \times 10^{-6}$
476.5	$0.056 \pm .002$	$0.121 \pm .004$	$0.31 \pm .01 \times 10^{-6}$
488.0	$0.056 \pm .002$	$0.124 \pm .004$	$0.32 \pm .01 \times 10^{-6}$
496.5	$0.055 \pm .002$	$0.126 \pm .005$	$0.32 \pm .01 \times 10^{-6}$
501.7	$0.051 \pm .004$	$0.122 \pm .009$	$0.30 \pm .02 \times 10^{-6}$
514.5	$0.049 \pm .004$	$0.126 \pm .009$	$0.30 \pm .02 \times 10^{-6}$

$$R = i_L / I_A \times N_e / N_p$$

$$R = \#e^- / \#photons \text{ absorbed}$$

$$N_e = \#e^- \text{ per } \mu A.$$

$$N_p = \#photons \text{ per mW.}$$

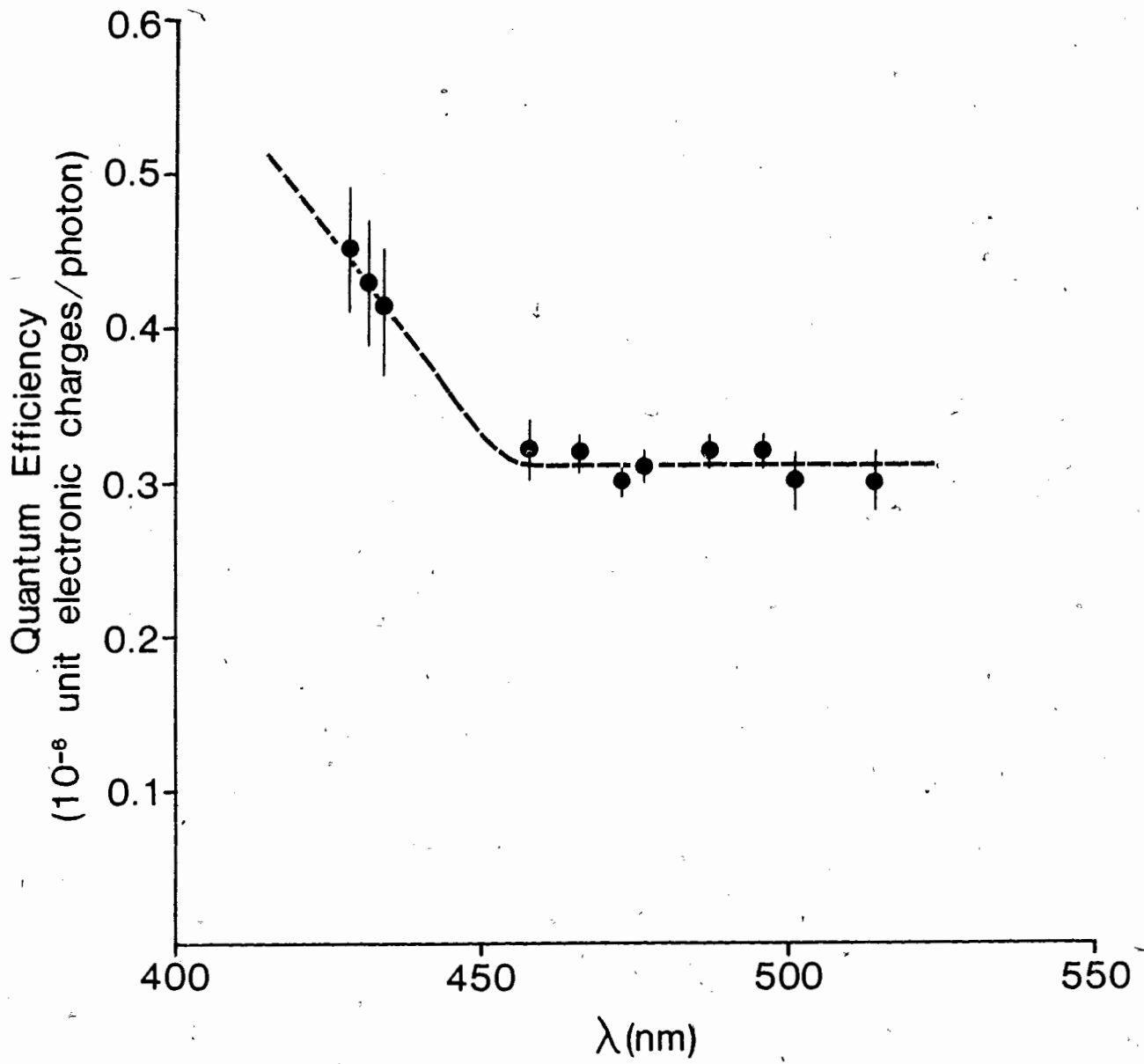
The graph of R vs. wavelength (Figure 2.10) is consistent with an increase in the probability of dissociation with excitation energy. The error limits were estimated from the uncertainty in each of the graphs of photosignal vs. laser intensity.

Because of the consistency of these data with the original data and model, the problems associated with obtaining reproducible photosignals were not immediately apparent. However, further photocurrent measurements demonstrated that the results were not consistently reproducible. A better control of the variables affecting the system seemed necessary. Thus, by improving the optics, the electronics, sample preparation, electrode preparation and temperature control, a significant improvement in reproducibility and more accurate data on quantum efficiencies at different wavelengths were anticipated.

27a

FIGURE 2.10 -

QUANTUM EFFICIENCY VS. EXCITATION WAVELENGTH



REFERENCES:

1. K.H. Michaelian, K.E. Rieckhoff, E.M. Voigt, "Photoionic Dissociation of Electron Donor/Acceptor Complexes of Tetracyanoethylene in Solution", Chemical Physics Letters **1976**, 44, 482-483.
2. R.S. Mulliken, W.B. Person, "Molecular Complexes, A lecture and Reprint Volume"; Wiley Interscience: New York, **1969**.
3. K.H. Michaelian, K.E. Rieckhoff and E.M. Voigt, "Model Theory of Resonance Raman Excitation Profiles in Electron Donor/Acceptor Complexes", Chemical Physics Letters **1977**, 45, 250-254.

CHAPTER 3 - REINTERPRETING THE PHOTOSIGNAL

The investigation of the effects of different variables on the photosignals measured in charge transfer solutions led to a major reinterpretation of the earlier experimental results. In section 3.1 the shape and magnitude of the photosignal as well as its dependence on light exposure time, beam geometry and beam position will be discussed and compared with the original model. Following this, in section 3.2, another interpretation of the photosignal will be considered which includes convective effects in solution. This model accounts qualitatively for the observed photoresponse.

3.1.1 - PHOTOCURRENT, DEPENDENCE ON LIGHT EXPOSURE TIME

The chopping frequency of incident laser light on CT solutions was varied in order to study the effect of light exposure time per cycle on the measured photosignal. The experimental set-up is identical to that used previously and is shown in Figure 2.6. Figure 3.1 shows the photosignal as a function of chopping frequency. The photosignal increases as the chopping frequency is decreased. A graph of photosignal versus half cycle time ($t_{\text{chopper}}/2 = 1/2f_{\text{chopper}}$), or light exposure time per cycle, shows that the signal rises most rapidly in the first 10 ms. (Figure 3.2). As the half-cycle time is increased, the signal continues to rise. The previous measurements at 375 Hz. ($t_{\text{chopper}}/2 = 1.33$ ms.) did not correspond to steady state conditions.

FIGURE 3.1 - PHOTOSIGNAL VS. CHOPPER FREQUENCY

Sample : 4 ml. of 0.001 M. TCNE/DCE

2 ml. of mesitylene

V = 200 Volts

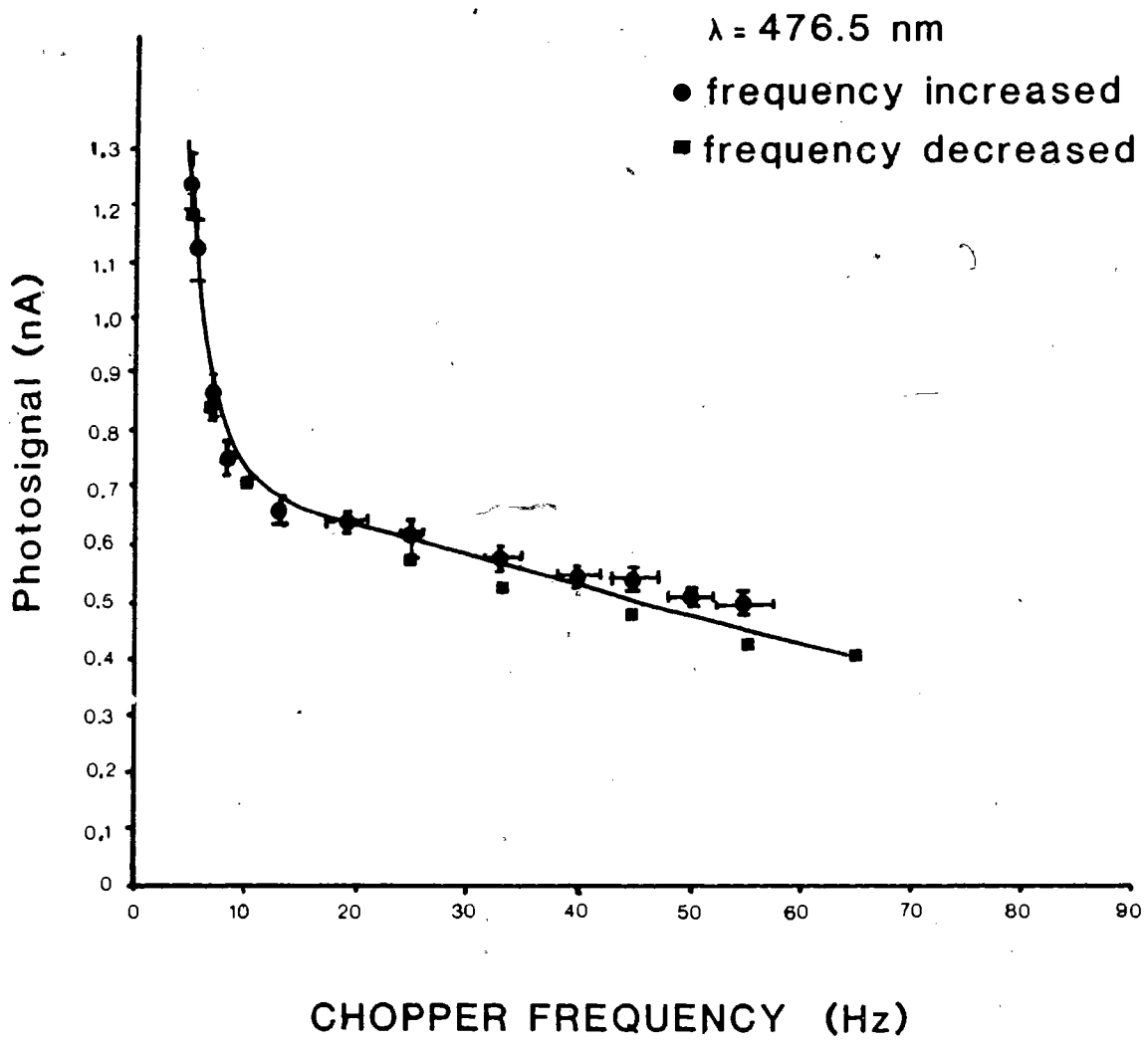


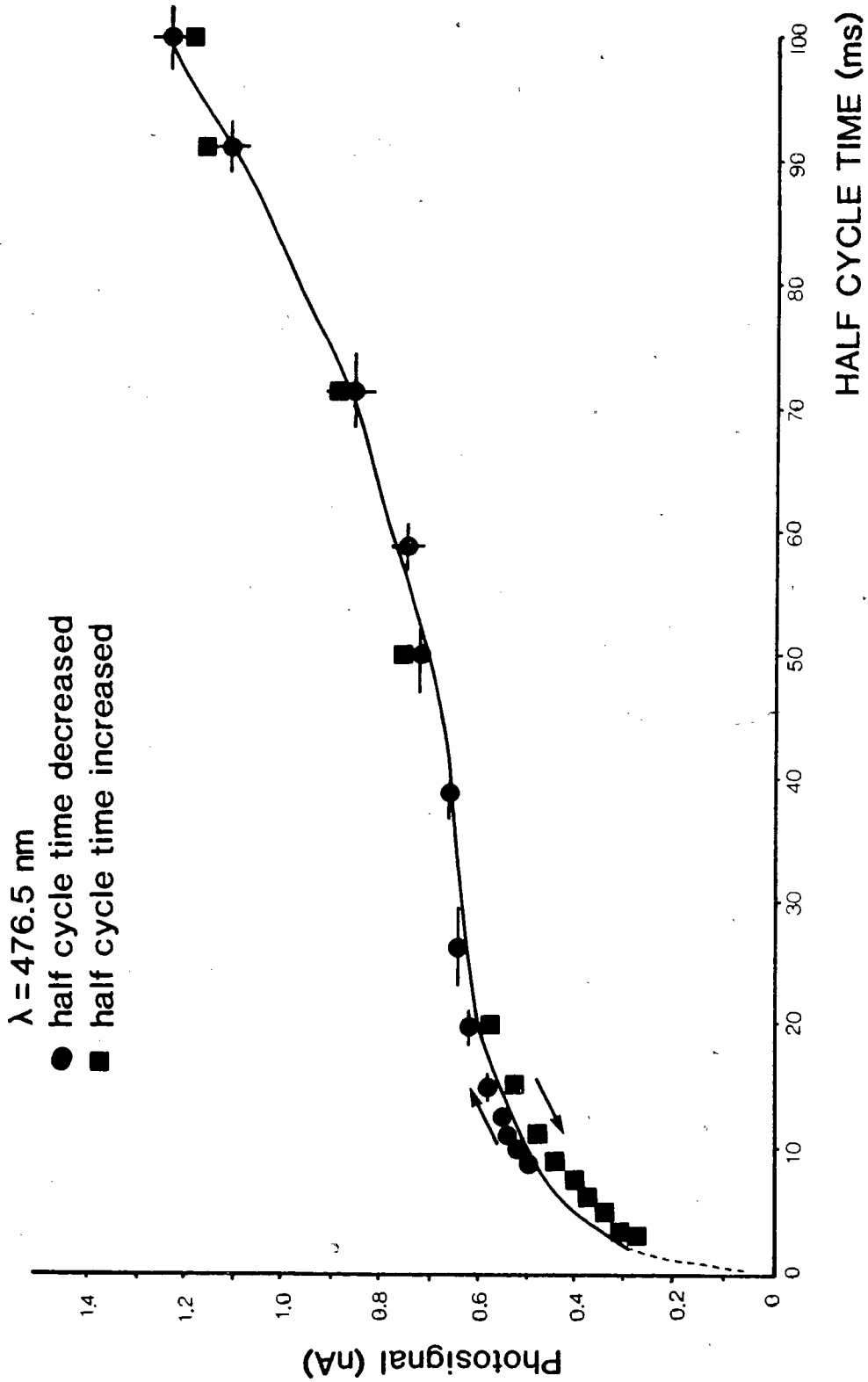
FIGURE 3.2 - PHOTOSIGNAL VS. HALF CYCLE TIME

Sample : 4 ml. of 0.001 M. TCNE/DCE

2 ml. of mesitylene

V = 200 Volts

31b



In the original model the fraction of the photoinduced charge reaching the electrodes per second should have been independent of the light-on time. Only the voltage dependent drift velocity and the ionic lifetimes were expected to change the rate of photocurrent generation at a given excitation wavelength.

The shape of the current response in time was investigated more closely using signal averaging techniques (Figure 3.3). The duration of the light exposure was varied using a chopper or camera shutter with a manual control. The overall DC current-time response was also measured directly (without averaging).

In Figure 3.4, the shape of the photosignal is shown for different chopping frequencies. Following illumination, a rapid change in current is observed. This is consistent with the observed dependence of the photosignal on half-cycle time (Figure 3.2). The increase in the signal magnitude with decreasing chopping frequency is also consistent with the data in Figures 3.1 and 3.2. Figure 3.5 shows the photocurrent response with longer light exposure times (1 - 20 sec). The current response levels out around 300 ms. (Figure 3.5a). This was beyond the range previously investigated in Figure 3.2.

Superimposed on the photosignal's sawtooth shape is the fluctuating DC current background. At higher frequencies (i.e. 375 Hz.) the magnitude of the noise could easily have overshadowed the photosignal. This explains



FIGURE 3.3 - SIGNAL AVERAGING APPARATUS



33b

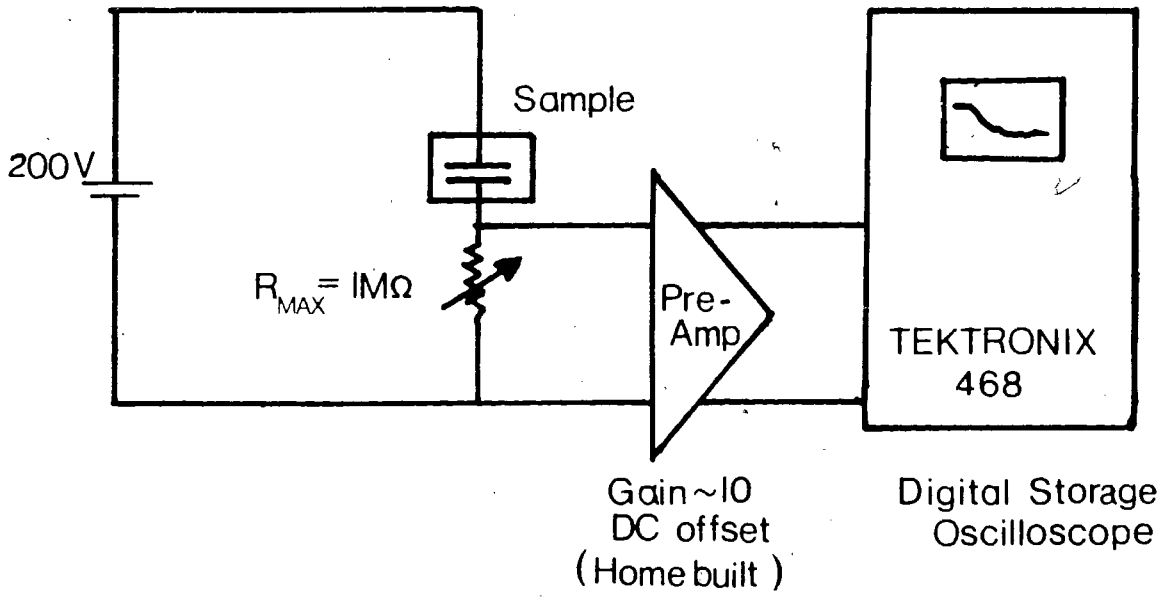


FIGURE 3.4 - PHOTOSIGNAL SHAPE

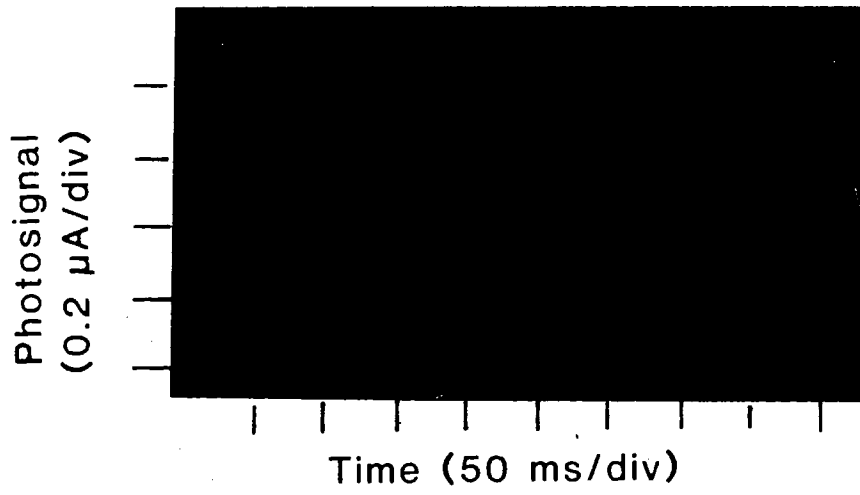
Sample : 4 ml. of 0.001 M. TCNE/DCE

2 ml. of mesitylene

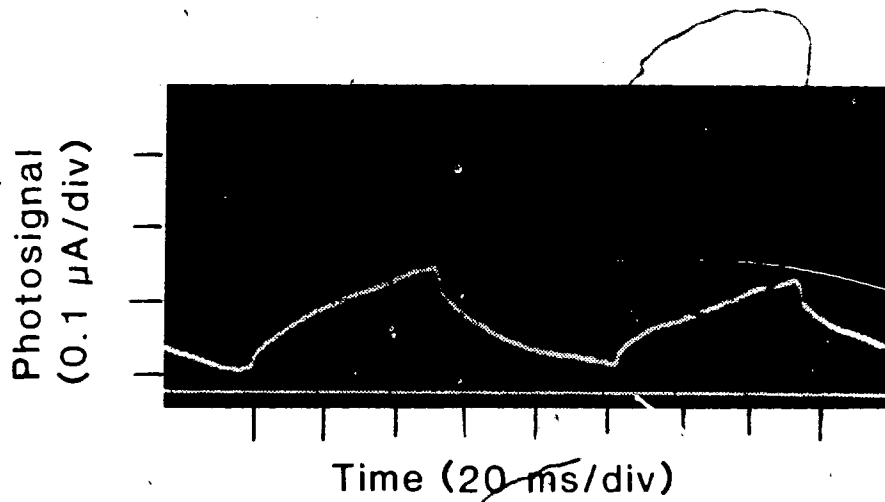
V = 200 Volts

$\lambda = 476.5$ nm.

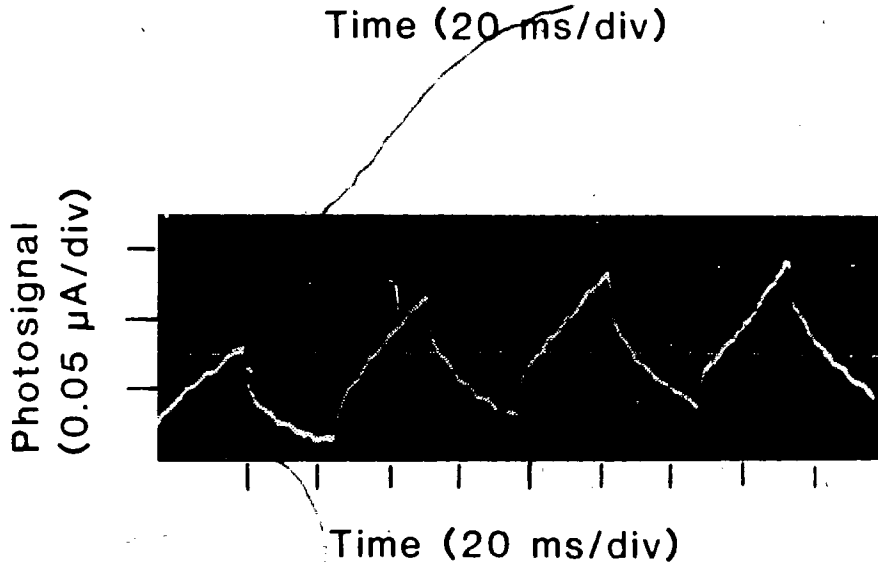
The current decreases following light exposure.



f = 5 Hz.



f = 10 Hz.



f = 20 Hz.

FIGURE 3.5 - PHOTOSIGNAL SHAPE

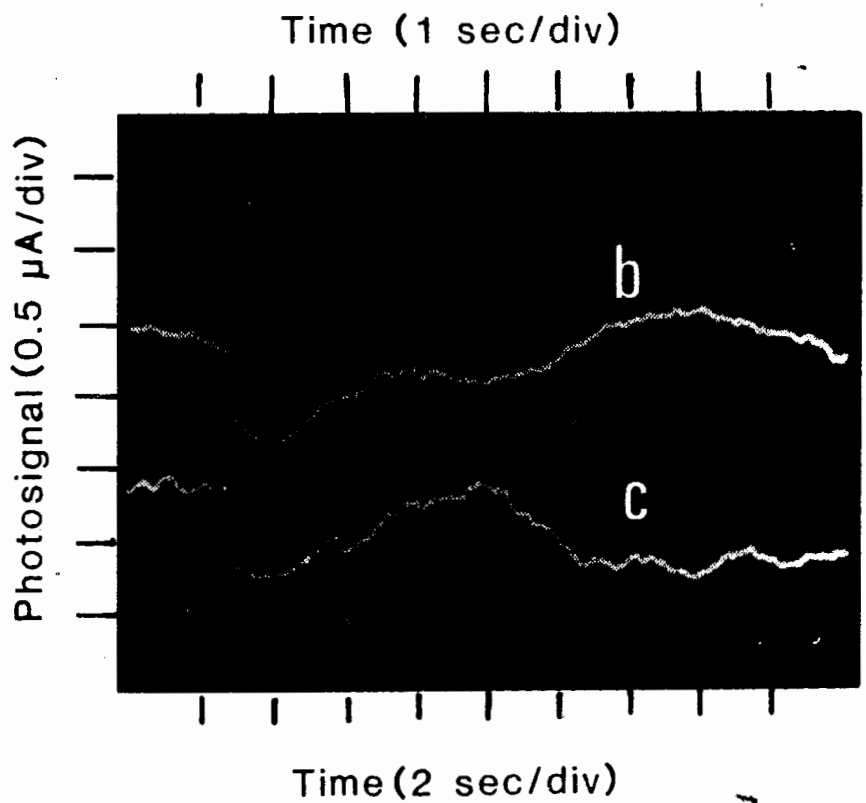
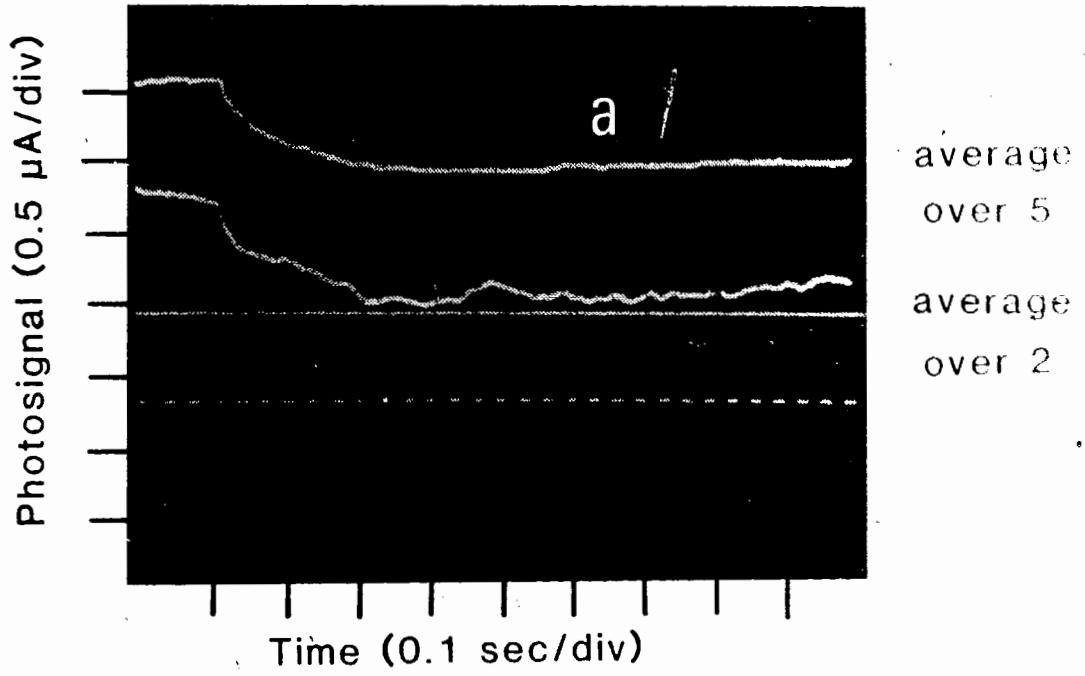
Sample : 4 ml. of 0.001 M. TCNE/DCE

2 ml. of mesitylene

$V = 200$ Volts

$\lambda = 476.5$ nm.

The current decreases following light exposure.



why the initial attempts to monitor the photosignal shape with an oscilloscope without signal averaging capability were unsuccessful.

The main features of the current response to light are summarized below for TCNE/Mesitylene/DCE samples. These features are demonstrated in Figures 3.5 and 3.6.

1. A sharp drop in current follows light exposure. The drop in DC background current is generally preceded by a delay time as shown in Figure 3.6 ($V = 10$ volts). One measurement with a chopping frequency of 35 Hz ($V = 200V$) did not show a delay time (delay time $< 250 \mu\text{sec.}$).
2. The rate of current drop declines and approaches zero, after which random fluctuations and noise are observed in the current response. (Figures 3.5b, 3.5c).
3. A sharp increase in current follows when light exposure is discontinued. (Figure 3.6 - DC response not averaged). This increase in current levels off, after which random fluctuations in the current are observed again (Figure 3.6).

The drop in current with incident light was not consistent with the previous assumption that photoionic dissociation would increase the number of charge carriers in solution.

FIGURE 3.6 - DC PHOTOCURRENT RESPONSE (no averaging)**Sample :** [TCNE] = 0.003 M.

[mesitylene] = 0.028 M.

V = 10 Volts **$\lambda = 482$ nm.**

The current recovery time with no incident light was approximately 4 minutes.

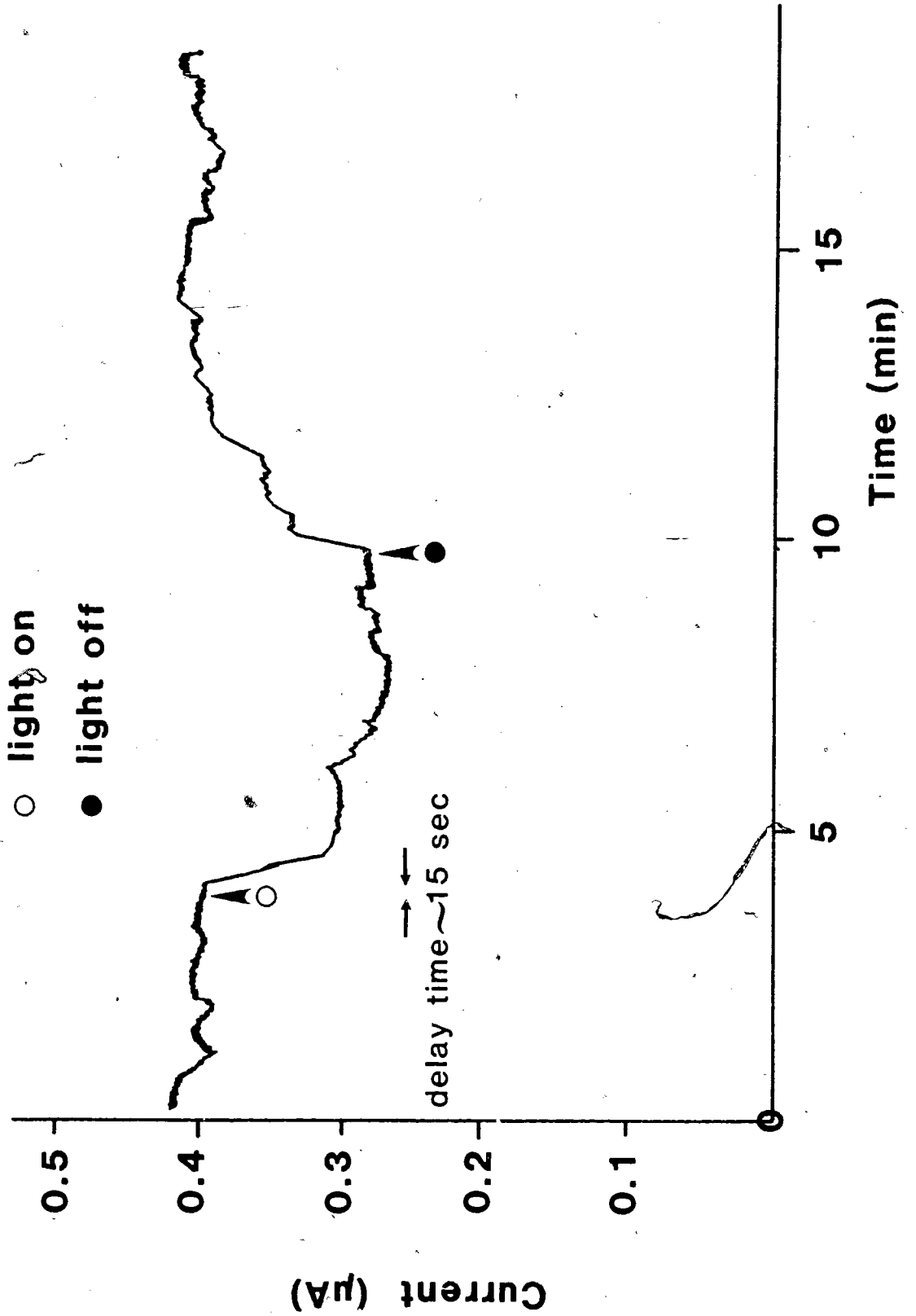


Table 3.1 shows the photoinduced change in the DC current at different voltages. In the range from 5 to 20 volts there is no longer a linear dependence of the photoresponse to the applied voltage. Such behaviour was not consistent with the expected contribution of drift velocity to the photocurrent. The photosignal magnitude and time response were also found to be sensitive to electrode preparation and voltage history.

3.1.2 - PHOTOSIGNAL GEOMETRY DEPENDENCE

Another group of observations that went beyond the previous work was the dependence of the photosignal on the geometry of the cell. Both the shape and position of the incident light beam were considered. Two different chopping frequencies (9.5 and 95 Hz.) were used with signal averaging.

The magnitude of the photosignal is larger with the light beam near the positive electrode (anode) than with the beam near the negative electrode (cathode). The decrease in photosignal is continuous as the beam is moved from the anode through the center of the cell to the cathode. Table 3.2 summarizes these observations, as well as the effects of beam shape.

Three beam profiles were considered: circular (0.5mm. diameter), vertical ($\approx 3 \times 0.5$ mm), and horizontal (1 x 2 mm). The vertically oriented beam profile results in larger photosignals for the same incident laser power. The number of photoinduced charge carriers should have been independent of

TABLE 3.1

DC CURRENT PHOTO RESPONSE

$\Delta DC/DC$ = fractional change in DC current
wavelength = 482 nm

Sample: [TCNE] = 0.003M [Mesitylene] = 0.028M

V	$\Delta DC/DC$	ΔDC	LASER POWER	PHOTO RESPONSE
25V	1/3	0.5 μA	4.9 mW \pm 20%	0.10 nA/(mW incident)
10V	1/4	0.1 μA	5.6 mW \pm 20%	0.018 nA/(mW incident)
5V	1/2.5	0.06 μA	3.8 mW \pm 20%	0.016 nA/(mW incident)

TABLE 3.2

GEOMETRY DEPENDENCE OF PHOTO-CURRENT SIGNAL

d = 2mm (Pt electrodes)

V = 200V

Wavelength = 476.5 nm

Photo-current measured with a storage scope, at a gain of 10.

BEAM GEOMETRY	f_{chopper}	SIGNAL (across $1M\Omega$)
circular beam: o 		
middle of cell	9.5 Hz	0.116 μA - 0.140 μA
near -ve plate	9.5 Hz	0.080 μA - 0.100 μA
near +ve plate	9.5 Hz	0.180 μA - 0.190 μA
glancing +ve plate	9.5 Hz	0.190 μA
glancing -ve plate	9.5 Hz	0.080 μA
glancing -ve plate	95 Hz	0.138 nA - 0.152 nA
-ve off center	95 Hz	0.15 nA
center	95 Hz	0.195 nA
+ve off center	95 Hz	0.23 nA
glancing +ve plate	95 Hz	0.30 nA
vertical beam: 		
center	95 Hz	0.244 nA
+ve off center	95 Hz	0.376 nA
-ve off center	95 Hz	0.154 nA
horizontal beam: = 		
	95 Hz	0.292 nA

beam location or shape according to the original model and so the preceding observations (Table 3.2) could not be reconciled with that model.

As a result of these observations and those in the previous section the originally proposed model for the mechanism of the photocurrent response in CT solutions had to be abandoned in favour of possible alternative explanations.

3.2.1 - EVIDENCE FOR CONVECTION AS A CHARGE TRANSPORT PROCESS IN CHARGE - TRANSFER SOLUTIONS

In an attempt to explain the photocurrent behaviour described in the previous chapter a convection mechanism for current transport was considered. Then the decrease in sample current under illumination could be explained by interruptions in the convection patterns in the cell induced by the absorption of light.

A lensing effect is observed in CT solutions for higher beam intensities ($I_0 \gg 10 \text{ mw}$, beam diameter $\approx 1 \text{ mm}$.) and clearly demonstrates that incident light can generate moving liquid density gradients in the sample. As a result of lensing, the size and shape of a transmitted light beam pulsate irregularly in time. A qualitative correlation can be made between the pulse time of the transmitted beam and the time required for the initial decrease in DC current after illumination. The characteristic decrease in current with illumination is still observable at higher light intensities. Although no

lensing was observed in samples during the photocurrent measurements discussed in the previous chapters, the possibility of light interfering with charge transport processes needed further investigation.

It was found that acoustic noise could also result in the disturbance of convection patterns and thus a decrease in the DC current. Figure 3.7 shows this using the periodic sound pulse (30 Hz.) from a strobe light (without sample illumination). The apparatus is shown in Figure 3.8. Each sound pulse results in a sudden decrease in sample current followed by smaller oscillations. Also it had been observed previously that the current response was very sensitive to mechanical vibrations (i.e. tapping the lab bench). Both vibration and light absorption could introduce liquid motion in a direction perpendicular to the applied field (cross-field) and thereby interfere with charge transport in the sample. These observations were consistent with, but did not prove in and of themselves, the existence of electroconvection in the charge transfer solutions. Further evidence was needed to establish the importance of convection in CT solutions and the role that it played in the photoresponse.

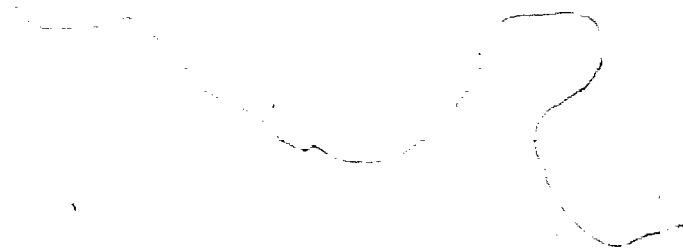
3.2.2 - EVIDENCE FOR CONVECTION IN AN ANALOGOUS SYSTEM - INDIGO (DYE)/DCE

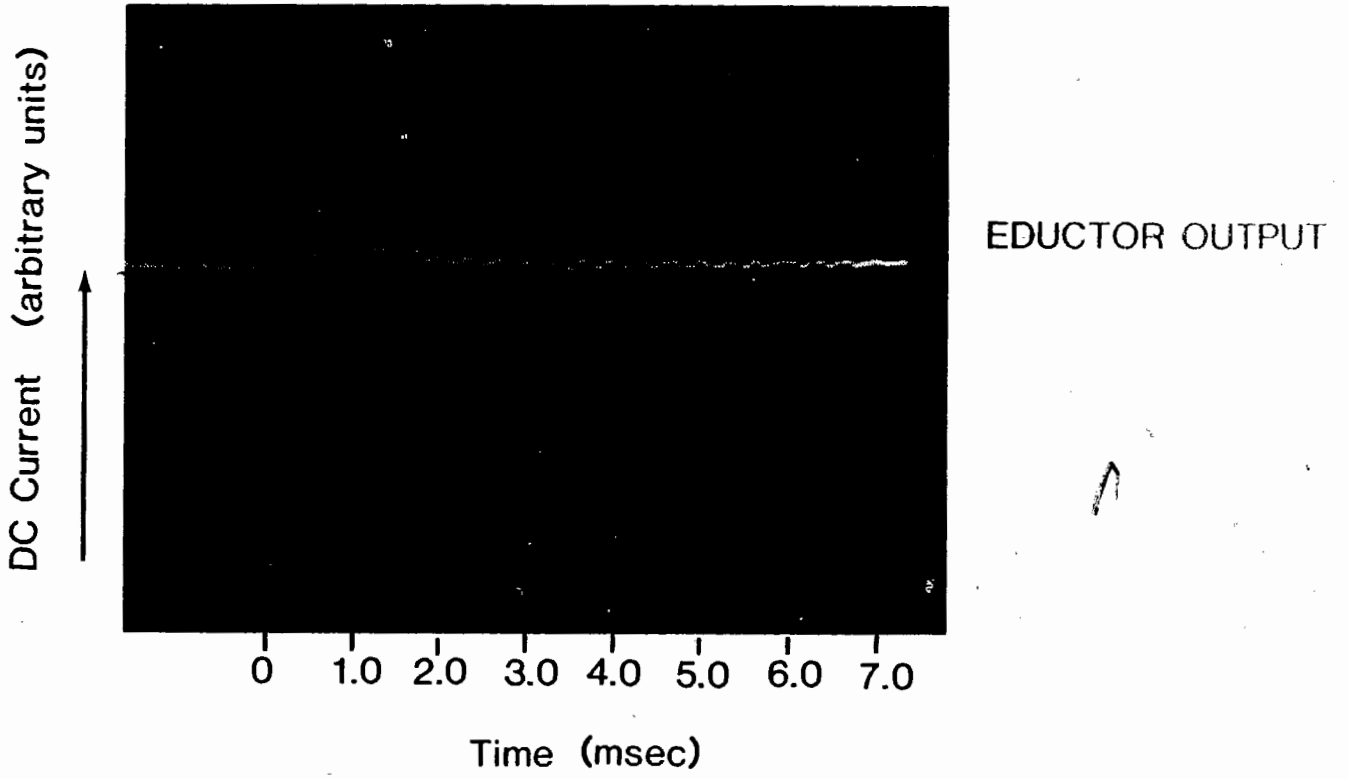
One method of observing convection in solutions is to introduce small 'neutral' particles which will indicate the flow pattern. Unfortunately, the particles introduced will tend to pick up charges and change the current

FIGURE 3.7 - DC CURRENT ACOUSTIC EFFECT**Sample : 4 ml. of 0.001 M TCNE/DCE****6 ml. of mesitylene****V = 200 Volts**

**The current decreases following each sound pulse (f = 30 Hz.)
and oscillates before returning to its initial value.**

f

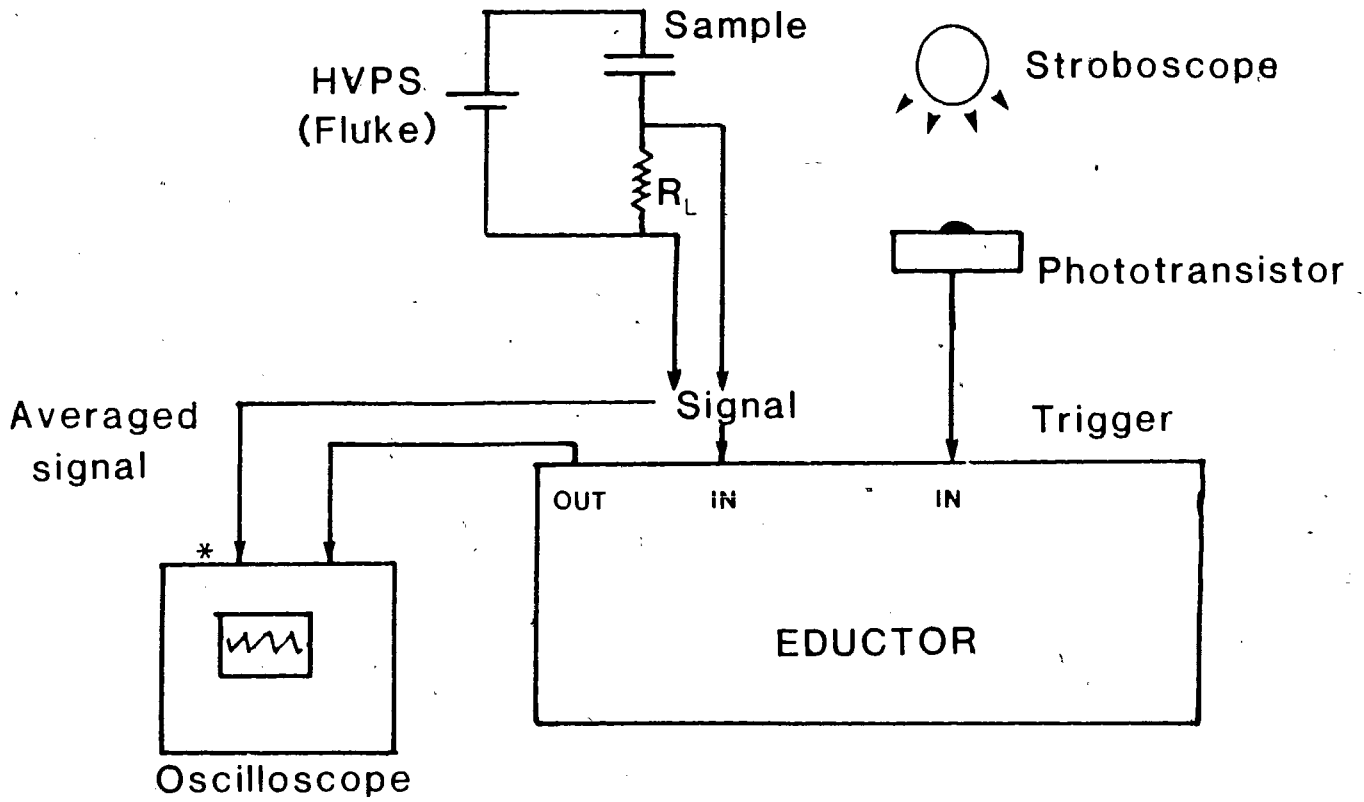




Handwritten marks at the bottom right of the page, including a checkmark and some illegible scribbles.

FIGURE 3.8 - SIGNAL AVERAGING APPARATUS, ACOUSTIC EFFECT





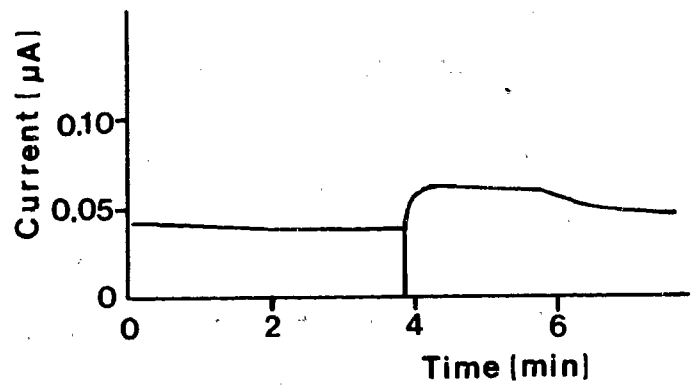
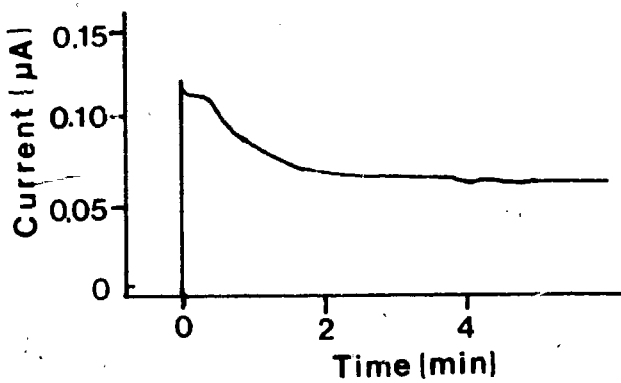
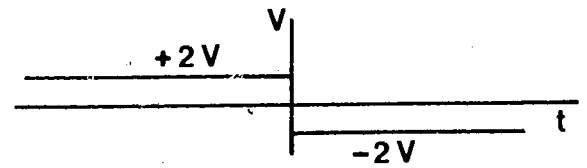
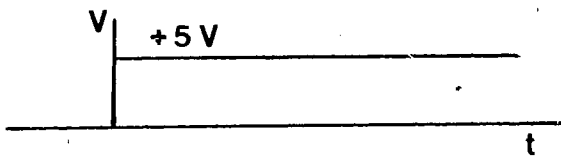
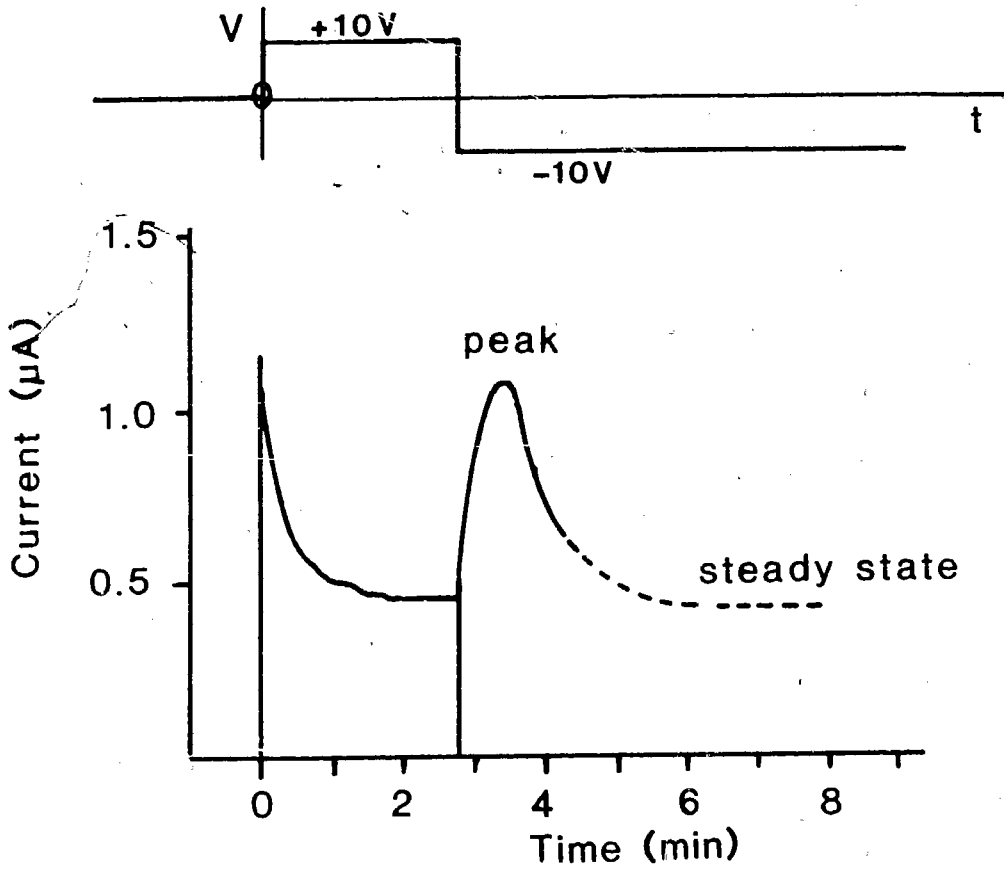
* Signal input to eductor is offset by oscilloscope

characteristics of a solution¹. Nevertheless, a useful analogous system was found for making qualitative comparisons with the TCNE/Mesitylene/DCE system: Indigo synthetic (Vat Blue 1) suspended in DCE. Indigo dye particles are electropositive (as demonstrated by the flow of particles under an applied electric field - Figure 3.12) and can easily be prepared as a suspension in DCE using an ultrasonic bath. The DC current responses of DCE solutions with TCNE or Indigo particles were qualitatively similar (see Figures 3.9 and 3.10). Also, both the Indigo/DCE and CT solutions absorbed incident light over a broad region of wavelengths (TCNE/mesitylene $\lambda_{\max} = 458$ nm, Indigo dye $\lambda_{\max} = 605$ nm²). Presumably, if convection was observed in the Indigo dye solution, and if the observed convection could be shown to be related to the photocurrent, then this would be a promising indication that the same mechanism is operative in the CT solutions.

To measure the dark DC current response for samples, a cell with platinum electrodes (the same cell that was used for photosignal measurements previously) was connected in series with a load resistor ($R_L = 10K\Omega$). The current was then measured over time by monitoring the signal across the load resistor after a step voltage was applied.

The application of voltage to DCE solutions without prior voltage exposure is followed by an immediate decrease in the current. A steady state current is approached as the rate of current change decreases in time. On voltage reversal the current peak is displaced in time (Figures 3.9 and 3.10). The

FIGURE 3.9 - DC CURRENT RESPONSE OF TCNE/DCE**Sample: [TCNE] = 0.002 M.****platinum electrodes****FIGURE 3.10 - DC CURRENT RESPONSE OF INDIGO/DCE
(Pt electrodes)**



measured steady state conductivities for the Indigo/DCE samples $[(2-4) \times 10^{-7} \Omega^{-1} \text{m}^{-1}]$ are larger than those measured for DCE alone $(10^{-9} - 10^{-8} \Omega^{-1} \text{m}^{-1})$, and of the same order of magnitude as conductivities for TCNE/DCE samples $(\approx 10^{-6} \Omega^{-1} \text{m}^{-1}$ for $[\text{TCNE}] = 0.002\text{M})$.

The effect of illumination on the Indigo Blue/DCE suspension with applied voltages from 1 to 40 volts is presented in Figure 3.11. A He-Ne laser was used to illuminate the system (wavelength = 632.8 nm.). Both the direction and magnitude of the DC photocurrent response vary with voltage. Above 5 volts the DC current decreases with sample exposure to light after a delay time (Figure 3.11), just as had been previously observed in CT solutions. Below 5 volts the sample current actually increases with incident light. This increase in photocurrent with illumination had not been previously observed in CT solutions.

The fundamental difference in photoresponse at different voltages could only be interpreted by considering the dye particle patterns in the Indigo/DCE system. The patterns were observed with light scattered from the suspended particles. Only one view was recorded, namely the one looking down at the top of the platinum electrode cell. Figure 3.12 and Table 3.3 summarize these observations. Below 5 volts, no evidence of turbulence is observed in the indigo/DCE solution. The dye particles move away from the anode with voltage application. This results in a well defined front beyond which nothing appears to be in suspension. In this voltage region the current increases with incident light. This increase can

**FIGURE 3.11 - PHOTOCURRENT REPOSE OF INDIGO/DCE AT
DIFFERENT VOLTAGES**

○ light on

● lightoff

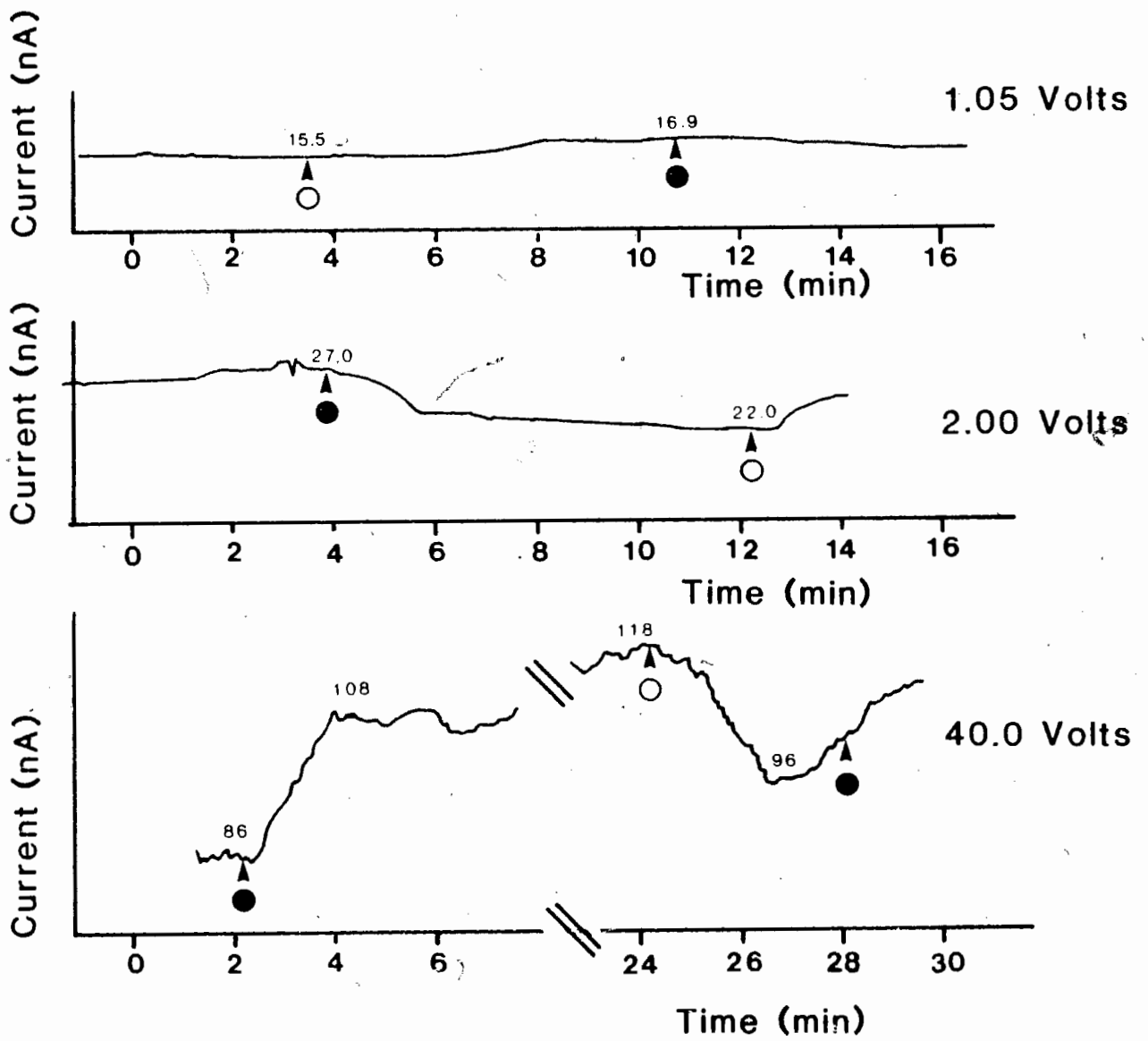


**FIGURE 3.12 - DYE PARTICLE PATTERNS IN INDIGO/DCE AT
DIFFERENT VOLTAGES**

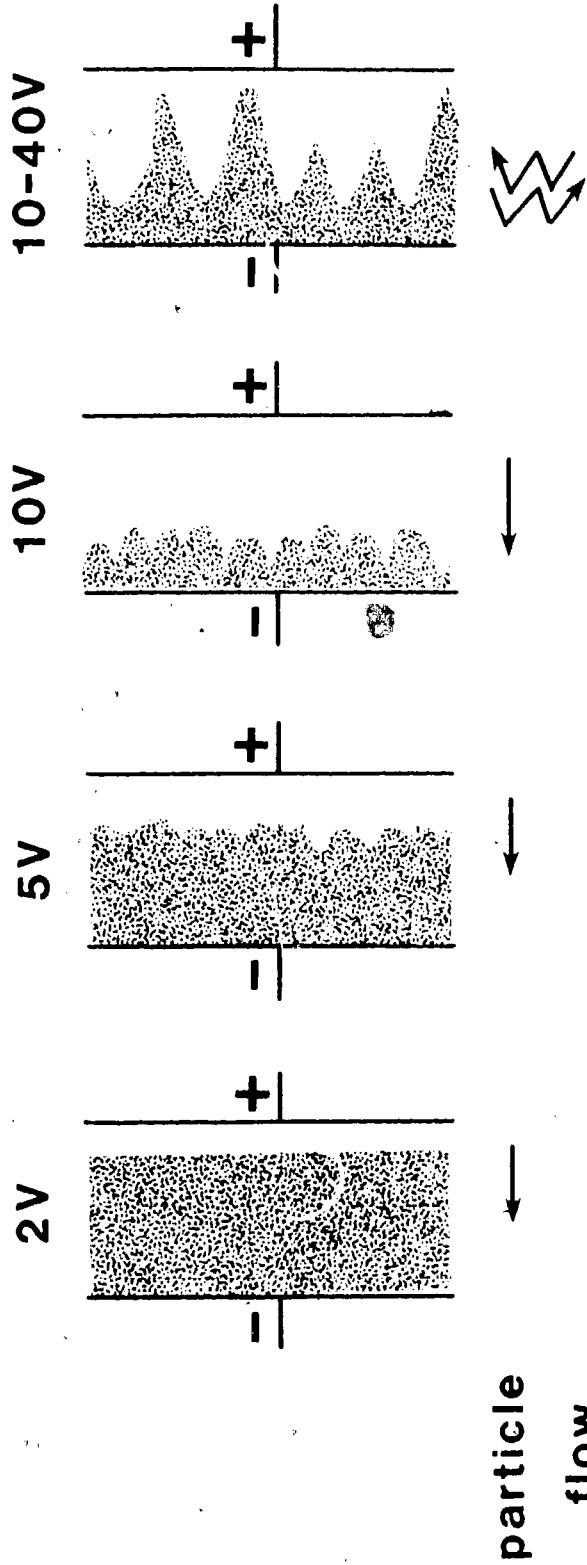


TABLE 3.3
INDIGO/DCE ELECTROCONVECTIVE PATTERNS

VOLTAGE	COMMENTS
1.05 V	No turbulence; dye particles form a clean front; positive photoresponse.
2.0 V	No turbulence; dye particles form a clean front; positive photoresponse.
5.0 V	There are some irregularities in the dye front
10.0 V	Some mixing of dye particles; negative photoresponse
15.0 V	Lots of mixing of dye particles
40.0 V	Turbulence; zig zag motion of particles; negative photoreponse.

be accounted for by the reduction in solvent viscosity with temperature and the resulting increase in particle mobilities. At 5 volts some irregularities are observed in the line dividing the regions of high and low dye particle density, however there is still no significant mixing of the solution.

In the region above 5 volts, the dye particle patterns give definite indications of turbulence and mixing: the dye front develops point irregularities and bands of high and low particle densities form fairly stable patterns over the time of observation. Within the overall pattern, particles execute a zig-zagging motion back and forth across the cell. The voltage range above 5 volts results in a decrease in the current with incident light (Figure 3.11). The observation of a critical voltage, above which turbulence ensues, is characteristic of electrohydrodynamic phenomena observed in low conductivity liquids^{3,4} and is further discussed in Chapters 4 and 5.

All of these observations are consistent with the picture that incident light interrupts convective charge transport and therefore results in a decrease in the current carried through the Indigo/DCE solution. It is thus reasonable to propose that the same mechanism is responsible for the photocurrent response observed in CT solutions. In order to establish the role of convection as a charge transport process, the basic nature of conduction in DCE solutions had to be addressed.

REFERENCES:

1. A. Rich, J.L. Sproston, G. Walker, "Some Observations on Bulk Electroconvection in Electrically Stressed Liquid Dielectrics", Journal of Electrostatics **1982**, 12, 503-510.
2. J. Fabian, H. Hartmann, "Light Absorption of Organic Colorants"; Springer-Verlag: Berlin, Heidelberg, **1980**, pp116-123.
3. P.K. Watson, J.M. Schneider, H.R. Till, "Electrohydrodynamic Stability of Space-Charge-Limited Currents in Dielectric Liquids", The Physics of Fluids **1970**, 13, 1955-1961.
4. R.W.L. Snaddon, R.Poulter, "Mass Transfer and Dissipation in Unipolar Electrophoretic Flows", Journal of Physics D - Applied Physics **1980**, 13, 2263-2274.

Chapter 4

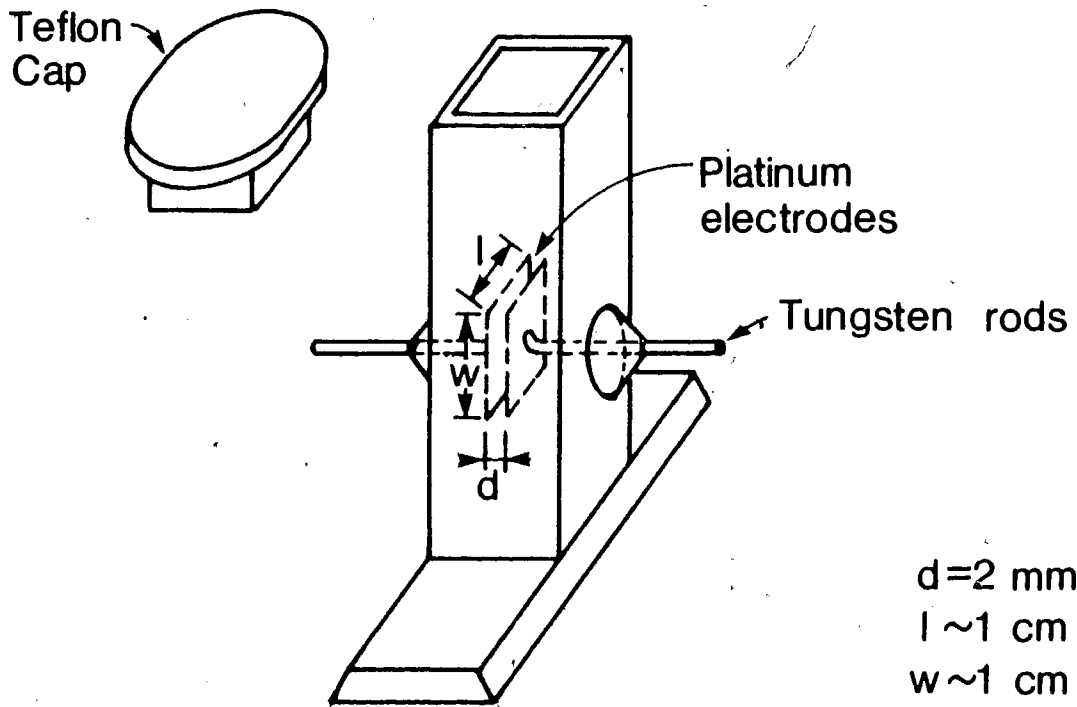
To assess the influence of convection in TCNE charge transfer solutions, the variables contributing to conduction were investigated. Only a few representative experiments performed on dichloroethane solutions with TCNE and mesitylene will be discussed in order to identify some important aspects of the conduction process. This chapter will summarize the features of the current response of TCNE/DCE and TCNE/mesitylene/DCE samples in three sections: [1] the dependence of conductivity on the concentration of TCNE and mesitylene [2] the shape of the current-time response, and [3] a description of current-voltage characteristics.

4.0 - MATERIALS AND METHODS for SECTIONS 4.1, 4.2, 4.3

The preparation of TCNE, mesitylene and DCE has already been discussed in the 'materials and methods' section of Chapter 1. A diagram of the sample cell with platinum (Pt) electrodes is given in Figure 4.1. This electrode configuration was identical to the one previously used for photoconductivity measurements. Two square Pt electrodes ($A \approx 1\text{cm}^2$) were separated by 2mm in a glass cell. The cells were sealed with a tight fitting teflon lid or covered with aluminum foil and wrapped with Teflon tape. Some measurements were carried out in fluorescent room light rather than in the dark but this had no observable effect on the current characteristics.

The DC current response of the sample was monitored by measuring the

FIGURE 4.1 - PLATINUM ELECTRODE CELL



signal across a load resistor in series with the sample cell (Figure 4.2). Typically, for 0.01M TCNE/DCE samples, measured resistances were of the order of 10 M Ω . A 10 k Ω load resistor would therefore only affect the current by about 0.1%. A 1M Ω resistor was used for some of the initial measurements on current peak times. The 1M Ω load resistor would not have changed the times at which maximum current readings were recorded although it would have affected the current readings by about 10%. The method of current measurement shown in Figure 4.2 was sufficiently accurate for our purposes since many of the experiments involved qualitative comparisons of signal shape, and since the results were liable to change significantly as a result of other variables.

The other variables affecting TCNE/DCE current response measurements included voltage history, sample-cell contact time and electrode preparation. Most 'steady state' measurements involved times of voltage application anywhere from 15 minutes to 8 hours. An experiment involving the measurement of current as a function of mesitylene concentration (Figure 4.5) was an exception since 'steady state' measurements were taken after about 6 minutes. Attempts to correlate current with TCNE concentration using the shorter runs were not fruitful. As a result of increasing the sample-cell contact time (at zero applied voltage) from 15 minutes to one hour, the steady state signal observed for a 0.004 M TCNE sample increased about two-fold.

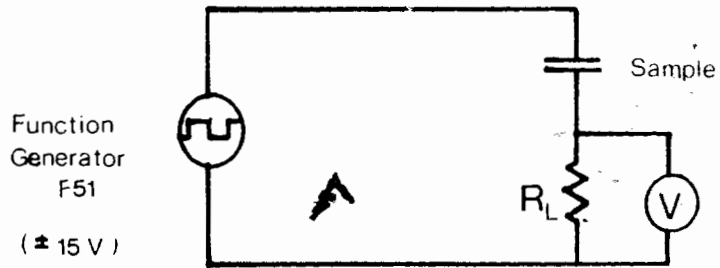
The same two Pt cells (Figure 4.1) were used repeatedly for the

FIGURE 4.2 - CURRENT MEASUREMENT

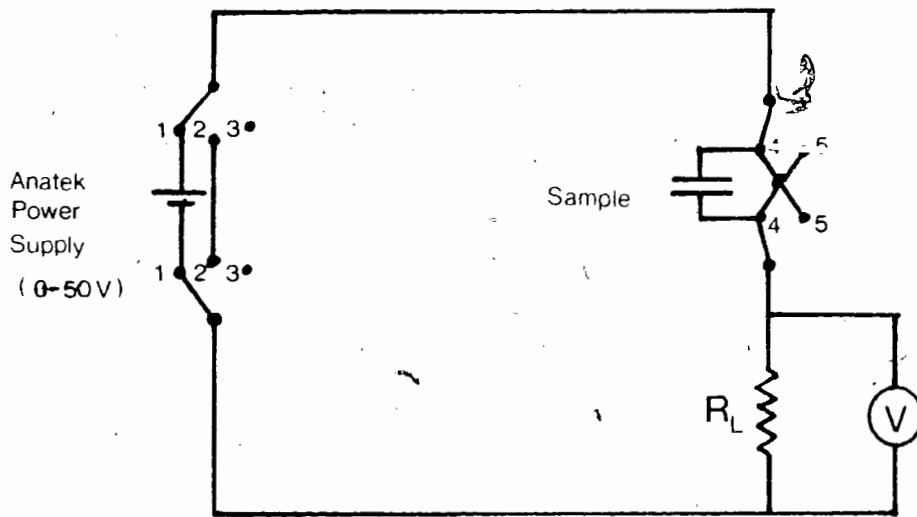
Square wave current reponse

Step Voltage current response

Square Wave Current Response



Step Voltage Current Response



Voltage
Switch
(1 $1V$
2 Short
3 Open)

Polarity
Switch
(4 $+$
5 $-$)

measurements described in this chapter. Cell cleaning was therefore an important aspect of the experimental work since electrode aging and degradation needed to be avoided in order to compare sets of data. Occasionally chemical deposits appeared on the electrodes after voltage treatments. It was difficult to ascertain any specific conditions that would generate deposits. Minute crystals of TCNE were sometimes observed on the Pt electrodes after a voltage treatment (< 50V). A drop of mesitylene turned the electrode a bright orange color characteristic of the TCNE/Mesitylene charge-transfer complex. In other instances, an orange-brown coating was observed. On the basis of information obtained later on the chemistry of TCNE, the orange deposit was probably a pentacyanopropenide salt ¹. A purple coating on the anode was observed twice during photosignal measurements (200 v applied) but was not observed with the current measurements at lower voltages. The purple coating was probably a TCNE⁻ salt. Thin films of M⁺ TCNE⁻ salts are reddish-blue or purple ². In order to maintain the Pt electrode surfaces, various cleaning methods were investigated to remove these deposits.

Cleaning methods were evaluated by comparing the currents measured through distilled DCE in the cell after different chemical treatments. This seemed a reasonable approach since, at the time, details of the electrode chemistry were not known. Table 4.1 shows the effect of different cell cleaning methods on the DCE current measurements. Chromerge cleaning was used for the runs shown in Figures 4.3, 4.4. The mesitylene-methanol-DCE treatment was used for the measurements shown

TABLE 4.1
DCE CURRENT RESPONSE
WITH DIFFERENT CLEANING METHODS

$$R_L = 5 \text{ K}\Omega \quad V = 15\text{V}$$

CLEANING METHOD	i_{peak} (na)	$i_{\text{steady state}}$ (na) *	K ($\Omega^{-1}\text{m}^{-1}$)
2 minute Chromerge soak + distilled H ₂ O rinses + Methanol rinses + DCE rinses	4	2	3×10^{-9}
Overnight DCE soak + Acetone rinses + DCE rinses	7	4	5×10^{-9}
15 minute hot Nitric Acid soak + distilled H ₂ O rinses + Methanol rinses + DCE rinses	40	20	27×10^{-9}
15 minute Benzene soak + DCE rinses	16	6	8×10^{-9}
Overnight DCE soak	60	12	16×10^{-9}
1/2 hr Methanol soak Methanol rinse DCE rinse	5	2	3×10^{-9}
Mesitylene rinse Methanol rinse overnight DCE soak	** 2.7	0.8 - 0.9	2×10^{-9}

* after 30 minutes

** $R_L = 10 \text{ K}\Omega$, $V = 10\text{V}$

in Figure 4.5.

The conductivity of DCE was used as a standard to check cell cleanliness before each set of runs. The criterion for including data on TCNE/DCE solutions was that the DCE standard had a conductivity less than one-tenth that of the sample. Thus the charge carriers in solution could be assumed to be largely the result of additives to the solvent (i.e. TCNE and mesitylene). The trace impurity charge carriers in highly purified dielectric solvents are difficult to identify.³

Efforts were made to keep water out of the samples. Part of the purpose of solvent and TCNE purifications was to remove water that might effect the measurements. The Pt cells were carefully sealed to prevent evaporation as well as water exposure. The contribution of water to the conductivity in TCNE/DCE solutions was initially thought to be small since the addition of a few drops of water to a 5 ml. TCNE/DCE sample had no immediate significant effect on the current. The important role of water in the conduction measurements was much better understood later when the charge carriers in our samples had been identified. (Refer to Chapter 6 for information on how little water was necessary to affect the system significantly).

4.1 - CONCENTRATION DEPENDENCE OF CONDUCTIVITY

One of the major issues to be addressed in interpreting conduction in TCNE

charge transfer solutions was the nature and generation of charge carriers in solution. The effects of both mesitylene and tetracyanoethylene on the DC currents have been considered and some results are shown in Figures 4.3, 4.4 and 4.5. Since the current response of the samples depended on a variety of variables such as voltage history, electrode preparation, electrode-sample contact time, to name a few, it was difficult to obtain reproducible conductivities at given concentrations. However, some basic trends appeared and these will be summarized.

The majority of the charge carriers in TCNE/DCE samples ($0.0002 \text{ M} < [\text{TCNE}]$) are the result of the presence of TCNE, since addition of TCNE to dichloroethane increases the measured conductivity. In Figure 4.3 the 'steady state' current is plotted vs. TCNE for three concentrations with the current measured in the following way: A single step voltage was applied to the sample and the current was assumed to be at steady state if it fluctuated by less than 15% over an extended period of time. An example of the first 5 minutes of a current response is shown in Figure 4.6. Note in Figure 4.3, that the lower the TCNE concentration is, the longer it takes for the current to reach steady state conditions. The steady state conductivity of the 0.01 M solution of TCNE is $(1.2 \pm 0.1) \times 10^{-6} \Omega^{-1} \text{m}^{-1}$. This is 2 orders of magnitude larger than the DCE conductivity of about $10^{-8} \Omega^{-1} \text{m}^{-1}$.

Figure 4.4 shows current vs. [TCNE] measurements using a different procedure. A square wave potential ($f = 0.0005 \text{ Hz}$, $T = 33 \text{ minutes}$) was applied to TCNE/DCE samples over the period of many hours. A typical

**FIGURE 4.3 - STEADY STATE CURRENT VS. [TCNE]
(SINGLE STEP APPLIED VOLTAGE)**

V = 10 Volts

The approximate time required for the current to stabilize to within $\pm 15\%$ is indicated with each data point.

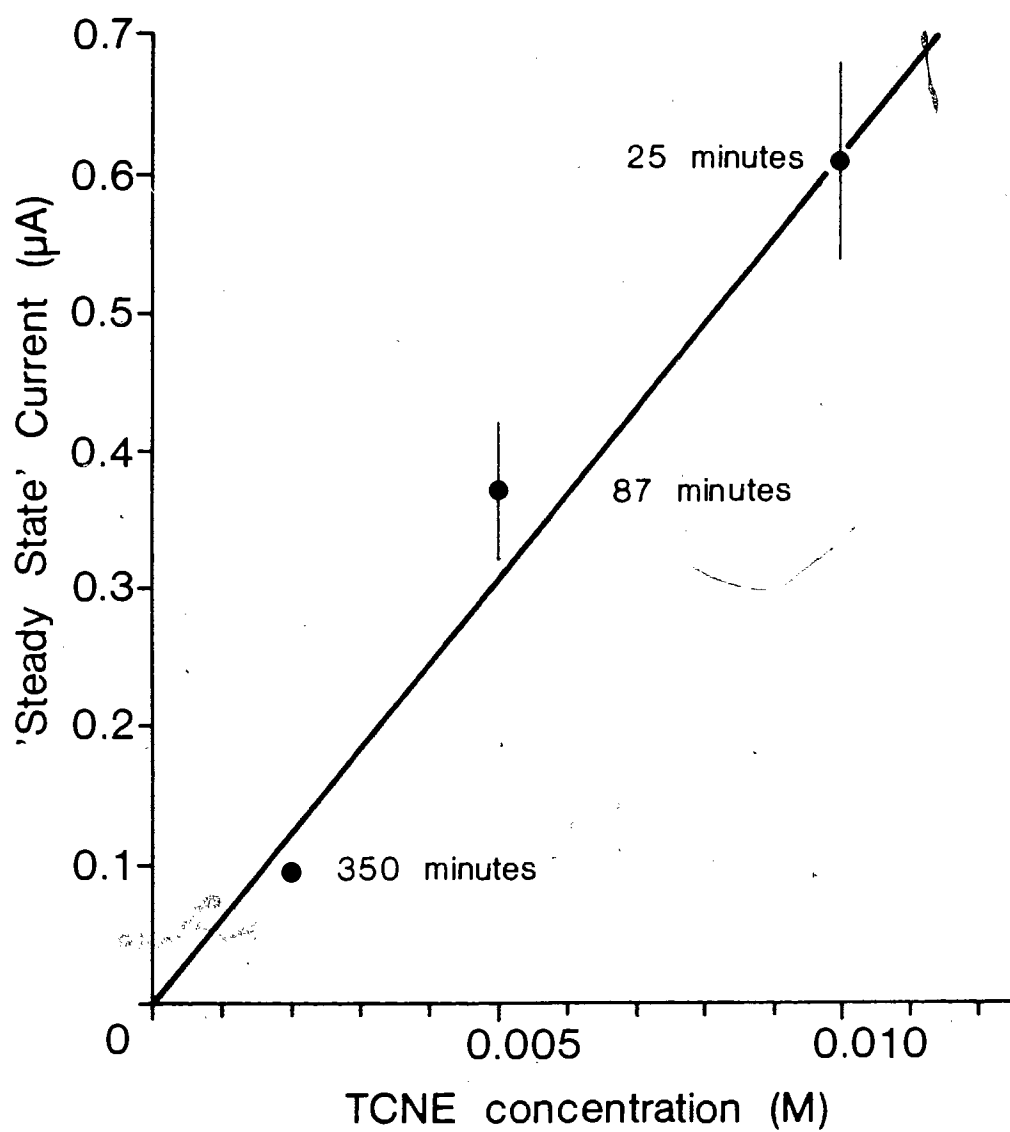


FIGURE 4.4 - PEAK AND STEADY STATE CURRENT VS. [TCNE]
(SQUARE WAVE VOLTAGE, $f=0.0005\text{Hz}$.)

$V = \pm 15.2$ Volts

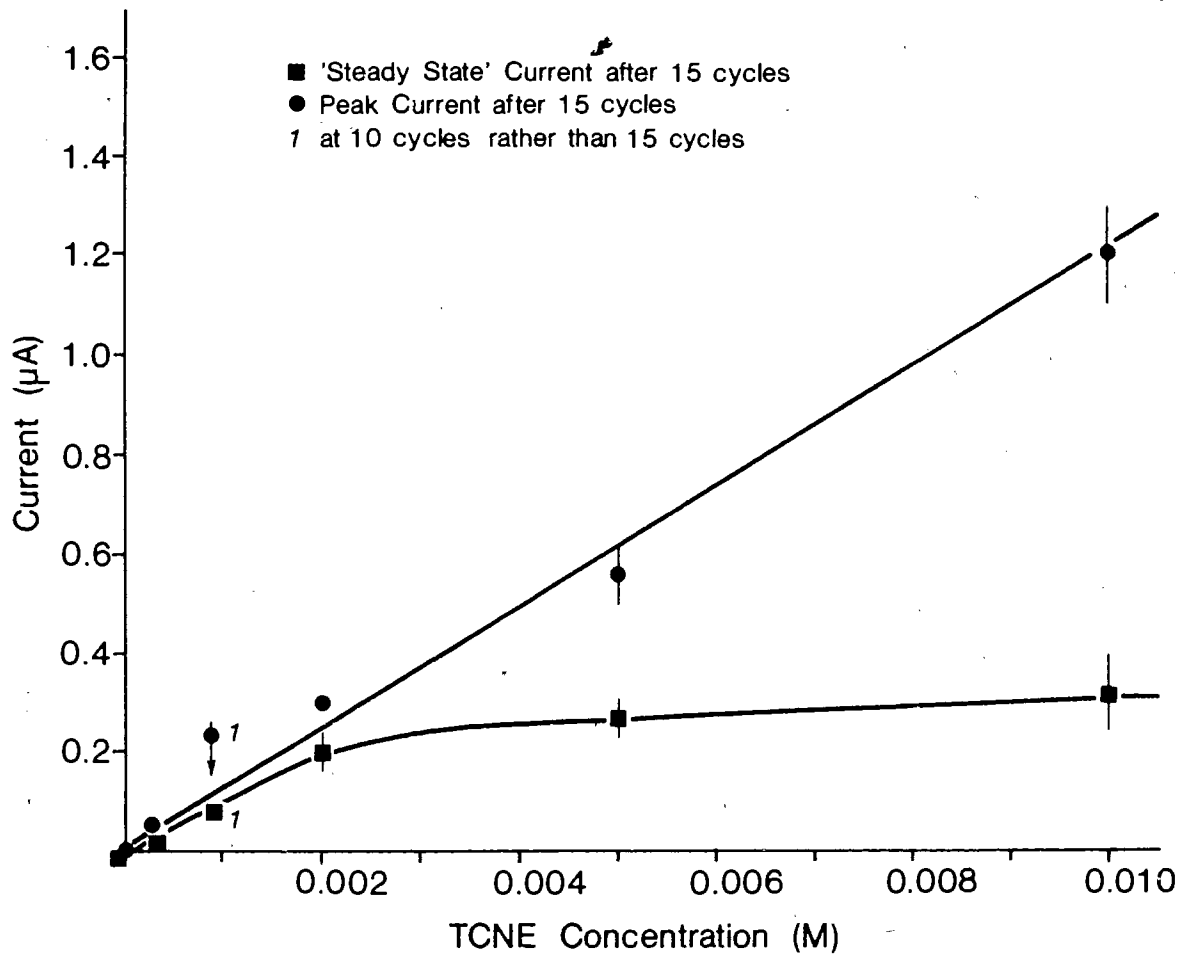
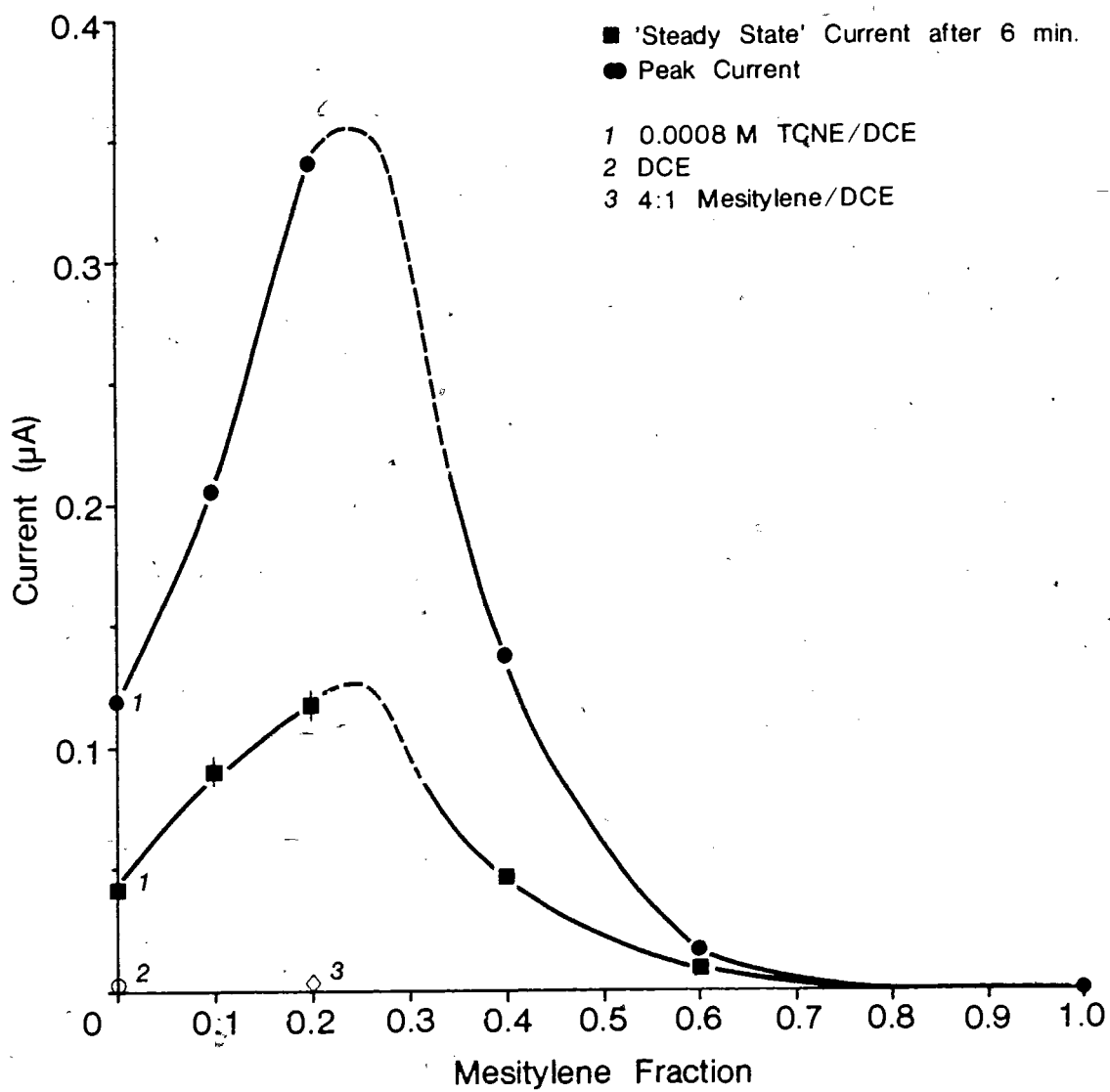


FIGURE 4.5 - CURRENT VS. MESITYLENE CONTENT

V = 10 Volts.

'steady state' currents were measured after about 6 minutes.

Sample: [TCNE] = 0.001 M. in DCE /mesitylene mixtures



current response is shown in Figure 4.7. The peak and 'steady state' currents (steady state = after 16 minutes) after each voltage reversal are plotted with respect to the number of cycles in Figure 4.8. Over consecutive cycles, the peak and 'steady state' currents decrease and level off after about 5 hours. Some other features of the square wave response over long periods of time will be discussed in Section 4.2. Values of i_{peak} and $i_{\text{steady state}}$ in the level region are plotted against TCNE concentration in Figure 4.4. An approximately linear relationship is observed between i_{peak} and [TCNE] up to 0.01M. The $i_{\text{steady state}}$ vs. [TCNE] curve levels off around concentrations of 0.005 M. The peak and steady state conductivities for a 0.01 M solution of TCNE are respectively $(1.6 \pm 0.2) \times 10^{-6} \Omega^{-1} \text{m}^{-1}$ and $(7 \pm 2) \times 10^{-7} \Omega^{-1} \text{m}^{-1}$ in this measurement. The 'steady state' conductivity measured using a one-step voltage application (Figure 4.3) lies between these values.

When these measurements were made, the major charge carriers in TCNE/DCE solutions had not yet been identified. All that could be concluded at the time was that TCNE related ions were in the solution. The dominant anion in solution was later identified as pentacyanopropenide which is a derivative of TCNE. (See Chapter 6). Cations in solution were thought to be solvent related. This was consistent with the idea that the weak charge transfer interaction between DCE and TCNE contributed to the presence of charge carriers in solution ^{4,5} (a different mechanism was later proposed for the generation of charge carriers in solution - Chapter 6)

FIGURE 4.6 - CURRENT RESPONSE TO A STEP VOLTAGE

$V = 10$ Volts

Sample: [TCNE] = 0.01 M. in DCE

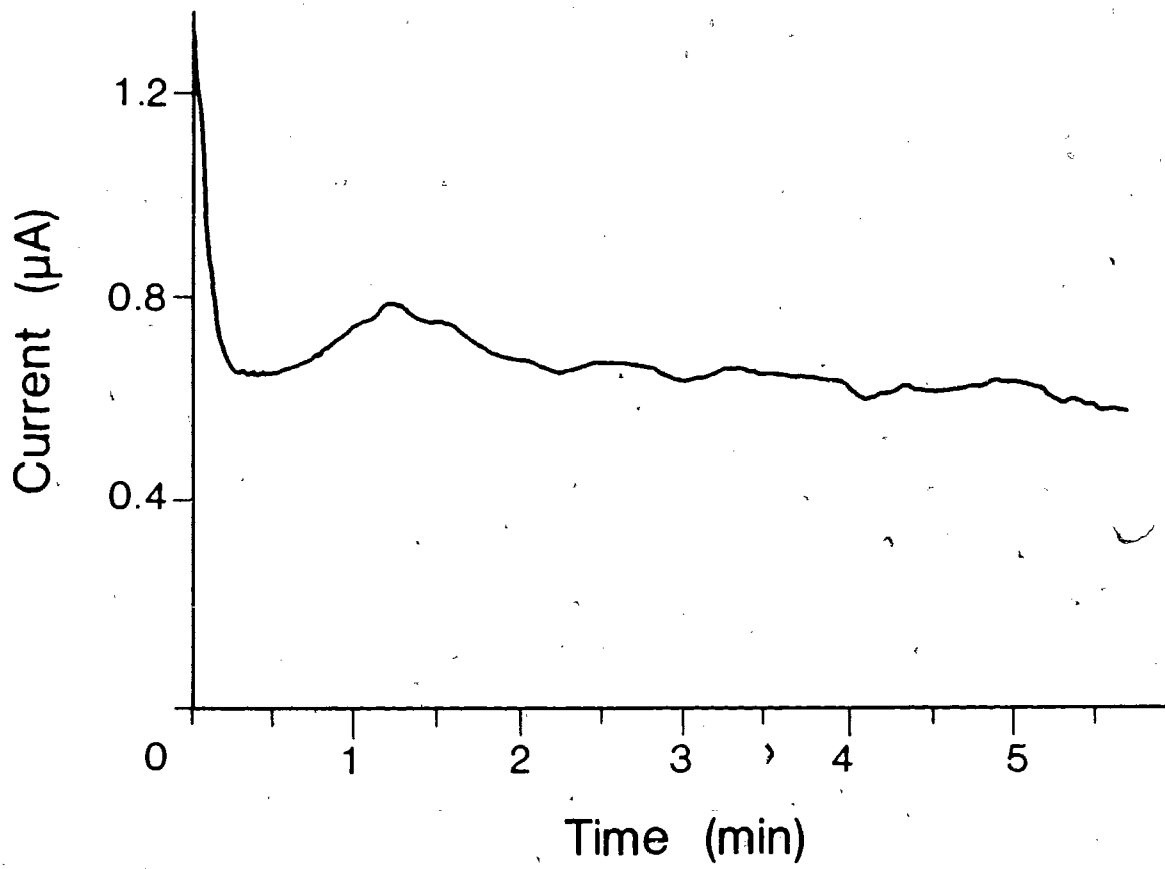
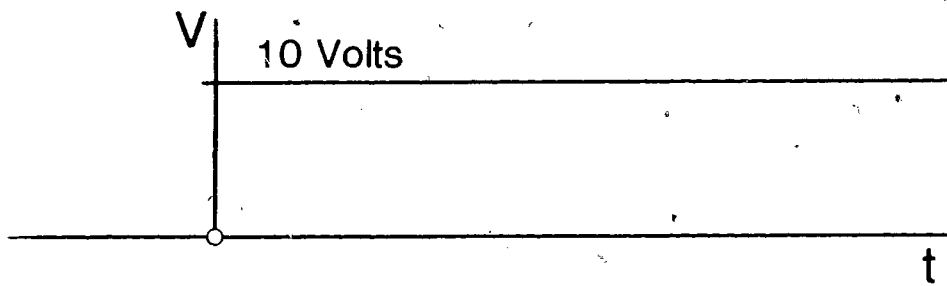


FIGURE 4.7 - SQUARE WAVE CURRENT RESPONSE $f = 0.0005 \text{ Hz.}$ $V = \pm 15 \text{ Volts}$ **Sample:** [TCNE] = 0.01 M. in DCE

The current response was measured after about 17 hours of voltage application.

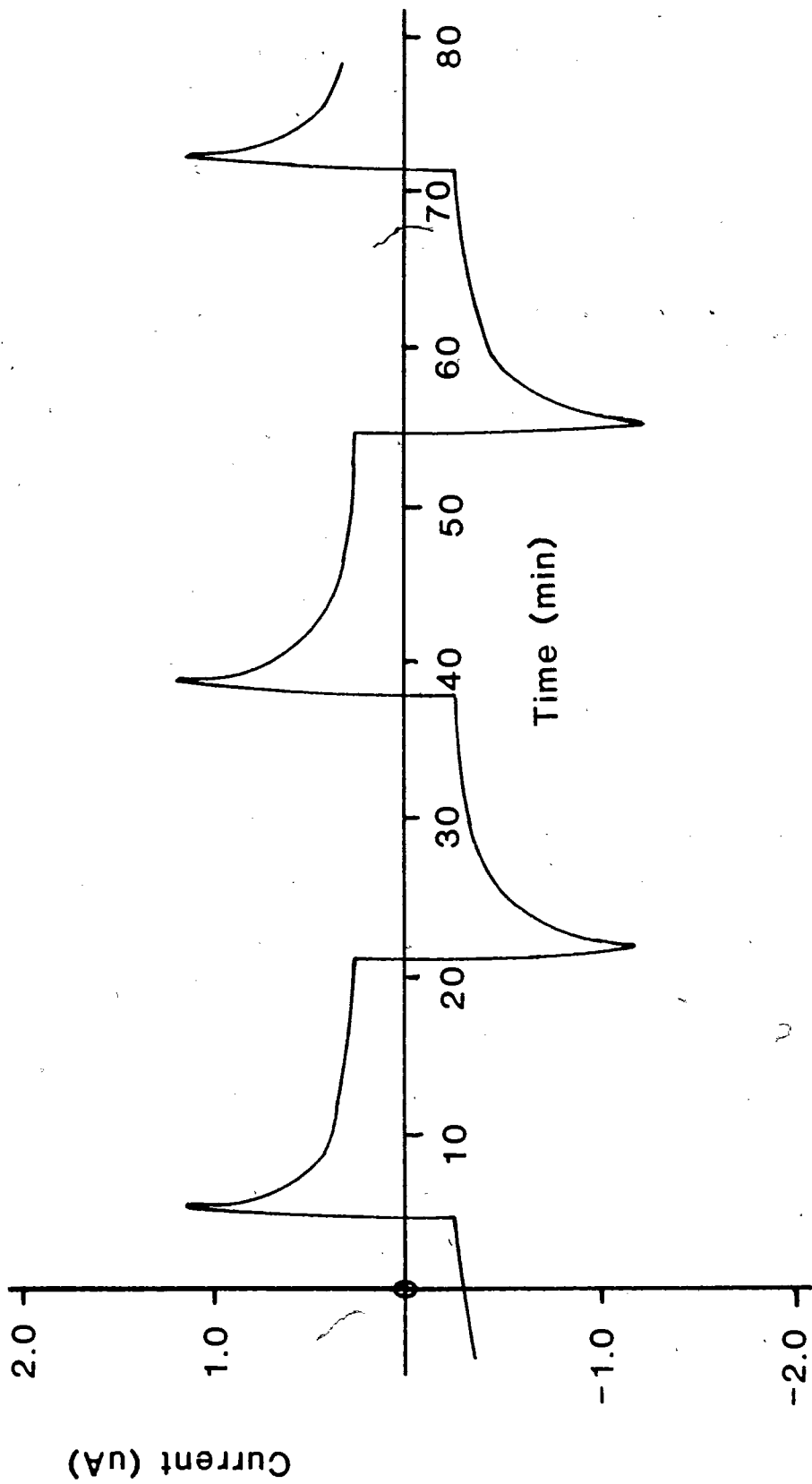
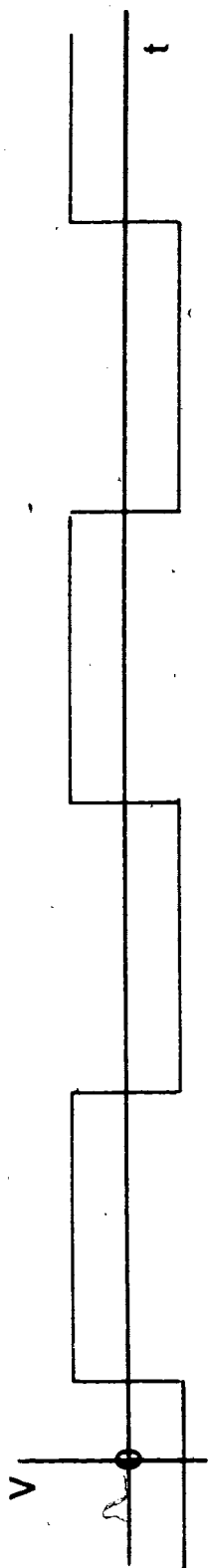
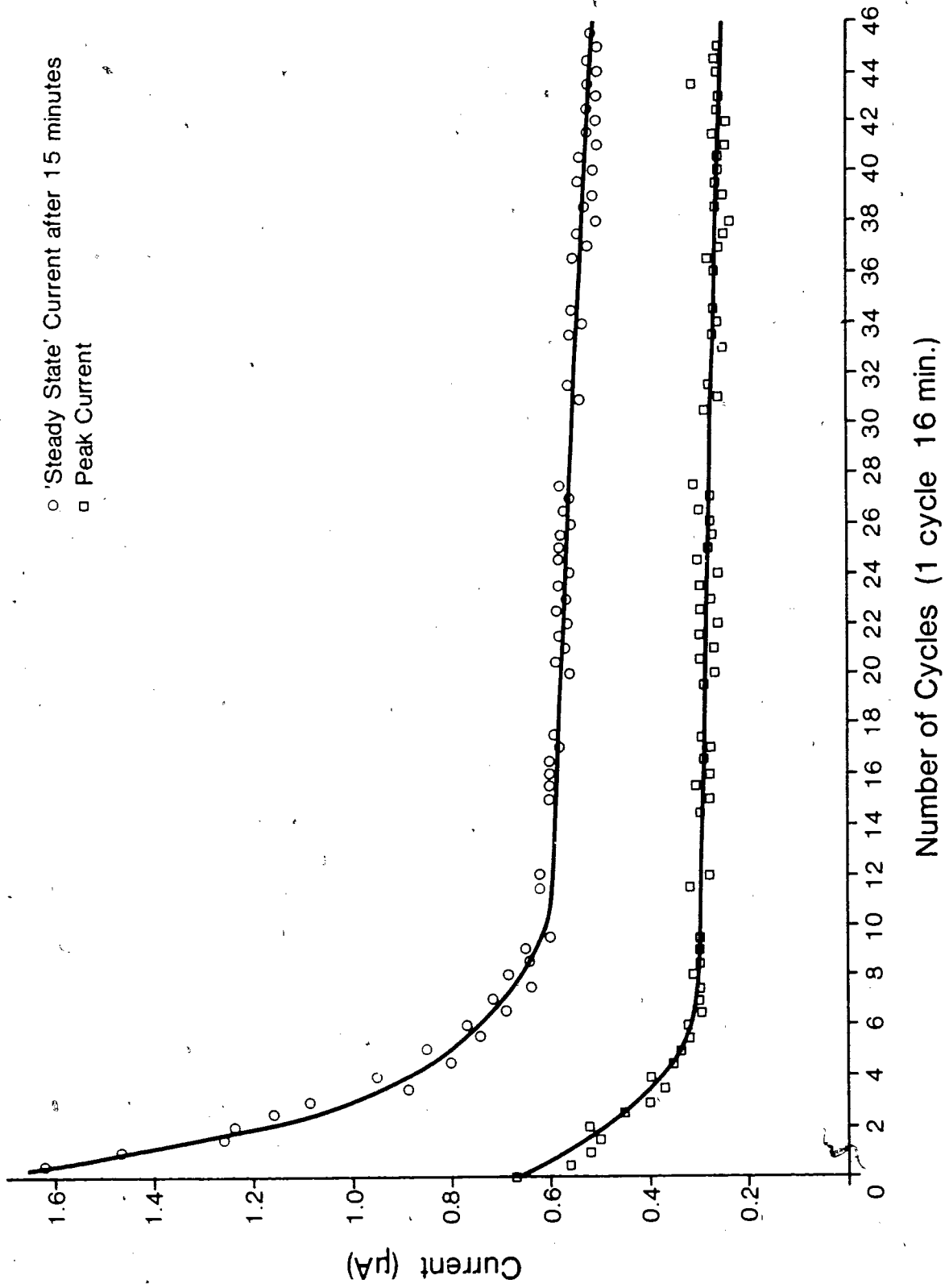


FIGURE 4.8 - PEAK AND STEADY STATE CURRENTS
VS. NUMBER OF SQUARE WAVE CYCLES

$f = 0.0005 \text{ Hz.}$

$V = \pm 15 \text{ Volts}$

Sample: [TCNE] = 0.005 M. in DCE



Number of Cycles (1 cycle 16 min.)

The addition of mesitylene to DCE does not result in a significant increase in the DC current over the DCE level. A sample with a 1.4 M concentration of mesitylene in DCE (0.2 = fraction of mesitylene in DCE) falls within the range of DCE peak conductivities measured at $(3-6) \times 10^{-9} \Omega^{-1}m^{-1}$ during a set of concurrent runs. By itself, mesitylene has a conductivity significantly less than $10^{-9} \Omega^{-1}m^{-1}$. Mesitylene, a non-polar liquid, does not stabilize free ions to the same extent as DCE.

Figure 4.5 shows how the DC current behaviour of a 0.001 M TCNE solution is influenced by the addition of mesitylene. The peak and 'steady state' currents (after about 6 minutes) are plotted as a function of the fraction of mesitylene in solution. For mesitylene/DCE fractions from 0 - 0.2 the current increases with the amount of mesitylene added. Beyond mesitylene fractions of 0.3 the current decreases with the fraction of mesitylene. The observed decrease in current at higher donor concentrations can be accounted for in terms of lowering the effective dielectric constant of the solution. The lower the dielectric constant, the less stable free ions are in solution⁶. In the lower mesitylene concentration range, the increase in solution conductivity with added mesitylene is probably the result of charge transfer interactions between TCNE and the donor molecules. Donor/acceptor complexes are known to dissociate spontaneously in liquids of sufficiently high dielectric constant⁷.

The nature of charge carriers in mesitylene/TCNE/dichloroethane samples

was not investigated in detail. The dominance of the TCNE related charge carriers for charge transfer solutions used in the earlier photosignal measurements ([TCNE] \approx 0.005M, [mesitylene] \approx .025M or 0.0035 volume fraction of mesitylene) became the reason for studying TCNE/DCE samples rather than the more complex mixture involving the donor molecules as well. The intention was to get a handle on the basic conduction processes in a simple, two component system before extending the work to a three component system.

4.2 - CURRENT/TIME RESPONSE:

ELECTRICAL BOUNDARY LAYERS and RESISTIVITY CHANGES

The measurements made in this section used the apparatus shown in Figure 4.2 and the methods described at the beginning of this chapter. The basic current response of TCNE/DCE to a square wave voltage is shown in Figure 3.9. With the initial application of voltage, an immediate decrease is observed in the current which eventually approaches a 'steady state' value. Following reverse biasing of the cell, the current peak is displaced in time and again the current falls to a 'steady state' value. The discussion of the current response will revolve around three main considerations: [1] electrical boundary layer or space charge effects [2] the resistivity or conductivity of the bulk of the solution [3] the effect of mixing or convection.

The type of current response shown in Figure 3.9 is quite typical of liquids with very low charge carrier concentrations or weak electrolyte solutions. Compare Figures 4.7 and 4.9 with the square wave current response for samples of Aerosol OT (a surfactant) in xylene studied by Novotny and Hopper⁸ (Figure 4.10). Aerosol OT weakly dissociates in xylene. In contrast, TCNE would not be expected to dissociate in DCE. However, low concentrations of pentacyanopropene, which is a strongly dissociating cyanocarbon acid, were later found to be a major source of charge carriers in our samples (See Chapter 6). Thus, the TCNE/DCE current behaviour observed is consistent with that of weak electrolytes.

FIGURE 4.9 - CURRENT VS. TIME FOLLOWING VOLTAGE REVERSAL**Sample:** [TCNE] = 0.01 M. in DCEFor $V = 10$ Volts, peak area $\approx 6 \times 10^{-5}C$

71b

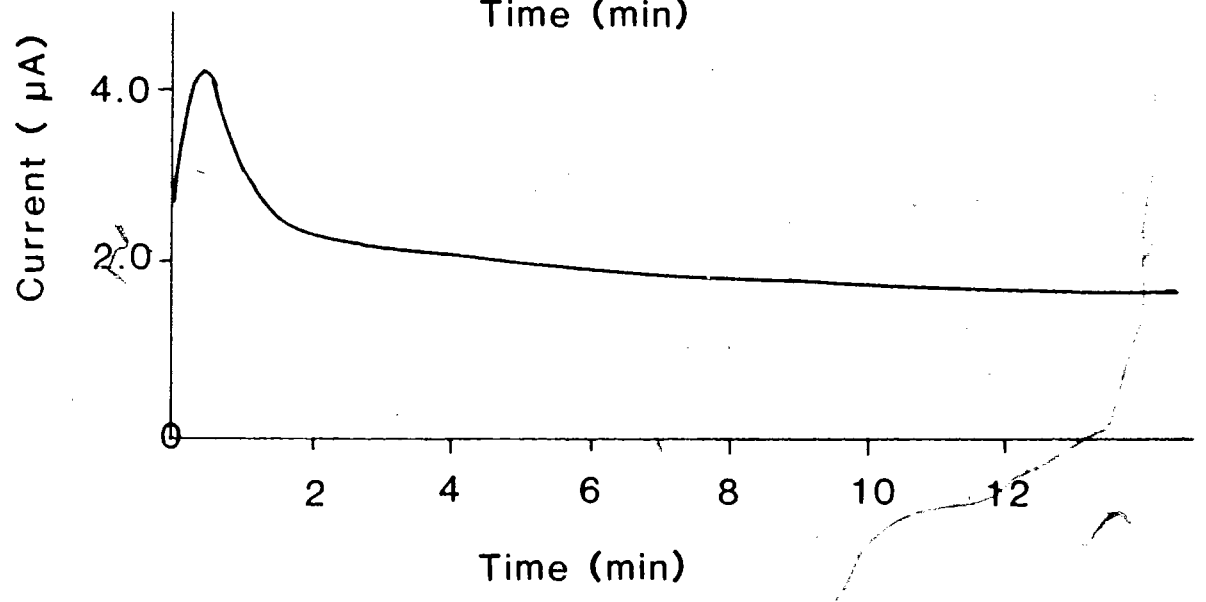
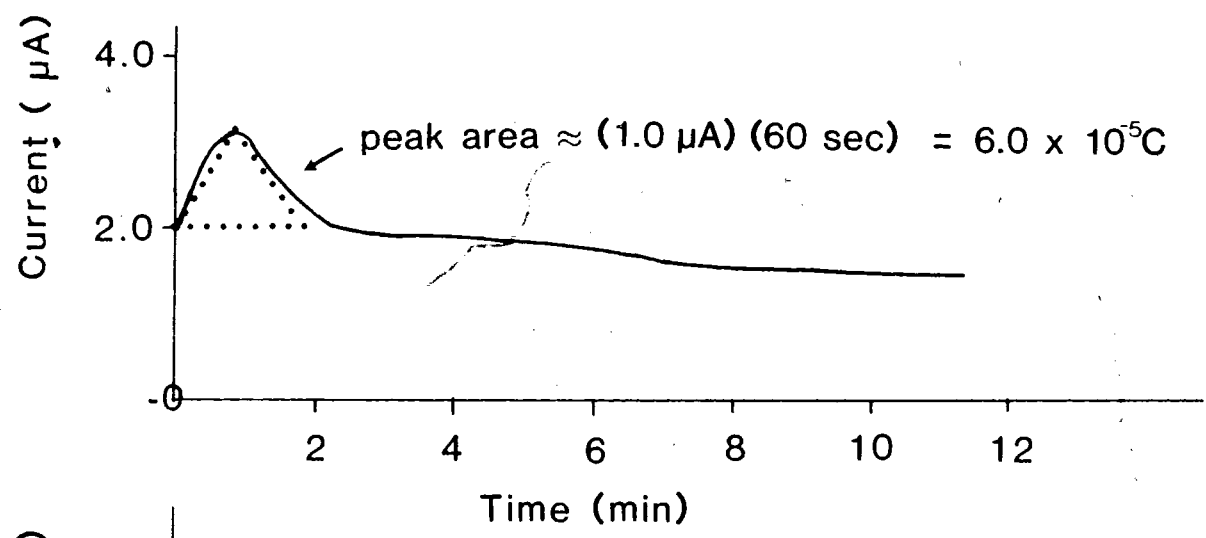
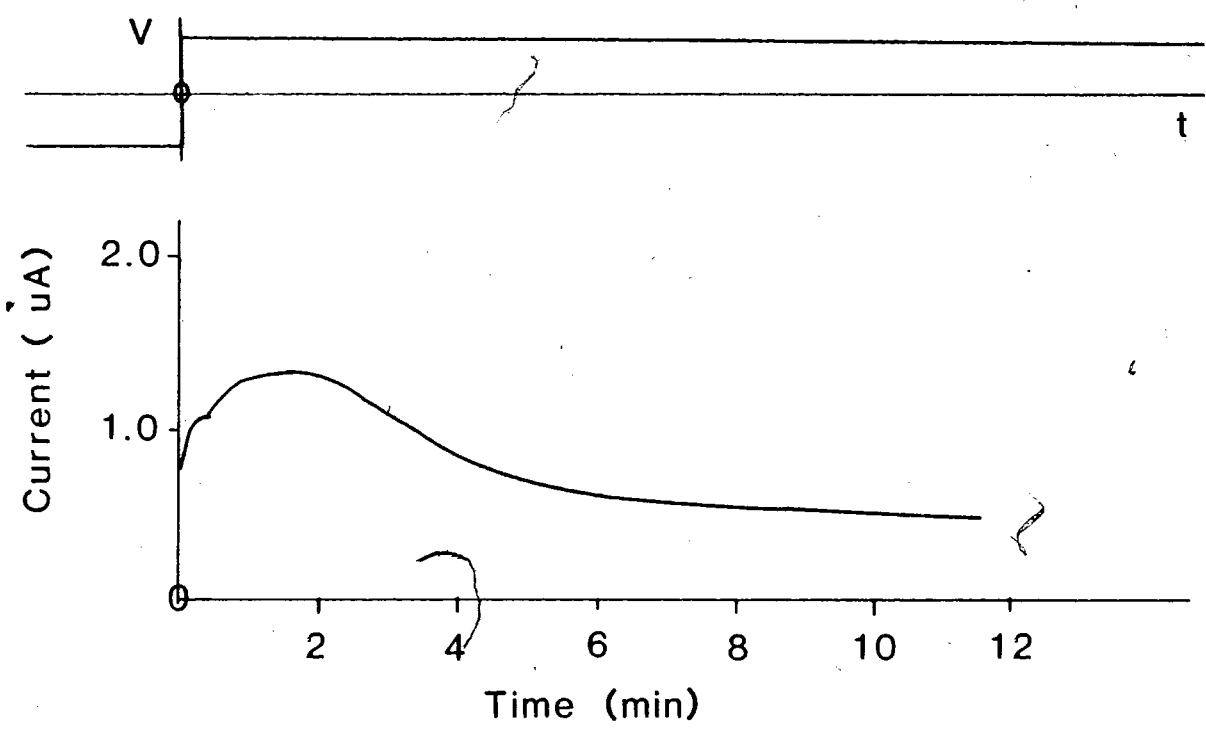
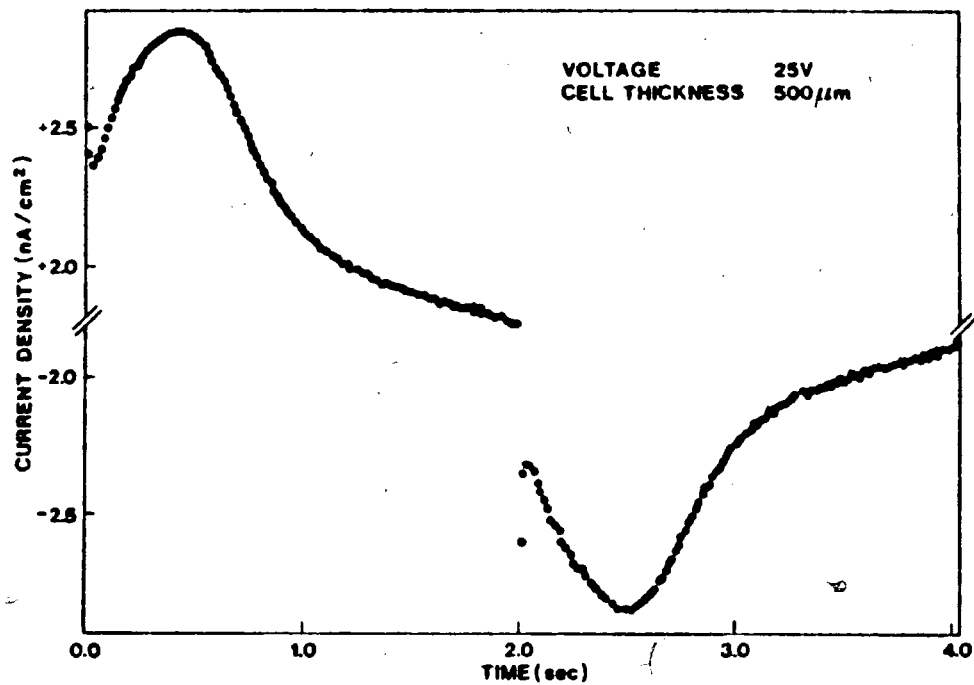
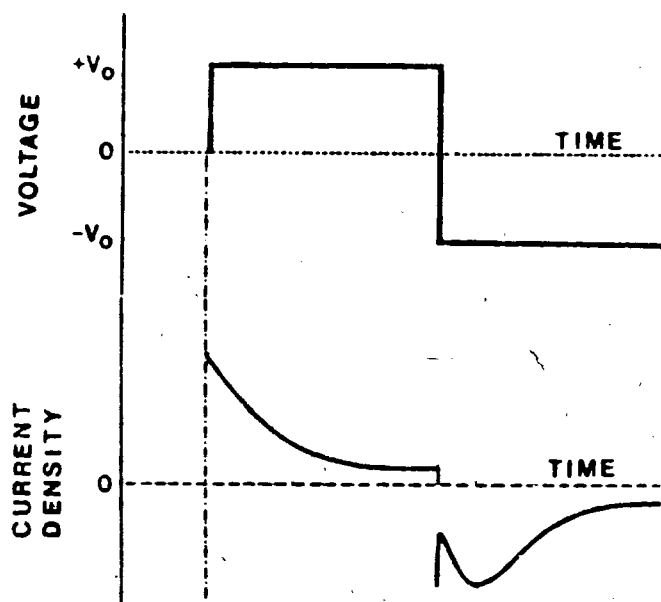


FIGURE 4.10 - CURRENT RESPONSE FOR AOT/XYLENE⁸



Typical current transient observed with square wave voltage excitation. The AOT concentration was 10^{-3}M .



Transient current behavior for first turn-on and field reversal waveforms.

Qualitatively, certain features of the current response in time can be discussed in terms of space charge at the electrodes (space charge layers = electrical boundary layers). Some characteristics of the current-voltage dependence (described in Section 4.4) can also be accounted for using boundary layers. Gibbings et. al.^{9, 10} have provided a description of electrical boundary layers in low conductivity liquids which will be summarized here. Prior to the application of voltage, electrical boundary layers (or double layers) exist at the metal-solution interface because of a chemical potential difference¹¹ (Figure 4.11, sketch 1 and 2). The sign of the space charge in solution depends on the electrode material, solvent and impurities present (which all effect the chemical potentials in the system). As a first approximation, it is assumed that the thickness of the electrical boundary layers is much less than the electrode spacing.

The application of a voltage (V) across a liquid causes negative space charge to collect at the anode and positive space charge to collect at the cathode (Figure 4.11, sketch 3 and 4). The space charge in the electrical boundary layers will be proportional to the applied potential¹⁰ ($Q \approx V$). The time required for the formation of the electrical boundary layer influences the current characteristics. Sketches of the net ion concentrations at both electrodes and the electrical potential profiles are shown with and without applied voltage in Figure 4.11.

In Figure 4.12, the potential across each of the electrical boundary layers

FIGURE 4.11 - ELECTRICAL BOUNDARY LAYERS ¹⁰

ϕ = electric potential

G = chemical potential

$+$ = positive space charge

$-$ = negative space charge

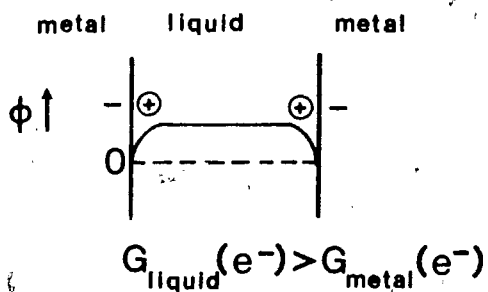
c = ion concentration

ρ = space charge density

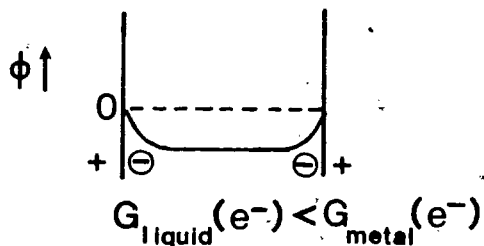
$\partial^2 \phi / \partial x^2$ is proportional to $-\rho$

ϕ vs. x

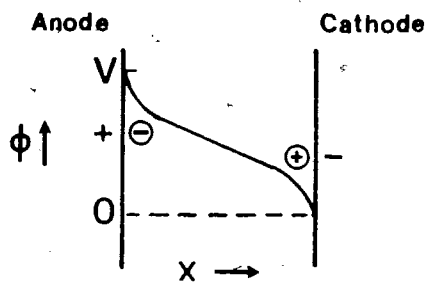
1. $V = 0$



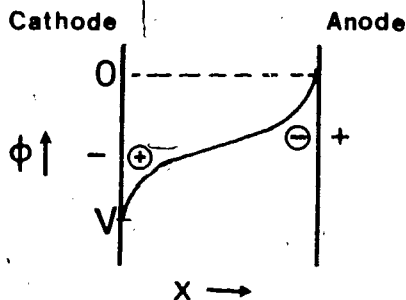
2. $V = 0$



3. forward bias



4. reverse bias



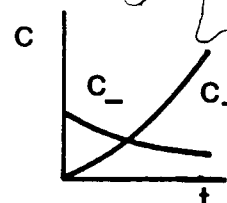
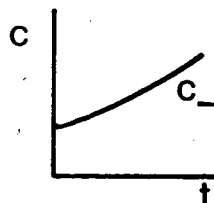
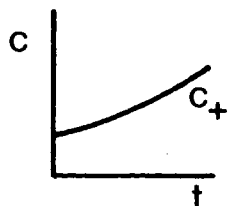
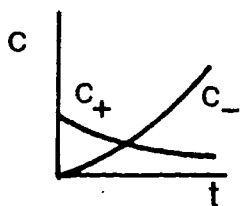
c vs. t

Anode

Cathode

Anode

Cathode

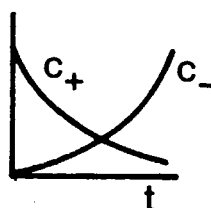
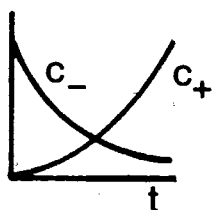


$t = 0 : 1$

$t = 0 : 2$

$t > 0$: forward bias 3

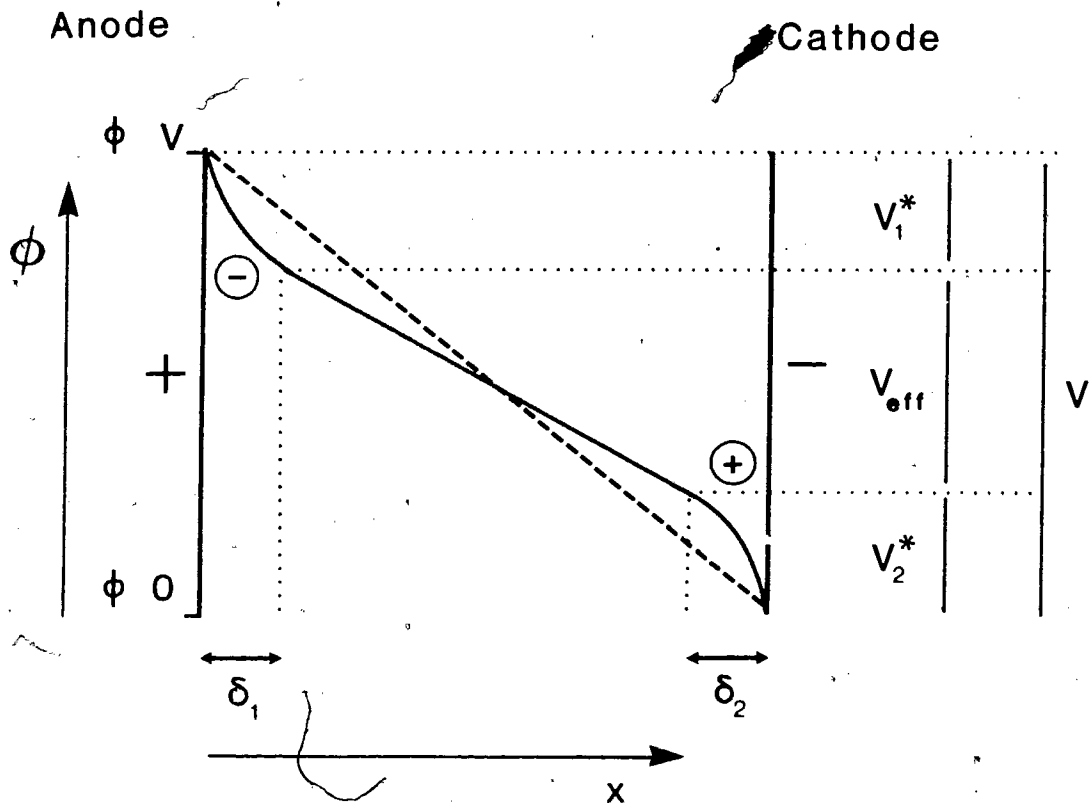
$t > 0$: forward bias 3



$t = 0 : 3$

$t > 0$: reverse bias 4

**FIGURE 4.12 - ELECTRICAL BOUNDARY LAYERS
AND ASSOCIATED POTENTIALS**



$$V = V_{\text{eff}} + V_1^* + V_2^*$$

V = applied voltage

V_{eff} = effective voltage across bulk of solution

V_1^*, V_2^* = electrical boundary layer potentials

δ_1, δ_2 = thickness of electrical boundary layers

\oplus = positive space charge

\ominus = negative space charge

(V_1^* and V_2^*) is sketched. The limiting value of the boundary potentials (as time \rightarrow infinity) depends on the applied voltage. The current through a weak electrolyte depends on the effective voltage (V_{eff}) across the bulk of the sample and the resistance of the sample. Since the sum of V_{eff} , V_1^* , and V_2^* must give the applied voltage V (Figure 4.10), the measured current can be written as shown below:

$$i = V_{\text{eff}}/R = (V - V_1^* - V_2^*)/R$$

The variation of current with time after an initial voltage application is accounted for qualitatively in terms of the growth of electrical boundary layers. As the charged layer at each electrode grows to some voltage-dependent limiting value, the effective voltage across the bulk of the solution decreases and so does the current.

Any time dependence of the resistance of the bulk of the solution can be incorporated into the equation.

$$V_{\text{eff}} = [V - V_1^*(t) - V_2^*(t)] / R(t)$$

$R(t)$, the effective resistance of the solution, depends on the ionic concentration between the electrodes.

$$R = d/(KA) = d/((\sum \Delta_i c_i)A)$$

where

d = distance across solution (m)

K = conductivity ($\Omega^{-1}m^{-1}$) = $\sum \Delta_i c_i$

Δ_i = equivalent conductance of the i^{th} ion ($\Omega^{-1}m^{-1}M^{-1}$)

c_i = concentration of the i^{th} ion in solution (M)

Returning to the interpretation of the current response after the initial voltage application, the resistance of the bulk of the sample can be expected to decrease as ions are dragged toward respective electrodes. This was verified with spectroscopic studies of the ion concentration in solution (Chapter 5). The decrease in conductivity, and accompanying increase of resistivity, would work together with boundary layer effects to decrease the current with time.

At long enough times after voltage application, and for sufficiently large space charge densities at the electrodes, convection establishes itself and reduces the magnitude of the electrical boundary layers. Whenever a net space charge is present in solutions, an unbalanced force (F) exists per unit volume of liquid and can generate sufficient pressure gradients for fluid flow to occur¹².

$F = \rho E$ where ρ = space charge density

E = electric field

$$P = \int_0^d (\rho E) dx \quad \text{where } P = \text{pressure generated from 0 to } d$$

In Gibbings work on kerosene ¹⁰, the onset of convection is marked by the current response levelling out. In the following discussion, it will be assumed that during the initial current vs. time response, convection has not yet had time to establish itself. However, if convection is established at steady state conditions, the current response immediately following voltage reversal will be affected by fluid flow because of its finite decay time. These assumptions were confirmed through spectroscopic work (Ch.5). Convective effects will be discussed in more detail in Section 4.4 and Chapter 5.

After voltage reversal, the temporal behaviour of the current response is difficult to account for in terms of space charge effects. The time displacement of the current peak appears to be related to ion transit times. The transit time for ions moving from one electrode to another in solution decreases as a function of the applied voltage. Experiment shows a definite correlation between the peak time displacement and voltage: the peak time is inversely proportional to the applied voltage in the range up to 15 volts (Table 4.2, Figure 4.9).

Since the current peak can be related to the drift velocity of ions moving through a constant distance, it is reasonable to propose that the time required for current carriers to travel from the electrodes to a point

TABLE 4.2

VOLTAGE DEPENDENCE OF CURRENT PEAK TIME

SAMPLE: 0.01M TCNE in DCE

VOLTAGE	PEAK TIME (t_p)	$V \cdot t_p$
15 V	30 ± 5 s	450 ± 75 Vs
10 V	49 ± 4 s	490 ± 40 Vs
5 V	90 ± 20 s	450 ± 100 Vs

half-way across the cell corresponds to the current peak time. Under these conditions the number of charge carriers in the bulk of the liquid would be a maximum. According to this model the expected travel time and current peak time (t_p) is given by

$$t_p = d/2v = d/2\mu E = d^2/2\mu V$$

where

d = distance between electrodes

$v = \mu E$ = effective* drift velocity of charge carriers

μ = effective* mobility of charge carriers

E = electric field in solution $\approx V/d$ **

V = applied voltage

* Both anions and cations would contribute to the effective drift velocity and mobility given in this expression. This mobility could include the effects of convection.

**the electric field in solution could not be assumed constant when there were ion concentration gradients present (Chapter 5).

Note: One could equally well propose that the charge carriers have to travel the full distance d to give a current pulse. This would only change the calculation by a factor of two.

If the relationship between the current peak time and voltage is correct as shown above, then the product of the two (Vt_p) should be a constant. The data in Table 4.2 show that this is indeed the case and the product, Vt_p , is a constant within the experimental uncertainty (This does not hold for square wave frequencies greater than $1/2t_p$. The peak displacement time decreases with increasing frequency. Figure 4.13 shows the current response to a square wave with $f > 1/2t_p$ for a thin Indium (In) electrode cell described in Section 4.4). From the measured value of 450 V s. for Vt_p , and the known electrode separation of 2 mm., an effective mobility of $0.4 \times 10^{-8} \text{ m}^2 \text{ V}^{-1} \text{ s}^{-1}$ is estimated. This mobility is in a range typical for charge carriers in polar organic liquids. The positive charge carriers in nitrobenzene have a mobility¹³ of $(1.6 - 2.3) \times 10^{-8} \text{ m}^2 \text{ V}^{-1} \text{ s}^{-1}$.

The amount of charge associated with the current peak after voltage reversal is about $6 \times 10^{-5} \text{ C}$. (Figure 4.9, $V = 10 \text{ Volts}$). The existence of a current pulse can be accounted for qualitatively in terms of electrical boundary layer charge migrating across the sample. However, an estimate of the amount of space charge associated with boundary layers shows that this interpretation is not reasonable. The amount of space charge associated with the boundary layers in solution could have been no larger than the metal electrode surface charge necessary to produce the applied voltage. For 10 volts applied across parallel metal plates and a dielectric liquid

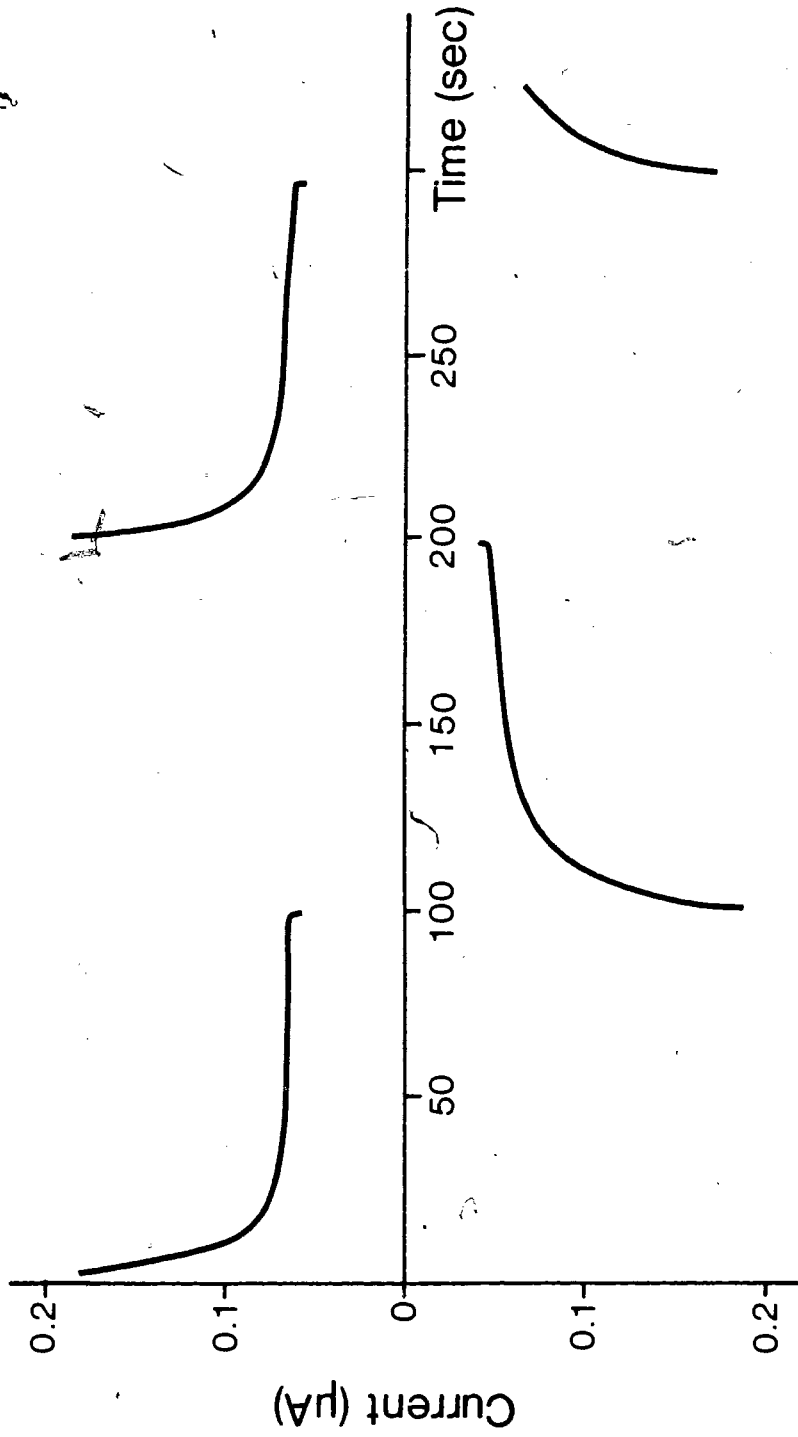
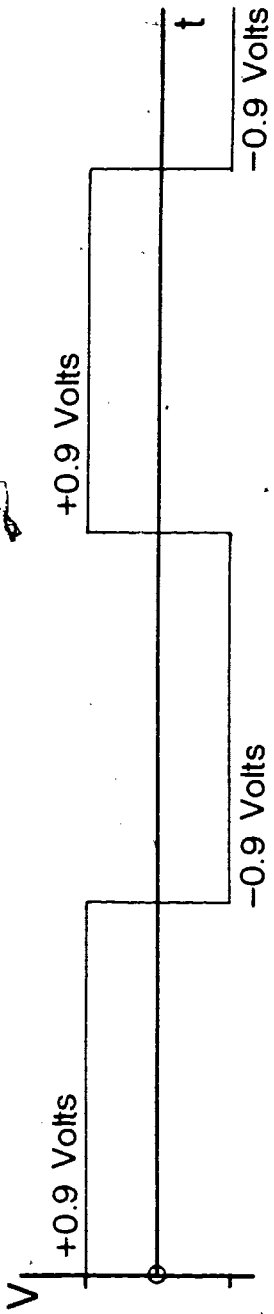


FIGURE 4.13 - CURRENT VS. TIME
(SQUARE WAVE VOLTAGE, $f = 0.005$ Hz.)

$V = 0.9$ Volts

$1/2f <$ transit time

Sample: [TCNE] = 0.01 M. in DCE



$$Q = \frac{\epsilon \epsilon_0 A V}{d} = \frac{10 (8.85 \times 10^{-12} \text{ CV}^{-1} \text{ m}^{-1}) (1 \times 10^{-4} \text{ m}^2) (10 \text{ V})}{(2 \times 10^{-2} \text{ m})}$$

$$= 4.4 \times 10^{-11} \text{ C}$$

where A = electrode area

d = electrode separation

ϵ_0 = 10 = dielectric constant for DCE

ϵ = permittivity of a vacuum

The charge associated with the current peak ($6 \times 10^{-5} \text{ C}$) is much too large to be accounted for only on the basis of a space charge originating in the boundary layers.

The displaced current peak in time also cannot be accounted for by considering the variation of V_{eff} in time. Immediately after voltage reversal

V_{eff} is a maximum given by

$$V_{\text{eff}} = V_{\text{app}} + (V_1^* + V_2^*)$$

where $(V_1^* + V_2^*)$ is the voltage developed across the boundary layers prior to the voltage reversal. The effective voltage decreases in time following voltage reversal.

The reversal of voltage may increase the conductivity of the solution by releasing ions into the solution (and this was later verified). The

concentration of ions associated with the current flux can be estimated given the speed of charge transport ($v = d/2t_p = 1 \times 10^{-3} \text{ m}/45 \text{ s} = 2.2 \times 10^{-5} \text{ m/s}$) and the current density (j) of about $2 \mu\text{A}/\text{cm}^2$.

$$j = 2ecv$$

$$c = j/2ev$$

$$= (2.0 \times 10^{-2} \text{ A/m}^2) / (2(1.6 \times 10^{-19} \text{ C/molecule})(2.2 \times 10^{-5} \text{ m/s}))$$

$$= 2.8 \times 10^{21} \text{ molecules/m}^3$$

This can be converted to a concentration of $4.7 \times 10^{-6} \text{ M}$, which is consistent with the concentration range later verified for anions in the system by spectroscopic studies (Chapter 5).

The width of current peaks after voltage reversal seems to indicate that diffusion processes contribute to charge transport. The width of the peak increases as a function of the travel time (Figure 4.9). Diffusion effects would not have been expected to be very significant in a system with convection as a contributing charge transport process. The Nernst-Planck equations describe mass transfer in solutions and include drift, diffusion, and convection terms. In one dimensional form:

$$j_i = \mu_i E(x) c_i(x) - D_i \frac{\partial c_i(x)}{\partial x} + c_i(x) v(x)$$

where j_i = current flux from the i^{th} ion ($\text{C}/(\text{m}^2\text{s})$)

μ_i = mobility of i^{th} ion ($\text{m}^2\text{V}^{-1}\text{s}^{-1}$) = $(z_i F/RT)D_i$

D_i = diffusion coefficient of i^{th} ion (m^2s^{-1})

c_i = concentration of i^{th} ion (mol/m^3).

E = electric field (Vm^{-1}) = $\partial V/\partial x$

v = liquid velocity (ms^{-1})

x = position relative to anode (m)

The width of a current peak was about equal to the transit time ($2t_p = 90$ seconds at $V=10$ Volts, Figure 4.9). A rough estimate of the time required for particles to diffuse through a mean distance of two millimeters (distance between electrodes) is given by the following equation: ¹⁴

$$x^2 = 2Dt$$

$$t = x^2 / (2D)$$

Calculating a value for the diffusion constant from the effective mobility of $0.4 \times 10^{-8} \text{ m}^2 \text{ V}^{-1} \text{ s}^{-1}$ gives $D = 1 \times 10^{-10} \text{ m}^2 \text{ s}^{-1}$. Using this in the preceding equation results in an average time of 330 minutes (5.5 hours) for ions to diffuse across 2 mm. Even for an order of magnitude calculation, this doesn't compare well with peak width times. Obviously, the contribution of diffusion to the shape of the current peak had to be reconsidered.

The importance of ion concentration gradients in the bulk of the solution is evidenced by the effect of mixing on sample current characteristics.

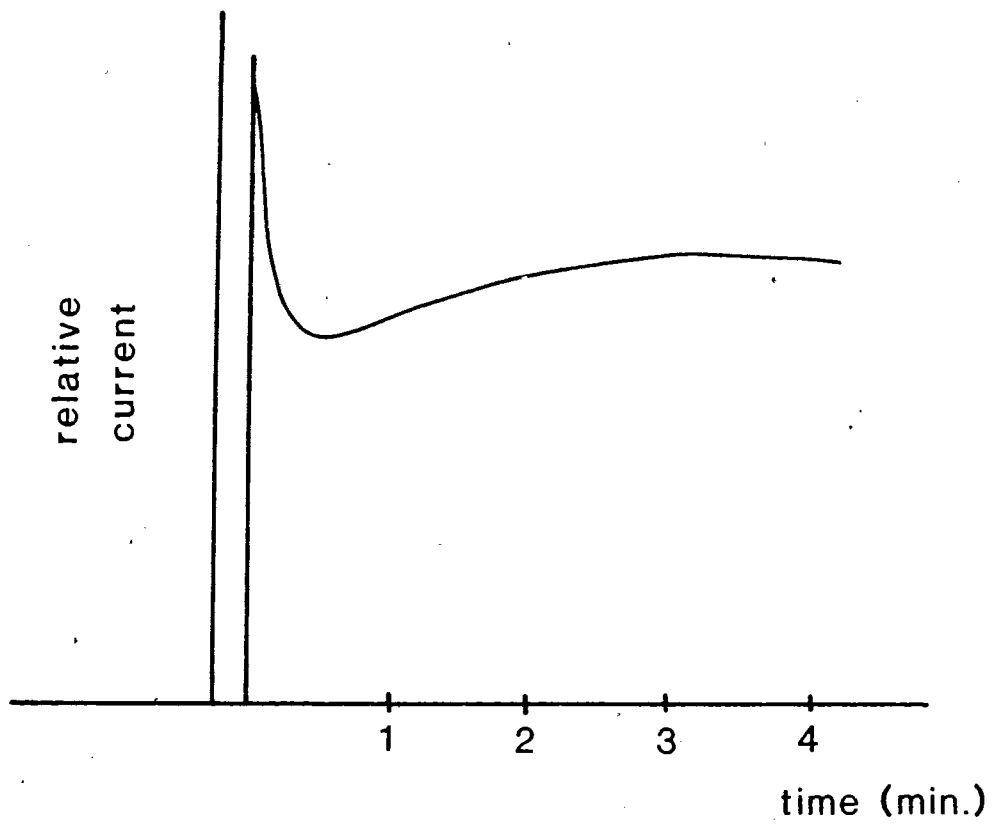
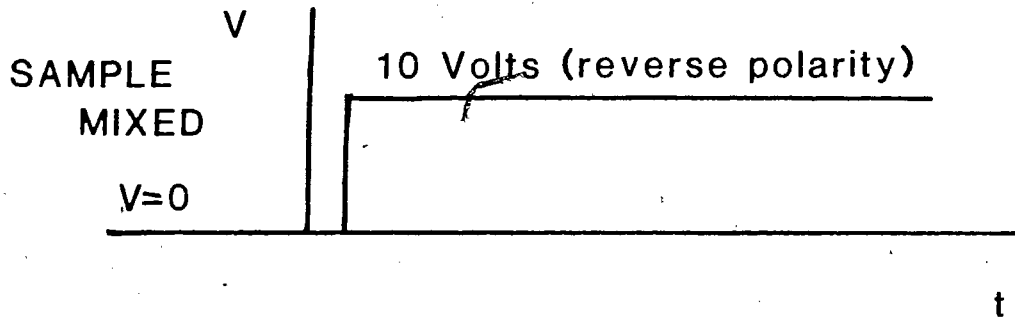
However, no quantitative estimates of $\partial c/\partial x$ could be obtained from these measurements. After a sample had been previously exposed to voltage the current peak was displaced in time with voltage reversal. If, after voltage exposure, the sample was physically mixed (using a pipette) before flipping the voltage again, then the current peak was no longer observed to be displaced in time (Figure 4.14). The immediate peaking of the current with a step in voltage is similar to that observed for samples without previous voltage exposure (Figure 3.9).

Mixing destroys any ion concentration gradients in the bulk of the solution as well as reduces the electrical boundary layer charge. The effect of mixing the sample after voltage application essentially restores the cell to conditions like those before voltage was ever applied. This accounts for the immediate peaking of the current for the sample mixed after voltage application.

As a result of these initial studies on the current-time response of TCNE/DCE solutions it was clear that bulk ion concentrations and space charge significantly affected the current characteristics and would have to be incorporated into a model for conduction in the system. However, the behaviour of ion concentrations in space and time, and the relationship of this with the change in current with time, could not be unravelled with the experimental techniques employed. Further information on the behaviour of ion concentrations in solution as a function of position and time had to be obtained. A spectroscopic study of ion concentration behaviour is presented

**FIGURE 4.14 - CURRENT RESPONSE TO VOLTAGE REVERSAL
AFTER MIXING**

Sample: [TCNE] = 0.002 M. in DCE



in Chapter 5 and provides the basis of the interpretation of conduction of TCNE/DCE solutions.

4.2.1-CURRENT RESPONSE TO SQUARE WAVE VOLTAGE OVER MANY CYCLES

Application of a square wave voltage ($f = 0.0005$ Hz.) to the TCNE/DCE samples results in a decrease in the peak and steady state currents over many cycles (Figure 4.8). After about 8 hours the peak and steady state currents approach a limiting value. This behaviour was already referred to in Section 4.8. One explanation for the overall decrease in conductivity is that some ions, or other charge carrying particles, are irreversibly dragged out of the solution during voltage exposure over long periods of time. This effect is sometimes referred to as electrical purification¹⁵ or electrostatic cleaning. Another possibility for the overall current decrease is the continual growth of electrical boundary layers. This is not unreasonable because of a small asymmetry in the positive and negative cycle times of the square wave (a 4% difference in positive and negative cycle times for $f = 0.0005$ Hz.).

4.3 -TEMPERATURE and MECHANICAL VIBRATION

The effects of temperature and mechanical vibration on conduction in TCNE/DCE samples are considered in this section. The temperature dependence was studied by placing a carefully sealed sample in a circulating water bath. In thermal equilibrium the solution is homogeneous throughout

the cell, in contrast to local heating by a focussed laser beam. Table 4.3 shows that the steady state current increases with increasing temperature. As temperature increases, the viscosity of a fluid, and also the resistance to charge motion, usually decreases. A corresponding increase in the current is expected. Isotropic heating of a sample does not interfere with convection patterns (unless a change in liquid viscosity brings about a convective transition).

The effect of continuous mechanical vibration was observed by measuring the sample current with and without water circulation around the cell (without temperature change, of course). Water circulation is a simple way of providing fairly uniform vibration. The presence of external mechanical vibration decreases the current magnitude (Current without vibration = 0.36-0.49 μA .; Current with vibration = 0.28-0.39 μA ; [TCNE] = 0.004 M, $V = 10$ Volts, $R_L = 10\text{k}\Omega$). This behaviour is consistent with the previously observed decrease in current as a result of acoustic noise and localized illumination.

The change in conductivity with mechanical vibration can be qualitatively interpreted in two ways: [1] vibration interrupts convection patterns important to mass and charge transport by introducing cross-field liquid motion; [2] vibration disturbs electrical boundary layers and ion concentration gradients in the solution. The second option seems less likely since the disturbance of charged layers would decrease V_1^* and V_2^* and

TABLE 4.3

TEMPERATURE DEPENDENCE OF CONDUCTIVITY

SAMPLE: 0.04M TCNE in DCE $V = 10V$ $R_L = 10 K\Omega$

TEMPERATURE ($T \pm 0.25^\circ\text{C}$)	CURRENT (μA)
26.0	0.26 - 0.34
30.8	0.31 - 0.35
35.3	0.35 - 0.39
40.5	0.41 - 0.47

result in an increase in the current. Any disturbance of ion concentration gradients would also not be expected to decrease the sample current.

Convective effects on sample current response will be discussed further in Section 4.4.

4.4 - CURRENT VOLTAGE CHARACTERISTICS

Several experimental approaches were used to characterize the current-voltage response of TCNE/DCE and TCNE/mesitylene/DCE samples. The various approaches and sample responses will be discussed in this section. As in Section 4.2 some aspects of the i - V response can be interpreted in terms of changes in electrical boundary layers and bulk sample resistivity. The most interesting conclusions arrived at in these studies are related to electrohydrodynamic effects. Certain types of current behaviour are indicative of transitions in liquid flow such as those that had been previously observed in the Indigo Blue/DCE system (Chapter 3). 'Critical' voltage conditions for transitions in the convective behaviour of dielectric liquids have been reported in the literature ^{16, 17, 18}.

Electrohydrodynamic and conduction studies have already been carried out on systems with a variety of charge generation mechanisms. Unipolar and bipolar injection of charge have been extensively considered in the literature ^{19, 20, 21}. Electrohydrodynamic studies on weak electrolyte solutions are rare and apparently the instabilities in such systems are not well understood at present ¹⁸. Since the current response of TCNE/DCE solutions resembles that of weak electrolyte solutions, very little of the published work on electroconvection is applicable. Further difficulties regarding electrode injection and discharge processes arise which are specific to TCNE/DCE solutions.

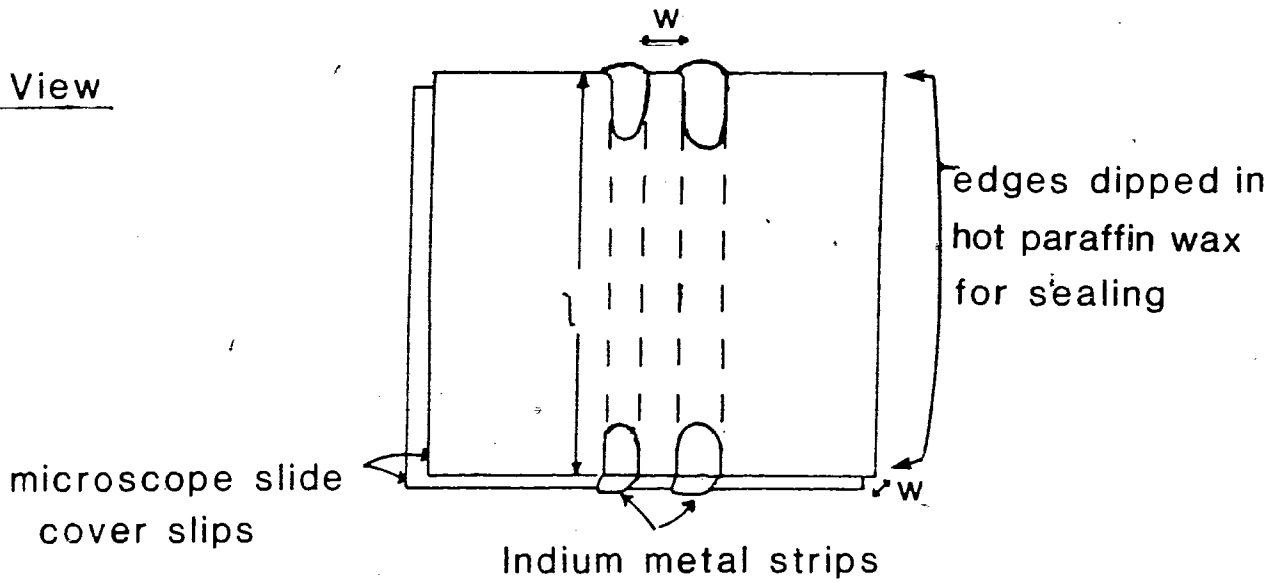
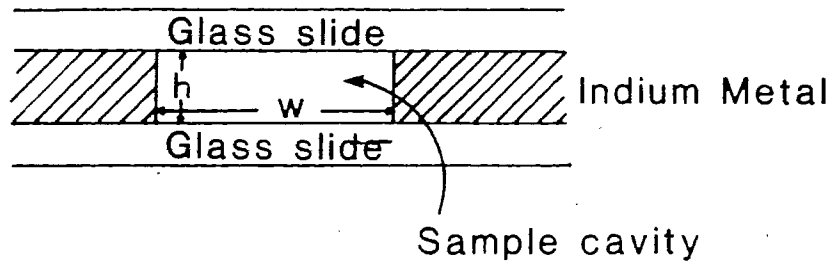
The interpretation of critical voltage behaviour in the TCNE/DCE systems in this study demonstrates a fundamental difficulty in the separation of convective effects and electrode injection/discharge processes (electrochemistry). The appearance of flow instabilities in dielectric liquids is critically dependent on the electrode boundary conditions²². The same would be expected to be true of the TCNE/DCE system. The experimental work described concerns different electrode geometries and materials. Instead of leading to a single interpretation of the current characteristics, the discussion presents several different interpretations that are all qualitatively consistent with the observations.

4.4.0 - EXPERIMENTAL

The types of measurements discussed in this section all involve the variation of current response with voltage. Current measurements were carried out using the method described at the beginning of this chapter. A Houston Omnigraphic 2000 X-Y recorder was used to record continuous i - V scans. Cell discharge currents after voltage application were monitored using the lower circuit in Figure 4.2.

Two types of electrode materials were used in the measurements: indium (In) and platinum (Pt). The Pt cell has already been described in Section 4.1. A thin cell construction was developed using In metal and is shown in Figure 4.15.

FIGURE 4.15 - THIN INDIUM CELLS

Top ViewSide View

Typical cell dimensions :

$$w = 1-2 \text{ mm.}$$

$$h = 0.1-0.2 \text{ mm.}$$

$$l = 30 \text{ mm.}$$

Typically, the electrode spacing in the thin In cell construction was 1mm. and the electrode areas were 30mm. x 0.1mm (Figure 4.15). Two In strips were sandwiched side by side between microscope slide cover slips. This In/glass arrangement was carefully heated on a hot plate to wet both glass surfaces with In metal. Once the cell was allowed to cool, the In/glass interfaces formed a good seal. The hollow between the electrodes could be filled with liquid samples by capillary action. A quick dip in hot paraffin wax was used to seal the cell at each end. The lifetime of the cells was from one to two days depending on the seal preparation and handling procedure. Other thin cell designs were tested and found to be inferior. The advantages of the thin In cell system include the simple, variable closed geometry and the disposability of the cells.

This thin, closed cell construction was chosen because the closed cell design eliminated any free liquid/air interfaces which could affect convection via surface instabilities²³, and the convective flow was substantially limited to one degree of freedom. Also, particle flow in the Indigo Blue/DCE analogue system could be clearly observed with the use of a microscope but it was difficult to correlate the current and particle behaviour in detail. Current peaks were qualitatively associated with particle transit times, and above about 5 volts convective patterns were observed. Generally, the stability of the i - V and i - t curves was improved over the Pt cells with their larger geometry. Initially, the stability improvement was associated with fewer available degrees of freedom for convective flow. Later results indicated that the improved stability could

also have been related to the electrode material being used.

RESULTS AND DISCUSSION

The current responses with stepwise and continuous changes in voltage will be discussed in terms of electrical boundary layer and ion concentration effects. Certain current voltage behaviour can also be interpreted in terms of convective transitions.

4.4.1 - IV RESPONSE (VOLTAGE STEPS)

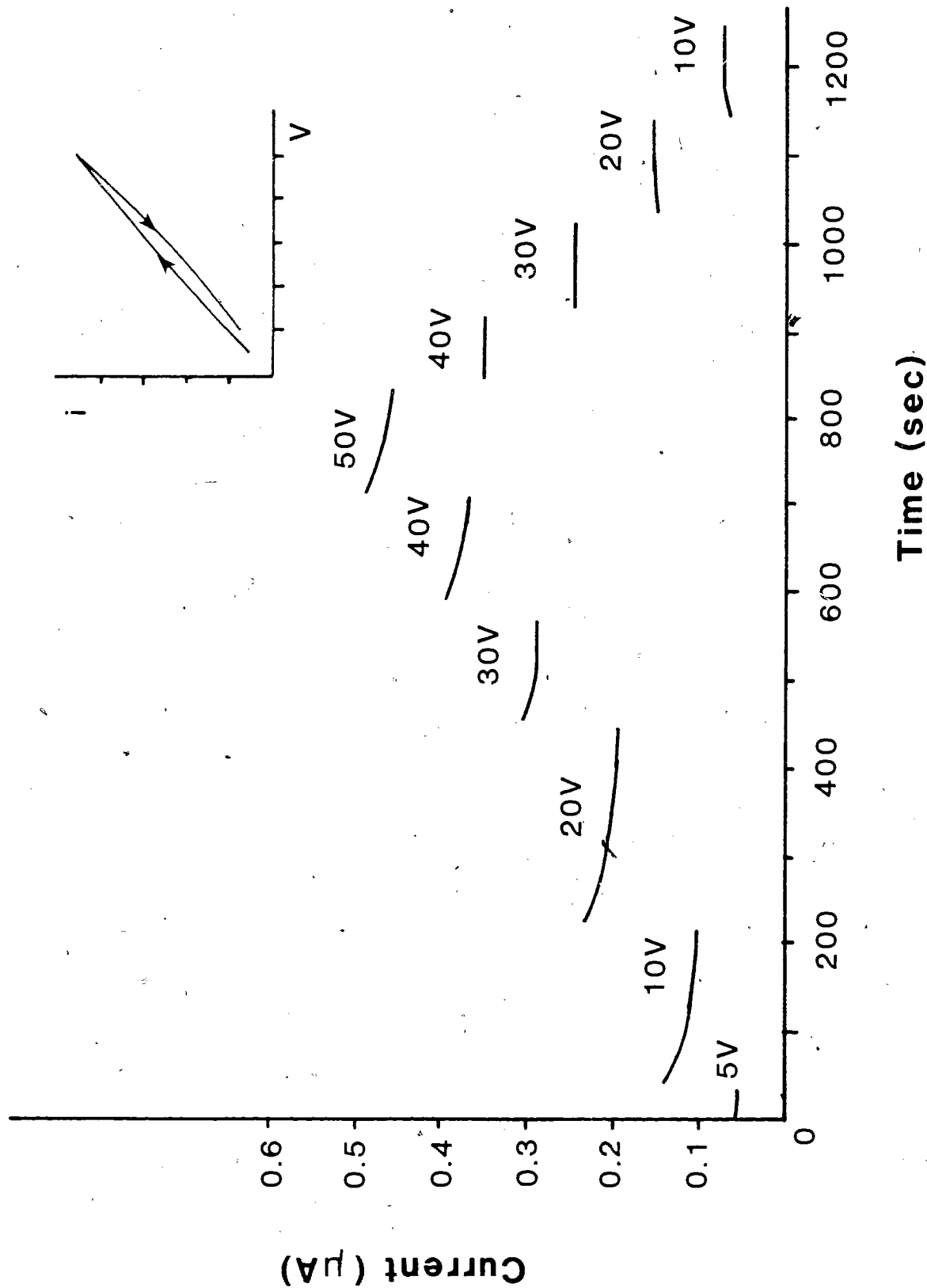
In Figure 4.16, the variation of current with voltage steps is shown. A thin In cell was used in this measurement. After each voltage step increase, the current slowly decreases in time to approach a 'steady state' value. Following each 10 volt decrease in voltage, the current approaches a new 'steady state value' immediately, or after a very slight increase in the current. The new 'steady state' current after a step-down in voltage is lower than that observed at the same voltage in the preceding voltage step-up sequence. As a result, the plot of i_{ss} vs. V shown in the corner of Figure 4.16 displays hysteresis. A similar sort of hysteresis (higher currents with increasing voltage rather than decreasing voltage) is observed for the i - V plots shown in Figures 4.20 to 4.23 for the slower voltage scan rates.

FIGURE 4.16 - CURRENT VS. TIME FOR VOLTAGE STEPS

Sample: [TCNE] = 0.01 M in DCE

indium electrodes

$w \approx 1\text{mm}$ $h \approx 0.1\text{mm}$.



Qualitatively, the hysteresis of the current response can be accounted for by discussing electrical boundary layer effects in the system. As in Section 4.2, the sample current can be expressed in terms of the applied voltage (V), the electrical boundary layer potentials (V_1^* and V_2^*), and the sample resistance (R).

$$i = V_{\text{eff}} / R = (V - V_1^* - V_2^*) / R$$

The potentials, V_1^* , V_2^* , and the associated charge layers at each electrode are an increasing function of the applied voltage. With each step-up in voltage, the electrical boundary layers grow in time and result in a current decrease. With each step-down in voltage, less space charge is supported at the electrodes and so a current increase results in time as the space charge diminishes.

As in Section 4.2, the change in bulk solution resistivity with time must also be considered ($i = V_{\text{eff}}(t) / R(t)$). Each voltage increase pulls more ions out of the bulk of solution, thereby increasing the resistivity. A voltage decrease releases the ions back into the solution. This sort of ion concentration effect was later observed, and the rate of ion release from the electrodes was much slower than the rate of ion depletion in the bulk of the liquid (Section 5.1.5). A combination of space charge effects and resistivity changes account qualitatively for the observed current behaviour with voltage steps.

The importance of space charge effects is demonstrated equally well by their apparent absence in the linear plot of current vs. voltage in Figure 4.17. In this example a Pt electrode cell is discharged between current measurements at different voltages. The peak currents (immediately following voltage application) are plotted vs. voltage. After approaching a steady state current, the cell is discharged by shorting out the two electrodes for about 4 minutes. Samples of the discharge current response are shown in Figure 4.18. Based on the linearity of the resulting i_{peak} vs. V plot, shorting out the cell was thought to have the effect of eliminating most of the space charge associated with the electrodes.

Initially, we hoped to gain information on the magnitude of the space charge at the electrodes by measuring the discharge current as a function of time. In Figure 4.19, the number of coulombs discharged through a Pt cell is plotted as a function of the previously applied voltage (electrode area = 1 cm^2). The 150 second discharge appears to level out around 50 to 60 microcoulombs at $V \geq 4.0$ volts, even though the peak current with applied voltage increases linearly with V (Figure 4.17). A charge of only 1.8×10^{-11} C/cm² would be required to generate 4 volts across 2mm of liquid with a dielectric constant of 10 (based on $Q = \epsilon \epsilon_0 \cdot AV/d$). This sets a limit for the amount of space charge stored in the electrical boundary layer, since any greater charge density associated with the solution interface would cancel the applied field. Since the number of coulombs discharged through the cell

FIGURE 4.17 - PEAK CURRENT (after discharge) VS. VOLTAGE

Sample: [TCNE] = 0.01 M. in DCE

platinum electrodes

d = 2mm

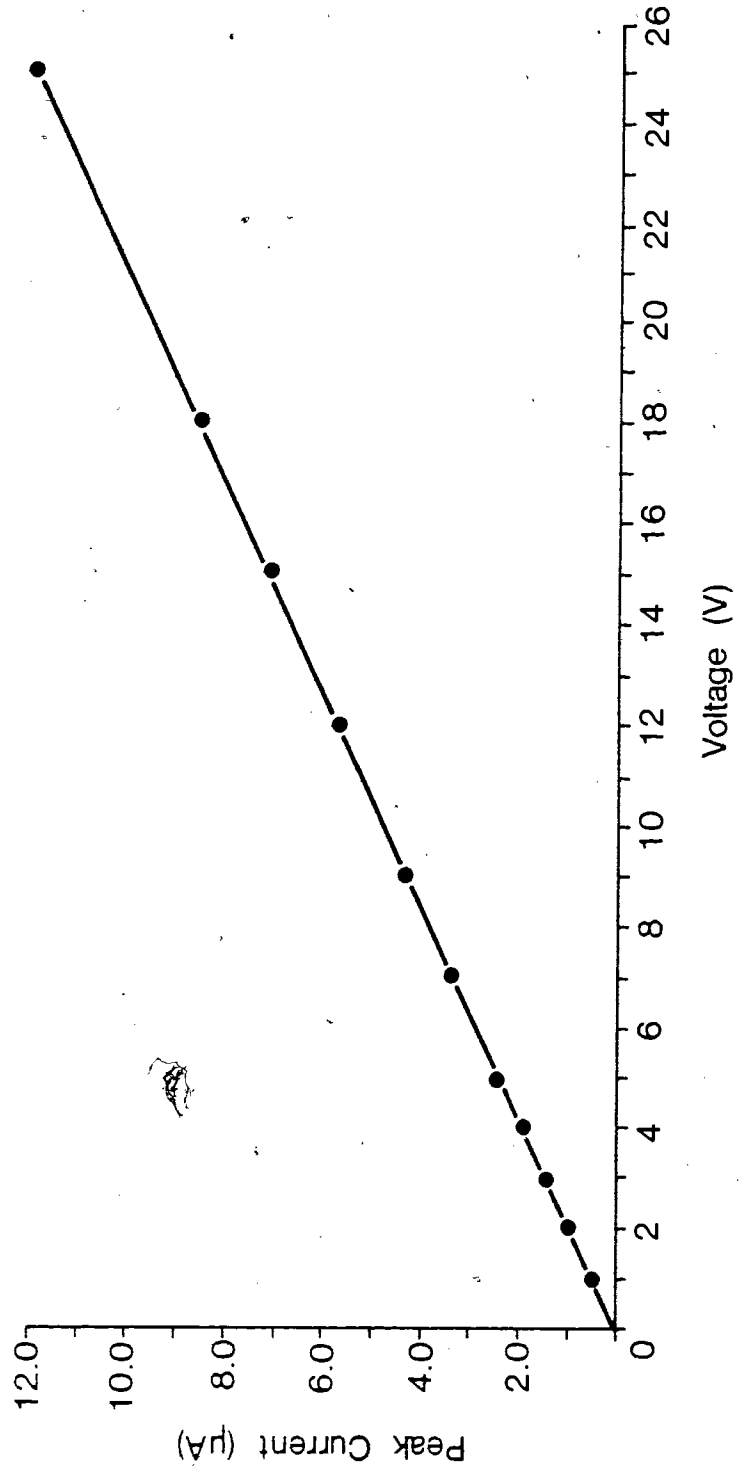


FIGURE 4.18 - DISCHARGE CURRENT VS. TIME

Sample: [TCNE] = 0.01 M. in DCE

platinum electrodes

d = 2mm

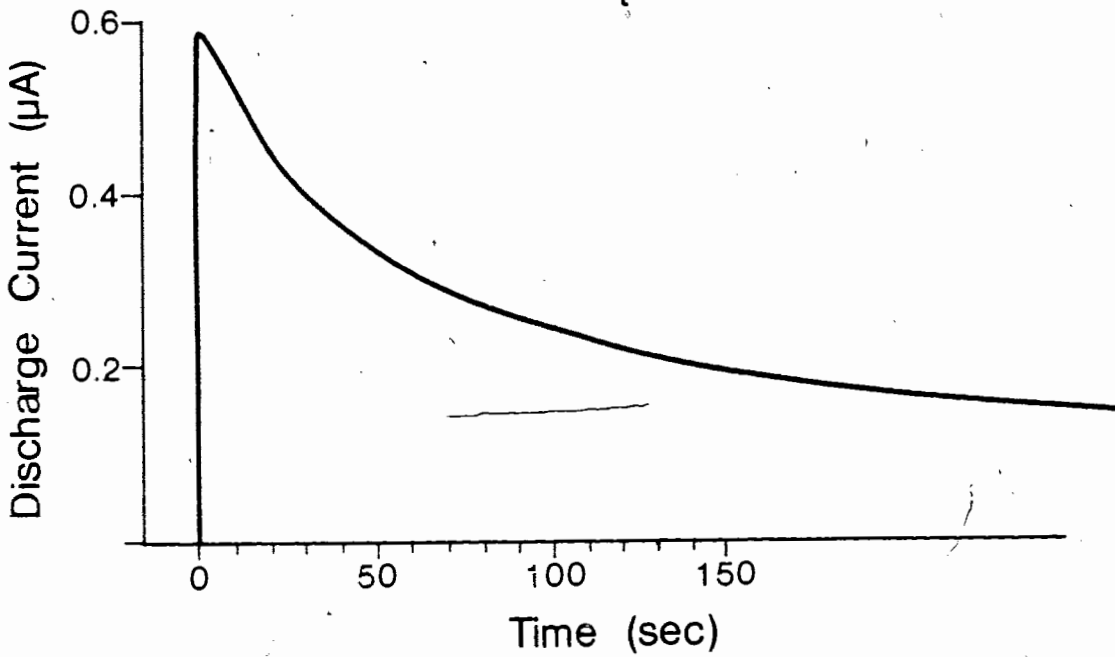
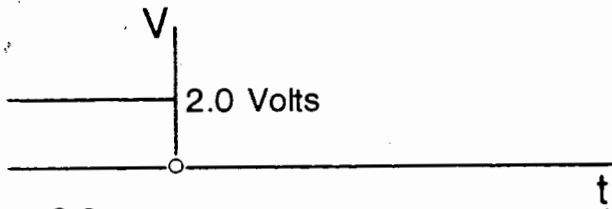
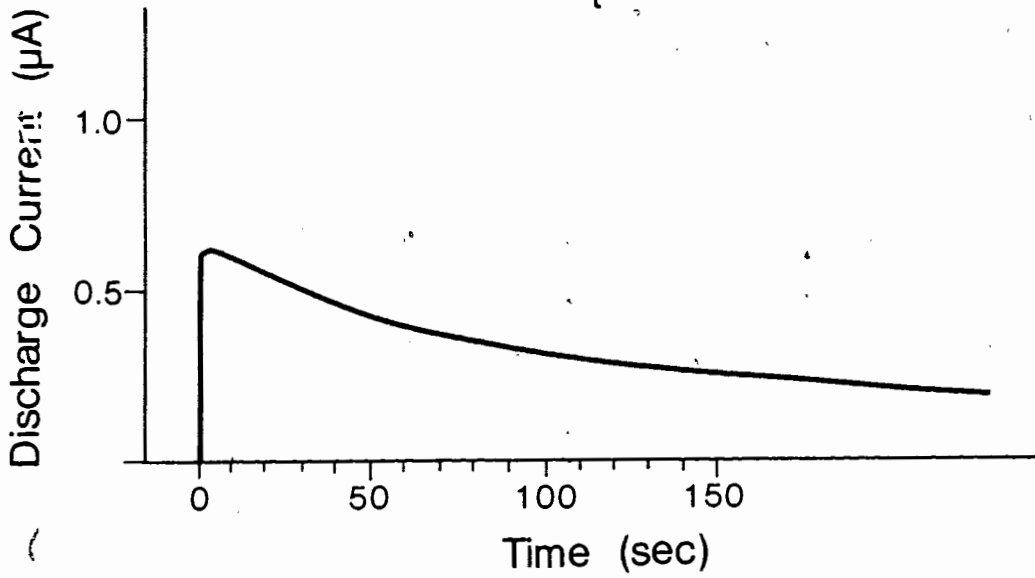
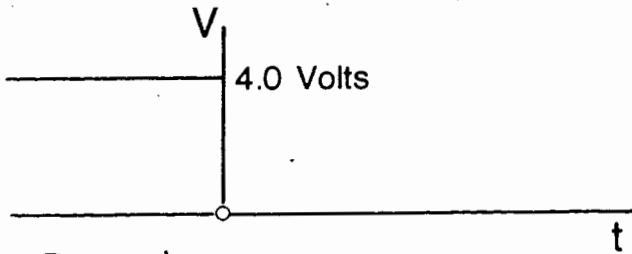


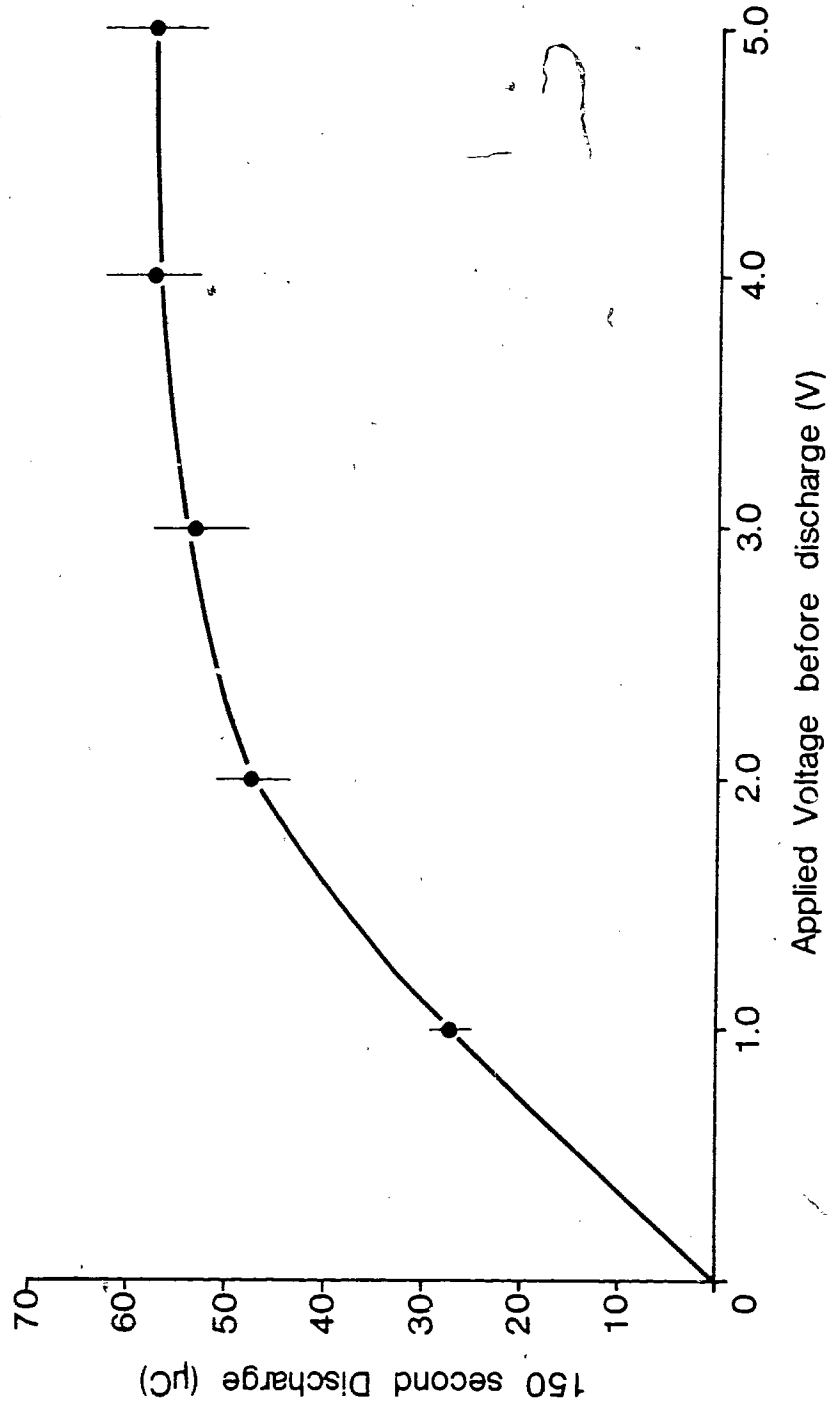
FIGURE 4.19 - Q DISCHARGED IN 150 SECONDS VS. VOLTAGE

Sample: [TCNE] = 0.01 M. in DCE

platinum electrodes

d = 2mm

Steady state conditions were approached prior to cell discharge



is six orders of magnitude larger than the maximum for electrical boundary layer charge, the discharge of electrical boundary layers obviously does not account for the current observed when the Pt cell is shorted. Electroactive species generated with voltage treatment probably revert back to their original oxidation state with voltage removal and thereby produce the discharge current. Even though the discharge current measurements don't give a handle on the magnitude of the space charge, or the electrical boundary layer potentials, presumably space charge effects are still an important consideration in modelling the conduction properties and related electrohydrodynamic behaviour of TCNE/DCE solutions.

Interestingly, there is a correlation between the discharge and current instabilities in TCNE/DCE solutions under the conditions discussed in the previous paragraph. The number of coulombs discharged through the Pt cell levels out around 4.0 volts. Current instabilities grow as a function of voltage beyond 4.0 volts and this type of behaviour can be associated with electrohydrodynamic instabilities. The current response below this critical voltage is smooth and decreases monotonically with time. Above the critical voltage, the 'steady state' current levels out or increases slightly with time. Growth in the concentration of any electroactive species near the electrodes is restricted by turbulent convection. This accounts qualitatively for the cell discharge levelling off beyond a critical voltage.

The preceding behaviour is consistent with a transition from laminar to turbulent flow at the critical voltage. The observations also demonstrate

the close relationship between electrohydrodynamic effects and electrode processes. There are three possible regimes of liquid flow: [1] stationary liquid (ions flow through without significant drag on the liquid) [2] laminar flow (smooth, non-turbulent flow) [3] turbulent flow²⁴. As space charge induced pressure gradients grow with increased applied voltage, the flow response of the liquid is expected to pass from stationary to laminar to turbulent behaviour. Further evidence for convective transitions will be discussed in the next section.

4.4.2 - IV RESPONSE (CONTINUOUS VOLTAGE SCANNING)

In this section, i - V characteristics with continuous voltage variation will be discussed in terms of space charge effects and convective transitions.

Figures 4.20 and 4.21 show sample i - V curves for scans with $V_{\max} > V > 0$ (Figure 4.20-triangular wave, Figure 4.21 - sinusoidal wave). Figure 4.22 shows i - V responses for voltages ranging between a positive and negative maximum value $-V_{\max} > V > V_{\max}$. The i - V responses with positive and negative voltages show reasonable symmetry about the origin over one cycle.

Decreasing the scan rate has the effect of decreasing the current magnitude at a given voltage. The slower the scan rate, the more time is available for space charge to collect at the electrodes and/or ion concentration to

**FIGURE 4.20 - CURRENT VS. VOLTAGE, ABOVE AND BELOW THE
CRITICAL FREQUENCY (TRIANGULAR WAVE VOLTAGE)**

Sample: [TCNE] = 0.01 M. in DCE

indium electrodes

$w = 1\text{mm}$ $h = 0.12\text{ mm}$

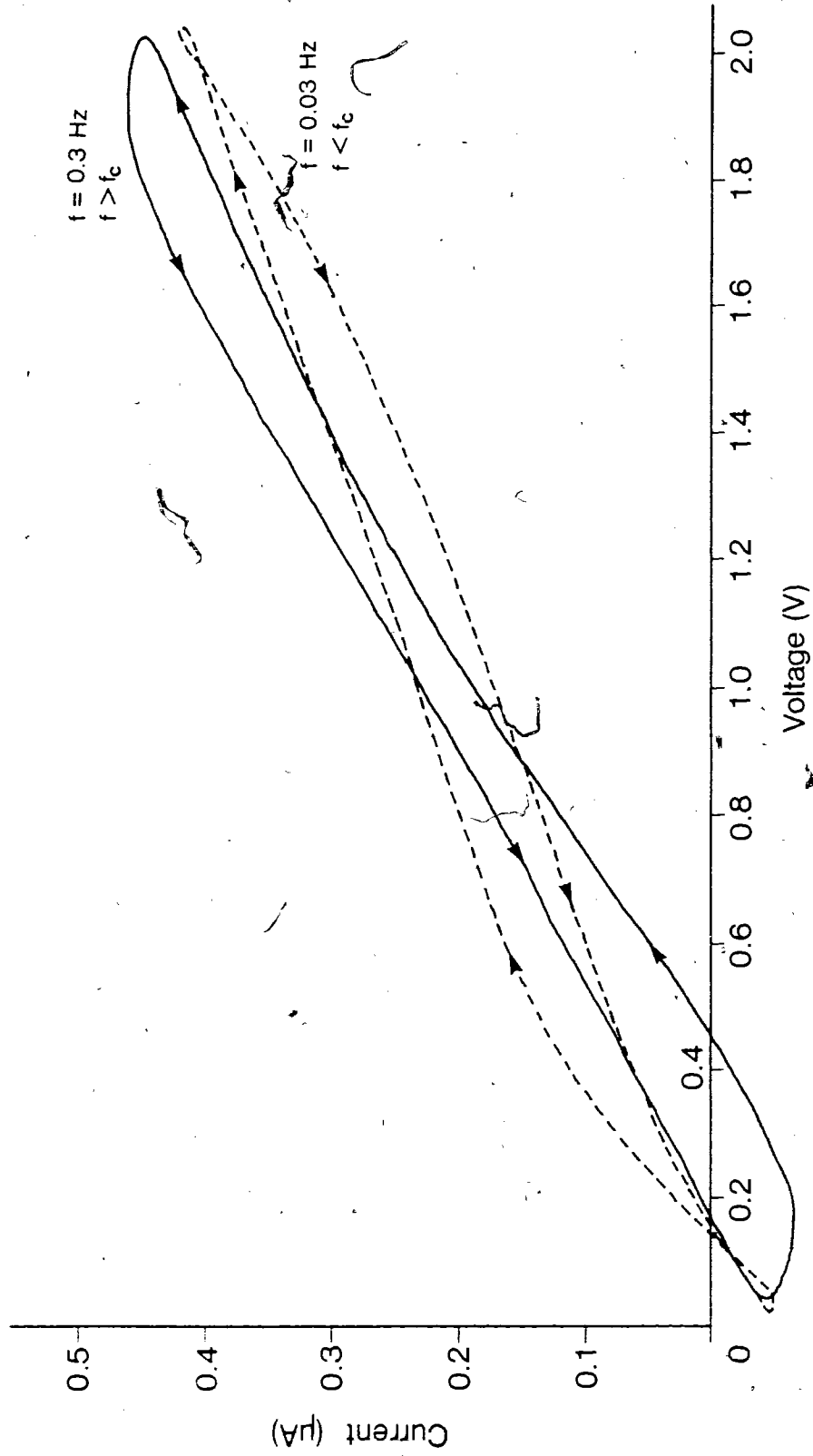


**FIGURE 4.21 - CURRENT VS. VOLTAGE, ABOVE AND BELOW THE
CRITICAL FREQUENCY (SINE WAVE VOLTAGE)**

Sample: [TCNE] = 0.01 M. in DCE

indium electrodes

w = 1mm h = 0.12 mm

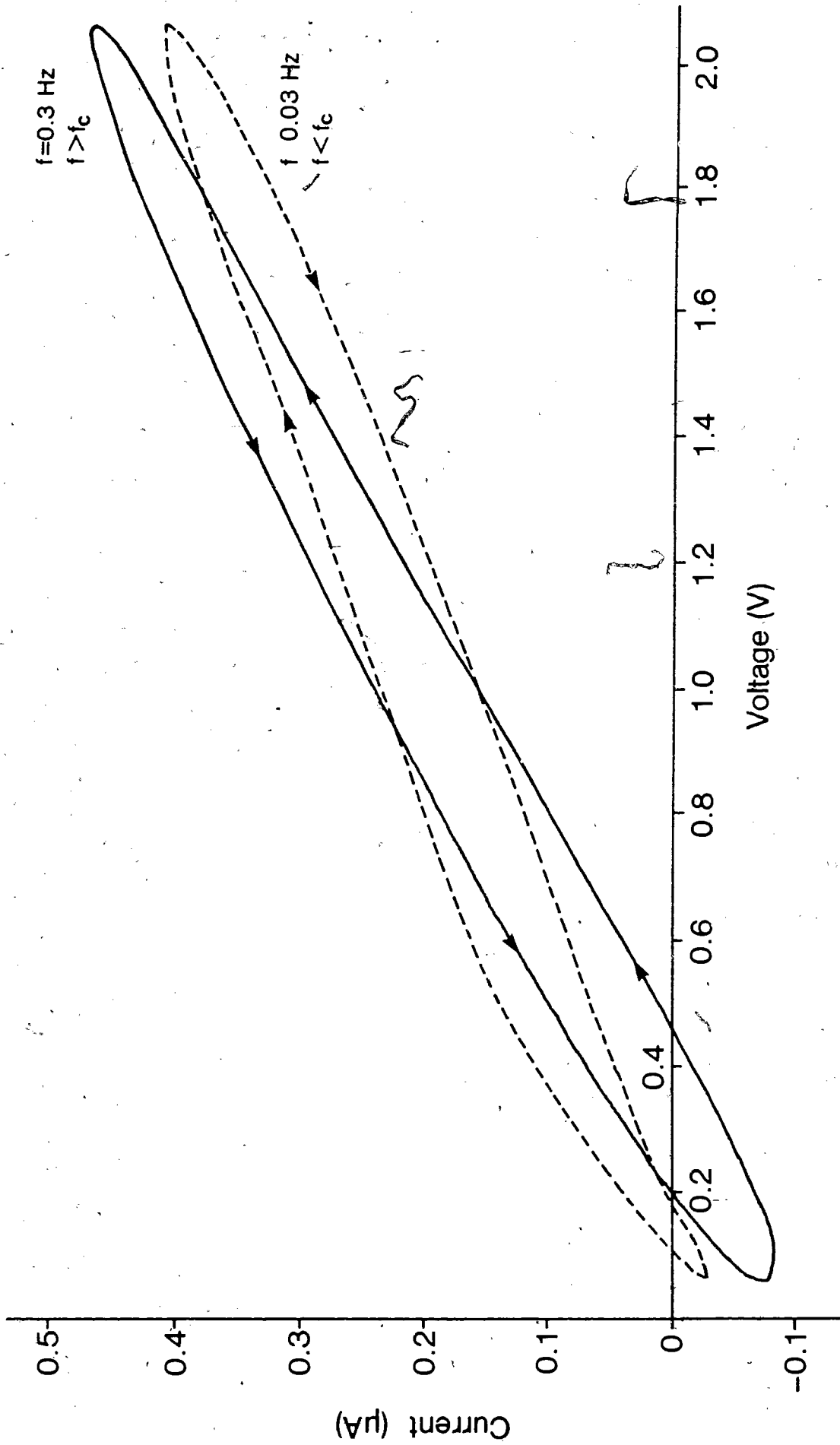
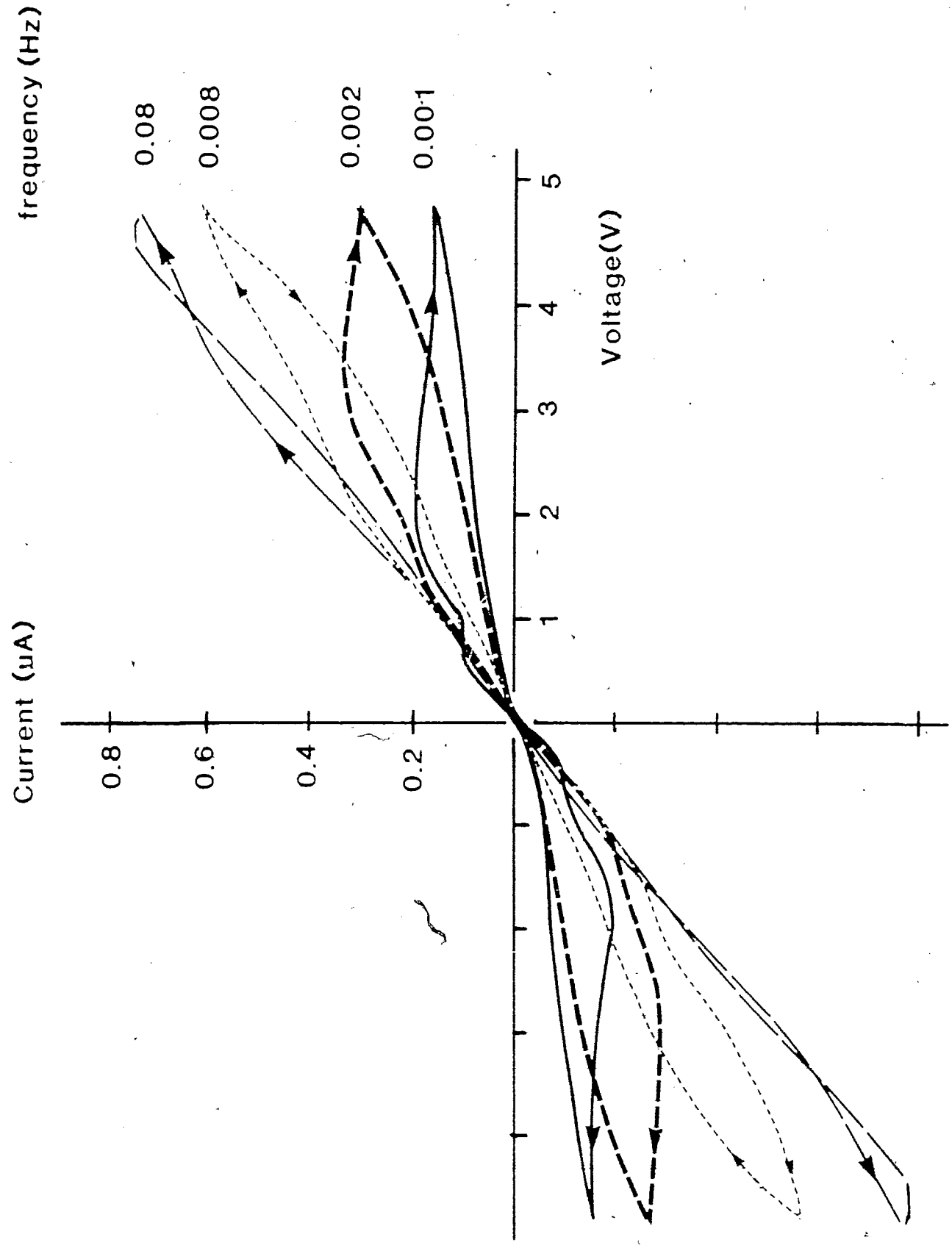


FIGURE 4.22 - CURRENT VS. VOLTAGE RESPONSE
AT DIFFERENT FREQUENCIES (TRIANGULAR WAVE VOLTAGE)

Sample: [TCNE] = 0.01 M. in DCE

indium electrodes

$w = 0.8 \text{ mm}$ $h = 0.08 \text{ mm}$



deplete in the bulk of the solution. The location of current plateaus is also a function of the scan rate. The slower the scan rate, the lower the voltages at which plateaus occur. The current decreases as a function of voltage after the second current plateau for the slowest scan rate in Figure 4.22. The preceding i - V curves were all measured using thin In cells and 0.01M TCNE/DCE solutions. Note the qualitative similarities between these data and the i - V curves for TCNE/Mesitylene/DCE solutions in a Pt cell (Figures 4.23.1 and 4.23.2). Again, the slower the scan rate the lower the voltage at which current plateaus appear.

There are two possible explanations for the plateaus in the current for unmixed samples: [1] the concentration of electroactive species diminishes near the electrodes via cell redox reactions; [2] electrohydrodynamic transitions at critical space charge densities alter the current characteristics. The evolution of concentration gradients or electrical boundary layers is expected to depend on both voltage and time, consistent with the observed behaviour of current plateaus. It is also possible that the combined effects of electroconvection and concentration depletion contribute to the location of current plateaus. Mixing, via the onset of turbulent convection, narrows concentration depletion layers and thus results in a further current increase after a plateau.

The decrease in current with voltage increase after the second plateau (Figures 4.22) is difficult to account for in terms of electrohydrodynamic transitions. The more reasonable explanation for this behaviour is that the

FIGURE 4.23.1 - CURRENT VS. VOLTAGE (f = 0.002 Hz. <
f_c, TRIANGULAR WAVE VOLTAGE)

Sample: 3 ml. of 0.001 M. TCNE/DCE

2 ml. of mesitylene

platinum electrodes

d = 2 mm

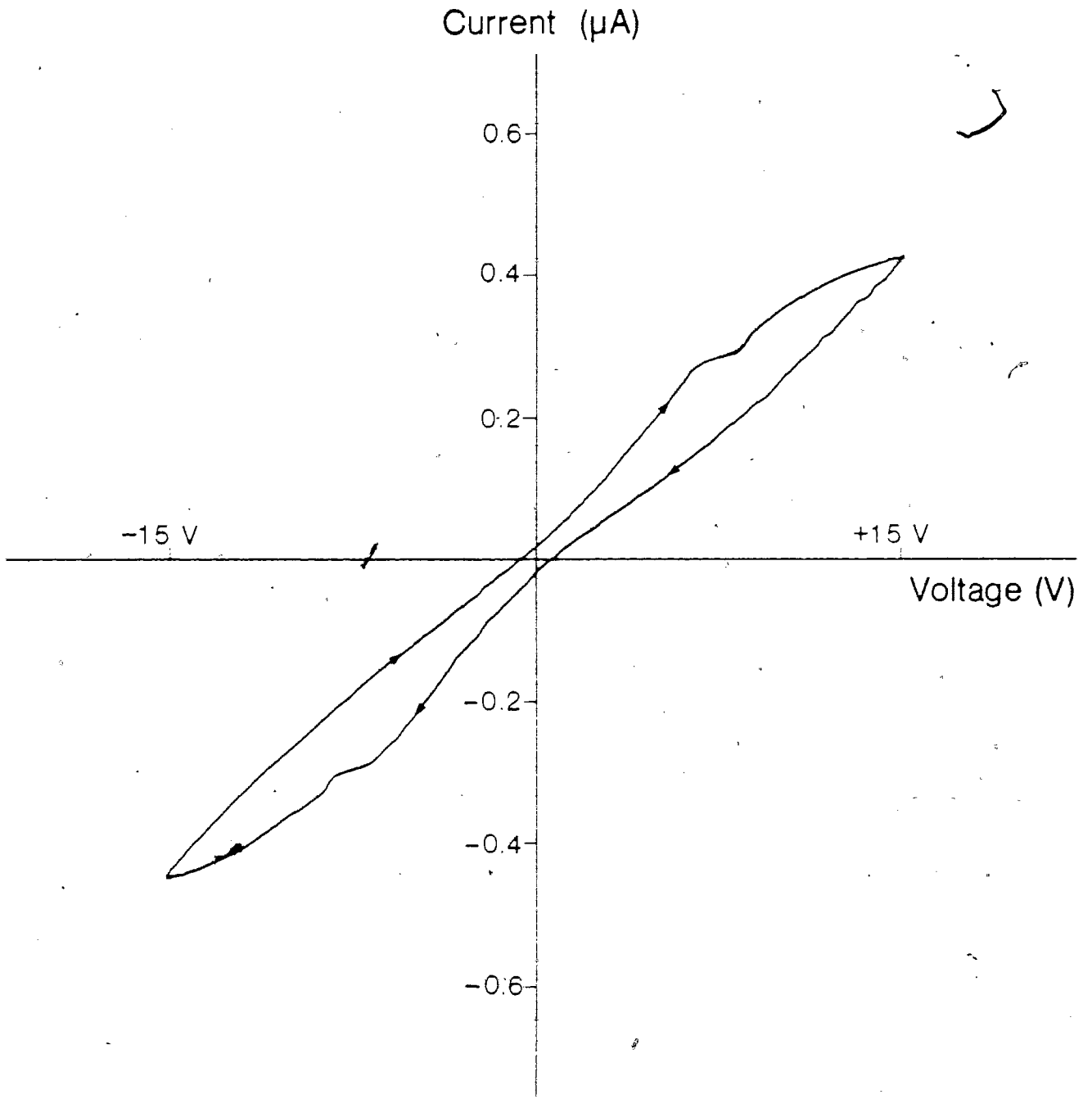


FIGURE 4.23.2 - CURRENT VS. VOLTAGE (f = 0.007 Hz. <
f_c, TRIANGULAR WAVE VOLTAGE)

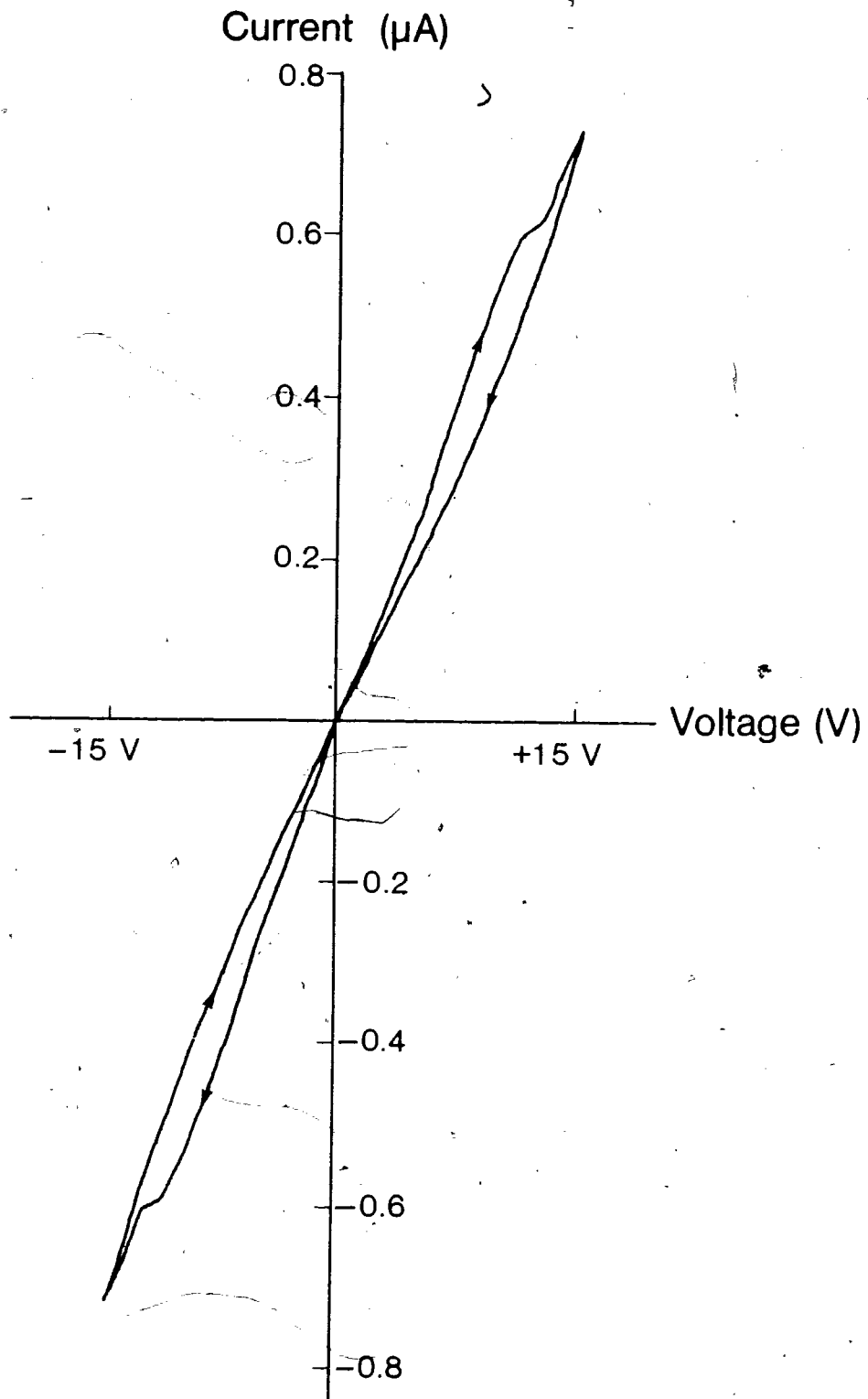
Sample: 3 ml. of 0.001 M. TCNE/DCE

2 ml. of mesitylene

NO MIXING

platinum electrodes

d = 2 mm



total concentration of electroactive species depletes not only near the electrode but also in the bulk of the sample.

Current plateaus disappear with external mixing. For a TCNE/Mesitylene/DCE sample (Pt electrodes, $d = 2$ mm), ~~i - V curves~~ with and without external mixing are shown in Figures 4.24 and 4.23.2, respectively. A linear dependence of the current on voltage is observed when the sample is continuously mixed using a magnetic stirrer. Mixing destroys any ion concentration gradients in the bulk of the solution and also decreases the electrical boundary layers. As has been discussed repeatedly, changes in space charge and bulk ion concentrations have an important influence on the current characteristics in an unstirred solution.

The i - V plot of the mixed CT sample is like that of a simple resistor. Note that the effective resistance of the mixed CT sample appears to be higher than that for the unmixed sample at the same scan rate, resulting in a lower current. This is consistent with observations previously reported in Chapter 3 and Section 4.3. When cross-field flow is introduced via mixing or localized heating, the charge transport efficiency decreases. External mixing eliminates any transitions in the flow properties of the medium and maintains a constant concentration distribution in the bulk of the solution.

The hysteresis behaviour of i - V curves can also be associated with transitions in convective flow. Triangular or sinusoidal waves with $V_{\max} > 0$ were used to observe i - V hysteresis in the thin In/TCNE/DCE system. At

**FIGURE 4.24 - CURRENT VS. VOLTAGE (f = 0.007 Hz. <
f TRIANGULAR WAVE VOLTAGE)**

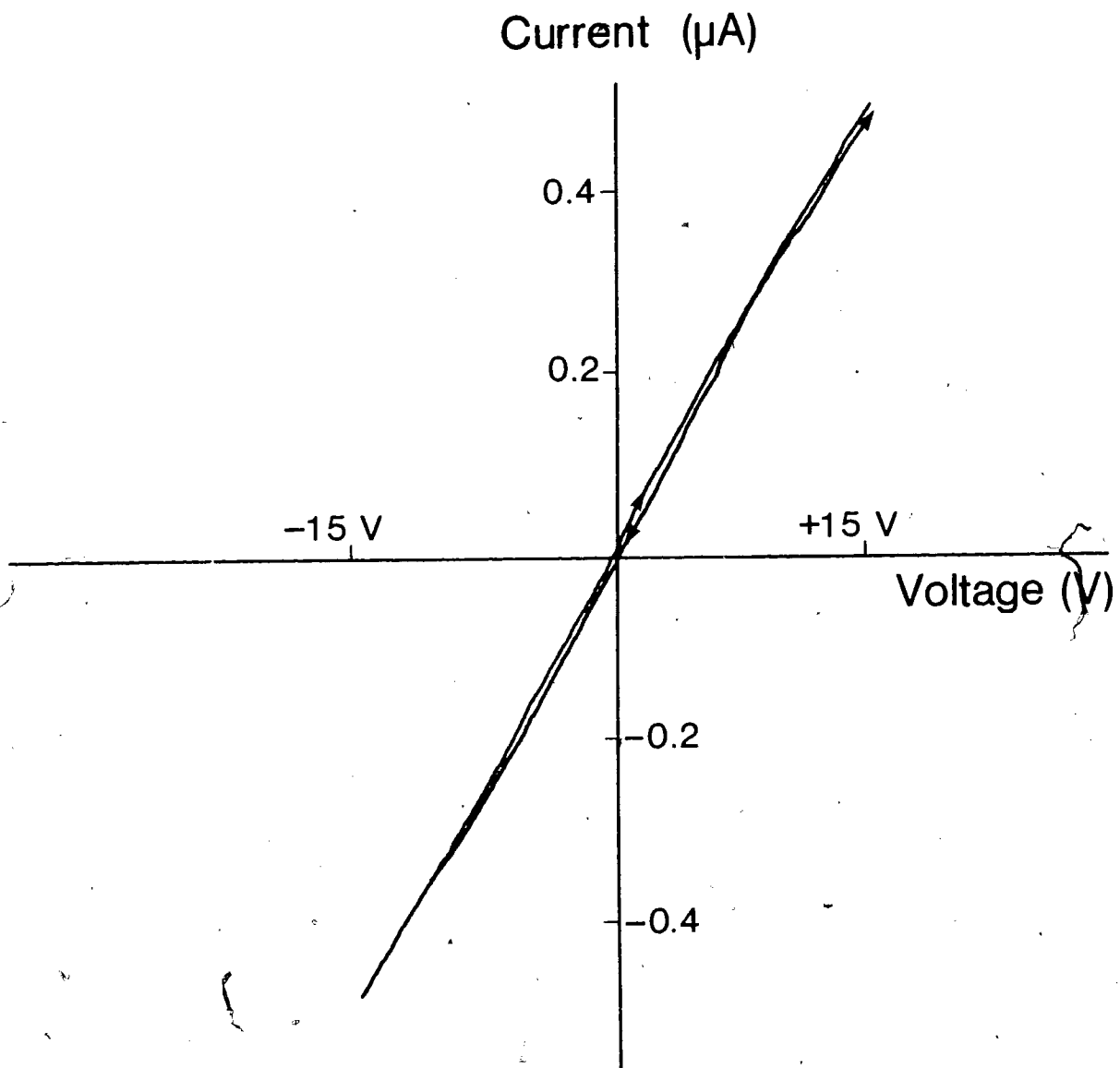
Sample: 3 ml. of 0.001 M. TCNE/DCE

2 ml. of mesitylene

WITH MIXING

platinum electrodes

d = 2 mm.



'critical' voltage scanning frequencies the hysteresis behaviour changes character. Above a certain voltage scanning frequency the current response lags behind the voltage, and the i - V curve loops counterclockwise (Figures 4.20, 4.21). Below a certain frequency the current tends to plateau with increasing voltage, or loop clockwise. Figures 4.25 and 4.26 show the gradual shape variation of i - V curves for scanning frequencies above and below the critical frequency. The frequency at which i - V hysteresis changes character is voltage dependent.

Figures 4.27 and 4.29 show the dependence of the critical frequency on voltage amplitude using log-log graphs for two sets of measurements. Plots of $1/f_c$, or the critical time (t_c), against voltage are shown in Figures 4.28 and 4.30. The two sets of measurements used different electrode spacings and cell thicknesses. The timing between runs was about 15 minutes in Figure 4.30 and was only about 5 minutes in Figure 4.28.

The power law relationship between t_c and V , ($t_c = V^n + a$), is given by the log-log plots in Figures 4.26 and 4.27 and 'coincidentally' gives values of $n = 0.5, 1.5, \text{ and } 2.0$. At this point it is difficult to attach particular significance to the values of the exponent 'n', other than that a change in 'n' appears at a critical voltage. In each graph, the transition in the voltage dependence of t_c and f_c occurs at 4.0 - 4.3 volts. This corresponds to the voltage at which a jump in the discharge current occurs in a thin In cell with somewhat different geometry (Figure 4.31). The change in the

FIGURE 4.25 - I/V RESPONSE WITH CHANGING FREQUENCY
(SINE WAVE VOLTAGE)

Sample: [TCNE] = 0.01 M. in DCE

indium electrodes

$w = 1 \text{ mm.}$ $h = 0.1 \text{ mm}$

$V_{\text{max}} = +1.0 \text{ Volt}$

$i_{\text{max}} \approx 0.12 \mu\text{A.}$

frequency
(Hz.)

0.30

0.25

0.20

0.10

0.05

$f_c \sim 0.20$ Hz.

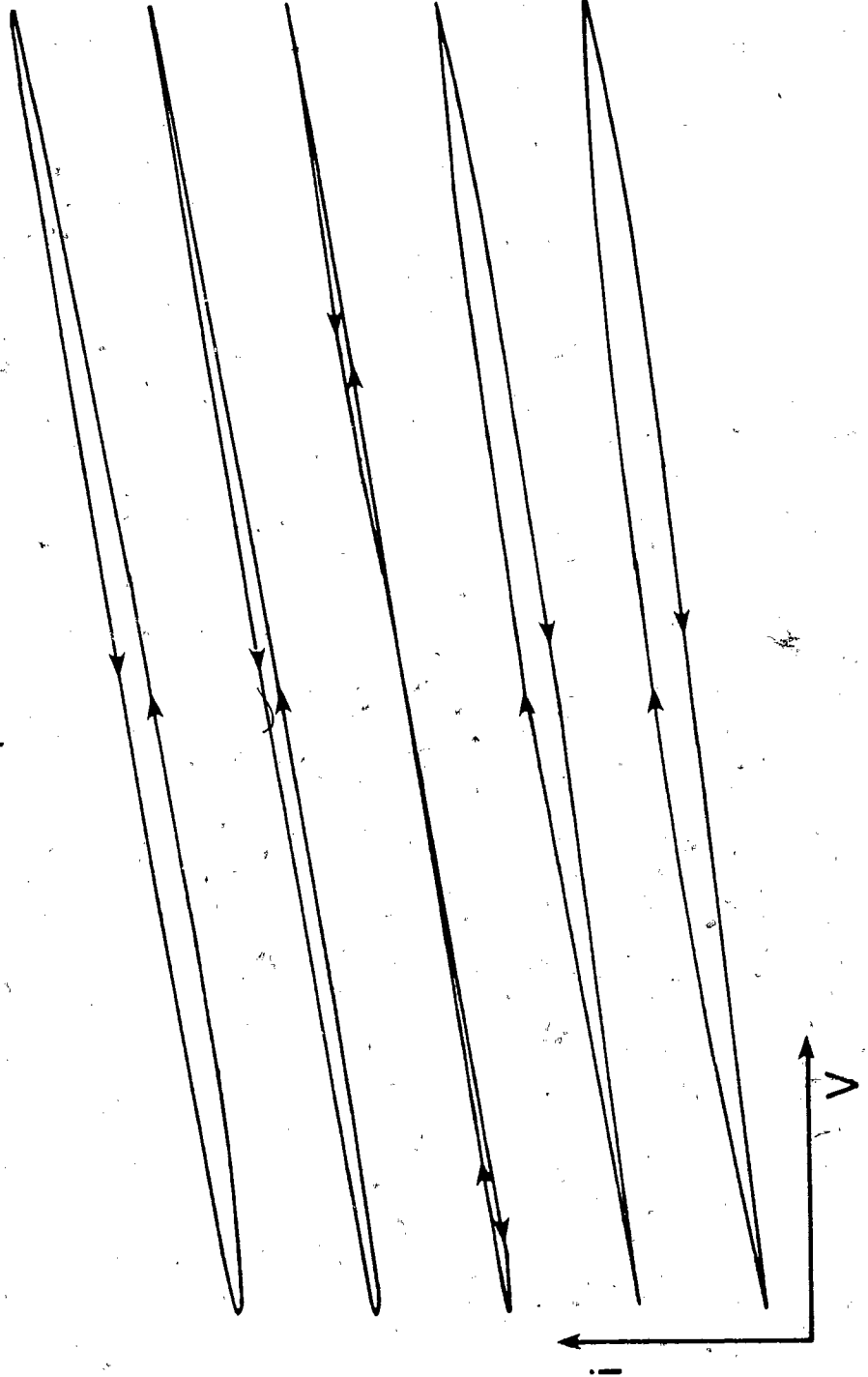


FIGURE 4.26 - I/V RESPONSE WITH CHANGING FREQUENCY
(TRIANGULAR WAVE VOLTAGE)

Sample: [TCNE] = 0.01 M. in DCE

indium electrodes

w = 1 mm. h = 0.1 mm

$V_{\max} = +1.0$ Volt

$i_{\max} \approx 0.12 \mu\text{A}$.

115b

$f_c \sim 0.45 \text{ Hz.}$

frequency
(Hz.)

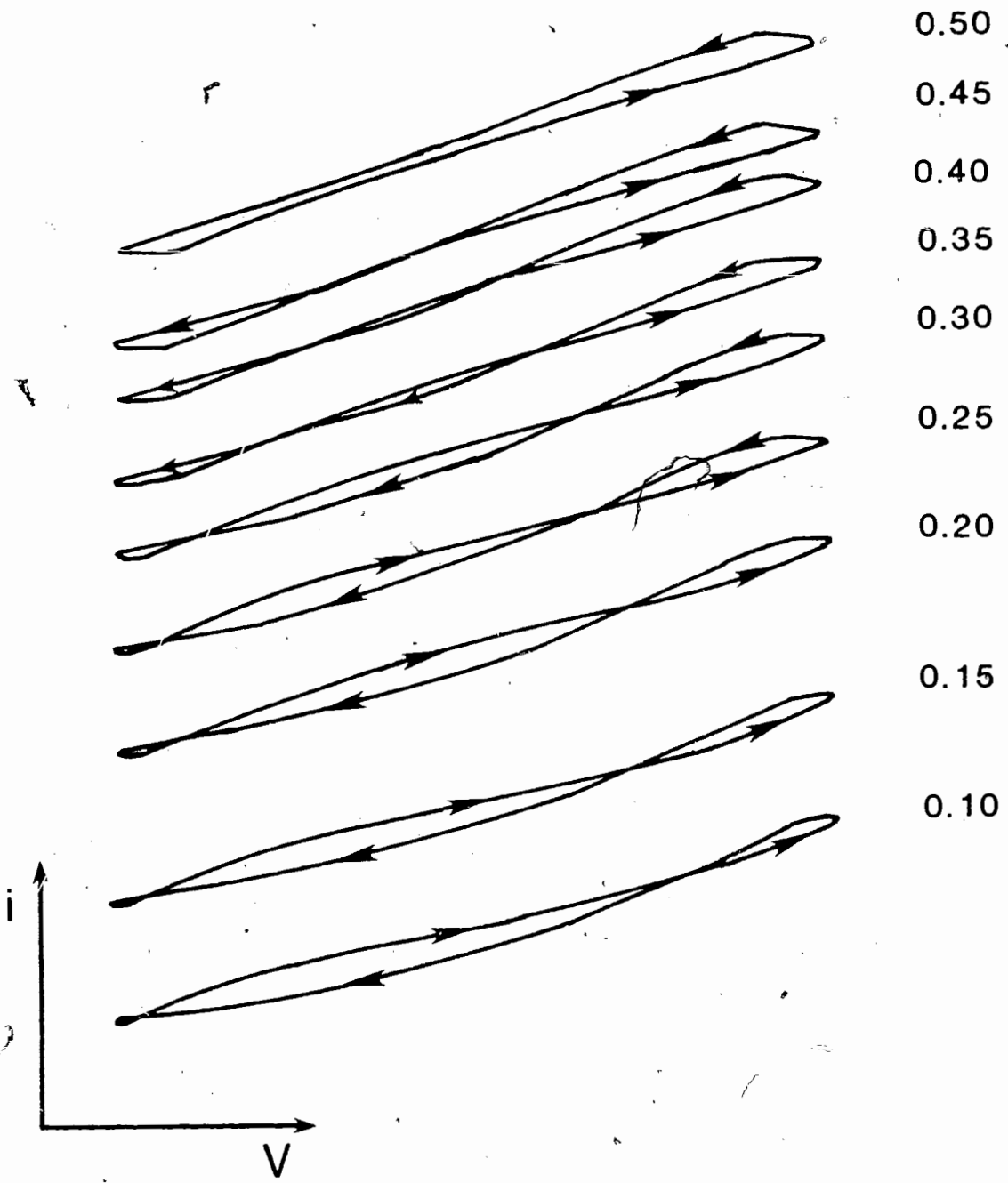


FIGURE 4.27 - CRITICAL FREQUENCY VS. VOLTAGE AMPLITUDE
(TRIANGULAR WAVE VOLTAGE)

Sample: [TCNE] = 0.01 M. in DCE

indium electrodes

w = 1 mm. h = 0.09 mm

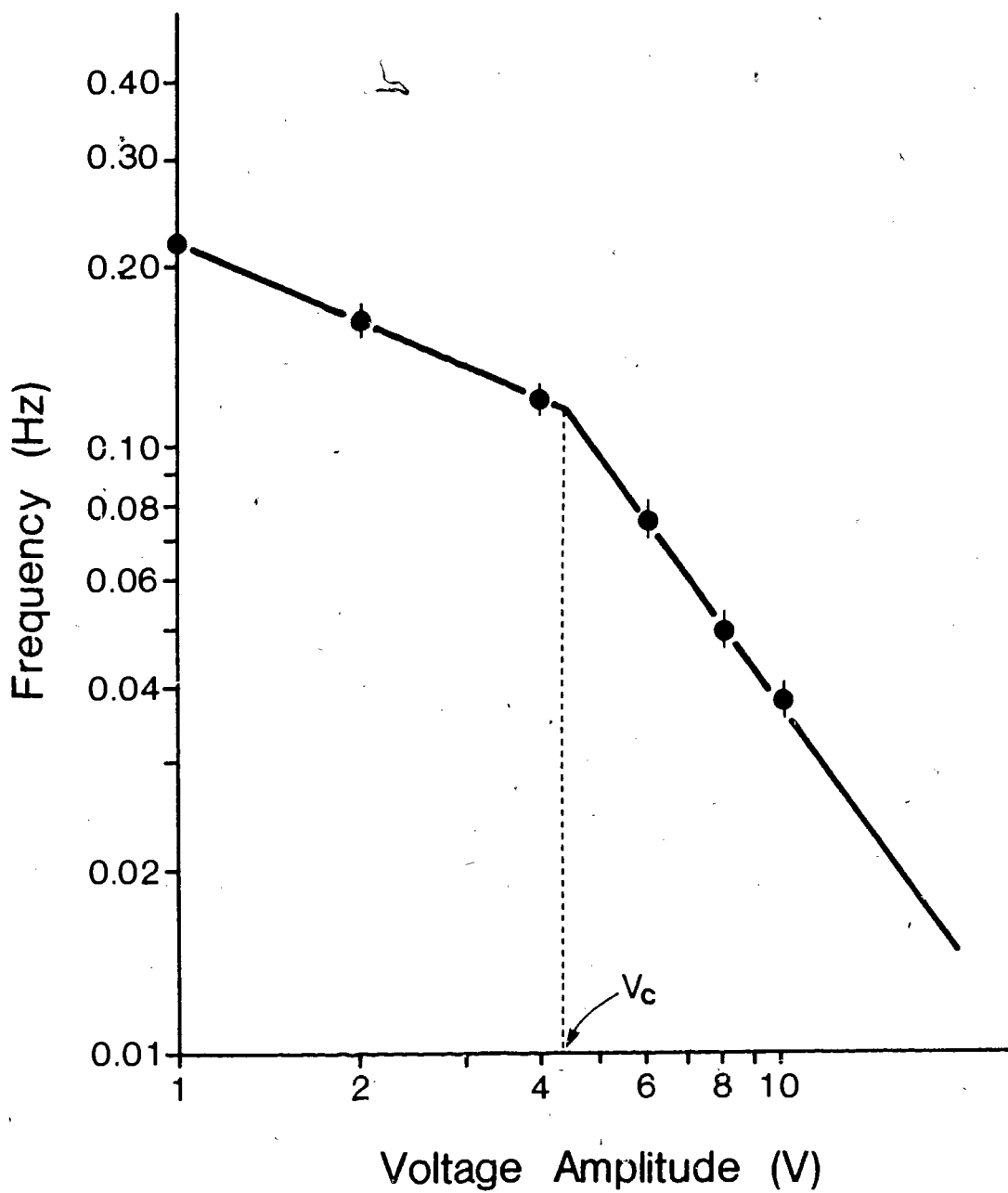


FIGURE 4.28 - CRITICAL TIME VS. VOLTAGE AMPLITUDE
(TRIANGULAR WAVE VOLTAGE)

Sample: [TCNE] = 0.01 M. in DCE

indium electrodes

w = 1 mm. h = 0.09 mm

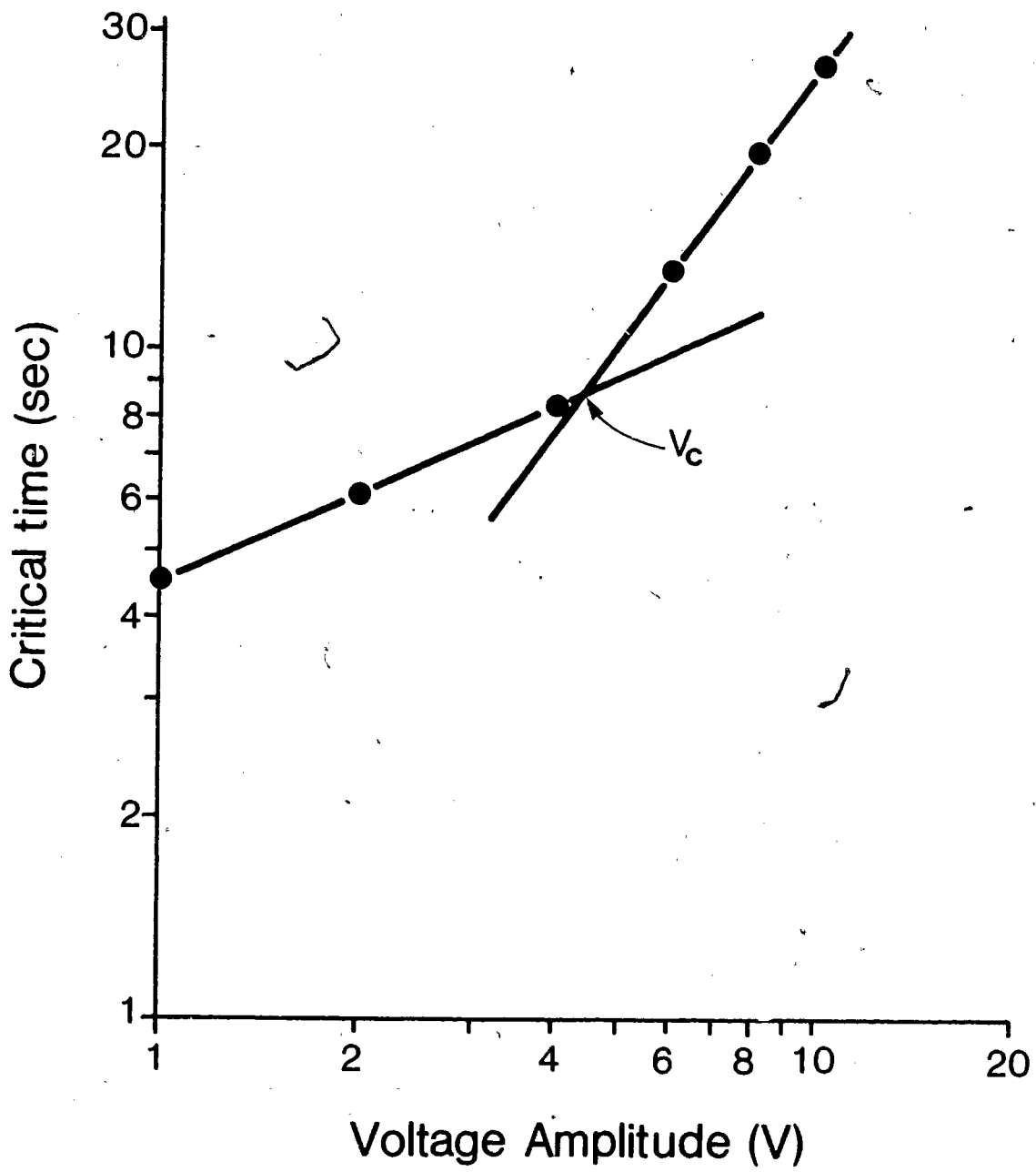


FIGURE 4.29 - CRITICAL FREQUENCY VS. VOLTAGE AMPLITUDE
(TRIANGULAR WAVE VOLTAGE)

Sample: [TCNE] = 0.01 M. in DCE

indium electrodes

w = 1.5 mm. h = 0.11 mm

■ measurements taken from low to high voltage

● last measurement

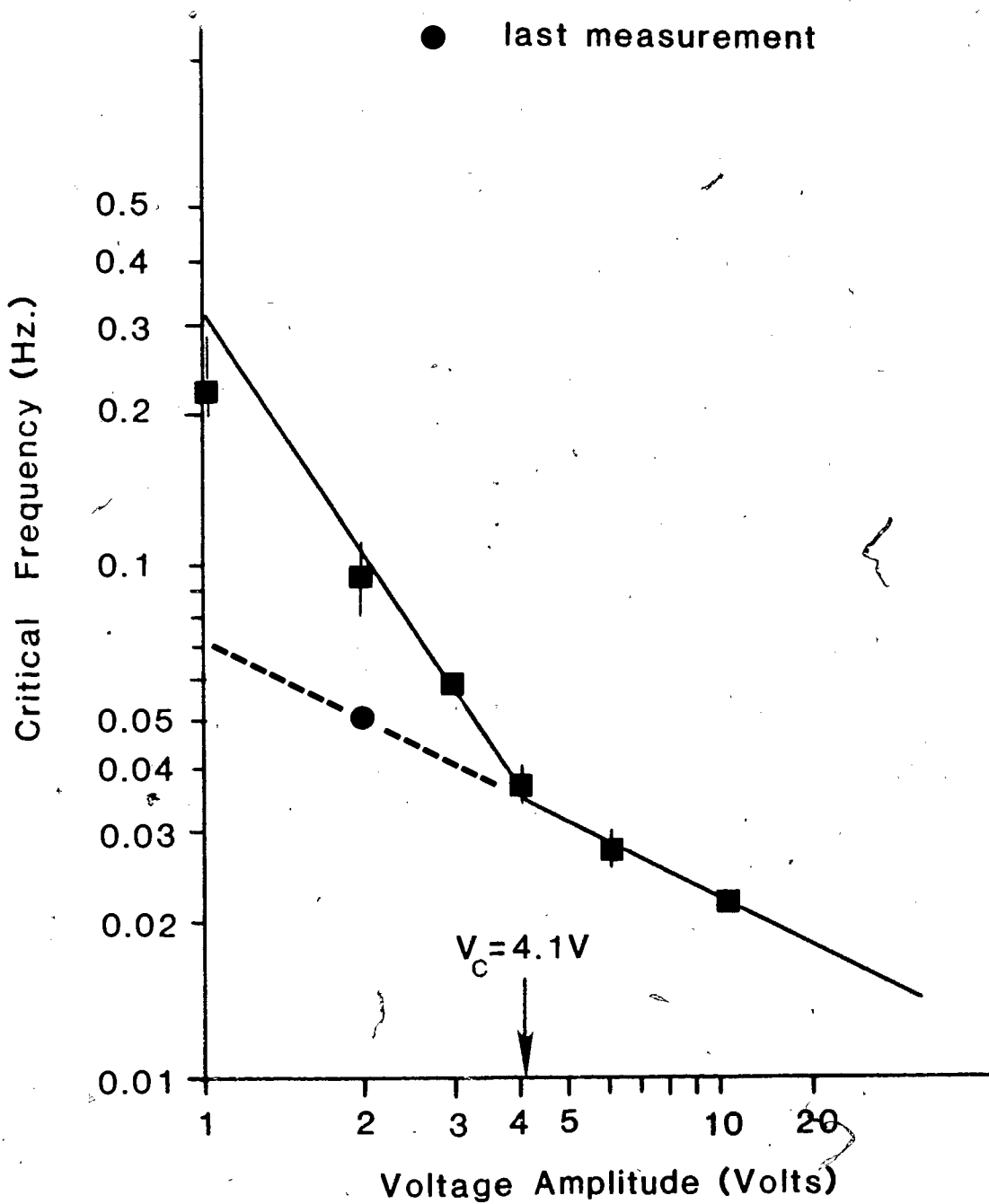


FIGURE 4.30 - CRITICAL TIME VS. VOLTAGE AMPLITUDE
(TRIANGULAR WAVE VOLTAGE)

Sample: [TCNE] = 0.01 M. in DCE

indium electrodes

w = 1.5 mm. h = 0.11 mm.

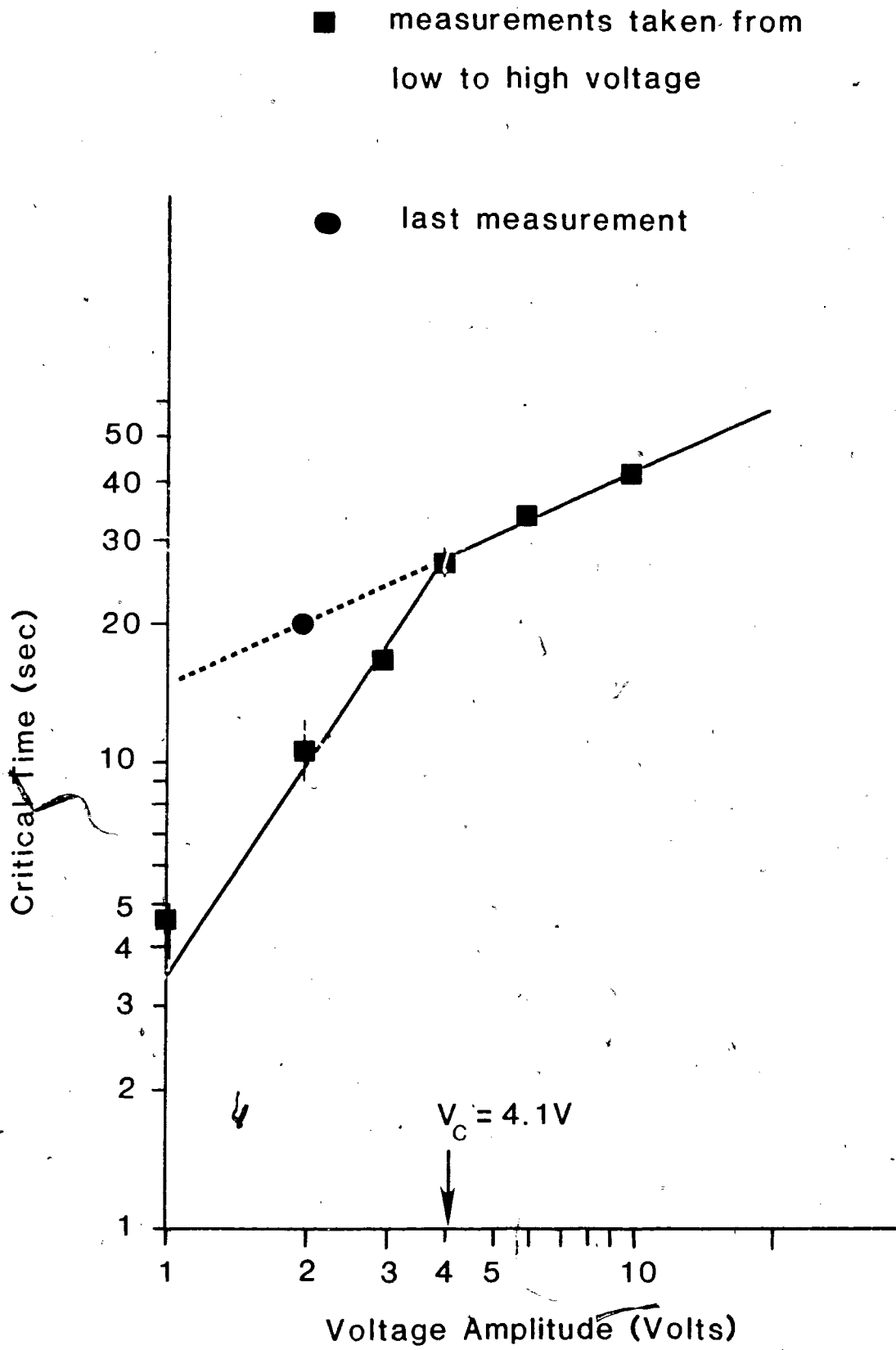
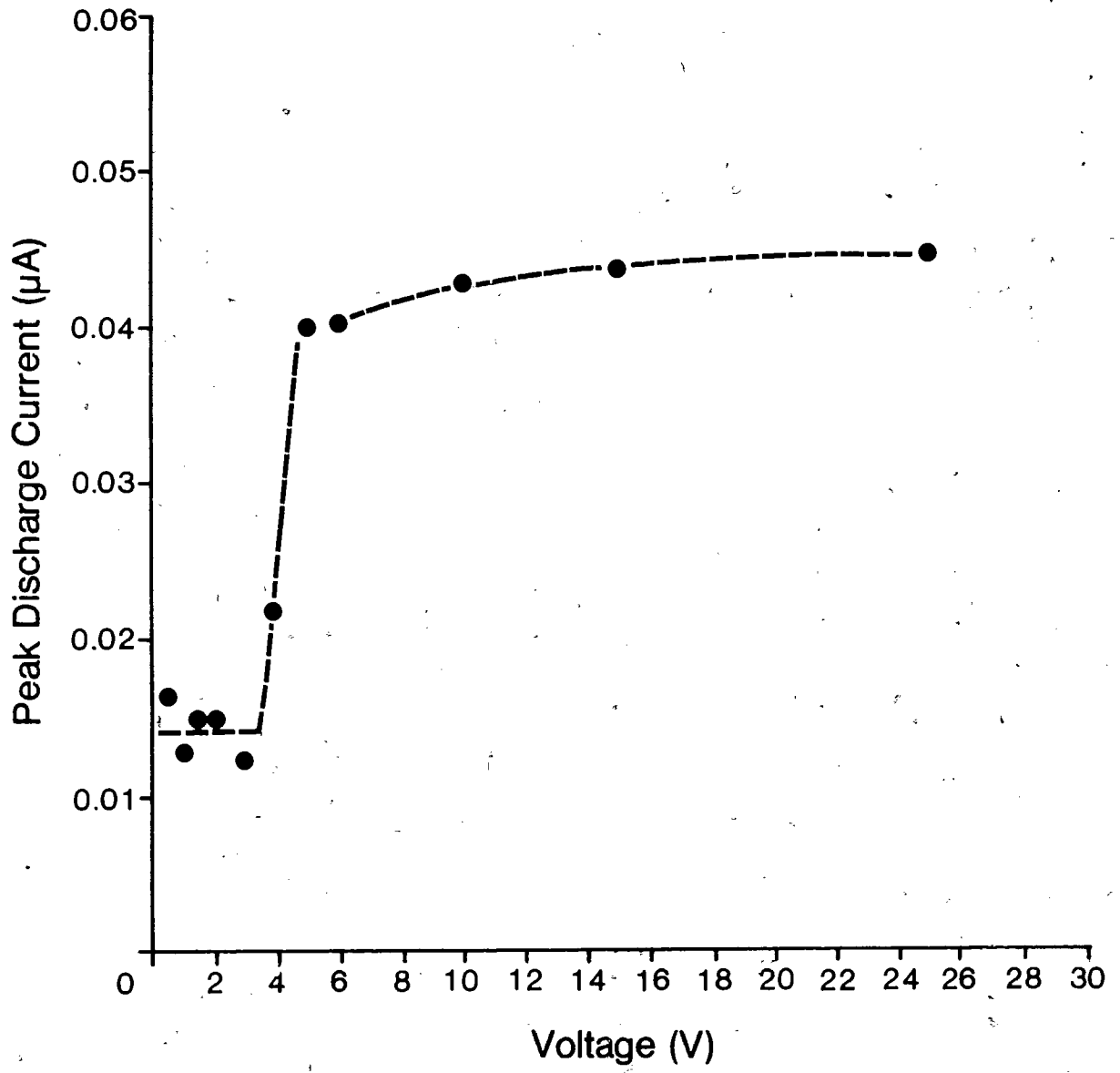


FIGURE 4.31 - DISCHARGE CURRENT VS. VOLTAGE

Sample: [TCNE] = 0.01 M. in DCE

indium electrodes

w = 2 mm. h = 0.2 mm



discharge current may reflect a change in electrode processes at 4 Volts, which in turn relates to mass flow in the cell.

Below 4 volts in Figure 4.28, $t_c = ((V)^{0.5} + a)$ and above this voltage $t_c = ((V)^2 + b)$. In Figure 4.30, $t \approx ((V)^{1.5} + c)$ and $t \approx ((V)^{0.5} + d)$ below and above 4 volts, respectively. Thin In cells of different geometry were used in each case so the applied field was not the same at the critical voltage. The difference in geometry also affects the nature of fluid flow, and this may account for the difference in the log-log plots of t_c vs. V even though the critical voltage remains at about the same value.

The variation of critical frequencies in time is included as an uncertainty in the plots of f_c versus V . For the 1.0 and 2.0 Volt measurements in Figure 4.29, f_c increases with time (i.e. at 1.0 V, f_c changes from about 0.20 Hz to 0.22 Hz. in 50 seconds). In the measurements taken at higher voltages, f_c decreases in time (i.e. at 10.0 V, f_c changes from 0.025 Hz. to 0.023 Hz. in 140 seconds). All but one of the critical frequencies were recorded in order from low to high voltage amplitudes. One measurement of f_c at 2.0 Volts (indicated by a circle in Figure 4.29) followed a measurement at 10.0 Volts. The initial value for f_c is lower than the previously observed value. As time progresses f_c increases slowly to approach the value previously observed (in about 40 minutes f_c varied from 0.05 Hz to 0.07 Hz). In Figure

4.29, the f_c value of 0.05 Hz. at 2.0 Volts fits on the line characteristic of higher voltages in the plot. As the value for f_c increases it approaches the line characteristic of lower voltages. Further comments will be made about these plots after some possible qualitative models for the critical time, t_c , have been proposed below.

The critical times observed for i - V hysteresis at a particular voltage could have been the result of a decay time in convective flow, or the result of a characteristic time for charging or discharging electrical boundary layers. A closer look at the data lends some merit to both of these proposals. Consider the current response for voltage scanning frequencies greater than f_c (Figures 4.20, 4.21). The current continues to rise even after the voltage begins to decrease. There are two feasible explanations for this behaviour and both need to be considered in modelling the critical time. One explanation is that the inertia of liquid flow in the system carries extra current with it even after the voltage has decreased. The speed of convective flow is an increasing function of the voltage ($v \approx V$, or $v \approx V^2$)^{20, 23}. The relaxation time for convective flow depends on the speed, viscosity, and density of the liquid. As the maximum applied voltage increases, the speed of flow also increases and hence the time constant associated with slowing down the flow is expected to increase. This is consistent with what is observed in the graph of t_c vs. V in Figures 4.28 and 4.30.

Another explanation for the current lag is in terms of charging the

electrical boundary layers at each electrode. The time constant for such a process is estimated using a simple RC circuit to model a space charge layer and the neighbouring solution. The sample resistance is typically about 10 M Ω . The observed time constants are in the range of 5 - 50 seconds which indicates boundary layer capacitances of the order of 0.2 - 2 μ F. According to the Guoy-Chapman theory²⁵, the differential capacitance of a double layer ($C_d = dp/dV$, where p =surface charge density, V =effective potential across the double layer) is a strong function of the voltage and ion concentration. The double layer capacitance increases with voltage and decreases with ion concentration. For 1:1 electrolytes with concentrations of 0.01 M. and $V=100$ mV, the differential capacitance is predicted to be about 100 μ F/cm² or about 3 μ F for the thin electrode geometry²⁶. The comparison cited here is somewhat strained since in our samples the ion concentrations were about 10⁻⁶M, and the boundary layer potentials were difficult to estimate. The limiting voltage range for electrochemical work on DCE with a supporting electrolyte is reported to be 2.3 \pm 0.2 Volts [anode] and 2.2 \pm 0.1 Volts [cathode]²⁷. This gives an upper limit for boundary layer voltages. At any rate, it appears reasonable to suggest effective electrical boundary layer capacitances of the order of 0.2-2.0 μ F in our samples.

Since the electrical boundary layer capacitance is expected to increase with voltage, thereby increasing the characteristic charging time, this model is consistent with the observations. Transitions in the capacitance of the boundary layers as a function of voltage may occur as the result of changes

in electrochemical kinetics or convective transitions. The mixing as a result of convection will tend to narrow the boundary layer as well as decrease the amount of surface charge. Convective flow will also influence the resistivity of the solution which in turn will have an effect on the critical time.

Obtaining the explicit power laws ($t_c = V^n + b$) in given voltage regions is difficult using either critical-time model. Atten and Malraison suggest that the speed of liquid convection varies as the square of the voltage ($v \propto V^2$) or directly with the voltage ($v \propto V$)²⁰. Using the first relationship one can qualitatively account for the V^2 dependence of t_c in Figure 4.28 if t_c is proportional to v , and if the solution resistance does not vary significantly as a function of the voltage amplitude (the steady state ion concentration was, however, observed in spectroscopic studies to be a function of the voltage). Derivations of the possible power laws between fluid flow relaxation times and the applied voltage from first principles were considered to be beyond the scope of this work.

Formulating a relationship for the voltage dependence of t_c by modelling the electrical boundary layer capacitance is not straightforward, either. Since recent models for double layer capacitance generally require the simplifying assumptions available in solutions with larger ion concentrations, there is no general theoretical description that fits the conditions in our samples.

In the discussion of i - V characteristics and critical voltage behaviour in TCNE/DCE samples, the difficulty of separating convective and electrochemical effects becomes apparent. The results to be discussed in Chapter 5 do not resolve this problem, but do give insight into the close relationship between ion concentration behaviour at the electrode interface and the appearance of flow instabilities.

REFERENCES:

1. W.J. Middleton, E.L. Little, K.K. Coffman, V.A. Engelhardt, "Cyanocarbon Acids and their Salts", Journal of the American Chemical Society **1958**, 80, 2795-2806.
2. M. Itoh, "Dimerization and Electronic Absorption Spectra of Tetracyanoethylene Anion in Solution and in Solid", Bulletin of the Chemical Society of Japan **1972**, 45, 1947.
3. A.J. Pearmin, B.Makin, A.W.Bright, "Purification, Impurity Content and Resistivity of Nitrobenzene", 4th International Conference on Conduction and Breakdown in Dielectric Liquids. **1972**, T.J. Gallagher, Editor; 68.
4. R.E. Merrifield, W.D. Phillips, "Spectroscopic Studies of the Molecular Complexes of Tetracyanoethylene", Journal of the American Chemical Society **1958**, 80, 2778-82
5. F. Gutmann, J.P. Farges, In "Modern Aspects of Electrochemistry", No. 13; J. O'M. Bockris, B.E. Conway, Editors; Plenum Press: New York, **1979**, p 361.
6. M.V. Ramanamurti, P.V.S.S. Prabhu, "Conductometric Studies of Charge Transfer Complexes in Solution", Electrochimica Acta **1982**, 27, 461-464.
7. F. Gutmann, J.P. Farges, In "Modern aspects of Electrochemistry", No. 13; J. O'M. Bockris, B.E. Conway, Editors; Plenum Press: New York, **1979**, p 362.
8. V. Novotny, M.A. Hopper, "Transient Conduction of Weakly Dissociating Species in Dielectric Fluids", Journal of the Electrochemical Society **1979**, 126, 925-929.

9. J.C. Gibbings, G.S. Saluja and A.M. Mackey, "Current Decay and Fluid Convection in a Conductivity Cell", Static Electrification 1975, Institute of Physics Conference Series No.27; A.R. Blythe, Editor; 18.
10. A.M. Mackey and J.C. Gibbings, "Charge Convection in Electrically Stressed, Low-Conductivity Liquids", Journal of Electrostatics **1981**, 9, 355-366.
11. A.J. Bard, L.J. Faulkner, "Electrochemical Methods"; John Wiley and Sons: New York, **1980**, Ch.12.
12. W.F. Pickard, "Ion Drag Pumping I: Theory", Journal of Applied Physics **1963**, 34, 246.
13. T.J. Gallagher, "Simple Dielectric Liquids", Oxford University Press: London, **1975**, p17.
14. W.J. Moore, "Physical Chemistry", 4th Edition; Prentice-Hall: Englewood Cliffs, New Jersey, **1972**, p 163.
15. I. Adamczewski, "Ionization, Conductivity and Breakdown in Dielectric Liquids"; Taylor and Francis Ltd.: London, **1969**, pp 139-140.
16. J.M. Schneider, P.K. Watson, "Electrohydrodynamic Stability of Space-Charge-Limited Currents in Dielectric Liquids I: Theoretical Study II: Experimental Study", The Physics of Fluids **1970**, 13, 1948-1961.
17. T.J. Gallagher, "Simple Dielectric Liquids", Oxford University Press: London, **1975**, pp13-15
18. P. Atten, B. Malraison, S. Ali Kani, "Electrohydrodynamic Stability

of Dielectric Liquids Subjected to A.C. Fields", Journal of Electrostatics **1982**, 12, 477-488.

19. P. Atten, J.C. Lacroix, "Non-Linear Hydrodynamic Stability of Liquids Subjected to Unipolar Injection", Journal de Mecanique **1979**, 18, 468-510.
20. B. Malraison, P. Atten, "Chaotic Behavior of Instability Due to Unipolar Ion Injection in a Dielectric Liquid", Physical Review Letters **1982**, 49, 723-726.
21. Y. Aikawa, H. Shimoda, K. Kobayashi, A. Takahashi, S. Takeda, T. Sakata, M. Sukigoro, "Electrohydrodynamic Dissipative Structure in Unipolar and Bipolar Injection Cases", The Bulletin of the Chemical Society of Japan **1982**, 55, 654-659.
22. J.C. Gibbings, "Interaction of Electrostatics and Fluid Motion", Electrostatics 1979, Institute of Physics Conference Series No.48; J. Lowell, Editor; 145.
23. A. Rich, J.L. Sproston, "Some Observations on Bulk Electroconvection In Electrically Stressed Liquid Dielectrics", Journal of Electrostatics **1982**, 12, 503.
24. T.J. Gallagher, "Simple Dielectric Liquids", Oxford University Press: London, **1975**, p 13.
25. A.J. Bard, L.R. Faulkner, "Electrochemical Methods"; John Wiley and Sons: New York, **1980**; p 507.
26. A.J. Bard, L.R. Faulkner, "Electrochemical Methods"; John Wiley and Sons: New York, **1980**; p 508.
27. T. Osa, T. Kuwana, Journal of Electroanalytical Chemistry **1969**, 22, 389-406.

CHAPTER 5 - ION CONCENTRATION BEHAVIOUR WITH APPLIED VOLTAGE

In this chapter, experiments correlating the current response and sample ion concentration will be discussed. Each of the samples, TCNE/DCE and $\text{TEA}^+\text{PCP}^-/\text{DCE}$, have charge carriers with visible absorption peaks (Chapter 6). Concentration changes in the range 10^{-6} - 10^{-7} M. are monitored as a function of time and position with simultaneous current measurements. This leads to a discussion of the different contributions to the ion transport in the system.

After describing the experimental details in Section 5.0, the temporal behaviour of the ion concentration with voltage treatment is presented in Section 5.1. This is followed by a description of the evolution of the concentration profiles in space and time in Section 5.2. Finally, in Section 5.3, the electrohydrodynamic instabilities in low conductivity liquids are discussed as the basis of a theoretical model explaining the results.

5.0 - EXPERIMENTAL

The studies of ion concentration behaviour in TCNE/DCE solutions were carried out using the sample cells shown in Figure 5.1. Visible or visible/UV Hellma cells with a 1.000 cm path length contained the samples. Al foil electrodes were used in most of the reported measurements. Al foil was chosen as the electrode material in many of these preliminary experiments since it was readily available, disposable and cheap. Pt and In

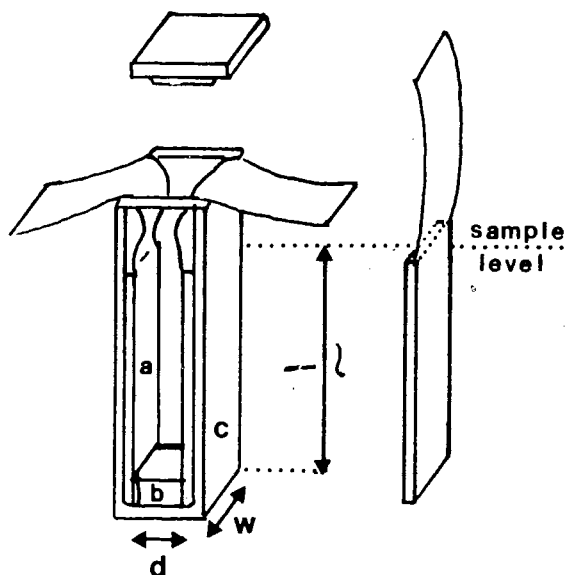
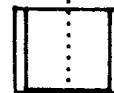
FIGURE 5.1 - SAMPLE CELLS AND ELECTRODES

7

3

Beam position

$$x = d/2$$



a) Aluminum foil electrode

$$A = 2.8 \text{ cm}^2$$

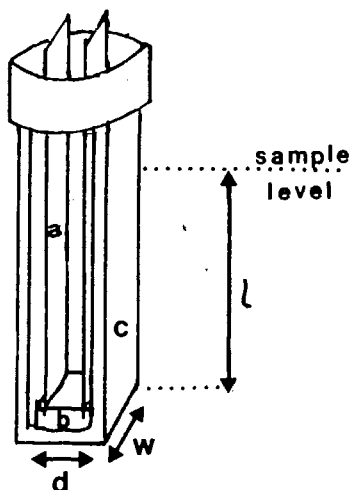
b) Teflon spacer

c) Cuvette (1.000 cm.)

$$d = 7.3 \pm 0.2 \text{ mm}$$

$$w = 8.3 \pm 0.2 \text{ mm}$$

$$l = 34 \pm 2 \text{ mm}$$



a) Platinum electrode

b) Teflon spacer

c) Cuvette (1.000 cm.)

$$d = 6.0 \pm 0.2 \text{ mm}$$

$$w = 6.0 \pm 0.2 \text{ mm}$$

$$l = 24 \pm 2 \text{ mm}$$

electrodes were also used. In electrodes were prepared from a thin sheet of the metal in the same way as the Al electrodes.

Al electrodes were prepared by wrapping foil around glass rectangles for support. Teflon spacers were used to position the electrodes in the cell (Figure 5.1). Note the substantial difference in electrode geometry compared with that in the Pt and In cells described in Chapter 4. The change in geometry was made to accommodate the use of 1 cm. spectroscopic cells. This change was, of course, expected to affect electrohydrodynamic behaviour in the samples.

Each electrode extended outside the cell for electric contacts. Care was taken to keep the foil away from the glass on the inside of the cell above the liquid to minimize sample loss via capillary action. Fresh electrodes were prepared for each experiment. Sample sealing consisted of a teflon cap and a small (1"x1") square of plastic foil which was secured around the top of the cell using teflon tape. The plastic (from Baggies®) did not dissolve in DCE or react with TCNE. The same sealing procedure was used with the In electrode cell. Unfortunately, the Pt electrode cell was more difficult to seal and used only over shorter runs because of evaporation.

Both electric and optical responses were monitored simultaneously. The current through the cell was monitored using a Keithley digital multimeter (model 177) with a chart recorder output. The switching circuit for voltage reversal and cell shorting ($V=0$) is shown in Figure 4.2. Both Cary 17 and

Cary 210 spectrophotometers were used for UV/VIS measurements of optical absorbance versus time or wavelength. The CARY 17 allowed coarse adjustment of the beam position between the electrodes.

The optical responses shown in Figure 5.16 were recorded using apparatus in which the beam position between electrodes could be continuously varied (Figure 5.2). In this case the light source was a Coherent 2000 K Krypton ion laser (413.1 nm, beam width \approx 0.2 mm.). Transmission changes through the sample were monitored by dividing the photomultiplier signals from sample and reference beams after amplification. It was necessary to offset the divider voltage to observe changes in sample transmission in time on a chart recorder. Changes in concentration were estimated from changes in the divider output using

$$\Delta c = (1/B) \log I_0/I = (1/B) \log V_0/V$$

where Δc = change in concentration (M = moles/liter)

B = molar absorption coefficient ($M^{-1}cm^{-1}$)

I = transmitted light intensity

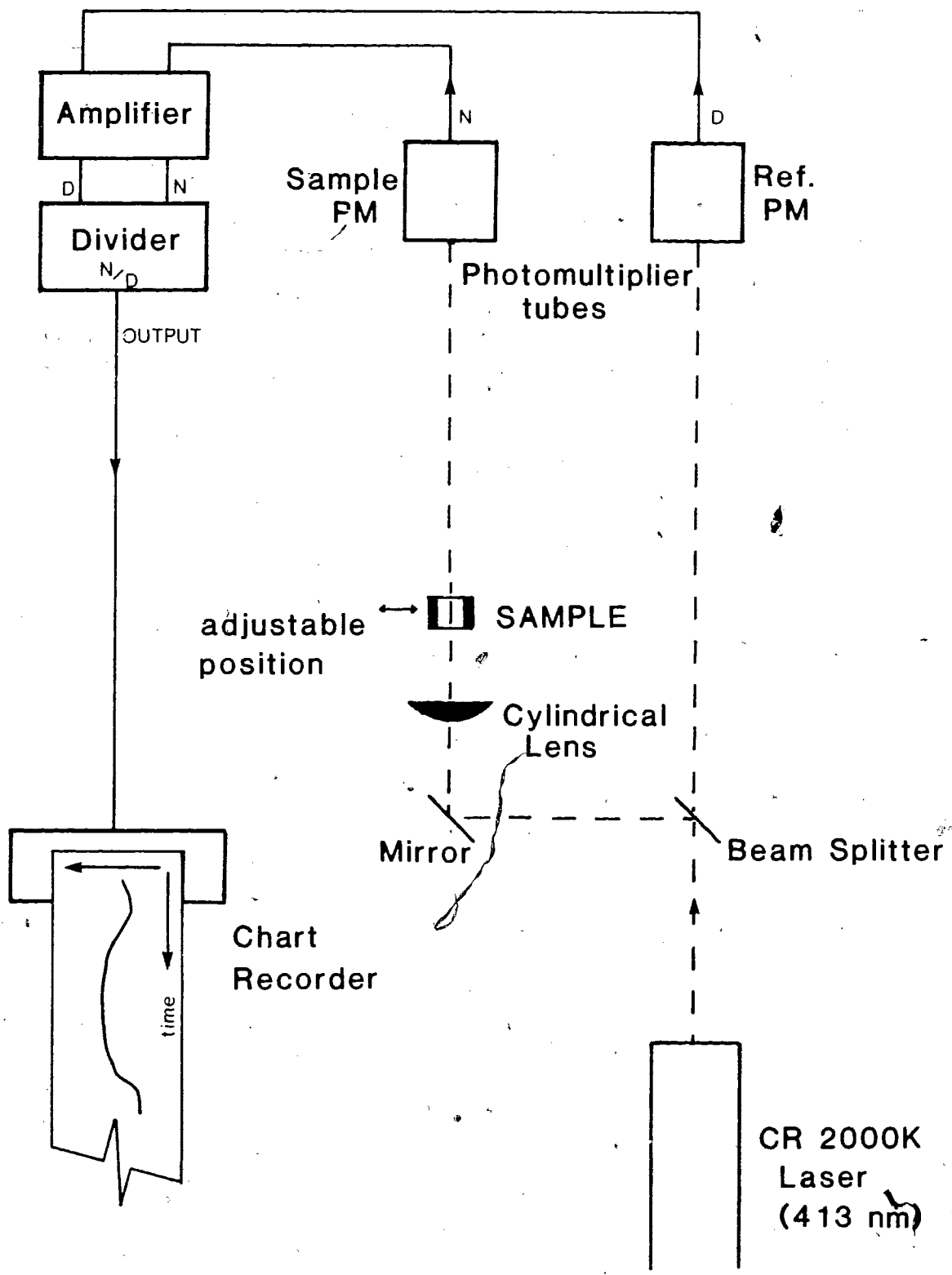
I_0 = reference light intensity

V = divider output (Volts) $\approx I$

V_0 = reference divider output (Volts) $\approx I_0$

I_0 and V_0 were arbitrarily chosen reference values.

FIGURE 5.2 - APPARATUS, SPATIALLY ASYMMETRIC
CONCENTRATION RESPONSE



The plots of transmission profiles in space and time required some alterations of the experimental set up just described (Figure 5.3). A high pressure mercury lamp with an interference filter (415 nm) was used as the light source. The beam was focussed to a width of 0.5 - 1.0 mm. through the sample. A potentiometer readout was arranged to give a measure of the cell position. Plots of divider output vs. beam position were scanned manually in sequence.

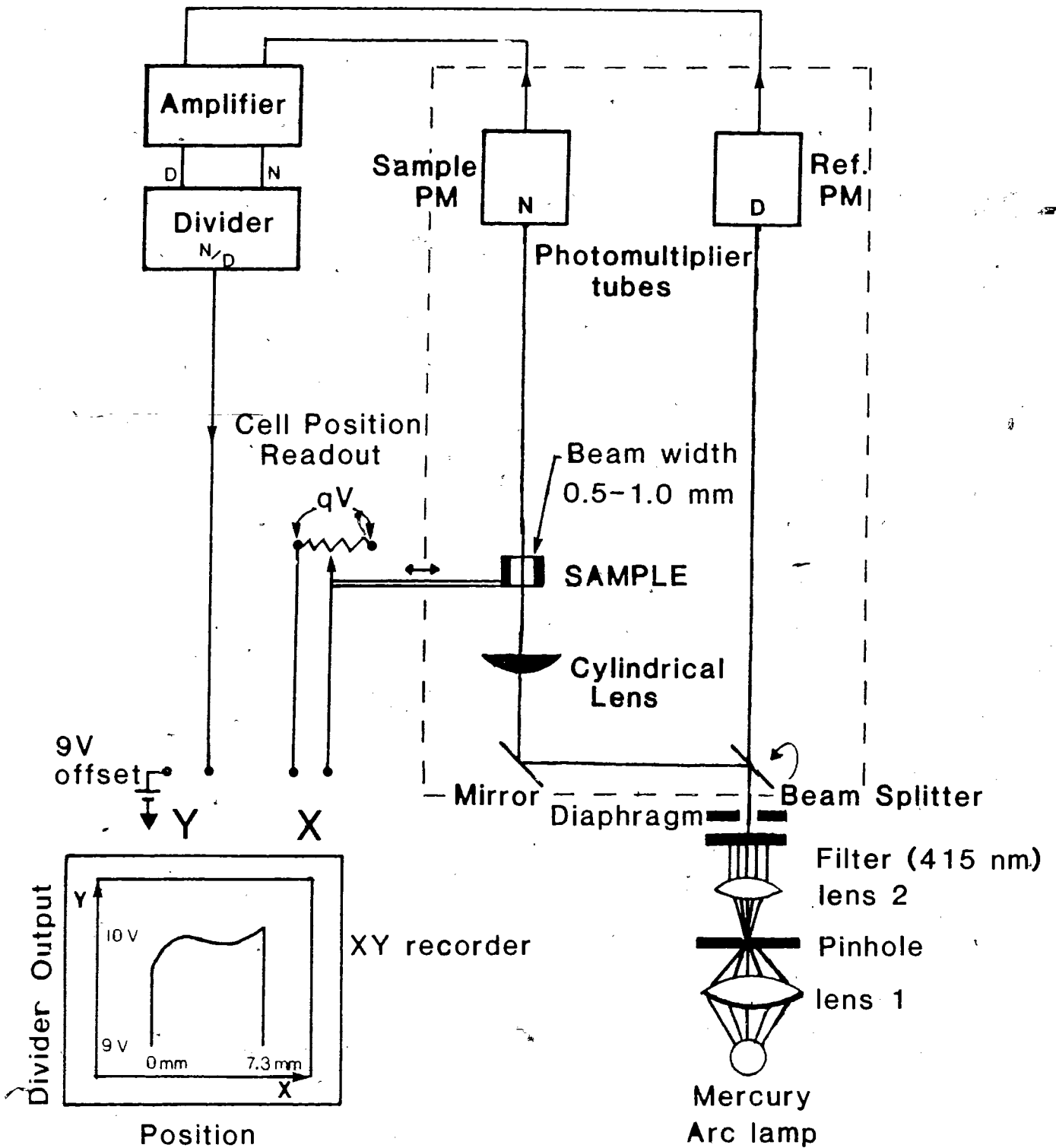
TCNE/DCE sample preparation was already discussed in Chapter 1. For the purpose of comparing spectral and electrical properties of an analogue weak electrolyte solution, samples of a pentacyanopropenide (PCP^-) salt in DCE were prepared. Tetraethylammonium-1,1,2,3,3 pentacyanopropenide ($\text{TEA}^+ \text{PCP}^-$) was prepared according to the method of Middleton et. al.¹ The salt of PCP^- ($\text{TEA}^+ \text{PCP}^-$) dissolved easily in DCE. Pt and Al electrode systems were used in the $\text{TEA}^+ \text{PCP}^-$ /DCE measurements.

5.1.1 - CONCENTRATION VS TIME BEHAVIOUR

The correlation of current response and ion concentration changes verified some of the ideas discussed in Chapter 4 about transient behaviour in the sample resistivity. In this section, the temporal behaviour of ion concentration response at the center of the samples will be discussed. The PCP^- concentration was monitored spectroscopically in the range from 400 to 420 nm where the molar absorption coefficient is $(2.2 \pm 0.1) \times 10^4 \text{ M}^{-1} \text{ cm}^{-1}$



FIGURE 5.3 - APPARATUS, TRANSMISSION PROFILES



(Chapter 6).

Figures 5.4, 5.5 and 5.6 show the response of $\log I_0/I$ vs time (at 415 nm.), after an initial voltage application, and after a voltage reversal. The current response is also shown. The application of voltage to a sample without previous voltage exposure results in an approximately exponential decrease of absorbance in time which is preceded by a short delay time. Except for the delay time, the current and optical absorbance parallel one another. With voltage reversal the optical response again parallels that of the current except for a time lag in the optical response. Both current and absorbance increase to a maximum before decaying to steady state conditions. This type of optical and electric response is characteristic for all TCNE/DCE samples observed. However, the magnitude of absorbance changes is sensitive to sample and electrode preparation, as well as to voltage history.

Optical absorbance changes are a function of the wavelength. A possible contribution by electroconvection to the optical response is assumed negligible compared with the effect of changes in PCP^- ion concentration. Spectral scans of TCNE/DCE solutions at different times during voltage application are shown in Figure 5.7. The two peaks observed at about 400 and 420 nm correspond to peaks in the PCP^- spectrum. Ion concentrations are in the range 10^{-7} - 10^{-6} M. before and during voltage application.

Stable spectra of PCP^- could not be monitored during voltage application

FIGURE 5.4 - LOG I_0/I VS. TIME, CURRENT VS. TIME. (1a, 1b)

Sample: [TCNE] = 0.01 M. in DCE

aluminum electrodes

d = 7.3 mm.

V = 50 Volts

$\lambda = 415$ nm.

137b

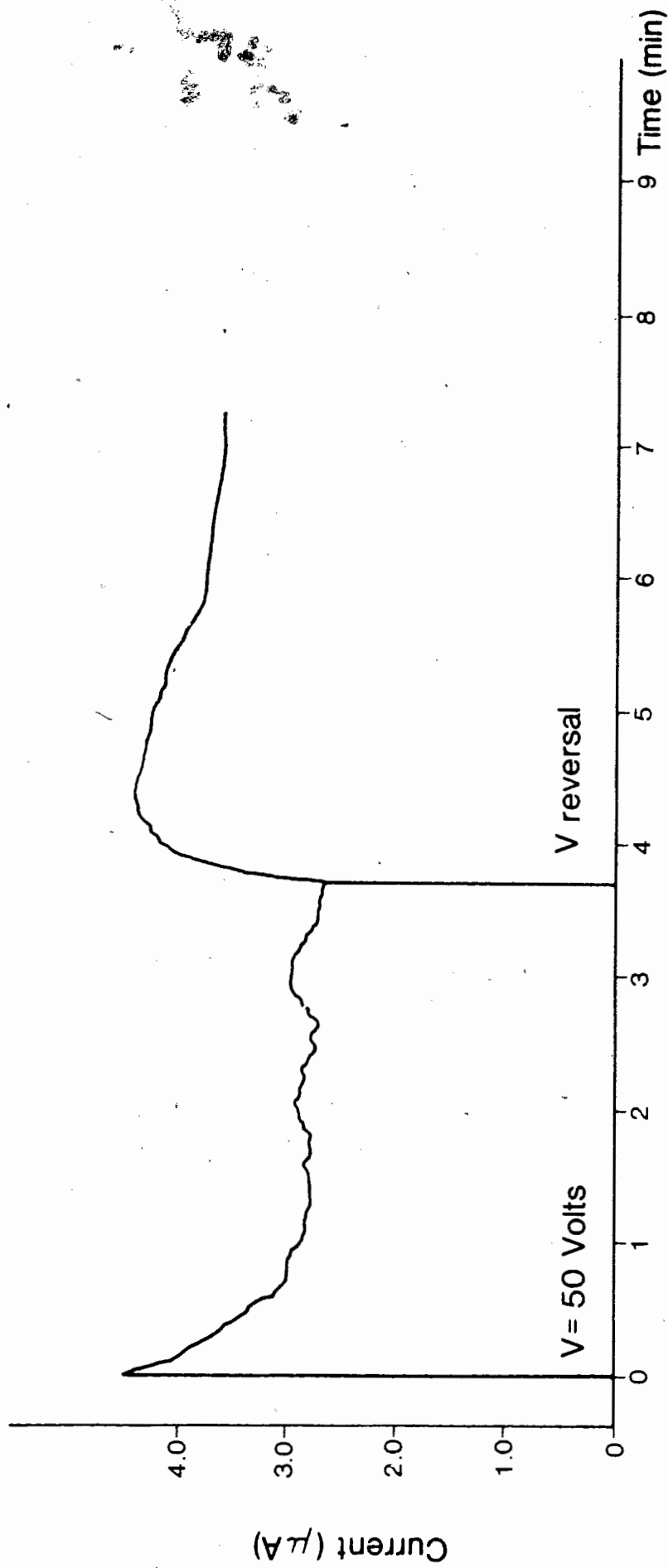
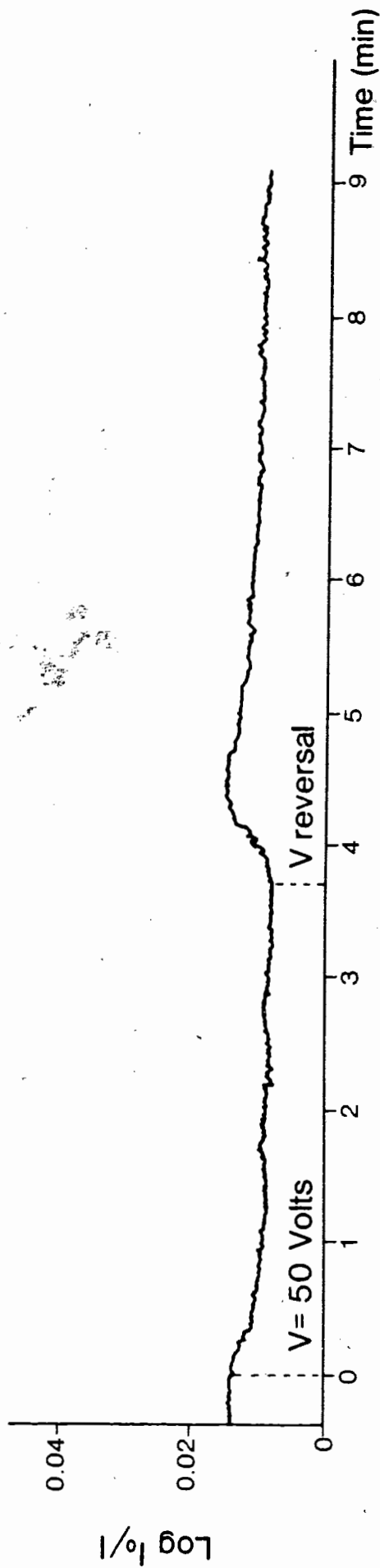


FIGURE 5.5 - LOG I_0/I VS. TIME, CURRENT VS. TIME, (2a)

Sample: [TCNE] = 0.01 M. in DCE

aluminum electrodes

d = 7.3 mm.

V = 50 Volts

$\lambda = 415$ nm.

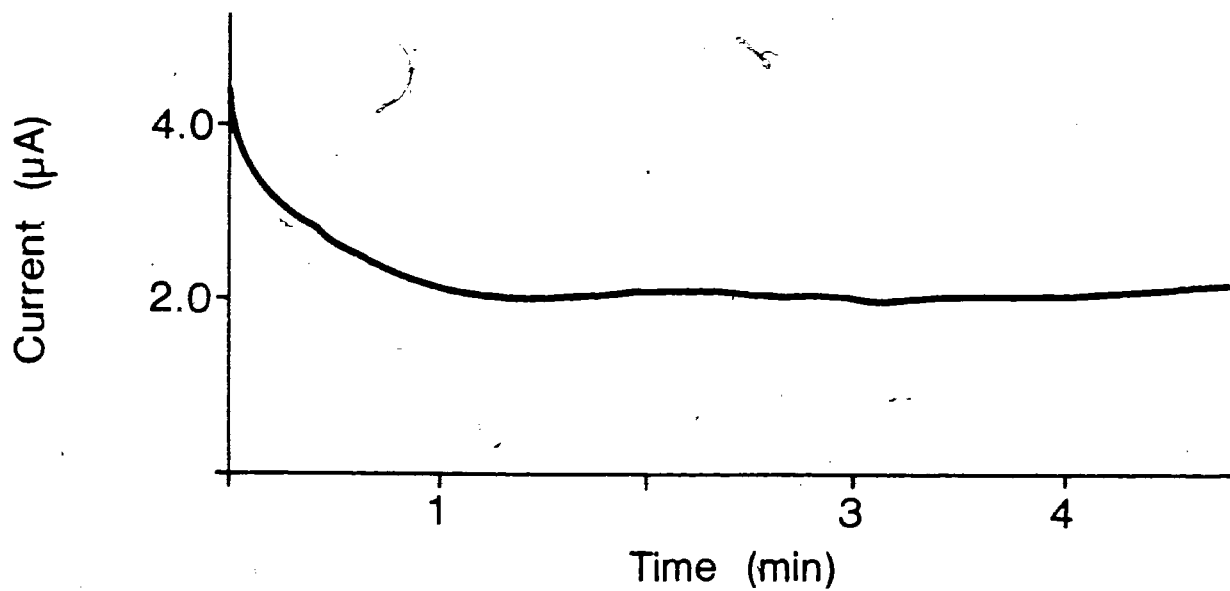
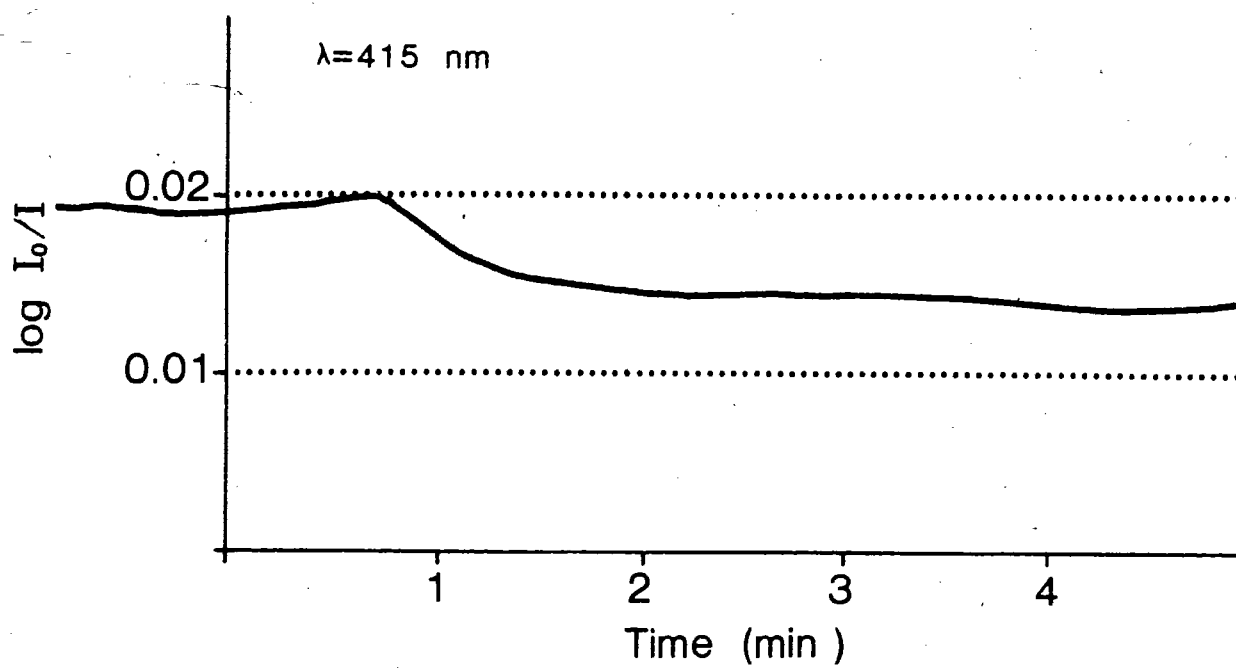
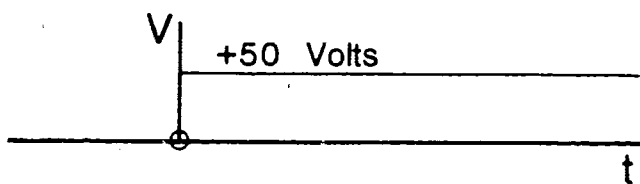


FIGURE 5.6 - LOG I_0/I VS. TIME, CURRENT VS. TIME, (1d)

Sample: [TCNE] = 0.01 M. in DCE

aluminum electrodes

d = 7.3 mm.

V = 50 Volts

λ = 415 nm.

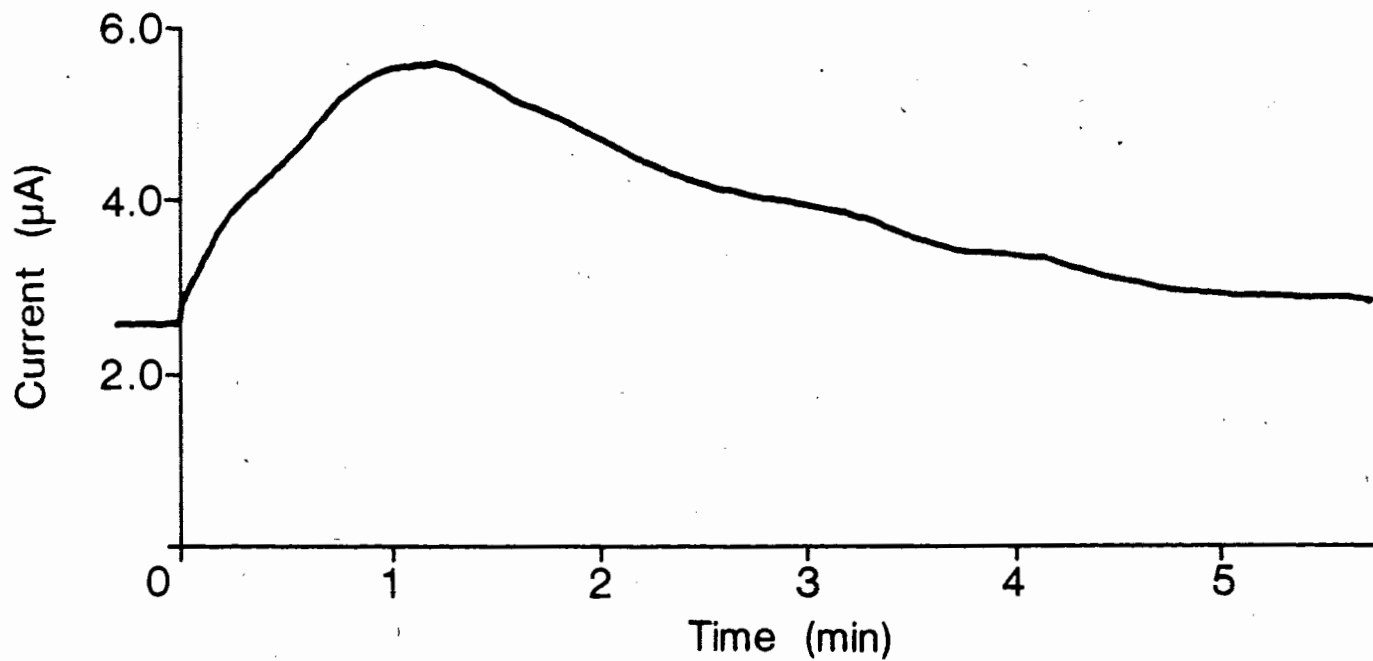
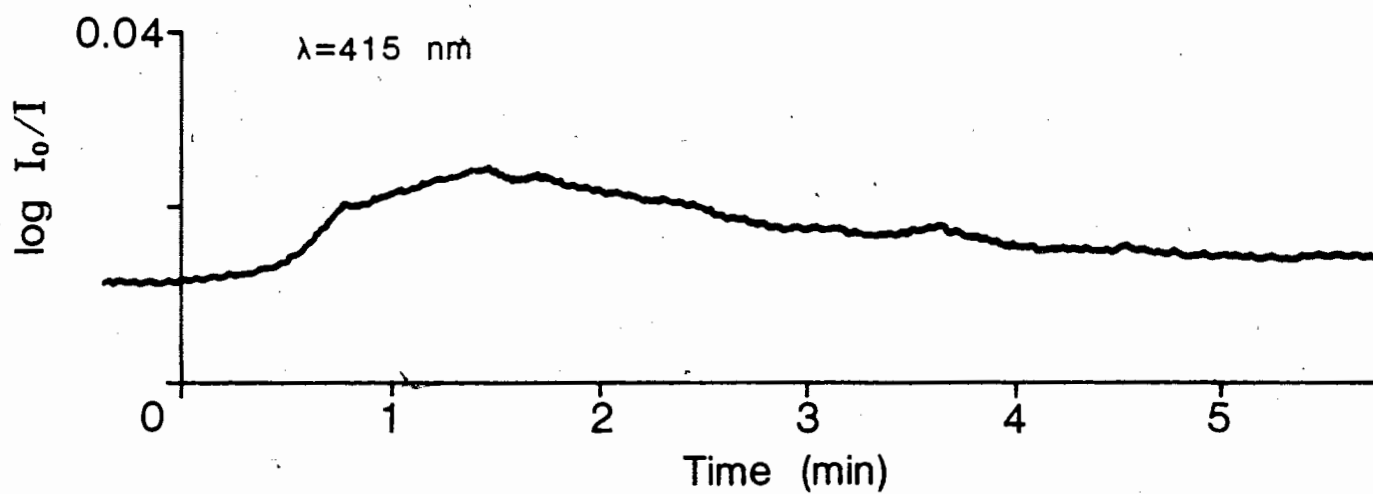
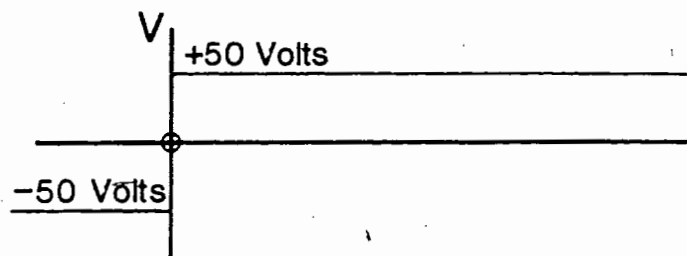


FIGURE 5.7 - ABSORPTION SPECTRUM OF TCNE/DCE
AT DIFFERENT TIMES AFTER VOLTAGE APPLICATION

Sample: [TCNE] = 0.01 M. in DCE

aluminum electrodes

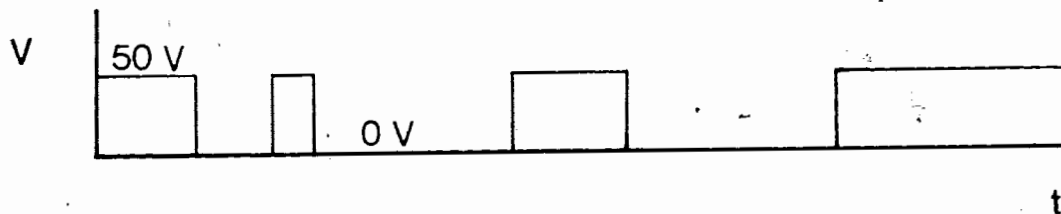
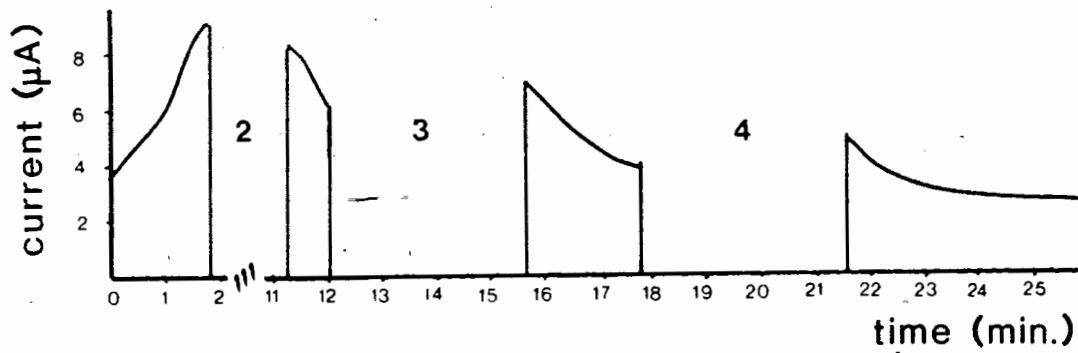
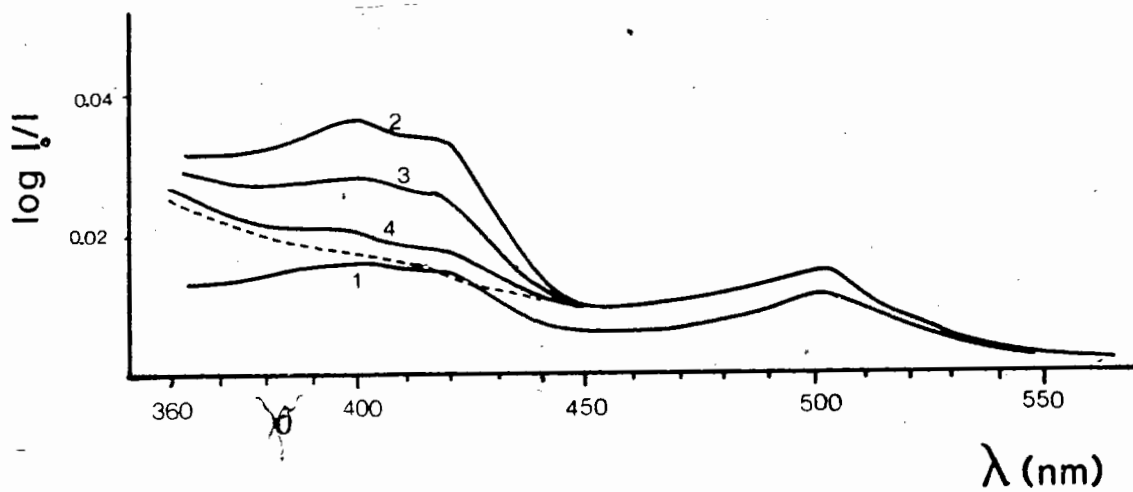
d = 7.3 mm.

V = 50 Volts

SPECTRUM 1: Prior to voltage application

SPECTRUM 2: At the current peak

SPECTRUM 3, SPECTRUM 4: After the current peak



since significant changes in $\log I_0/I$ took place in the time of a spectral scan (≈ 2 minutes). By setting the voltage to zero first, a fairly stable spectrum could be measured at different stages of voltage exposure. The ion concentration at $x = d/2$ stabilizes about a minute after the removal of applied voltage (see Section 5.1.3 for sample response with $V=0$).

An increase in background optical absorbance, particularly at wavelengths shorter than 400 nm., is observed after voltage application (compare scans 1 and 4 in Figure 5.7). It is possible that other non-ionic chromophores were being produced at the electrodes or in the bulk of the solution. Since the voltage was set to zero during scans, electroconvective effects should not have had an influence on the spectral background. Part of the change in background absorption can be attributed to baseline drift.

Table 5.1 shows typical transient times for TCNE/DCE current and optical absorbance with applied voltage. The half-times of the approximately exponential decay in current and optical absorbance agree within the experimental error ($t_{1/2} = 18 \pm 2$ s for $V = 50$ Volts, $d = 7.3 \pm 0.2$ mm. and aluminum electrodes). The delay time is not included in the absorbance half-time. A time of about $3t_{1/2}$ is required to reach steady state (SS) conditions. Characteristic times for the current and absorbance to peak (t_p) also agree within the experimental error for a given trial. t_p was not a constant in different trials with the same applied voltage, cell geometry and TCNE concentration.

TABLE 5.1
DRIFT VELOCITY ESTIMATES FROM
CHANGES IN CURRENT AND CONCENTRATION

Sample: 0.01 M TCNE/DCE
Cell: Aluminum Foil

$$v = \frac{\Delta i}{2Ae\Delta c} = \frac{\Delta i}{B \Delta c}$$

$$V = 50V \quad d = 7.3 \pm 0.3 \text{ mm} \quad B = (54 \pm 0.4) \times 10^4 \text{ A M}^{-1} \text{ m}^{-1} \text{ s}$$

Trial	Decay or Peak	Δi (μA)	Δc (M)	Calculated v (m/s)	Transient time $t_{1/2}$ or t_p (s)
1a	Decay	1.8 ± 0.2	2.7 ± 0.5	12 ± 4	20 ± 5 (i)
	to S. S.		$\times 10^{-7}$	$\times 10^{-5}$	18 ± 3 (c)
1b	peak	17 ± 0.3	32 ± 0.5	10 ± 4	40 ± 10 (i)
			$\times 10^{-7}$	$\times 10^{-5}$	35 ± 5 (c)
1c	peak	2.1 ± 0.2	2.7 ± 0.5	14 ± 5	70 ± 20 (i)
			$\times 10^{-7}$	$\times 10^{-5}$	70 ± 20 (c)
1d	peak	3.2 ± 0.2	5.5 ± 0.6	10 ± 3	65 ± 10 (i)
			$\times 10^{-7}$	$\times 10^{-5}$	70 ± 10 (c)
1e	peak	4.1 ± 0.2	8.2 ± 0.7	9 ± 2	68 ± 6 (i)
			$\times 10^{-7}$	$\times 10^{-5}$	70 ± 10 (c)
2a	decay	2.4 ± 0.2	2.7 ± 0.5	16 ± 4	16 ± 2 (i)
	to ss		$\times 10^{-7}$	$\times 10^{-5}$	18 ± 3 (c)
2b	peak	1.4 ± 0.1	4.1 ± 0.5	6 ± 1	30 ± 10 (i)
			$\times 10^{-7}$	$\times 10^{-5}$	30 ± 10 (c)
3b	peak	2.4 ± 0.1	2.7 ± 0.5	16 ± 5	65 ± 5 (i)
			$\times 10^{-7}$	$\times 10^{-5}$	85 ± 25 (c)
3c	peak	2.3 ± 0.1	4.1 ± 0.1	10 ± 2	65 ± 5 (i)
			$\times 10^{-7}$	$\times 10^{-5}$	60 ± 20 (c)

* the time to reach steady state (ss) current was about $3t_{1/2}$

Note: Delay time not included for t_p (c).

$$v_{\text{avg}} = (11 \pm 5) \times 10^{-5} \text{ m/s}$$

$$\mu = (1.6 \pm 0.7) \times 10^{-6} \text{ m}^2/\text{Vs}$$

$$\left(\text{time to travel } \frac{d}{2} \right) = \frac{d}{2v} = 22-60 \text{ s}$$

The correlation between electric and optical response can be interpreted qualitatively in terms of the effect of ion concentration changes on the effective resistance of the solution. A current maximum results when the number of charge carriers in the bulk of the solution is also at a maximum. At steady state conditions both the current and sample ion concentration are at a minimum. Although a qualitative correlation exists between current and ion concentration, contributions from space charge effects, convection and anisotropic concentration distributions must also be considered in interpreting the current response.

5.1.2 - ION DRIFT VELOCITY ESTIMATES IN TCNE/DCE

Drift velocities are estimated in this section using measured values of the current and PCP^- concentration in TCNE/DCE solutions. It is reasonable to assume that current conduction is dominated by PCP^- and H^+ in TCNE/DCE samples (See Section 5.1.4). Given a homogeneous ion distribution between electrodes, the drift velocity can be expressed as

$$v = i/(2Aec) = j/(2ec)$$

where i = measured current (C s^{-1})

j_c = current density ($\text{C s}^{-1}\text{m}^{-2}$)

A = electrode area (m^2)

e = unit electronic charge = 1.6×10^{-16} C

$2c = c_T = \text{total number of charge carriers } (\bullet/\text{m}^3) = c_- + c_+$

$c \approx \text{measured PCP}^- \text{ concentration } (\bullet/\text{m}^3) \approx c_-$

$c_+ = c_- \text{ in order to maintain charge neutrality}$

$v = \text{effective drift velocity } (\text{ms}^{-1})$

Prior to voltage application and under steady state conditions a homogeneous ion distribution exists. Measurements of ion concentration distribution at the current peak also showed a reasonably even distribution of ions in solution (Section 5.2). These three conditions will be used to estimate ionic drift velocities.

$$v_o = i_o / (2Aec_o)$$

$$v_{ss} = i_{ss} / (2Aec_{ss})$$

$$v_p = i_p / (2Aec_p)$$

where the subscripts refer to the conditions

o = immediately after initial voltage application

ss = at steady state current

p = at the peak current

It is convenient to express drift velocities in terms of concentration differences at different times because of the uncertainty in estimating a

baseline which represents zero concentration.

$$v = \Delta i_{\text{decay}} / (2Ae\Delta C_{\text{decay}})$$

$$v = \Delta i_p / (2Ae\Delta C_p)$$

where

$$\Delta i_{\text{decay}} = i_o - i_{ss}$$

$$\Delta C_{\text{decay}} = C_o - C_{ss}$$

$$\Delta i_p = i_p - i_{ss}$$

$$\Delta C_p = C_p - C_{ss}$$

Table 5.1 shows drift velocity estimates from measured values of Δc and Δi . The calculated values for the drift velocity range from $(6-16) \times 10^{-5} \text{ ms}^{-1}$ with an average of $(11 \pm 5) \times 10^{-5} \text{ ms}^{-1}$. A mobility of $(1.6 \pm 0.7) \times 10^{-8} \text{ m}^2 \text{ V}^{-1} \text{ s}^{-1}$ is calculated from the average drift velocity. This is the same order of magnitude as the mobility of $0.4 \times 10^{-8} \text{ m}^2 \text{ V}^{-1} \text{ s}^{-1}$ estimated in Chapter 4 using peak transient times.

The largest drift velocity estimate is obtained using the measured values of i_o and c_o . For trial #1a (shown in Figure 5.4)

$$c_o = (3.7 \pm 0.6) \times 10^{-7} \text{ M.}$$

$$i_o = 4.5 \pm 0.1 \text{ } \mu\text{A.}$$

giving $v_0 = (2.3 \pm 0.6) \times 10^{-4} \text{ ms}^{-1}$

and $\mu = (3 \pm 1) \times 10^{-8} \text{ m}^2 \text{V}^{-1} \text{ s}^{-1}$

The mobility value of $(3 \pm 1) \times 10^{-8} \text{ m}^2 \text{V}^{-1} \text{ s}^{-1}$ in TCNE/DCE agrees with the effective ionic mobility of $\text{PCP}^- \text{TEA}^+$ in DCE (Section 5.1.4) within the experimental uncertainty. Ions moving with this estimated drift velocity take 18 ± 6 seconds to move halfway across the cell. This corresponds to the halftime for current and concentration decay after voltage application.

The lower effective velocities and mobilities estimated in Table 5.1 can be accounted for qualitatively by considering the effects of space charge after voltage application. Immediately following voltage application, space charge effects are not significant and so the effective field across the bulk of the sample is just proportional to V_{app}/d . In the absence of convective effects, the drift velocity can be written as

$$v = \mu E = \mu V_{\text{eff}}/d = \mu(V_{\text{app}} - V_1^* - V_2^*)/d$$

where $V_1^*, V_2^* =$ electrical boundary layer potentials

The effective voltage across the bulk of the sample decreases as electrical boundary layer potentials V_1^* and V_2^* grow. Thus, since μ and d are constant in the expression above, space charge effects bring about a decrease in the drift velocity after the initial voltage application. Space

charge effects can suppress or enhance the drift velocities calculated from Δi_p and Δc_p in Table 5.1. Following voltage reversal, the electrical boundary layer charges change sign. All of the drift velocities estimated from Δi_p and Δc_p are lower than the value calculated after initial voltage application.

Since the contribution of electrical boundary layers to ion velocities cannot be assessed quantitatively, the tabulated drift velocity values in Table 5.1 are only rough estimates. The effective ionic mobility calculated at conditions immediately following voltage application in TCNE/DCE is compared with the mobility measured in TEA⁺PCP⁻/DCE in the next section.

5.1.3- ELECTRIC AND OPTICAL RESPONSE OF TEA⁺ PCP⁻/DCE

The current response of DCE solutions with a dissolved pentacyanopropenide salt (TEA⁺ PCP⁻ = tetraethylammonium 1,1,2,3,3 pentacyanopropenide) can be interpreted directly in terms of the concentration of PCP⁻ in solution. Figure 5.8 shows the dependence of current on the concentration of TEA⁺PCP⁻ dissolved in DCE. The concentrations of any other ions in solution are insignificant compared with PCP⁻ and TEA⁺. The pure solvent DCE had a conductivity 2 orders of magnitude lower than the samples.

Figures 5.9 and 5.10 show plots of $\log I_0/I$ vs. time and current vs. time for PCP⁻TEA⁺ dissolved in DCE. The PCP⁻ concentrations are similar to those previously observed in TCNE/DCE solutions. Note that the transient behaviour of the current and $\log I_0/I$ is very similar to that of TCNE/DCE solutions, except that the ratio of peak to steady state currents is greater in TEA⁺ PCP⁻/DCE samples. The presence of TCNE in DCE provides possible mechanisms for the continuous generation of PCP⁻ in the bulk of the solution and at the cathode [i.e. (TCNE + H₂O → PCPH → PCP⁻ + H⁺) and (TCNE + e⁻ cathode → TCNE⁻ + H₂O or O₂ → PCP⁻)]. For this reason, the steady state PCP⁻ concentration in TCNE/DCE solutions is expected to be higher than that observed in TEA⁺ PCP⁻/DCE samples.

The observed transient times for the optical and electric response of TEA⁺PCP⁻/DCE are shown in Table 5.3. The qualitative correlation between

FIGURE 5.8 - CURRENT (i_0) vs. $[TEA^+ PCP^-]$ in DCE

platinum electrodes

$d = 9.0$ mm.

$V = 20$ Volts

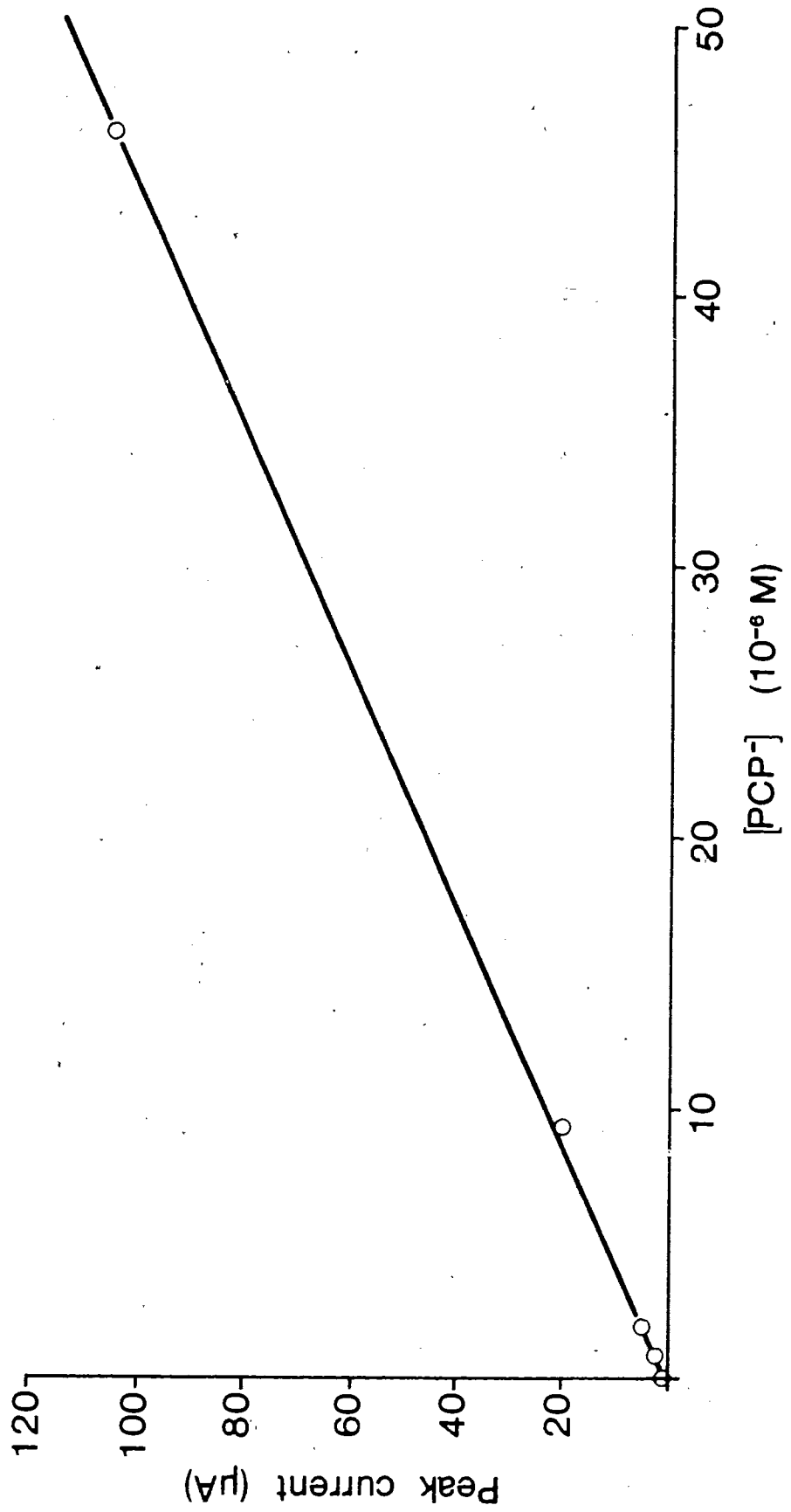


FIGURE 5.9 - LOG I_0/I VS. TIME, CURRENT VS. TIME

Sample: $[\text{TEA}^+\text{PCP}^-] = 2.1 \times 10^{-6} \text{ M.}$

platinum electrodes

$d = 9.0 \text{ mm.}$

$V = 10 \text{ Volts}$

$\lambda = 400 \text{ nm.}$

150b

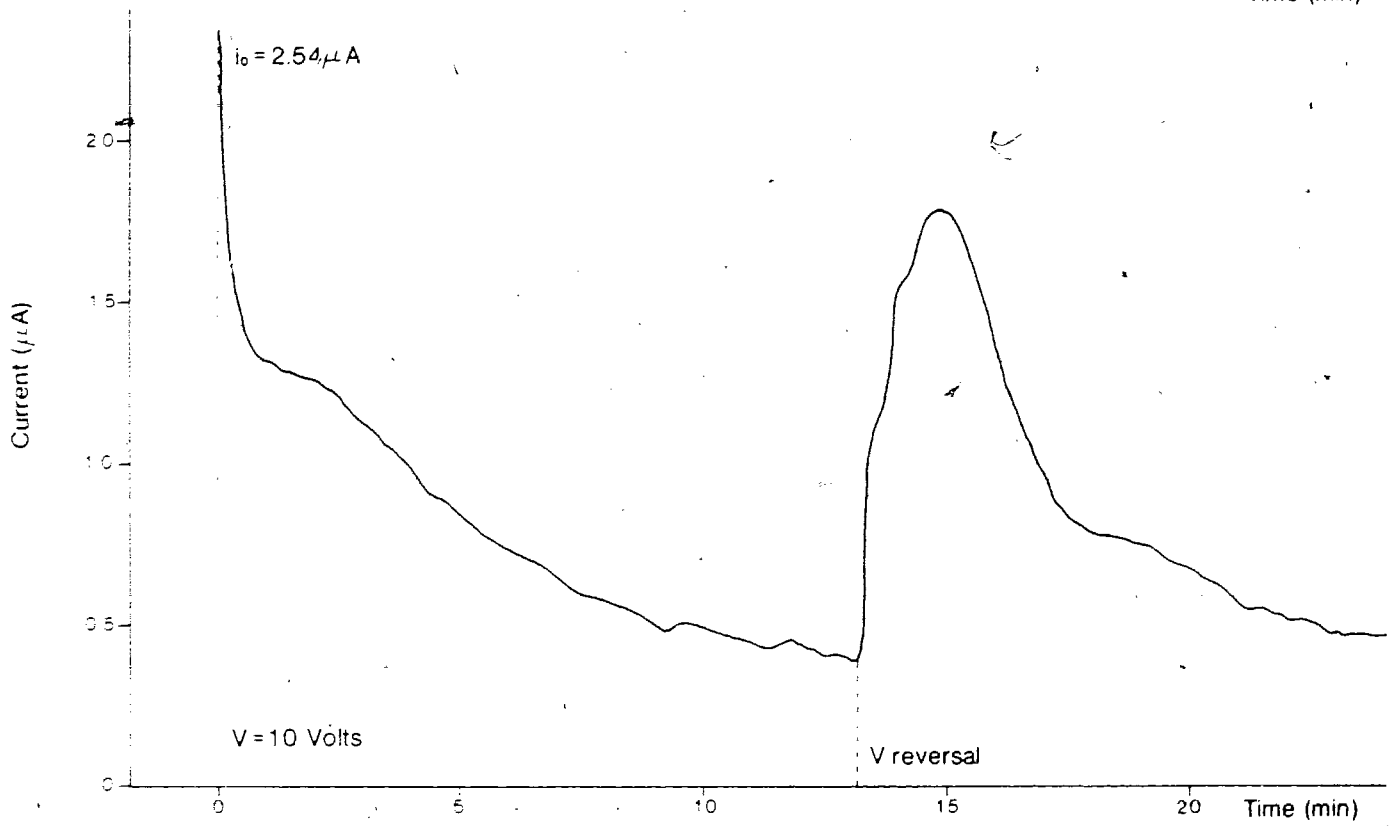
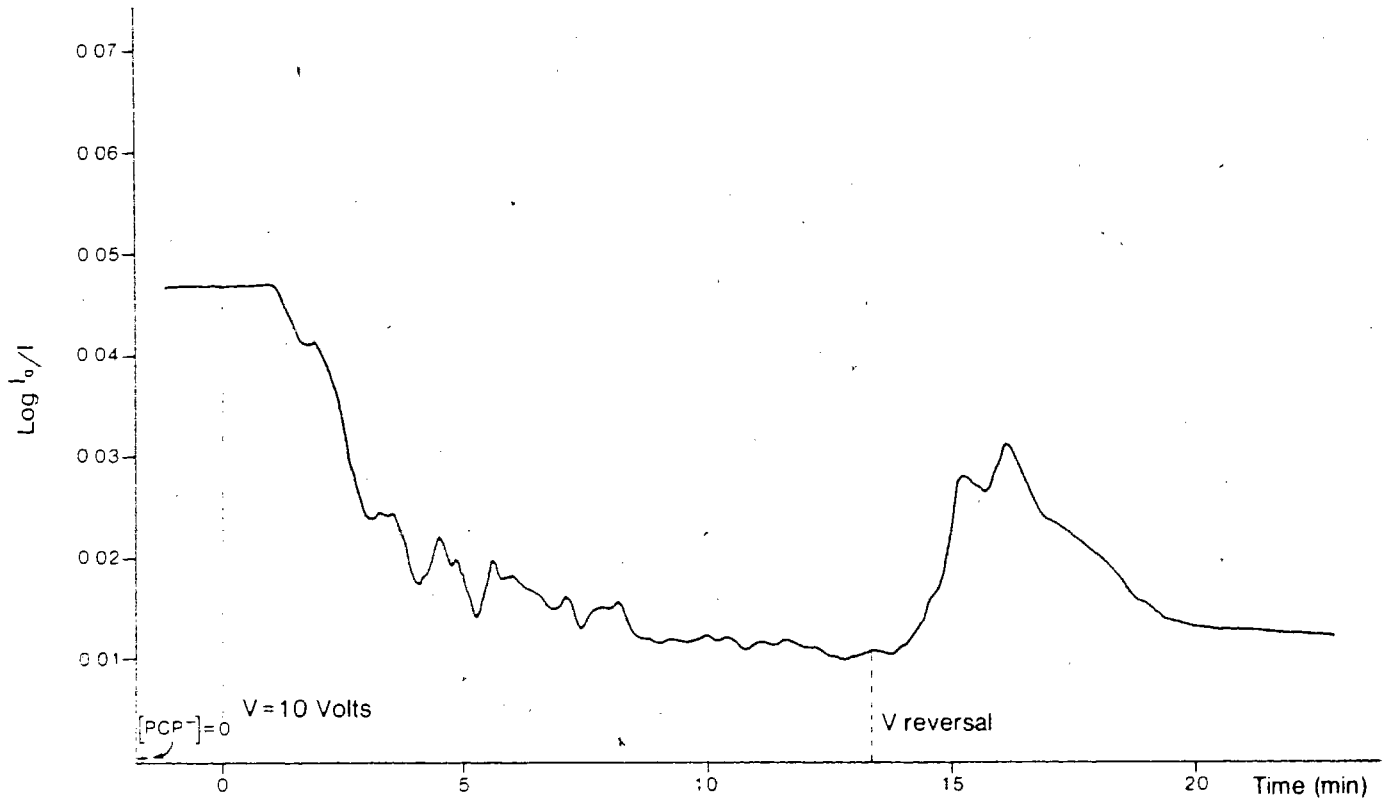


FIGURE 5.10 - LOG I_0/I VS. TIME, CURRENT VS. TIME,

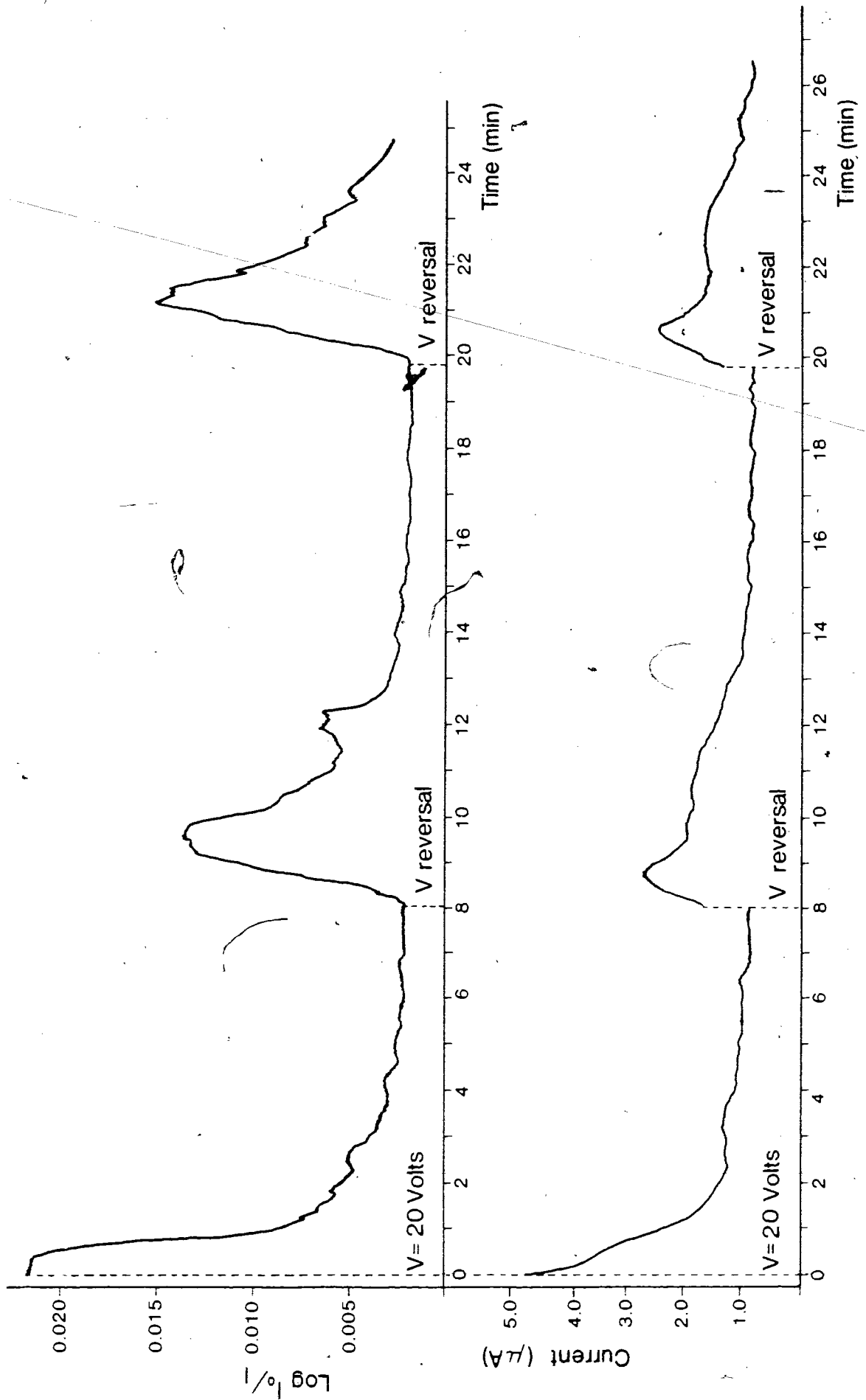
Sample: $[\text{TEA}^+\text{PCP}^-] = 2.1 \times 10^{-6} \text{ M.}$

aluminum electrodes

$d = 7.3 \text{ mm.}$

$V = 20 \text{ Volts}$

$\lambda = 400 \text{ nm.}$



Handwritten mark

optical and electric response remains, except that the current peaks earlier than the ion concentration. The peak times decrease with increasing voltage.

Table 5.3 shows drift velocity estimates for TEA⁺PCP⁻/DCE samples. Changes in the current and optical absorbance (Δi , Δc) are used in these estimates. Table 5.2 shows estimates of drift velocities using absolute current and concentration measurements (i , c). A comparison of drift velocities v_o , v_p and v_{ss} in the Pt electrode system demonstrates evidence of space charge effects. The steady state drift velocity is smaller than that observed after initial voltage application. This is consistent with the effective voltage across the sample being reduced via space charge effects. In both electrode systems v_o and v_p have similar values.

An enhancement of the steady state drift velocity is observed in the Al electrode system. The steady state drift velocity is about double v_o . A simple explanation for this effect is that convection contributes to ion transport in the system at steady state conditions

Mobilities calculated from i_o and c_o in both electrode systems agree within the experimental uncertainty. For TEA⁺PCP⁻/DCE solutions.

$$\mu_{Al} = (4.0 \pm 0.9) \times 10^{-8} \text{ m}^2 \text{ V}^{-1} \text{ s}^{-1}$$

TABLE 5.2
DRIFT VELOCITY ESTIMATES FROM CURRENT AND CONCENTRATION DATA

Sample: TEA⁺PCP⁻/DCE Cell#1: Platinum, d = 9.0 ± 0.2mm
Cell#2: Aluminum, d = 7.3 ± 0.2mm

Electrodes; Applied Voltage	i_o (μA)	c_o (M)	v_o (m/s)	μ (m ² /Vs)
Platinum 10V	2.54 ± 0.05	2.1 ± 0.1 x 10 ⁻⁶	4.3 ± 0.6 x 10 ⁻⁵	3.9 ± 0.7 x 10 ⁻⁸
Aluminum 20V	5.4 ± 0.4	9.5 ± 0.7 x 10 ⁻⁷	11 ± 2 x 10 ⁻⁵	4.0 ± 0.9 x 10 ⁻⁸

Electrodes; Applied Voltage	i_{ss} (μA)	c_{ss} (M)	v_{ss} (m/s)
Platinum 10V	0.39 ± 0.03	4.5 ± 0.5 x 10 ⁻⁷	1.6 ± 0.3 x 10 ⁻⁵
Aluminum 20V	0.88 ± 0.08	7 ± 2 x 10 ⁻⁸	2.3 ± 0.1 x 10 ⁻⁴

Electrodes; Applied Voltage	i_{ss} (μA)	c_p (M)	v_p (m/s)	
Platinum 10V	1.82 ± 0.02	1.36 ± 0.08 x 10 ⁻⁶	4.8 ± 0.7 x 10 ⁻⁵	
Aluminum 20V	2.7 ± 0.08	5.9 ± 0.4 x 10 ⁻⁷	9 ± 2 x 10 ⁻⁵	*1
Aluminum 20V	2.6 ± 0.1	6.5 ± 0.4 x 10 ⁻⁷	7 ± 1 x 10 ⁻⁵	*2

$$v = (i / B c) \text{ where } B_{Pt} = (2.8 \pm 0.2) \times 10^4 \text{ sA/Mm}$$

$$B_{Al} = (5.4 \pm 0.4) \times 10^4 \text{ sA/Mm}$$

* c_p values used at $t_p = 80s$ would have resulted in artificially low values of the drift velocity.

$$c_p^{\#1} = (3.4 \pm 0.6) \times 10^{-7} \text{ M} \quad v^{\#1} = (1.5 \pm 0.4) \times 10^{-4} \text{ m/s}$$

$$c_p^{\#2} = (3.6 \pm 0.6) \times 10^{-7} \text{ M} \quad v^{\#2} = (1.3 \pm 0.3) \times 10^{-4} \text{ m/s}$$

TABLE 5.3
DRIFT VELOCITY ESTIMATES FROM
CURRENT AND CONCENTRATION CHANGES

Sample: TEA⁺PCP⁻/DCE Cell#1: Platinum, d = 9.0 ± 0.2mm
Cell#2: Aluminum, d = 7.3 ± 0.2mm

Electrodes; Voltage	Decay or Peak	i_0 (μA)	c_0 (M)	CALCULATED v_{drift} (m/s)	transient times $t_{1/2}$, t_p
Platinum 10V	decay to SS	2.15 ± 0.08	1.7 ± 0.1 × 10 ⁻⁶	4.5 ± 0.8 × 10 ⁻⁵	*40 ± 5 100 ± 10
	Peak	5.4 ± 0.4 × 10 ⁻⁷	9.5 ± 0.7 × 10 ⁻⁵	11 ± 2 × 10 ⁻⁸	4.0 ± 0.9

From Table 5.2: $v_0 = (4.3 ± 0.6) × 10^{-5}$ m/s

Time to travel d/2 is approximately 105 seconds.

* A slower decay time was superimposed on the current response.

	Decay to ss	4.5 ± 0.5	8.8 ± 0.9 × 10 ⁻⁷	9 ± 3 × 10 ⁻⁵	45 ± 6 25 ± 2
Aluminum 10V	Peak #1	1.8 ± 0.1	** 5.2 ± 0.6 × 10 ⁻⁷	6 ± 2 × 10 ⁻⁵	40 ± 10 80 ± 10
	Peak #2	1.7 ± 0.1	** 5.9 ± 0.4 × 10 ⁻⁷	5 ± 1 × 10 ⁻⁵	40 ± 10 80 ± 10

From Table 5.2: $v_0 = (11 ± 2) × 10^{-5}$ m/s

Time to travel d/2 is approximately 33 seconds.

** Δc_p values used at $t_p = 80$ s after voltage reversal and resulted in artificially low values of v .

At $t_p = 40$ s:

$$\Delta c_{O_1} = (3.4 ± 0.6) × 10^{-7} \text{ M} \quad v_{O_1} = (1.5 ± 0.4) × 10^{-4} \text{ m/s}$$

$$\Delta c_{O_2} = (3.6 ± 0.6) × 10^{-7} \text{ M} \quad v_{O_2} = (1.3 ± 0.3) × 10^{-4} \text{ m/s}$$

$$\mu_{Pt} = (3.9 \pm 0.7) \times 10^{-8} \text{ m}^2 \text{V}^{-1} \text{s}^{-1}$$

These values also compare well with the ionic mobility of $(3 \pm 1) \times 10^{-8} \text{ m}^2 \text{V}^{-1} \text{s}^{-1}$ in TCNE/DCE.

The dominant negative charge carrier in TCNE/DCE and TEA⁺PCP⁻/DCE is PCP⁻. The positive charge carriers in the samples are H⁺ and TEA⁺, respectively. The cationic mobilities are similar judging by the agreement between measured effective ionic mobilities in both samples [$\mu = (\mu_- + \mu_+)/2$].

5.1.4 - PCP⁻ AND TCV⁻ CONTRIBUTIONS TO CONDUCTION

Both PCP⁻ and tricyanovinylalcoholate (TCV⁻) are ions produced by the reaction of TCNE with water. The effective basicity of a solution influences which of the two ions is more likely to be produced (See Chapter 6). A DCE sample with observable concentrations of both PCP⁻ and TCV⁻ was prepared by first reacting TCNE in deionized water followed by ultrasonic mixing of 10 μ l of this solution with DCE. Using this technique, no neutral TCNE remains in solution and the ultraviolet spectral absorbance can be monitored easily. Figure 5.11 shows the solution spectrum of this sample before voltage application and the TCV⁻ and PCP⁻ bands, at 296 and 410 nm. respectively (Chapter 6), are clearly displayed. The concentration of PCP⁻ in the TCNE-H₂O/DCE sample is in the same range [$(4.2 \pm 0.3) \times 10^{-7}$ M.] as in the 0.01 TCNE/DCE solutions. The TCV⁻ concentration in the

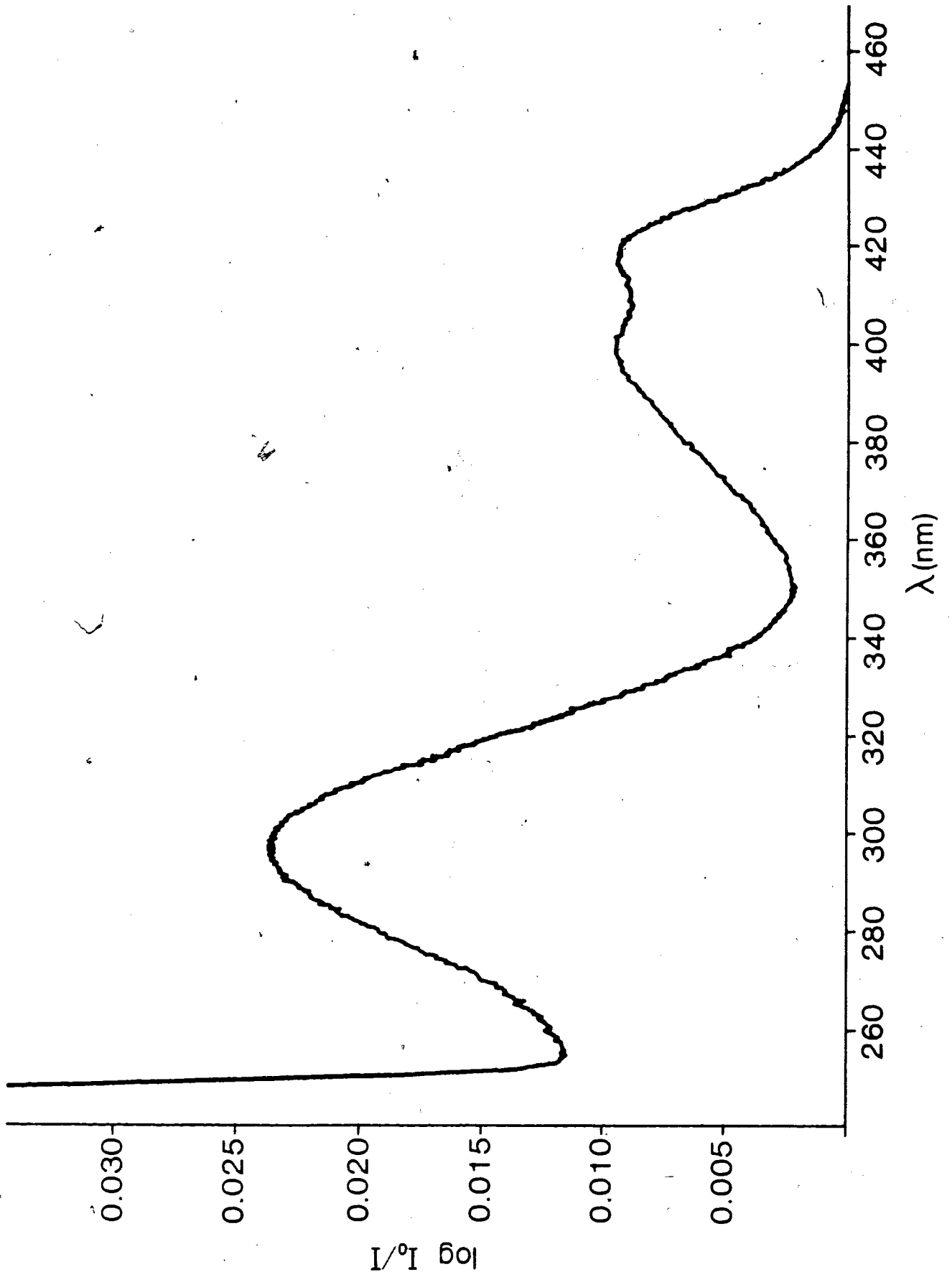
FIGURE 5.11 - SPECTRUM OF TCNE- H₂O/DCE

298 nm peak: $[TCV^-] = (2.1 \pm 0.2) \times 10^{-6} \text{ M}$

400 nm peak: $[PCP^-] = (4.2 \pm 0.3) \times 10^{-7} \text{ M}$

**TOTAL ANION
CONCENTRATION = $(2.5 \pm 0.2) \times 10^{-6} \text{ M}$**

156b



TCNE-H₂O/DCE sample is about 5 times that of PCP⁻ or $(2.1 \pm 0.2) \times 10^{-6}$ M. (using $B_{\text{tov}} = 1.1 \times 10^4 \text{ M}^{-1} \text{ cm}^{-1}$)².

A sample current of $i_0 = 16.0 \pm 0.5 \mu\text{A}$ was observed after initial voltage application ($V = 20$ Volts). The 296 nm. peak decays with time after voltage application. The contribution of TCV⁻ and PCP⁻ ions to the conductivity of TCNE-H₂O/DCE samples depends on the relative ionic mobilities. The equivalent conductance of PCP⁻ salt and TCV⁻ salt solutions are within 6% of one another³. Therefore the mobilities of PCP⁻ and TCV⁻ should also agree within 6% in these solutions. The effective ionic mobility estimated experimentally in TCNE-H₂O/DCE containing both TCV⁻ and PCP⁻ should be similar to mobilities calculated using TCNE/DCE and PCP⁻TEA⁺/DCE solutions.

As earlier mentioned, the drift velocity and effective mobility can be calculated using

$$v = \mu_{\text{eff}} E = i_0 / (2eAc_0)$$

$$\mu_{\text{eff}} = i_0 / (2eAc_0 E)$$

where $c_0 = c_{\text{pcp}} + c_{\text{tcv}}$

Estimating the ionic mobility as shown above gives a value of $(4 \pm 1) \times 10^{-8} \text{ m}^2 \text{ V}^{-1} \text{ s}^{-1}$ which agrees with the values obtained from other samples with

only PCP^- as a negative charge carrier.

The experimental observations are consistent with the additivity of PCP^- and TCV^- current contributions. It is therefore reasonable to conclude that the concentration of TCV^- in TCNE/DCE solutions under study is insignificant. If this had not been the case, the effective mobilities calculated from $[\text{PCP}^-]$ in TCNE/DCE would have been higher than that observed in $\text{TEA}^+\text{PCP}^-/\text{DCE}$, or TCNE- $\text{H}_2\text{O}/\text{DCE}$. Thus, although the absence of TCV^- in TCNE/DCE could not be verified by other means, the solutions behaved as if only PCP^- and its counterion contributed to conduction.

5.1.5 - RELAXATION OF CONCENTRATION WITH $V = 0$ IN TCNE/DCE

Variation of ion concentration in time with the removal of the applied voltage is shown in Figures 5.12 and 5.13. Figure 5.12 shows the effect of setting the voltage to zero after steady state current conditions (Apparatus is shown in Figure 5.2). About an hour is required to increase the ion concentration from c_{ss} to c_0 . The long time constant for the concentration change indicates a diffusion driven process.

Figure 5.13 shows the effect of setting the applied voltage to zero at non-steady state conditions in the cell. A Cary 17 spectrophotometer was used in these measurements. In each of the three examples the concentration at the center of the cell oscillates for one to two minutes

FIGURE 5.12 - $\Delta(\text{LOG } I_0/I)$ VS. TIME
VOLTAGE SET TO ZERO AFTER 20 V TREATMENT

Sample: [TCNE] = 0.02 M. in DCE

aluminum electrodes

d = 7.3 mm.

λ = 413 nm.

The absorbance after 60 minutes is comparable to the sample absorbance prior to voltage application.

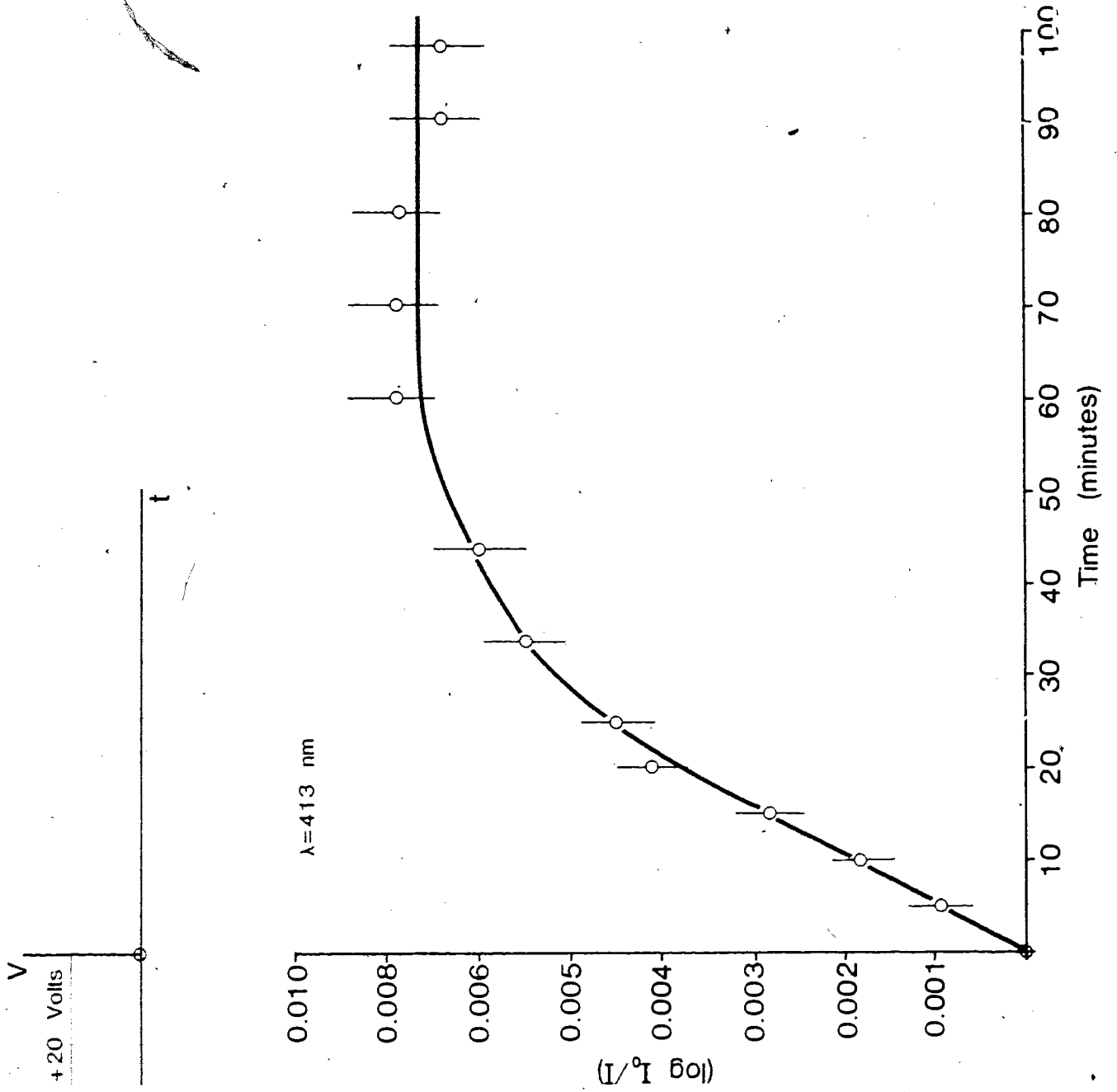


FIGURE 5.13 - (LOG I_0/I) VS. TIME

VOLTAGE SET TO ZERO BEFORE STEADY STATE

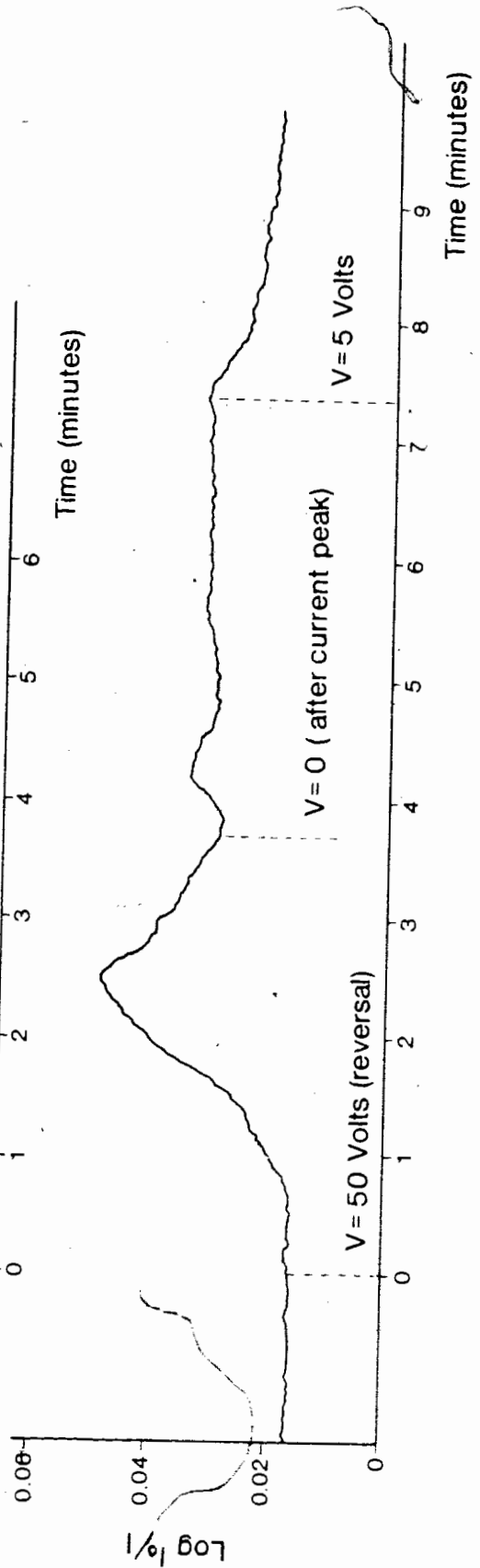
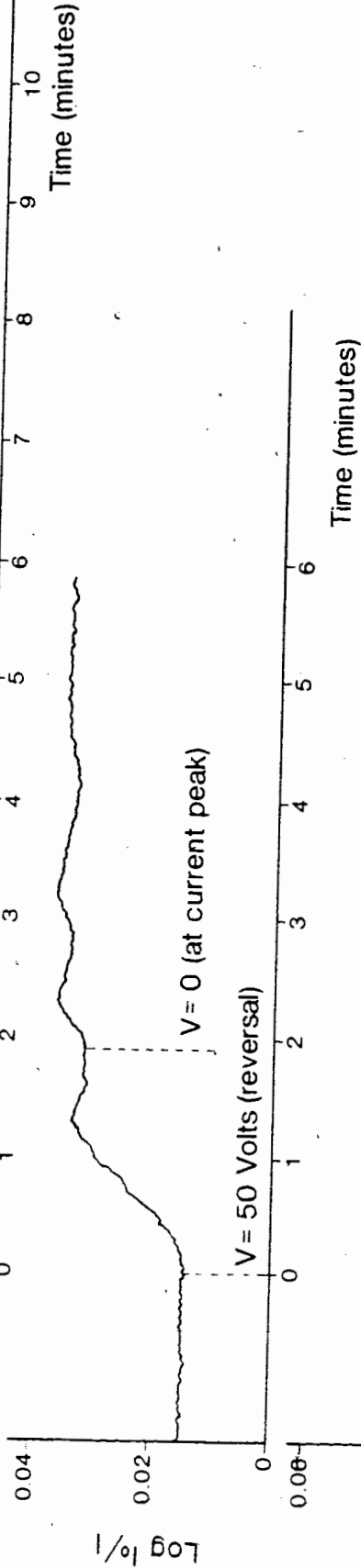
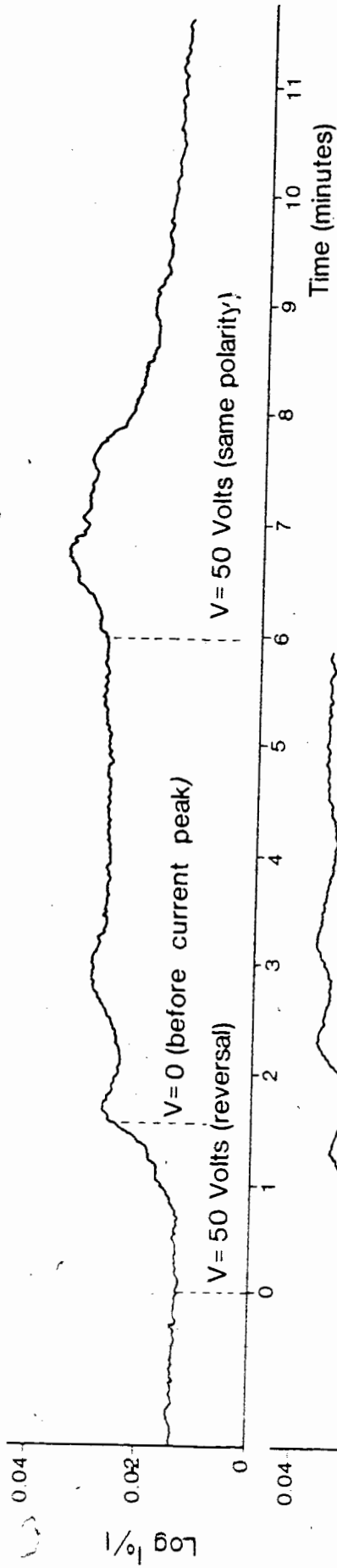
(open circuit)

Sample: [TCNE] = 0.01 M in DCE

aluminum electrodes

d = 7.3 mm.

λ = 415 nm.



before settling to a value very close to that observed at the time of voltage removal. The oscillation lasts somewhat longer when the voltage application is interrupted at the current peak. When the oscillations die down, diffusion processes dominate any further changes in the ion concentration. The source of the temporary instability in ion concentrations after voltage removal may be related to the relaxation of electrical boundary layers and space charge in solution, and/or to the dying down of convection flow patterns.

5.1.6 - CONCENTRATION GRADIENTS IN SOLUTION

The effect of ion concentration gradients on drift velocity and current response will be discussed in this section. The observation of transient concentration behaviour in solution requires, according to Fick's law, the presence of concentration gradients:

$$\partial c / \partial t = D \partial^2 c / \partial x^2$$

where D = diffusion coefficient (m^2/s)

Other experimental evidence supporting the existence of concentration gradients in solution includes the effect of external mixing on sample current response (Chapter 4).

In the estimates of drift velocity, a uniform ion concentration distribution was assumed under certain conditions. In general, however, the

concentration has to be considered a function of position and time. At a given time, the drift velocity will also generally be a function of position in order to maintain a constant current flux throughout the sample.

$$j = 2Aec(x)v(x) = \text{constant}$$

A drift velocity estimated using concentration measurements at a particular value of x applies only to that position.

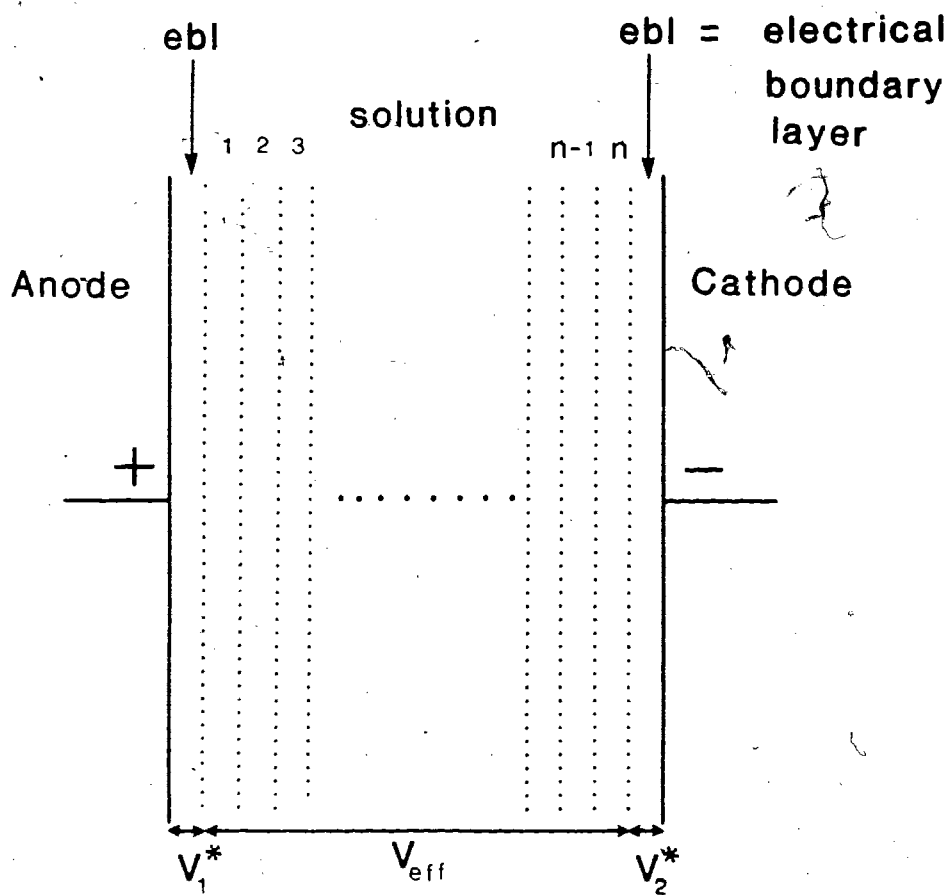
The dependence of concentration on position must be included in a discussion of the current response. The greatest contribution to sample resistance arises from that portion of the solution having the fewest charge carriers. The total resistance of the solution is given by summing resistances $R_i(x,t)$ of individual layers of solution between the electrodes (See Figure 5.14).

$$\begin{aligned} R(t) &= \sum_i R_i = \sum \Delta x_i / (K_i A) = \sum \Delta x_i / (\Delta_{eq} c^*(x,t) A) \\ &= 1 / (\Delta_{eq} A) \int^d (1/c^*(x,t)) dx \end{aligned}$$

$$\begin{aligned} \text{OR} &= \sum \Delta x_i / (2e\mu c_i(x,t) A) \\ &= 1 / (2e\mu A) \int^d (1/c(x,t)) dx \\ &= (\text{constant}) \int^d (1/c(x,t)) dx \end{aligned}$$

where R_i = resistance of i^{th} fluid layer (Ω)

FIGURE 5.14 - SOLUTION RESISTANCE



$$R_{total} = \sum_{i=1}^n R_i$$

$$V = V_1^* + V_2^* + V_{eff}$$

Δx_i = thickness of i^{th} fluid layer (m)

K_i = conductance of i^{th} fluid layer ($\Omega^{-1} \text{m}^{-1}$)

A = electrode area (m^2)

Δ_{eq} = equivalent conductance of solution ($\Omega^{-1} \text{m}^{-1} (\text{equiv} \text{m}^{-3})^{-1}$)

μ = effective mobility of ions in solution

$c^*(x,t)$ = equivalent concentration ($\text{equiv} \text{m}^{-3}$)

$2c_i(x,t)$ = total ion concentration, i^{th} layer at x and t ($*/\text{m}^3$)

$c_+ = c_- = c_i(x,t)$

and $R_i = \Delta x_i / (K_i A) = \Delta x_i / (2 \Delta_{\text{eq}} c^*(x,t) A) = \Delta x_i / (2 e c_i \mu A)$

Using this expression for the resistance, the current can be written according to this model as

$$i(t) = \frac{(V_{\text{app}} - V_1^*(t) - V_2^*(t)) (2e\mu A)}{\int_0^d (1/c(x,t)) dx}$$

$$\text{or } i(t) = \frac{(V_{\text{app}} - V_1^*(t) - V_2^*(t)) (\Delta_{\text{eq}} A)}{\int_0^d (1/c^*(x,t)) dx}$$

Convective effects can be included by introducing a new effective mobility $\mu(x,t,V)$.

In order to predict the current response in our samples, information on the magnitude and transient behaviour of electrical boundary layers is required. The variation of concentration in space and time also has to be mapped. In Section 5.2 some measurements of the evolution of concentration profiles in space and time will be discussed.

5.2.1 - SPATIAL CONCENTRATION BEHAVIOUR IN TIME

In this study the current response of organic solutions has been interpreted qualitatively in terms of the transient behaviour of sample ion concentration. Some features of ion concentration distributions in solution, such as the magnitude of concentration gradients, and the nature of concentration instabilities, can be observed directly by monitoring PCP^- concentration as a function of position and time.

With voltage application an initially homogeneous distribution of ion concentration evolves and develops spatial asymmetry. When the optical response (415 nm.) of a TCNE/DCE/Al system is monitored at a position closer to one electrode than the other, consecutive voltage reversals demonstrate asymmetry in ion concentration changes with respect to the anode and cathode. The optical responses are shown in Figures 5.15 and 5.16 and were measured using the CARY 17 and the Krypton laser arrangement (Figure 5.2) respectively.

The absorption vs. time profiles observed with the beam near the anode are broader and shallower than those observed near the cathode. The shape of these profiles can be accounted for if a pulse of PCP^- charge migrates from the negative to the positive electrode after each voltage reversal and disperses as it travels. A narrower absorption response is predicted with the beam near the cathode after voltage reversal. The asymmetry of PCP^- distribution must, however, be interpreted in terms of the total ion

FIGURE 5.15 - LOG I_0/I VS. TIME
BEAM POSITIONED CLOSER TO ONE ELECTRODE

Sample: [TCNE] = 0.01 M

aluminum electrodes

d = 7.3 mm

V = 50 Volts

λ = 415 nm.

$\lambda = 415 \text{ nm.}$

▼ time of voltage reversal

■ beam location

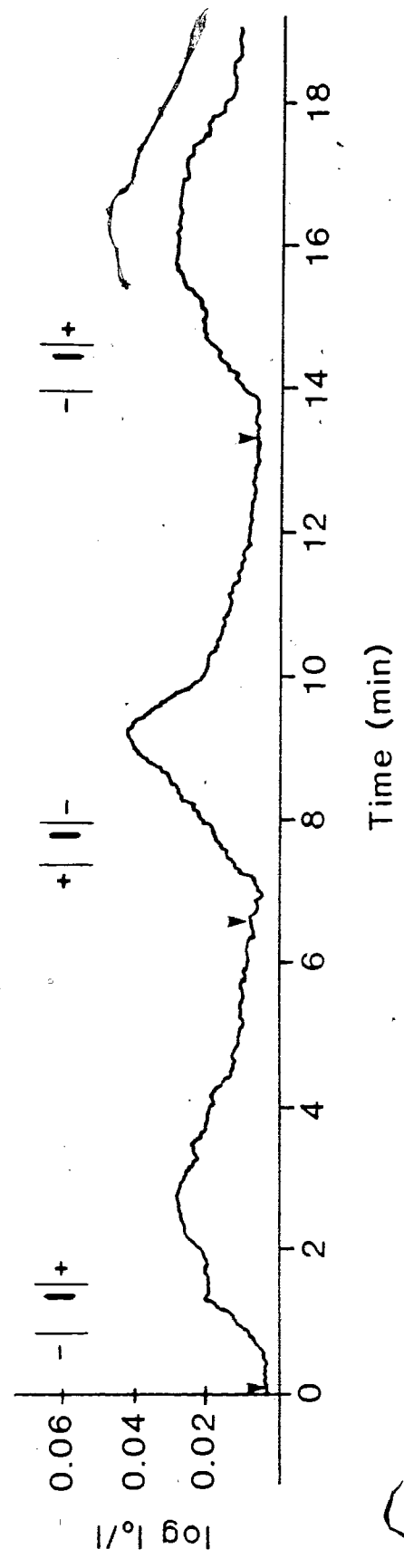


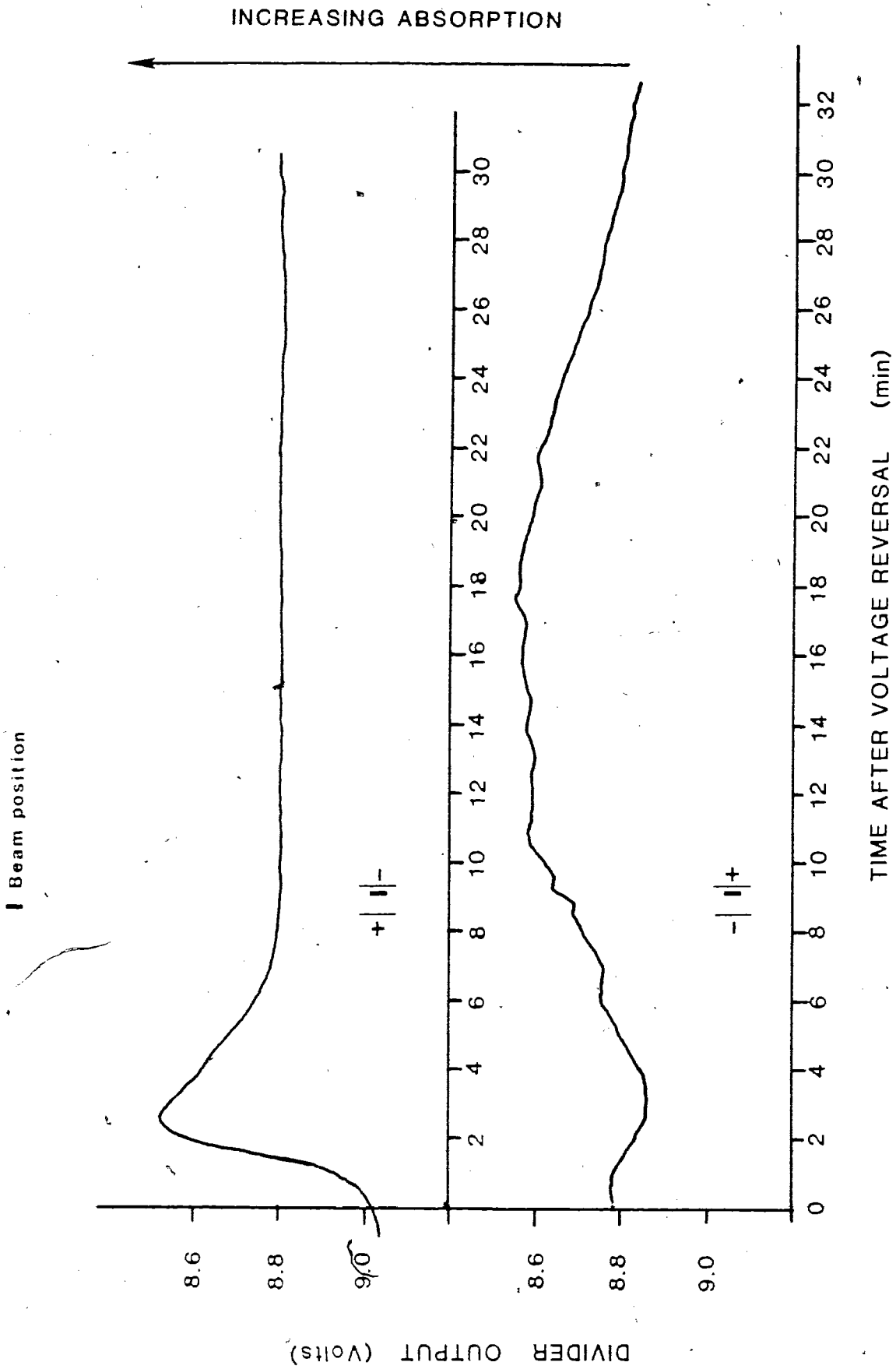
FIGURE 5.16 - ABSORPTION VS. TIME

Sample: [TCNE] = 0.02 M

aluminum electrodes

d = 7.3 mm.

V = 10 Volts



concentration. Concentrations of unbalanced negative space charge can never be expected to approach 10^{-7} M. (See Section 5.3 for typical space charge densities in solution). The preceding observations do not necessarily require a pulse of ion concentration travelling across the solution. The asymmetry of the optical response only demonstrates that the rate of ion concentration changes are greater at the cathode than at the anode in the TCNE/DCE/Al system. The asymmetry of the ion concentration behaviour could also have resulted from differences in anion and cation mobility, and/or anode and cathode processes.

Measurements of ion concentration changes as a function of position and time clearly show the importance of processes occurring at the electrode/liquid interface. However, the current response of samples is largely determined by the effective ion concentration in the bulk of the solution. The evolution of concentration profiles will be described in TCNE/DCE with Al, In and Pt electrodes. The data are recorded as a sequence of diagrams with relative optical transmission plotted against beam position. Higher transmission represents lower PCP^- concentration. Monitoring PCP^- as the dominant negative charge carrier in the system was equivalent to monitoring the behaviour of the total ion concentration at a given position in solution ($c_{total} \approx 2 c_{pcp}$). Only relative ion concentration changes in space and time could be estimated reliably with the measurements because of baseline drift in the apparatus.

Figures 5.17 to 5.21 show sequences of transmission profiles for

FIGURE 5.17 - TRANSMISSION PROFILE

Sample: [TCNE] = 0.04 M

aluminum electrodes

d = 7.3 mm.

V = 20 Volts

Scan 1 : prior to voltage application.

INITIAL VOLTAGE APPLICATION

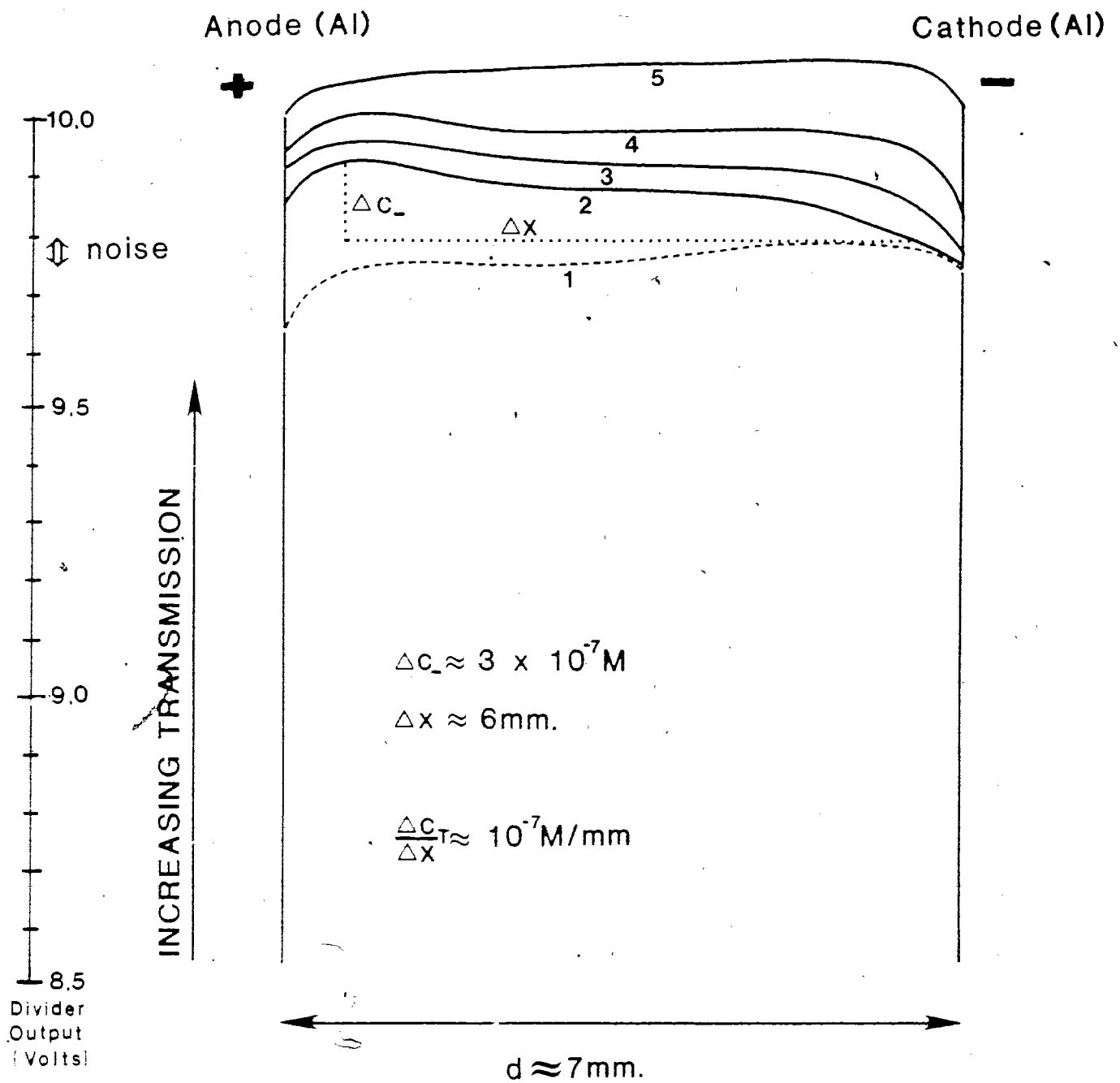


FIGURE 5.18 - TRANSMISSION PROFILE

Sample: [TCNE] = 0.04 M

aluminum electrodes

d = 7.3 mm.

V = 20 Volts

Scan 1: prior to voltage reversal

FIRST VOLTAGE REVERSAL

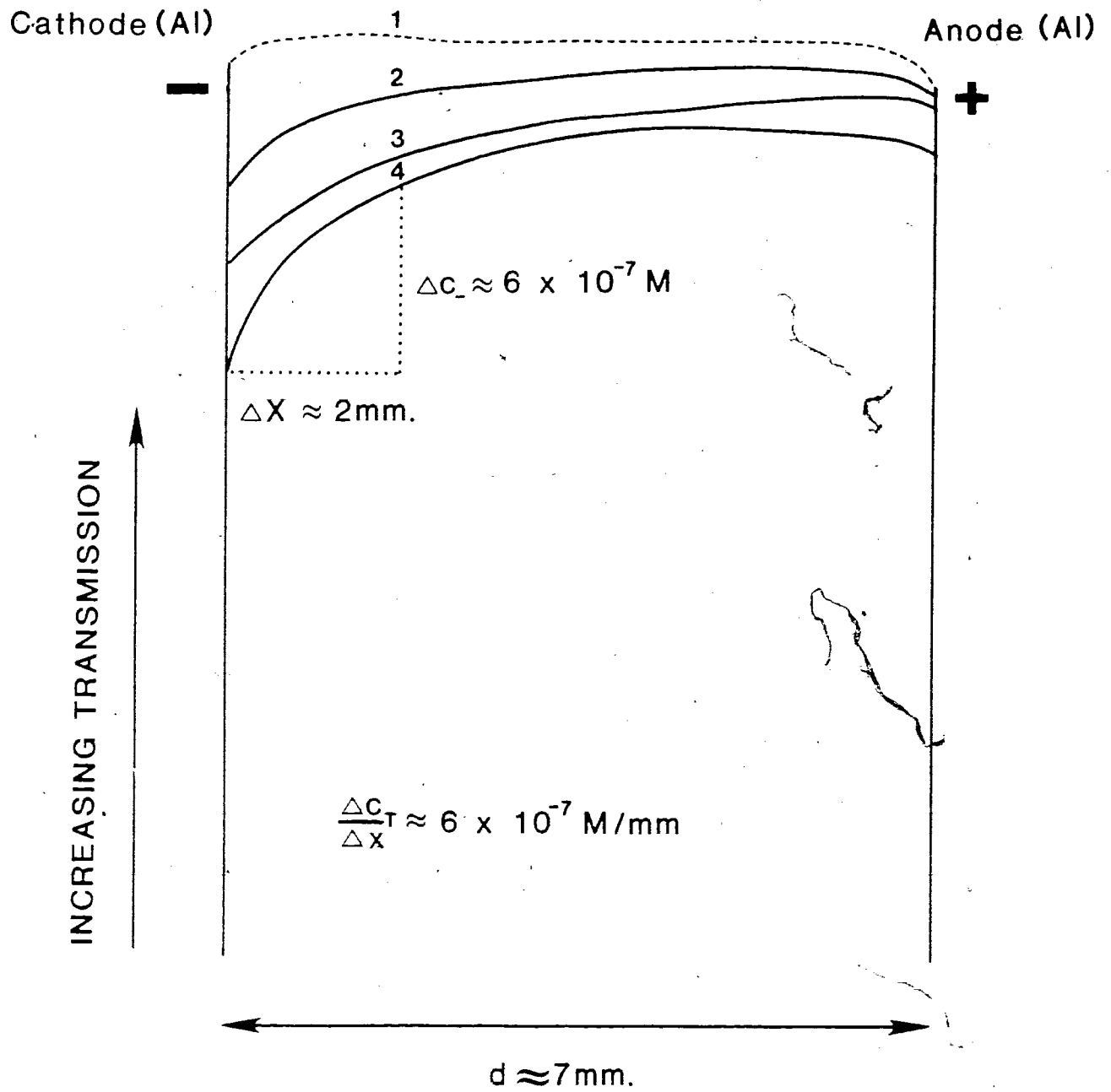


FIGURE 5.19 - TRANSMISSION PROFILE

Sample: [TCNE] = 0.04 M

aluminum electrodes

d = 7.3 mm.

V = 20 Volts

CONTINUATION OF FIRST VOLTAGE REVERSAL

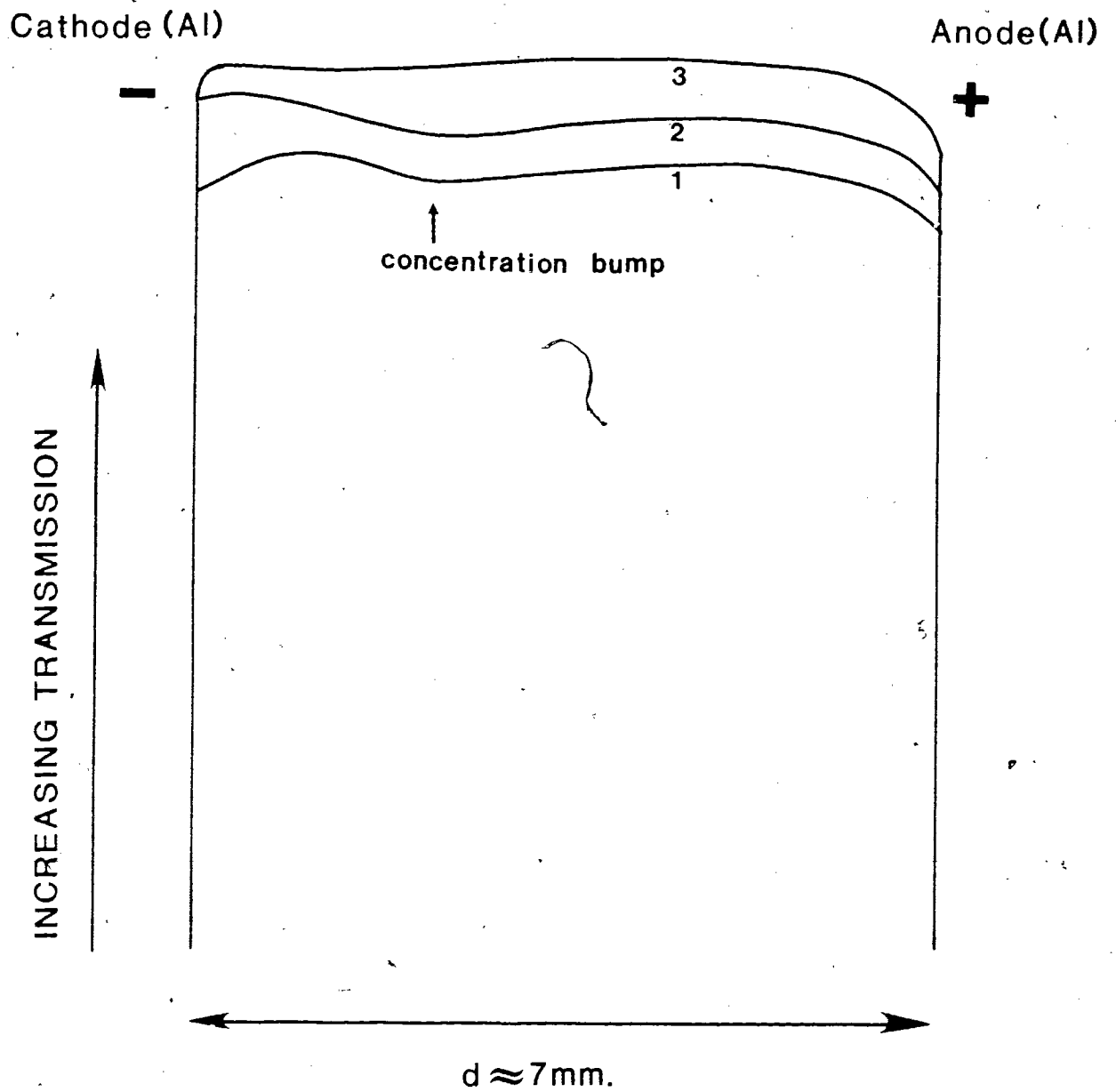


FIGURE 5.20 - TRANSMISSION PROFILE

Sample: [TCNE] = 0.04 M

aluminum electrodes

d = 7.3 mm.

V = 20 Volts

Scan 1: prior to second voltage reversal

SECOND VOLTAGE REVERSAL

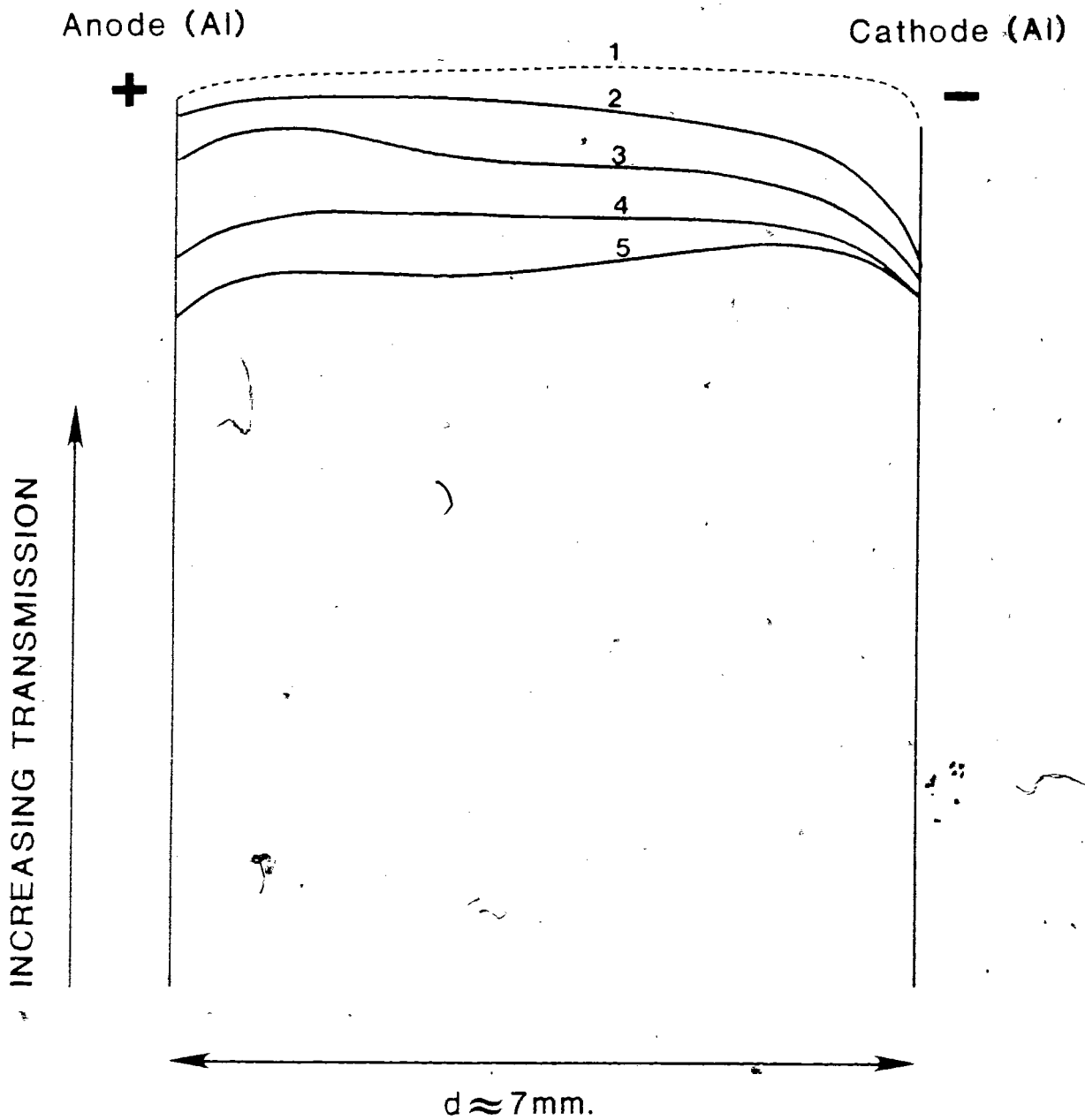


FIGURE 5.21 - TRANSMISSION PROFILE

Sample: [TCNE] = 0.04 M

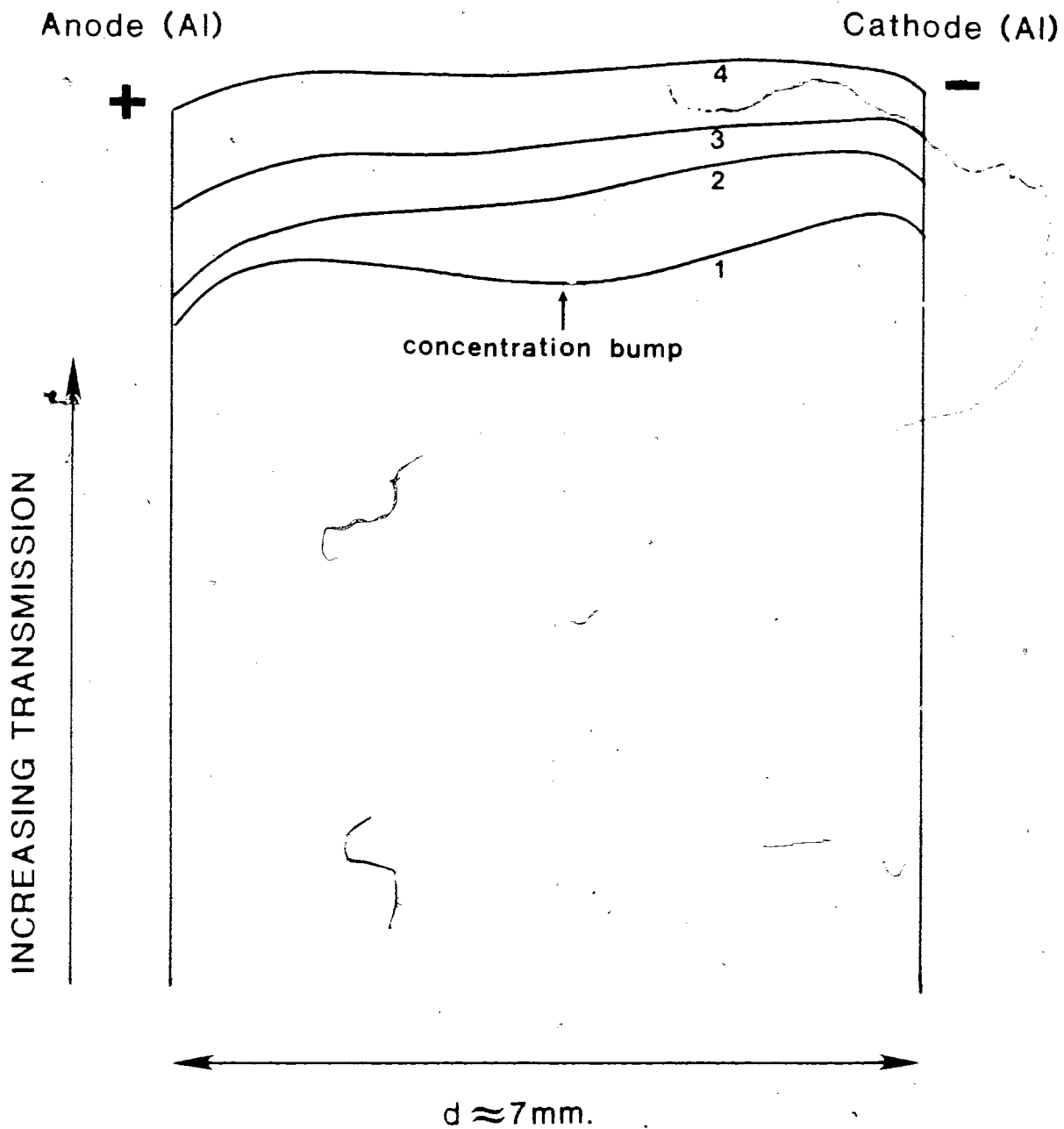
aluminum electrodes

d = 7.3 mm.

V = 20 Volts

Scan 4: 15 minutes after voltage reversal

CONTINUATION OF SECOND VOLTAGE REVERSAL



TCNE/DCE/Al. The first diagram shows the effect of initial voltage application on sample transmission. An increase in optical transmission at the anode corresponds to depletion of PCP^- . The decrease in PCP^- concentration spreads across the cell until a level optical response is observed at steady state. The decrease in overall ion concentration is accompanied by current decay.

After voltage reversal, decreasing transmission near the cathode indicates growth in the concentration of PCP^- (Figure 5.18). As the current peak is approached, the effective ion concentration increases and distributes fairly evenly across the cell. Beyond the current peak the overall ion concentration decreases to approach a steady state level (Figure 5.19). The second voltage reversal qualitatively reproduces the behaviour observed after the first polarity reversal (Figures 5.20 and 5.21).

The sequence of transmission profiles for TCNE/DCE with In electrodes are qualitatively similar to those with Al electrodes (Figure 5.22 and 5.23). The initial transmission profile is uneven but relative changes in PCP^- concentration at a given position are still observable. Similarities of the concentration response with Al and In electrodes reflect similarities in injection/discharge processes for the two metals in DCE. Both metals belong to the Boron group and form surface oxide layers. The $\log I_0/I$ vs. time, and current vs. time responses for a TCNE/DCE/In sample are similar to those observed using Al electrodes.

FIGURE 5.22 - TRANSMISSION PROFILE

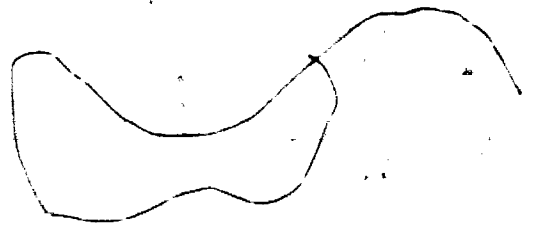
Sample: [TCNE] = 0.04 M

indium electrodes

d = 7.3 mm.

V = 20 Volts

Scan 1: prior to voltage application



INITIAL VOLTAGE APPLICATION

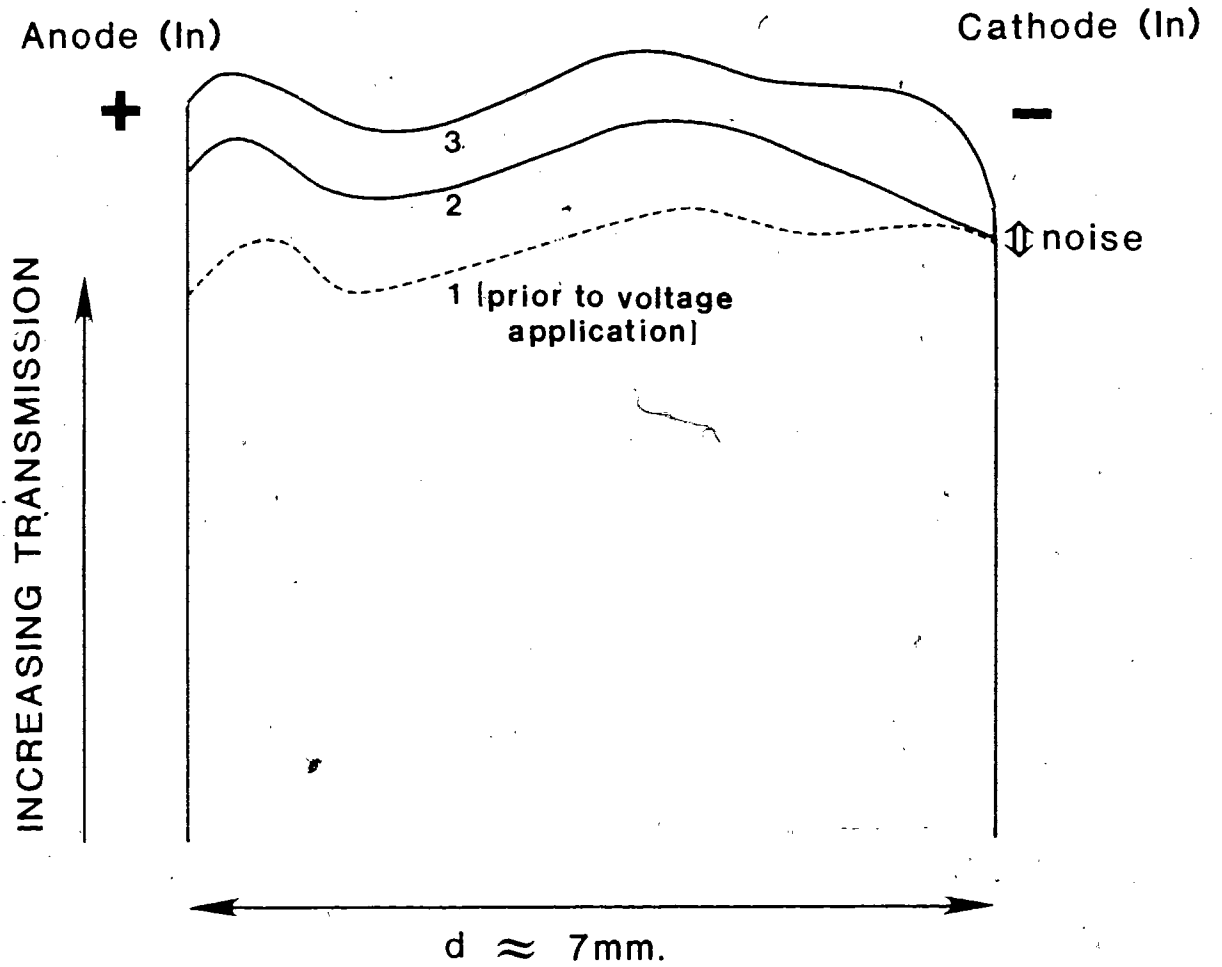
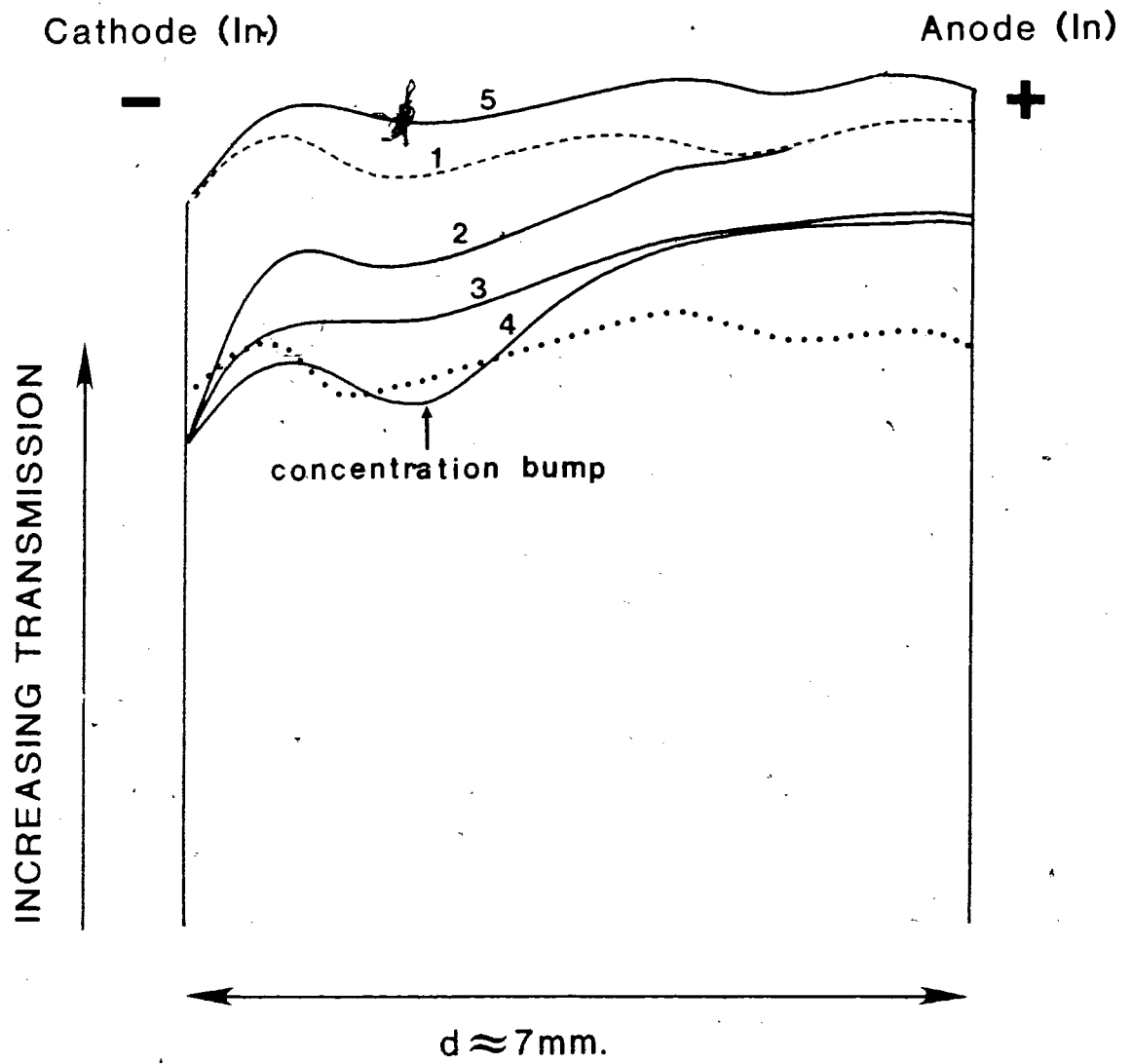


FIGURE 5.23 - TRANSMISSION PROFILE

Sample: [TCNE] = 0.04 M
indium electrodes^{4r}
d = 7.3 mm.
V = 20 Volts

Scan 5: 10 minutes after voltage reversal

FIRST VOLTAGE REVERSAL



Ion concentration behaviour in TCNE/DCE/Pt is different from that observed using Al or In electrodes, although the current response of the Pt system resembles qualitatively that of the other electrode systems. Sequences of transmission vs. position profiles are shown in Figures 5.24 to 5.26. Initial application of voltage decreases the transmission near the cathode. Instabilities in the concentration profiles follow a delay time during which ion concentration builds up at the cathode. In this sample concentration fluctuations were too rapid to be continuously monitored with the apparatus available. The increasing magnitude of concentration fluctuations with applied voltage (Figure 5.27) suggest that electrohydrodynamic effects play an important role in the system. It is also possible that the size of concentration gradients near the cathode increases as a function of voltage, and is therefore accompanied by larger drag forces (See Section 5.2.2).

After voltage reversal, a build-up in ion concentration is again observed near the Pt cathode and concentration instabilities persist. Higher ion concentration is maintained near the cathode in spite of the turbulent behaviour in the rest of the solution. TCNE^- , from the reduction of TCNE, could have contributed to the lower transmission observed near the Pt cathode. TCNE^- and PCP^- both absorb light at the monitored wavelength of 415 nm.

The data demonstrate that injection/discharge processes at a Pt surface are substantially different from those at Al and In surfaces. The absence of a surface oxide layer on Pt distinguishes its electrochemical behaviour from

FIGURE 5.24 - TRANSMISSION PROFILE


Sample: [TCNE] = 0.04 M

platinum electrodes

d = 6 mm.

V = 10 Volts

Scan 1: prior to voltage application



INITIAL VOLTAGE APPLICATION

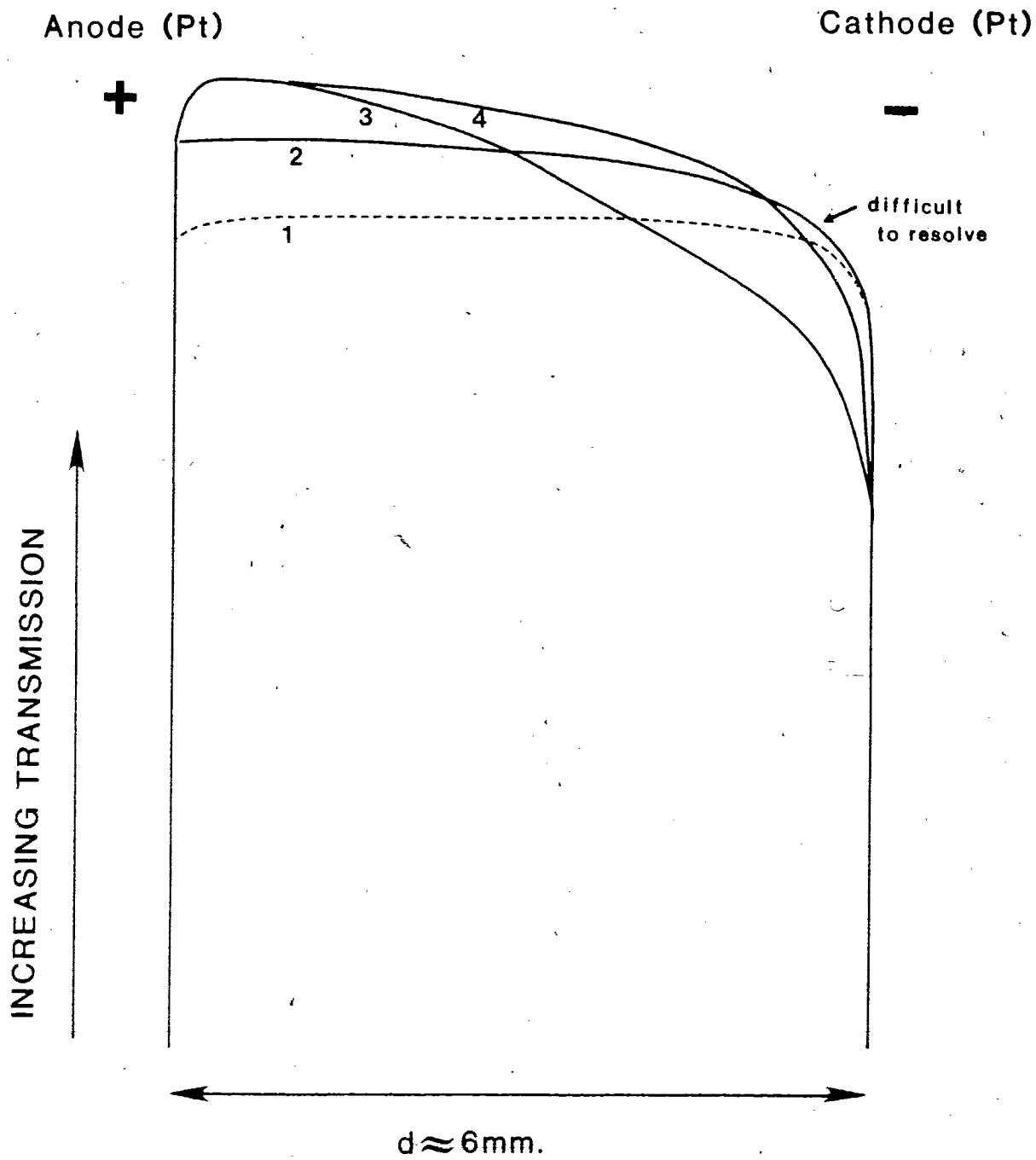


FIGURE 5.25 - TRANSMISSION PROFILE

Sample: [TCNE] = 0.04 M.

platinum electrodes

d = 6 mm.

V = 10 Volts

CONTINUATION OF FIRST VOLTAGE APPLICATION

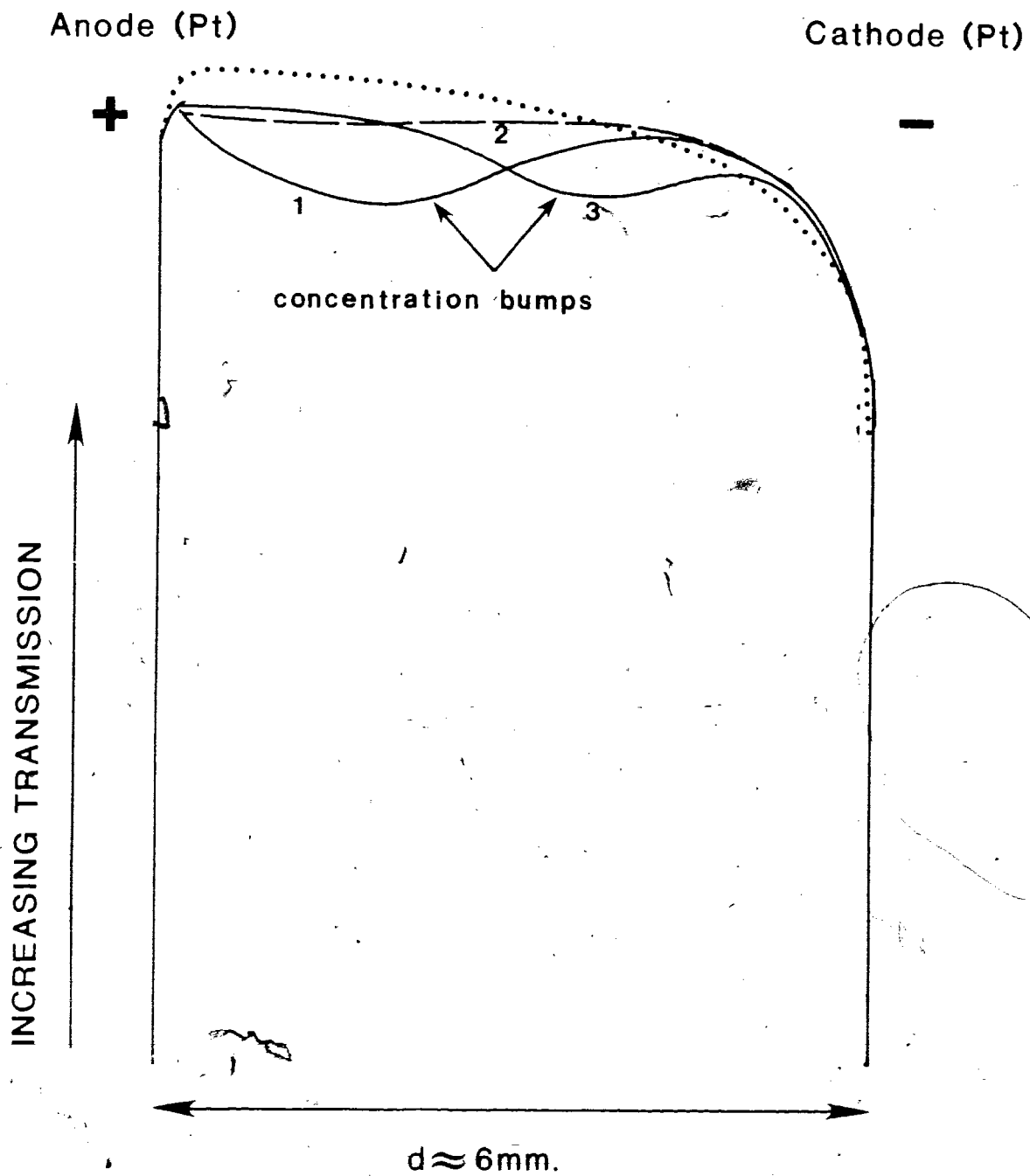


FIGURE 5.26 - TRANSMISSION PROFILE

Sample: [TCNE] = 0.04 M.

platinum electrodes

d = 76 mm.

V = 20 Volts

VOLTAGE REVERSAL

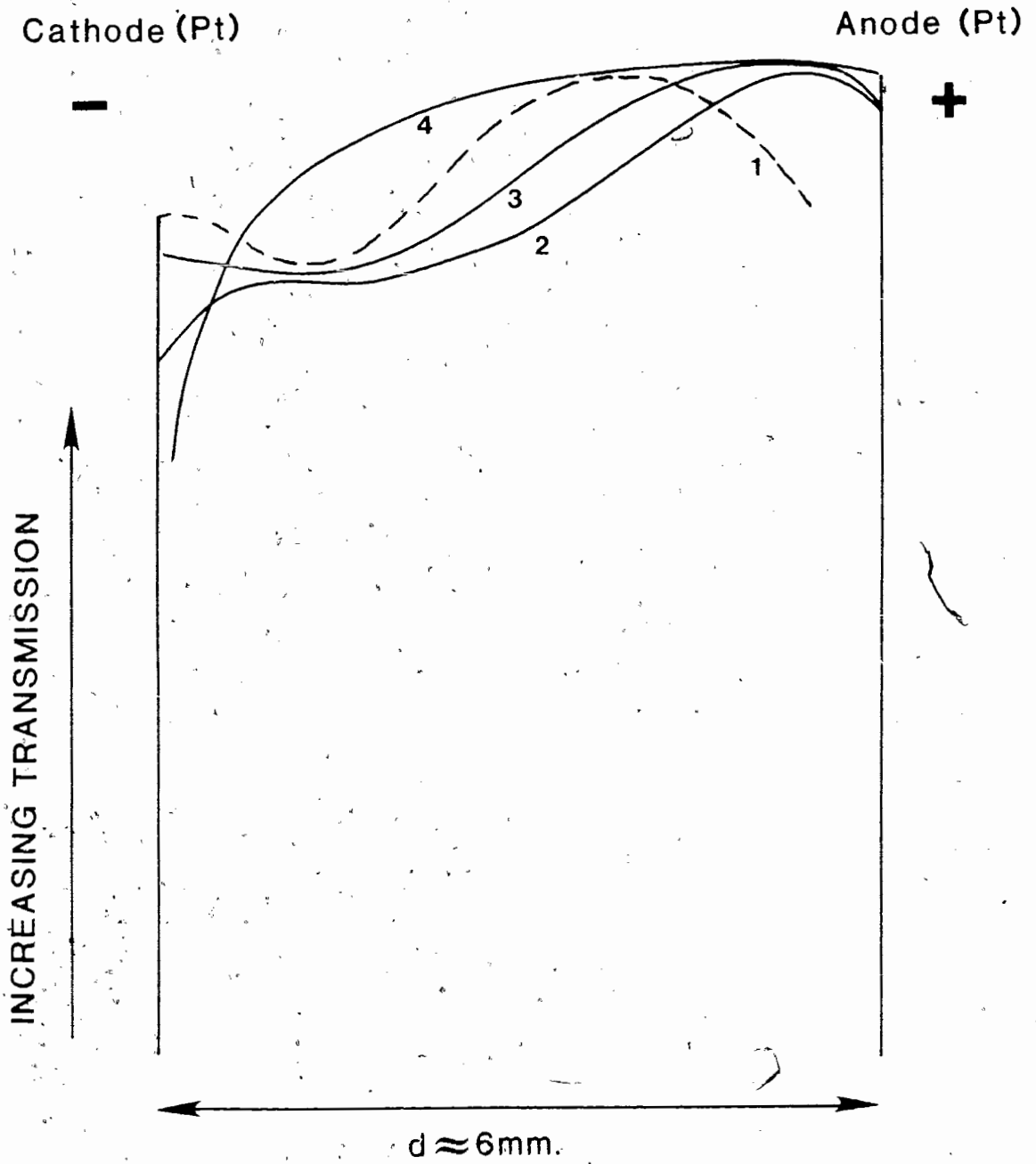



FIGURE 5.27 - LOG i_0/i FLUCTUATIONS AT DIFFERENT VOLTAGES

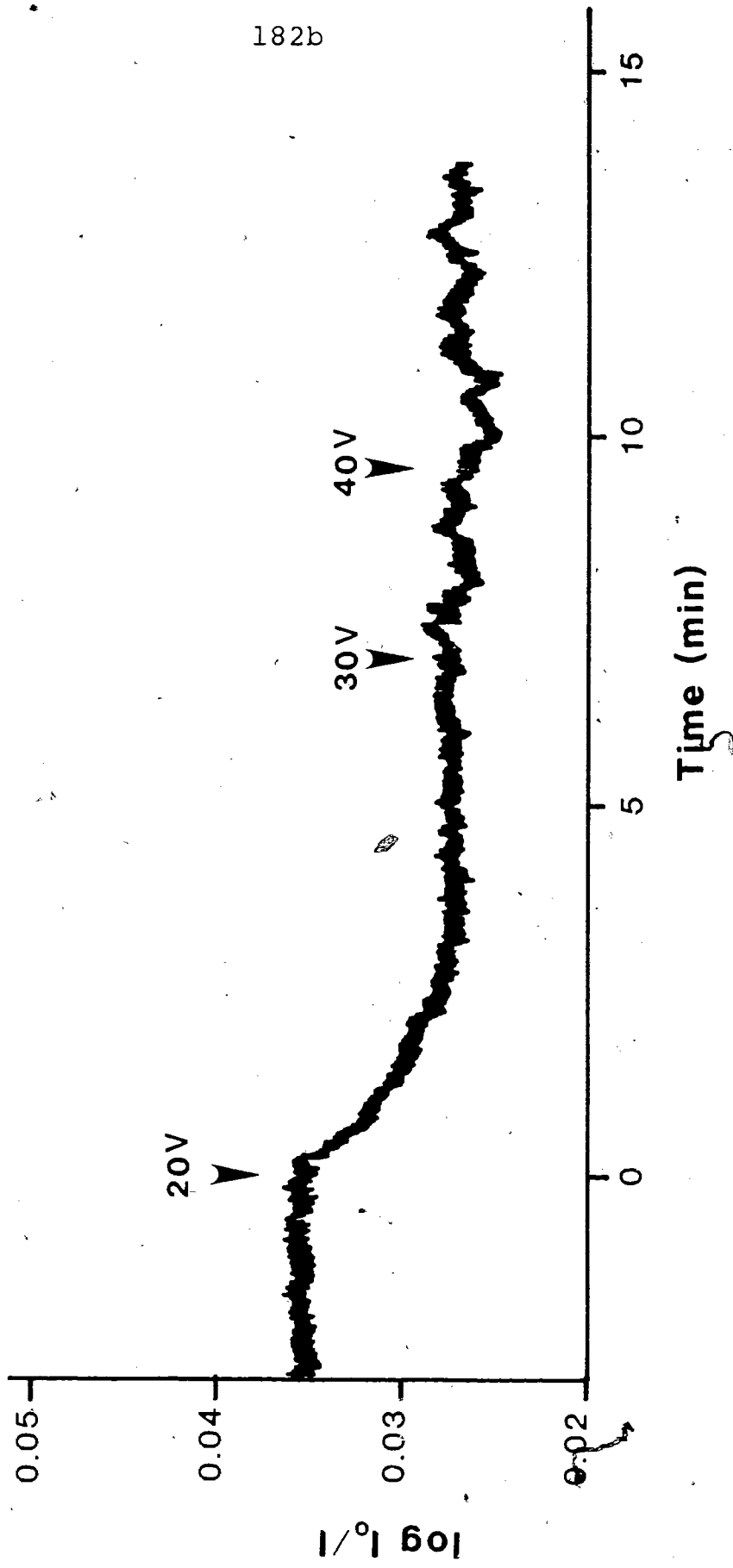
Sample: [TCNE] = 0.02 M. in DCE

platinum electrodes

d = 6 mm.



182b



that of In and Al. Another distinguishing feature of Pt metal is the possibility of d-orbital interactions with surface adsorbed molecules. For example, TCNE-Pt complexes are known which involve interaction of filled Pt d-orbitals with the empty π^* orbital of TCNE ⁴.

Electrode materials have a strong influence on concentration response and the appearance of hydrodynamic instabilities in the organic solutions under study. The importance of understanding electrode injection processes when studying low conductivity dielectric liquids is also discussed in the literature ⁵.

5.2.2 - CONCENTRATION GRADIENTS AND HYDRODYNAMIC INSTABILITIES

The observations just discussed have implications regarding ion concentration gradients and hydrodynamic instabilities in the liquid. A model correlating concentration gradients, space charge and convective instabilities will be discussed in Section 5.3. According to this model, unbalanced drag forces and pressure gradients in electrolyte solutions are associated with ion concentration gradients and space charge. The unbalanced force always points from high to low ion concentration regions in solution. The larger the concentration gradient, the larger the force on the liquid. Large enough forces lead to laminar or turbulent flow in the solution. The diffusion induced drag force per unit volume of liquid (F_d) can be estimated from concentration gradients in solution using

$$F_d = -kT (\partial c_T / \partial x)$$

where k = Boltzmann constant (J/K)

T = temperature (K)

c_T = total ion concentration

$\partial c_T / \partial x$ = concentration gradient (M/m^4)

A typical ion concentration gradient in the bulk of TCNE/DCE solutions during non-steady state current conditions can be estimated using Figure 5.17. A PCP^- concentration difference of 2.8×10^{-7} M. is observed over about 6 mm. This gives a concentration gradient of

$$\begin{aligned} (2\Delta c_{\text{pcp}}) / \Delta x &= 2 (3 \times 10^{-7} \text{ M}) / 6 \text{ mm.} = 1 \times 10^{-7} \text{ M/mm} \\ &= 6 \times 10^{22} / \text{m}^4 \end{aligned}$$

In Figure 5.18 and 5.24, larger concentration gradients of about 6×10^{-7} M/mm or $3.6 \times 10^{23} / \text{m}^4$ are observed. Concentration gradients of this size produce a force of 1.5×10^{-3} Newton per unit cm^3 of solution. This is equivalent to the weight of a 0.15 gm mass being applied as an unbalanced force to a 1.2 gm. portion of DCE.

Evidence of turbulent flow is observed in the TCNE/DCE/Pt system and preceded by growth in ion concentration near the cathode (Figure 5.24, 5.25). A net drag force on the liquid points from the cathode to the region of lower ion concentration in the bulk of the solution. Liquid flowing from the

cathode into the center of the cell in response to the unbalanced force reduces the build-up of ion concentration near the cathode.

In the TCNE/DCE/Al sample, the evolution of concentration profiles in time shows very smooth behaviour after the initial application of voltage. Concentration gradients were smaller than those observed after the initial voltage application in Pt. The absence of turbulence does not eliminate the possibility of laminar fluid flow in the system. Laminar flow would be expected to decrease the magnitude of concentration gradients in a smooth fashion.

After voltage reversal and the build up of ion concentration near the Al cathode, a temporary instability in the solution is marked by a bump in the concentration (Scan 1, Figure 5.19). Concentration bumps are also observed after the next voltage reversal, and under similar conditions in the TCNE/DCE/In system (Scan 4, Figure 5.23).

The temporary nature of fluid instabilities in TCNE/DCE/Al samples is in contrast to the continuous turbulent behaviour monitored in the TCNE/DCE/Pt system. In the Pt system a higher ion concentration is maintained at the cathode with respect to the bulk, whereas in the Al system the build-up of ion concentration is only temporary. At steady state conditions in TCNE/DCE/Al samples, concentration gradients disappear and fluctuations in concentration at a given position reach a minimum. This behaviour indicates the absence of turbulent flow.

Table 5.4 lists experimentally observed concentration gradients and diffusion induced drag forces per unit volume of liquid. The drag force is compared to solvent weight per unit volume. The drag force is a significant fraction of the solvent weight for the larger of the two concentration gradients considered. This corresponds to a situation in which hydrodynamic instabilities are observed in solution. When the drag force is only about 2% of the liquid weight, there is no evidence of hydrodynamic instabilities.

This behaviour supports a model in which ion concentration gradients are responsible for initiating fluid flow in weak electrolyte solutions. Steady state turbulent flow requires a mechanism for sustaining ion concentration gradients. Transient fluid instabilities indicate temporary establishment of concentration gradients in the bulk of the solution. The contribution of space charge effects to hydrodynamic instabilities will be considered in the next section.

TABLE 3.4
CONCENTRATION GRADIENTS AND
DIFFUSION-INDUCED DRAG FORCES

M/mm	$\partial c_T / \partial x$ */m ⁴	F_D (N/m ³)	$F_D / \rho_l g$	Fluid Flow
1×10^{-7}	6×10^{22}	2.4×10^2	0.02	stationary or laminar
6×10^{-7}	3.6×10^{23}	1.5×10^3	0.12	turbulence

$F_D / \rho_l g$ is the ratio of the diffusive drag force
to the weight of the liquid

$$\rho_l = \text{DCE mass density}^{20^\circ} = 1.2351 \times 10^3 \text{ kg/m}^3$$

$$\rho_l g = 1.21 \times 10^4 \text{ (N/m}^3\text{)}$$

5.3 - ELECTROHYDRODYNAMIC INSTABILITIES IN LOW CONDUCTIVITY ELECTROLYTE SOLUTIONS

Electrohydrodynamic instabilities are a general phenomenon in low conductivity solutions. However, the source of these instabilities in electrolyte solutions is still not well understood⁶. In this chapter a model is proposed that predicts the existence of pressure gradients in electrolyte solutions with concentration gradients. The contribution of space charge and diffusion to pressure gradients is considered.

Fluid flow can be initiated via unbalanced forces acting on a liquid. The presence of any space charge in solution will result in a drag force per unit volume of liquid if an electric field is applied

$$F_e = \rho_e E = \rho f_e$$

F_e = space charge drag force per unit volume (N/m³)

ρ = unbalanced charges per unit volume (#/m³)

e = unit electronic charge = 1.6×10^{-19} C

E = electric field (J/C)

f_e = force per unit electronic charge (N)

In the strictest definition of an electrolyte solution, no space charge exists

in the bulk of the liquid and so no pressure gradients are expected in an applied field. However, in the case of even small violations of charge neutrality in the bulk of the solution the space charge drag force must be considered.

A diffusion field will also result in an unbalanced drag force per unit volume of liquid with or without the benefit of an applied electric field.

$$F_d = c_T e E_d = c_T f_d = -kT (\partial c_T / \partial x)$$

where F_d = diffusion drag force per unit volume (Nt/m)

c_T = concentration of particles ($\#/m^3$)

$\partial c_T / \partial x$ = concentration gradient ($\#/m^4$)

E_d = diffusion field (J/C) = $(kT / (c_T e)) \partial c_T / \partial x$

f_d = diffusion force per particle = $(kT / c_T) \partial c_T / \partial x$

There is no fundamental difference in the way forces from space charge or diffusion are transferred to the liquid. In both cases the drag force exerted by the liquid on the moving particle is accompanied by an equal force in the opposite direction on the liquid (i.e. in the direction of particle motion).

Another source of unbalanced forces in chemical systems is the existence of mass density gradients (sometimes referred to as natural convection). Mass density gradients can arise from temperature gradients (Benard convection is a special case) or large enough concentration gradients. In the organic solutions under study, concentration differences of the order of 10^{-6} M. are not expected to result in significant mass density gradients. Significant temperature gradients would have been present only in the photocurrent measurements. Therefore, the contribution of density gradients to convection will be ignored.

The pressure developed across a liquid can be written in terms of the contributions from space charge and diffusion following the reasoning of Pickard ⁷ as

$$P = \int_0^d F dx = \int_0^d (F_d + F_e) dx$$

The contribution from gravitational effects is assumed to be negligible and the liquid is incompressible and without rotational motion. It is not the aim of this model to predict the details of hydrodynamic flow with given pressure gradients. The aim of this model is to suggest a general mechanism by which pressure gradients are established in an electrolyte liquid with applied voltage.

Under the influence of an applied field space charge and concentration gradients are not independent parameters. This can be shown using a few physical assumptions:

1. The current flux is approximately independent of position at a given time:

$$\partial \rho(x)/\partial t = -\partial j/\partial x \approx 0$$

2. Charge neutrality is approximately maintained at all positions in the solution:

$$c_+ = c_- = c(x)$$

$$c_+ - c_- = \rho(x) \ll c(x)$$

3. The Poisson equation in one dimension relates electric field gradients and space charge density in solution:

$$\partial E/\partial x = \rho e/(\epsilon \epsilon_0)$$

The concentration and electric field distributions at a given time can be related using the first assumption

$$j = 2\mu c(x)E(x) = \text{constant}$$

therefore

$$c(x)E(x) = \text{constant}$$

Since the product of electric field and concentration is constant with respect to position we have

$$\partial[c(x)E(x)]/\partial x = 0$$

$$c(x) \partial E(x)/\partial x = -E(x) \partial c(x)/\partial x$$

Using the Poisson equation to rewrite $\partial E(x)/\partial x$ and rearranging gives

$$-\frac{(\epsilon\epsilon_0)E}{ec} \frac{\partial c}{\partial x} = \rho \quad (1)$$

Equation (1) relates the concentration gradient present at a given position in solution to the space charge density at the same position. Using conditions applicable to the organic solutions under study, the space charge density, ρ , can be shown to be much less than the ion concentration.

$$\text{Using } \partial c/\partial x = 3.6 \times 10^{23} / \text{m}^4$$

$$c = 7 \times 10^{-7} \text{ M} = 4.2 \times 10^{20} / \text{m}^3$$

$$\epsilon = 10$$

$$E = V/d = 20V/(7.3 \times 10^{-3} \text{ m}) = 2.8 \times 10^3 \text{ V/m}$$

gives

$$\rho = 1.3 \times 10^{15} / \text{m}^3 \ll c$$

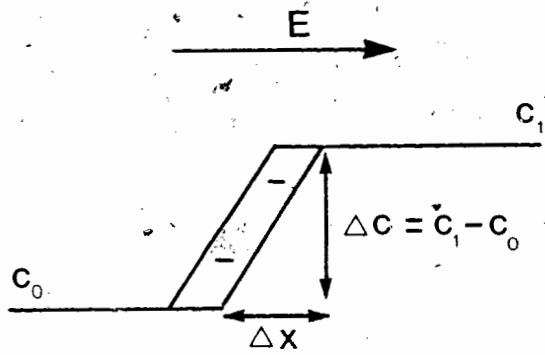
or $\rho = 2.2 \times 10^{-12} \text{ M}$

$$\rho/c = 3 \times 10^{-6}$$

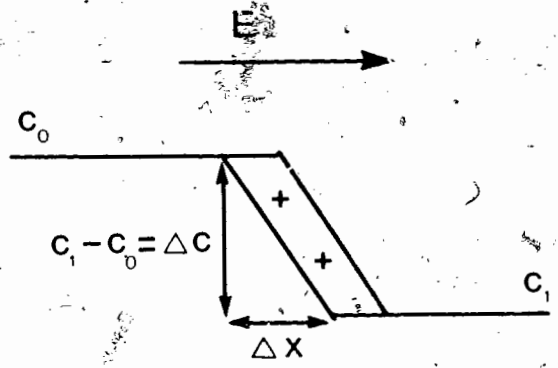
For a positive concentration gradient and positive applied field, the space charge is negative. The space charge for positive and negative concentration gradients is sketched in different fields in Figure 5.28. In each case the space charge enhances the electric field in the region of low ion concentration and diminishes the electric field in the region of high ion concentration. This allows a constant current flux to be maintained on either side of the concentration gradient.

Given the transient nature of concentration gradients and current flux in the solutions under study, it is reasonable to question whether a well defined space charge distribution can be associated with a concentration gradient in solution at a given time. In order to estimate a characteristic time for establishing the space charge distribution required to maintain constant current flux as a function of position imagine the following situation: A portion of a concentration gradient with a positive slope exists in a solution without applied electric field (Figure 5.29). No space charge is associated with the ion distribution under these conditions. With the application of an electric field in the positive direction, some separation of charge results in

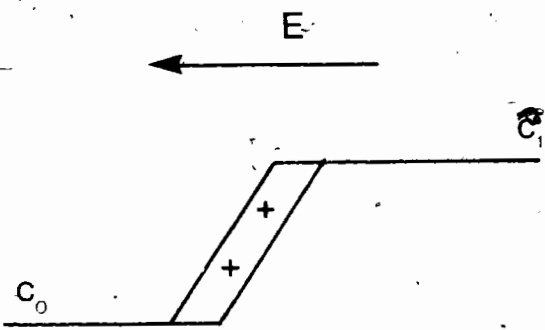
**FIGURE 5.28 - SPACE CHARGE ASSOCIATED WITH
ION CONCENTRATION GRADIENTS TO MAINTAIN
A CONSTANT CURRENT FLUX**



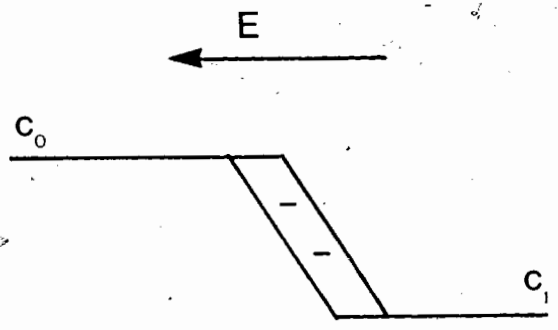
$\frac{\Delta c}{\Delta x} > 0 \quad E > 0 \quad \rho < 0$



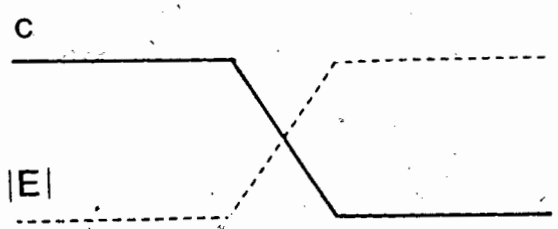
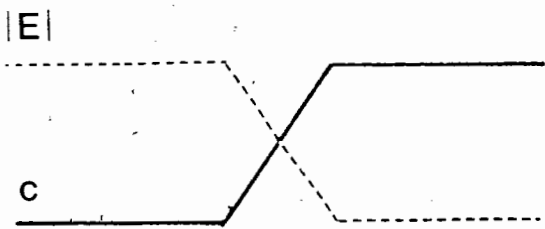
$\frac{\Delta c}{\Delta x} < 0 \quad E > 0 \quad \rho > 0$



$\frac{\Delta c}{\Delta x} > 0 \quad E < 0 \quad \rho > 0$

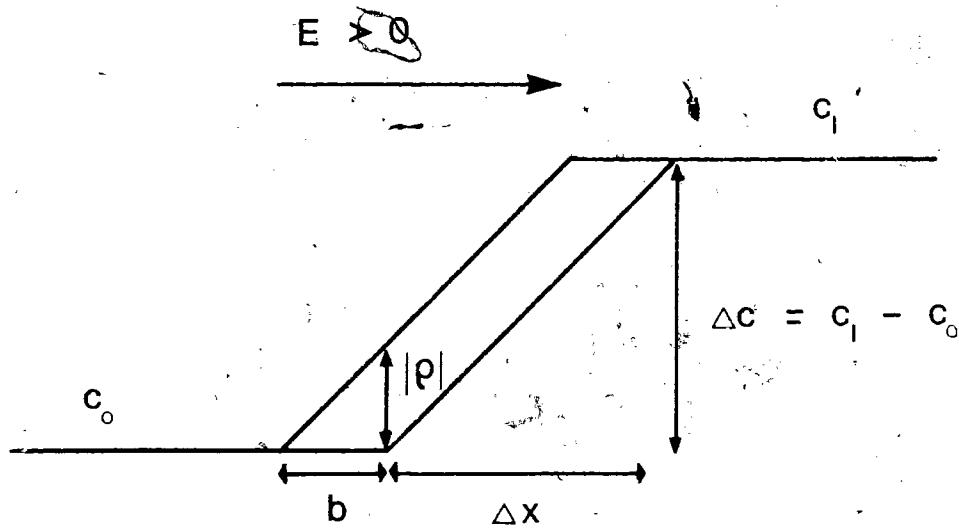
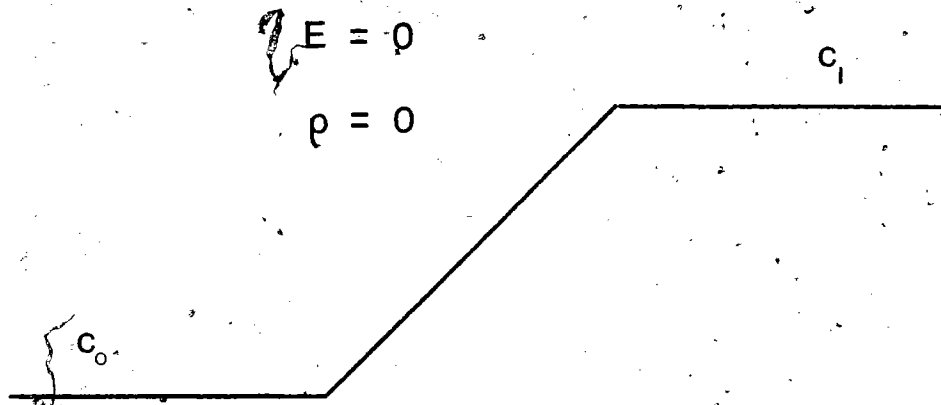


$\frac{\Delta c}{\Delta x} < 0 \quad E < 0 \quad \rho < 0$



$c|E| = \text{constant}$

**FIGURE 5.29 - FORMATION OF A SPACE CHARGE LAYER ON A
CONCENTRATION GRADIENT**



$$\frac{|p|}{b} = \frac{\Delta c}{\Delta x}$$

$p < 0$

the region with the gradient. In this example, negative charge moves from the high ion concentration region to the low ion concentration region. The result is an unbalanced negative space charge in the region of the concentration gradient. Once the conditions for constant current flux are met, the space charge is defined in terms of the concentration gradient (Equation 1).

The characteristic time (t_{sc}) for meeting the condition of constant current flux for a given concentration gradient depends on how quickly the negative and positive charge profiles separate to form the desired space charge distribution. Negative and positive charges initially separate at a speed v_{sep} which is the sum of the individual ion velocities.

$$v_{sep} = \mu_+ E + \mu_- E = 2\mu E$$

The thickness of the space charge layer (b) at constant current flux is given by the product of v_{sep} and the time, t_{sc} .

$$b \approx v_{sep} t_{sc}$$

The characteristic time, t_{sc} , can be rewritten in terms of ρ , $\partial c / \partial x$, μ , and E using the similar triangles in Figure 5.29. From the triangles

$$\rho / (v_{sep} t_{sc}) = \Delta c / \Delta x \text{ or } \partial c / \partial x$$

hence,

$$t_{sc} = \rho / ((\partial c / \partial x) v) = \rho / ((\partial c / \partial x) \mu E)$$

Substitution of Equation (1) into the previous equation gives

$$t_{sc} = (\epsilon \epsilon_0) / (\mu e c) \quad (2)$$

Note that t_{sc} is independent of the magnitude of the concentration gradient, as well as of the electric field. t_{sc} increases with decreasing ion concentration. A characteristic time for establishing constant current flux for a solution of given concentration can be estimated using physical constants applicable to the organic solutions in this study.

Using $\mu = 3 \times 10^{-8} \text{ m}^2 \text{V}^{-1} \text{s}^{-1}$

$$c = 10^{20} / \text{m}^3$$

results in $t_{sc} = 0.18 \text{ ms} \lll d/v_{drift} \approx 45 - 225 \text{ s}$

Since t_{sc} is much smaller than typical times for changes in concentration gradients, it is reasonable to associate a well defined space charge density

with a given concentration gradient in solution. It is also reasonable to assume that current flux is constant as a function of position in the cell.

The relative contributions of diffusion and space charge to liquid drag forces might be expected to vary with electric field and concentration. The ratio of space charge and diffusion forces per unit volume can be written

$$\frac{F_e}{F_d} = \frac{\rho_e E}{kT(\partial c_T / \partial x)} = \frac{\rho_e E}{kT(2\partial c / \partial x)}$$

Using equation (1) for ρ gives

$$\frac{F_e}{F_d} = \frac{(\epsilon\epsilon_0) E^2}{2(kT) c} \quad (3)$$

This ratio determines the concentration and electric field conditions for which space charge effects can be expected to dominate diffusion effects. At high fields and low ionic concentrations, space charge effects are expected to dominate. This is consistent with the appearance of electroconvective phenomena in low rather than high conductivity liquids. The range of this ratio under experimentally observed conditions in this study is from about 10^{-7} to 10^{-1} (Table 5.5).

Equation (3) obviously has some consequences for experimental work on

TABLE 5.5

TYPICAL F_e / F_D VALUES
FOR EXPERIMENTAL CONDITIONS

C (M)	C ($^*/m^3$)	E (V/m)	F_e / F_D
10^{-8}	6×10^{18}	6.8×10^3	8.5×10^{-2}
10^{-7}	6×10^{19}	2.7×10^3	1.4×10^{-3}
10^{-6}	6×10^{20}	1.3×10^2	3.1×10^{-7}

electrohydrodynamic instabilities in liquids. In order to select a sample for studying the contribution of space charge effects to hydrodynamic instabilities in DCE, the ratio of E^2/c must be much larger than $9.1 \times 10^{-11} \text{ V}^2/\text{m}^5 = (2kT/\epsilon\epsilon_0)$ at 293°K. Table 5.6 lists values of fields and concentrations for which space charge and diffusion contributions to the liquid drag force are equal. Even exceedingly pure solvents with ion concentrations of the order of 10^{-12} M would have diffusion drag forces contributing to hydrodynamic instabilities at low enough electric fields.

As a rule, the inclusion of diffusion drag forces has been ignored in electrohydrodynamic studies. This approach is warranted in systems with unipolar injection as the only source of charge carriers. However, diffusion drag forces must be considered in industrial dielectric liquids such as fuels, mineral oil, and solvents according to our model.

TABLE 5.6

CONDITION FOR $F_e / F_D = 1$

$$F_e / F_D = (1.1 \times 10^{10}) E^2 / c$$

{c in (*/m³) E in (V/m)}

c (M)	c (*/m ³)	E (V/m)
10 ⁻¹²	6 × 10 ¹⁴	2.3 × 10 ²
10 ⁻⁶	6 × 10 ²⁰	2.3 × 10 ⁵
1	6 × 10 ²⁶	2.3 × 10 ⁸

Note: The potential limits for a DCE solution with 0.1 M of n-Bu₄NCIO₄ of supporting electrolyte are

anode : 2.13 to 2.48 Volts

cathode: -2.07 to -2.32 Volts

from T. Osa, T. Kuwana, Journal of Electroanalytical Chemistry 1969, 22, 389-406.

REFERENCES:

1. W.J. Middleton, E.L. Little, K.K. Coffman, V.A. Engelhardt, "Cyanocarbon Acids and their Salts", Journal of the American Chemical Society 1958, 80, 2795-2806.
2. R.H. Boyd, "Ionization Behaviour of Cyanocarbon Acids", Journal of Physical Chemistry 1963, 67, 737-744.
3. R.H. Boyd, "The Solution Conductance of Cyanocarbon Salts", Journal of Physical Chemistry 1961, 65, 1834-1843.
4. G. Henrici-Olive, S. Olive, "Coordination and Catalysis"; Verlag Chemie: Weinheim, New York, 1976; pp.110-112
5. J.C. Gibbings, "Interaction of Electrostatics and Fluid Motion", Electrostatics 1979, Institute of Physics Conference Series, No.48; J. Lowell, Editor; 145.
6. P. Atten, B. Malraison, S. Ali Koni, "Electrohydrodynamic Stability of Dielectric Liquids subjected to A.C. Fields", Journal of Electrostatics 1982, 12, 477-488.
7. W. F. Pickard, "Ion Drag Pumping", Journal of Applied Physics 1963, 34, 246.

CHAPTER 6 - SOME CYANOCARBON CHEMISTRY

Chemical and electrochemical processes contributing to the production of charge carriers in the organic solutions under study are considered in this chapter. The chemistry of the 1,1,2,3,3 pentacyanopropenide anion (PCP^-), and the tricyanovinylalcoholate anion (TCV^-) are discussed. The electrochemical generation of TCNE^- in solution is also considered.

6.0 - EXPERIMENTAL

The tetraethylammonium salt of pentacyanopropenide (TEA^+PCP^-) was prepared according to the method of Middleton et. al.¹ except that TEA^+Cl^- was used as a reactant instead of TEA^+Br^- . The TEA^+PCP^- salt dissolves easily in a variety of solvents. Spectra were recorded with the CARY 210 spectrophotometer.

Acetonitrile (CH_3CN) was twice distilled under nitrogen, using P_2O_5 as drying agent. Spectroscopic grade DCE was distilled once under the same conditions. Tetrahydrofuran and 2-Methyltetrahydrofuran were distilled under nitrogen and sodium metal was used as a drying agent. If solvents were not used immediately, they were stored under nitrogen.

The sample preparation used to study the reaction of TCNE and water in DCE and CH_3CN will now be described. Water is very soluble in CH_3CN , but is

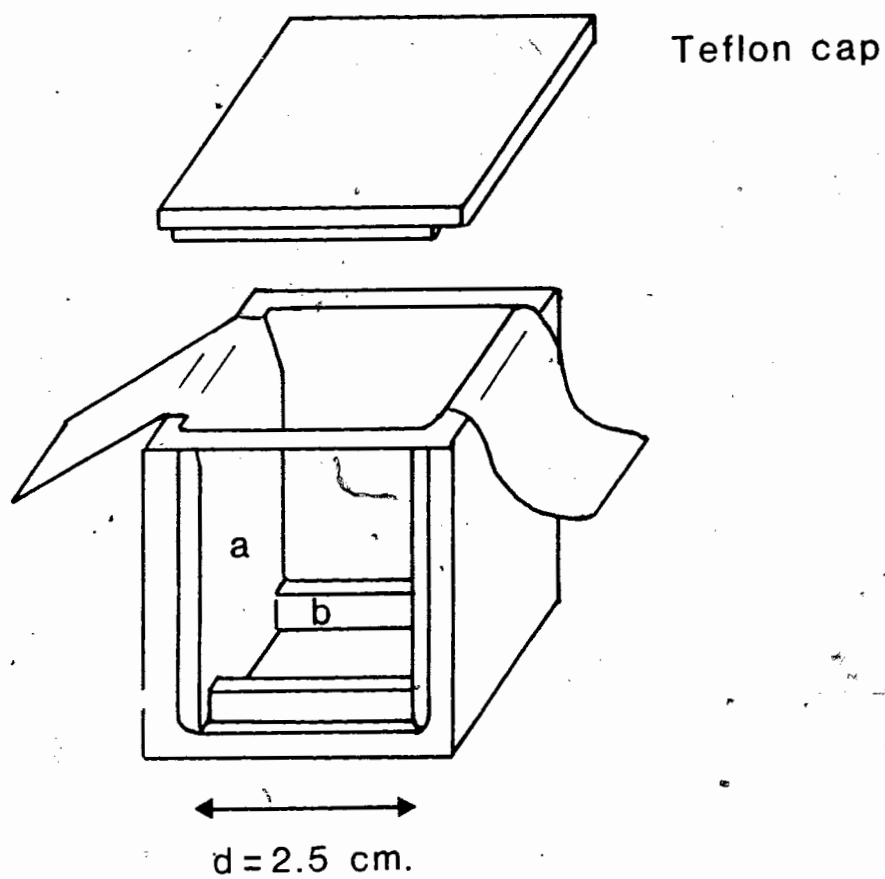
poorly soluble in DCE (0.16% by weight at 20 C)². Micropipettes were used to introduce distilled water directly into CH₃CN solutions of TCNE. The samples were then vigorously shaken, transferred to a 1.000 cm. spectroscopic cell (Hellma), and carefully sealed with parafilm and teflon tape. Water was added to TCNE/DCE samples by first saturating a portion of the solvent with water. By adding different fractions of H₂O saturated DCE to the sample, the concentration of water could be varied. Changes in the visible spectrum of TCNE/solvent samples were monitored with the CARY 210.

The preparation of voltage treated samples of TCNE/CH₃CN was carried out using the Al electrode cell shown in Figure 6.1. Voltage was applied for about an hour until steady state had been reached. After voltage treatment, the solution was removed from this cell and sealed in a 1.000 cm. spectroscopic cell using parafilm and a teflon tape wrapping. Again, the CARY 210 was used to record the chemical changes in the cell spectroscopically.

6.1 - RESULTS AND DISCUSSION

Absorption spectroscopy can be used to monitor the chemistry of cyanocarbon ions in solution. Each of the anions, PCP⁻, TCY⁻ and TCNE⁻, has an intense ultraviolet or visible spectrum with peak molar absorption coefficients from 7100 to 22,400 M⁻¹cm⁻¹ (Figures 6.2³, 6.3⁴). PCP⁻ in

**FIGURE 6.1 - CELL FOR PREPARATION OF TCNE⁻
FROM TCNE/CH₃CN**



a) Aluminum foil electrode

Area = 6.3 cm^2

b) Teflon spacer

**FIGURE 6.2 - ABSORPTION SPECTRUM OF TCNE, TCNE⁻
IN METHYLTETRAHYDROFURAN³**

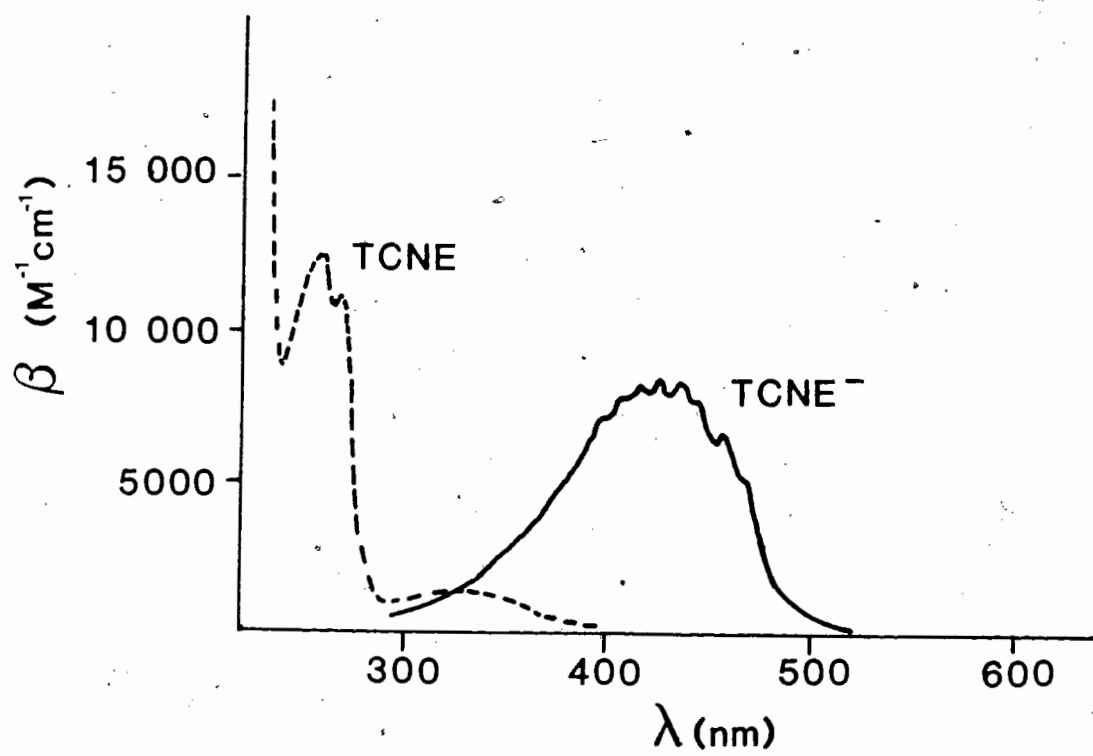
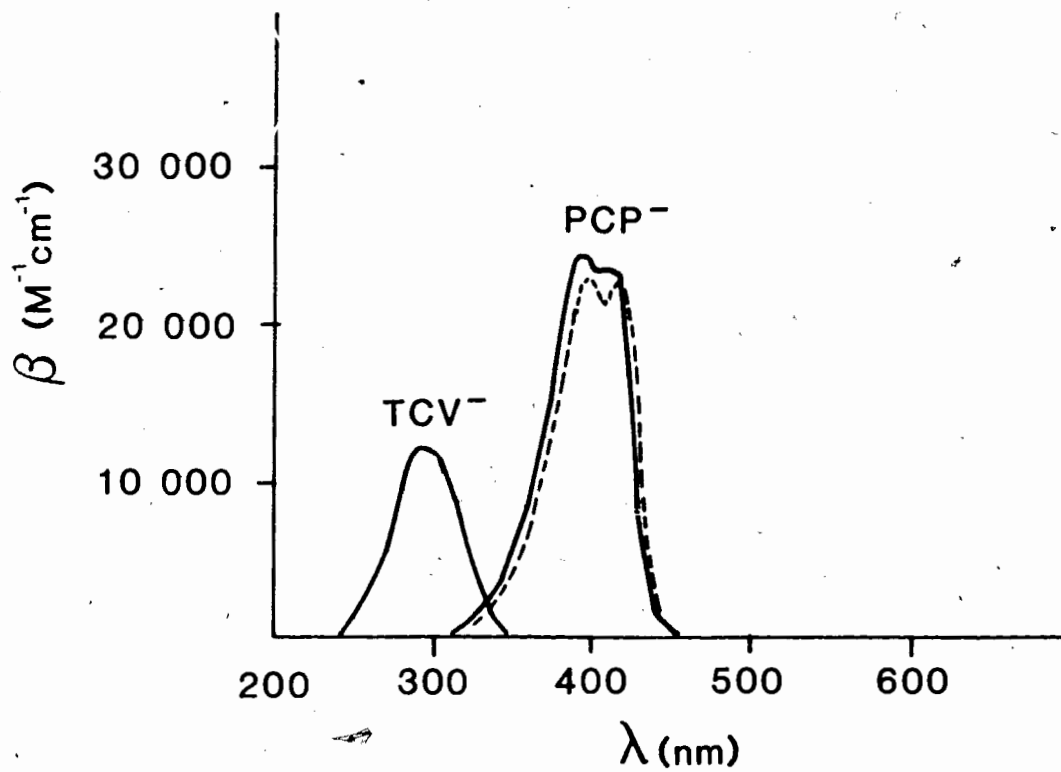


FIGURE 6.3 - PCP⁻, TCY⁻ ABSORPTION SPECTRA IN WATER⁴



————— PCP^- in water, TCV^- in water

----- PCP^- in acetone/ CCl_4 , $\epsilon=10.31$

DCE is characterized by a band with two peaks at 414 and 398 nm. Table 6.1 lists the peak positions of PCP^- in several solvents. Figure 6.4 shows the spectrum of PCP^- in DCE with peaks at 417 and 398 nm. TCV^- has a single peak at 295 nm in water (Figure 6.3). The TCNE^- spectrum has a number of vibronic peaks and a maximum absorbance at 425 and 435 nm. in CH_3CN . The TCNE^- peaks in CH_3CN are compared with those reported in the literature ⁵ in Table 6.2.

Figure 6.5 ⁴ shows the structure of the cyanocarbon anions PCP^- , TCV^- . PCP^- and TCV^- have conjugate acids which also have intense spectra in the UV/VIS region (Figure 6.6 ⁶). The protonated forms of PCP^- and TCV^- have pK_a values of < -8.5 and -5.3 respectively ^{6,7}.

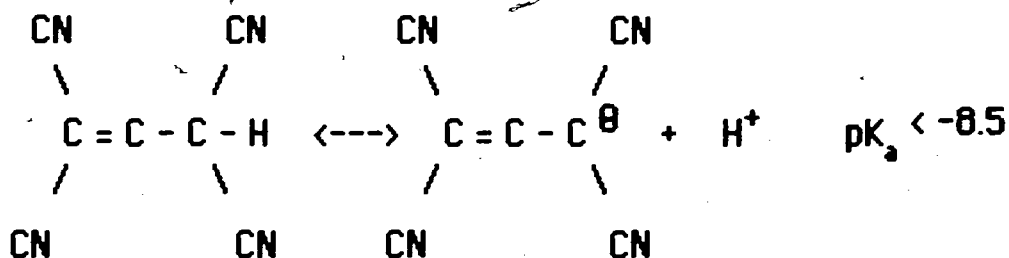
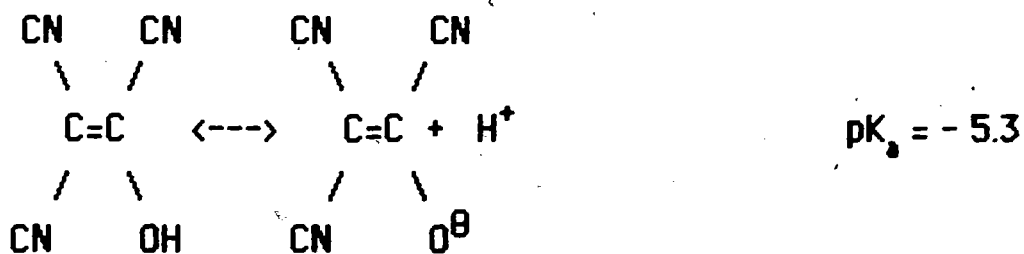


TABLE 6.1

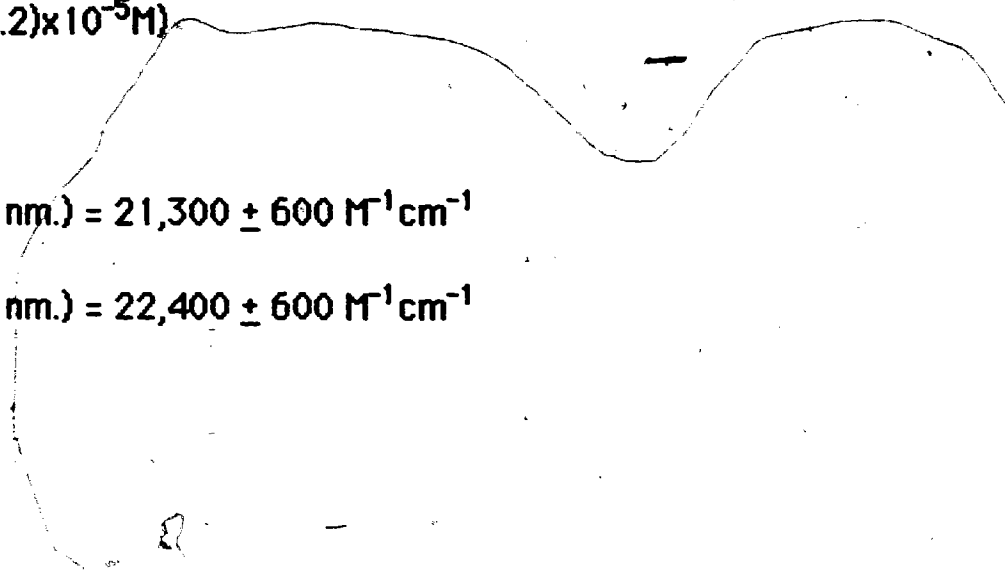
PCP⁻ PEAKS IN DIFFERENT SOLVENTS

Solvent	λ_1 (nm)	λ_2 (nm)
H ₂ O $\epsilon_{25^\circ} = 78.5$	395 ± 1	414 ± 1
CH ₃ CN $\epsilon_{25^\circ} = 27.5$	395 ± 1	414 ± 1
2-MTHF	396 ± 1	416 ± 1
DCE $\epsilon_{25^\circ} = 10.4$	398 ± 1	417 ± 1
CCl ₄ * $\epsilon_{25^\circ} = 2.23$	395 ± 2	420 ± 2

* TEA⁺ PCP⁻ was insoluble in CCl₄.

These peaks were measured in a sample of reagent grade CCl₄ saturated with TCNE. The undissociated form of PCP⁻ may contribute to the spectrum.

FIGURE 6.4 - PCP⁻ ABSORPTION SPECTRUM IN DCE
 $((5.6 \pm 0.2) \times 10^{-5} \text{M})$



$\epsilon (418 \text{ nm.}) = 21,300 \pm 600 \text{ M}^{-1} \text{ cm}^{-1}$

$\epsilon (398 \text{ nm.}) = 22,400 \pm 600 \text{ M}^{-1} \text{ cm}^{-1}$

210b

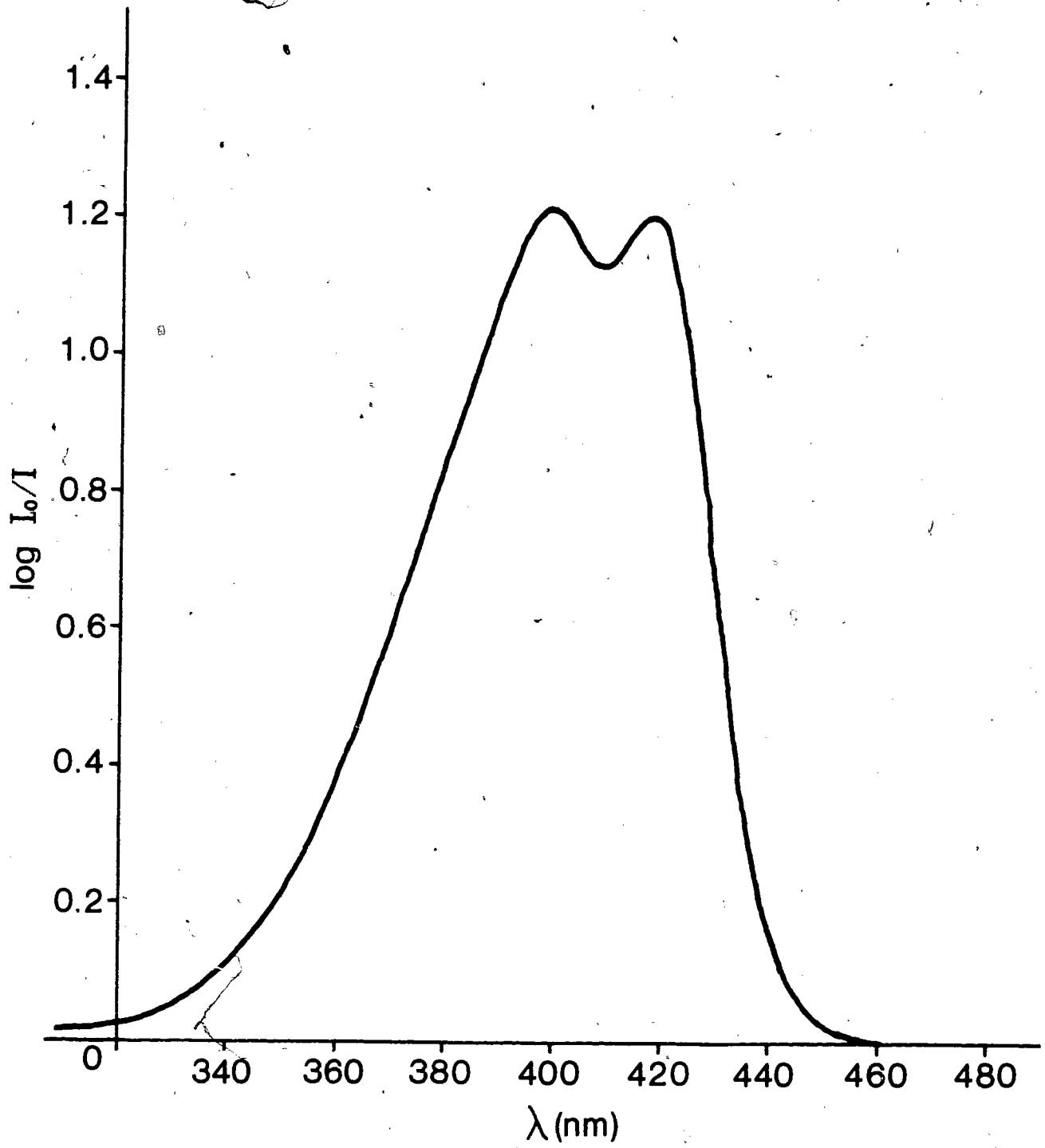
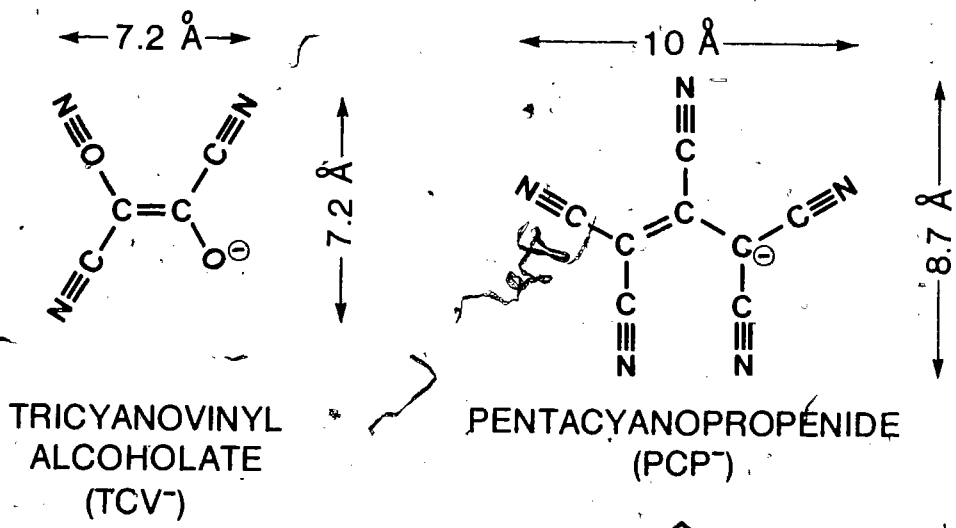


TABLE 6.2

SPECTRUM OF TCNE⁻ IN CH₃CN

λ measured (± 1 nm)	λ (literature) ⁵	β (literature) ⁵
468	468	4400
458	457	5670
446	445	6520
435	435	7100
425	425	7100
417	416	6890
407	407	6200
399	398	5460
390	390	4660
382	382	3810
374	374	3070
366	366	2440

FIGURE 6.5 - PCP⁻ .TCV⁻ STRUCTURES ⁴



RESONANCE FORMS

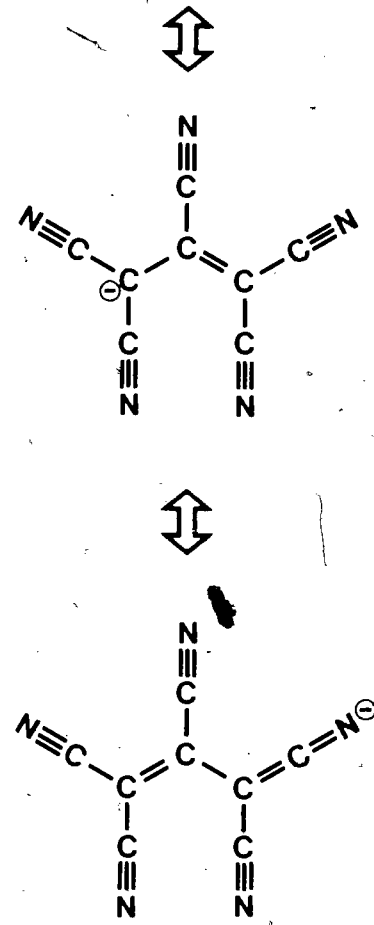
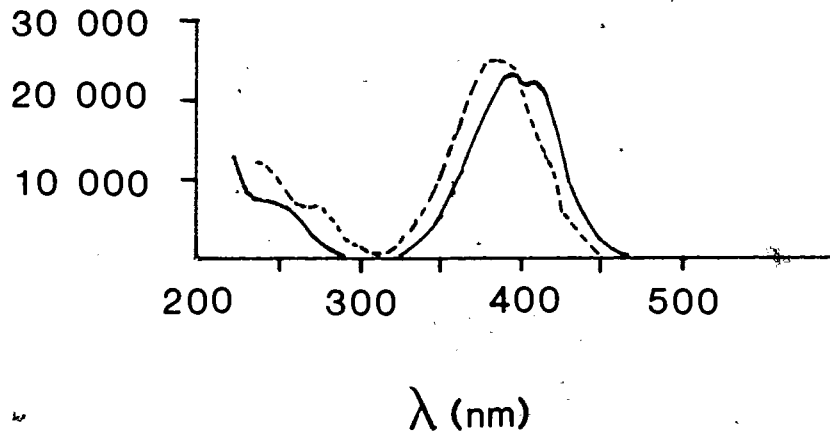
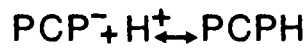
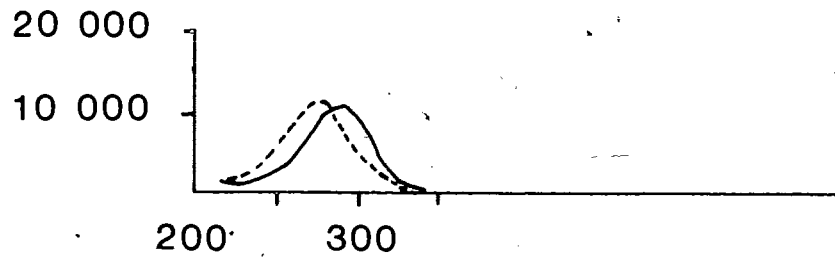
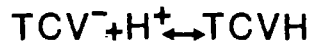


FIGURE 6.6 - PROTONATED FORMS OF TCV⁻ AND PCP⁻ ⁶



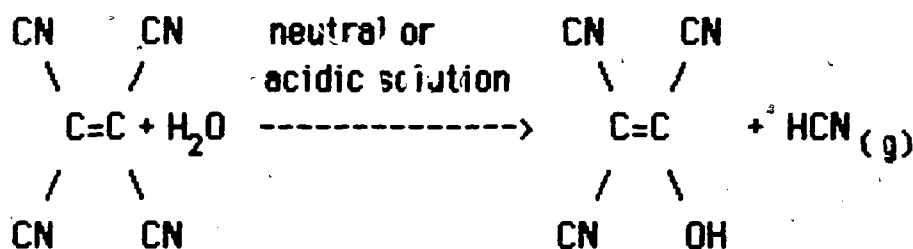
- undissociated form in
sulfuric acid of high concentration
- anionic form in water

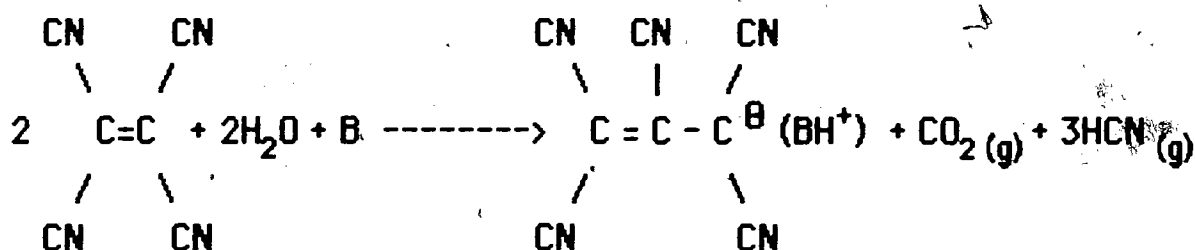
The strength of these cyanocarbon acids, which rivals that of HCl ($pK_a \approx -7$), is related to the resonance stabilization energy of the anions ⁷.

Resonance forms of PCP^- are shown in Figure 6.5. The spectrum of the conjugate acid of TCV^- (275 nm) is shifted to shorter wavelengths than the anion (295 nm.)⁶. Much the same effect is observed for the PCP^- conjugate acid except some dissociated PCP^- contributes to the shifted spectrum shown in Figure 6.6 ⁶.

6.1.1 - REACTIONS OF WATER AND TCNE IN SOLUTION

Both PCP^- and TCV^- are possible products of the reaction of water with TCNE ¹. Neutral to acidic conditions favour formation of tricyanovinylalcohol (or tricyanoethanol). The presence of a base favours the formation of PCP^- . The following reactions are representative of chemistry involving TCNE and water:





B = pyridine, quinoline

BH⁺ = pyridinium, quinolinium

Quaternary ammonium salts of PCP⁻ can be prepared by dissolving TCNE in a sodium bicarbonate solution (aqueous) and adding quaternary ammonium chloride or bromide salts. The mechanism for reactions producing PCP⁻ is not well understood. Tricyanoethanol is not a likely reaction intermediate
1,8

Conditions leading to PCP⁻ generation in solutions of DCE and CH₃CN relate to the conductivity studies. PCP⁻ is the dominant negative charge carrier in TCNE/DCE and TEA⁺PCP⁻/DCE solutions. Addition of water to TCNE/DCE and TCNE/CH₃CN samples results in the growth of PCP⁻ concentration. The set of spectra in Figure 6.7 shows the change in the sample absorbance in time after the addition of 40 μl of water to 3 ml. of 0.04M TCNE/CH₃CN. A plot of [PCP⁻] vs. time is shown in Figure 6.8 for three TCNE/CH₃CN samples with different water concentrations. In each sample a rapid increase in PCP⁻ anion concentration is initiated by the addition of water and is followed by

FIGURE 6.7 - TCNE/CH₃CN SPECTRA AFTER ADDITION OF WATER

Sample: 3 ml. of 0.04 M TCNE/DCE
 40 μ l water

Time after water addition

Scan 1:	3 min
Scan 2:	27 min
Scan 3:	55 min
Scan 4:	92 min
Scan 5:	151 min

216b

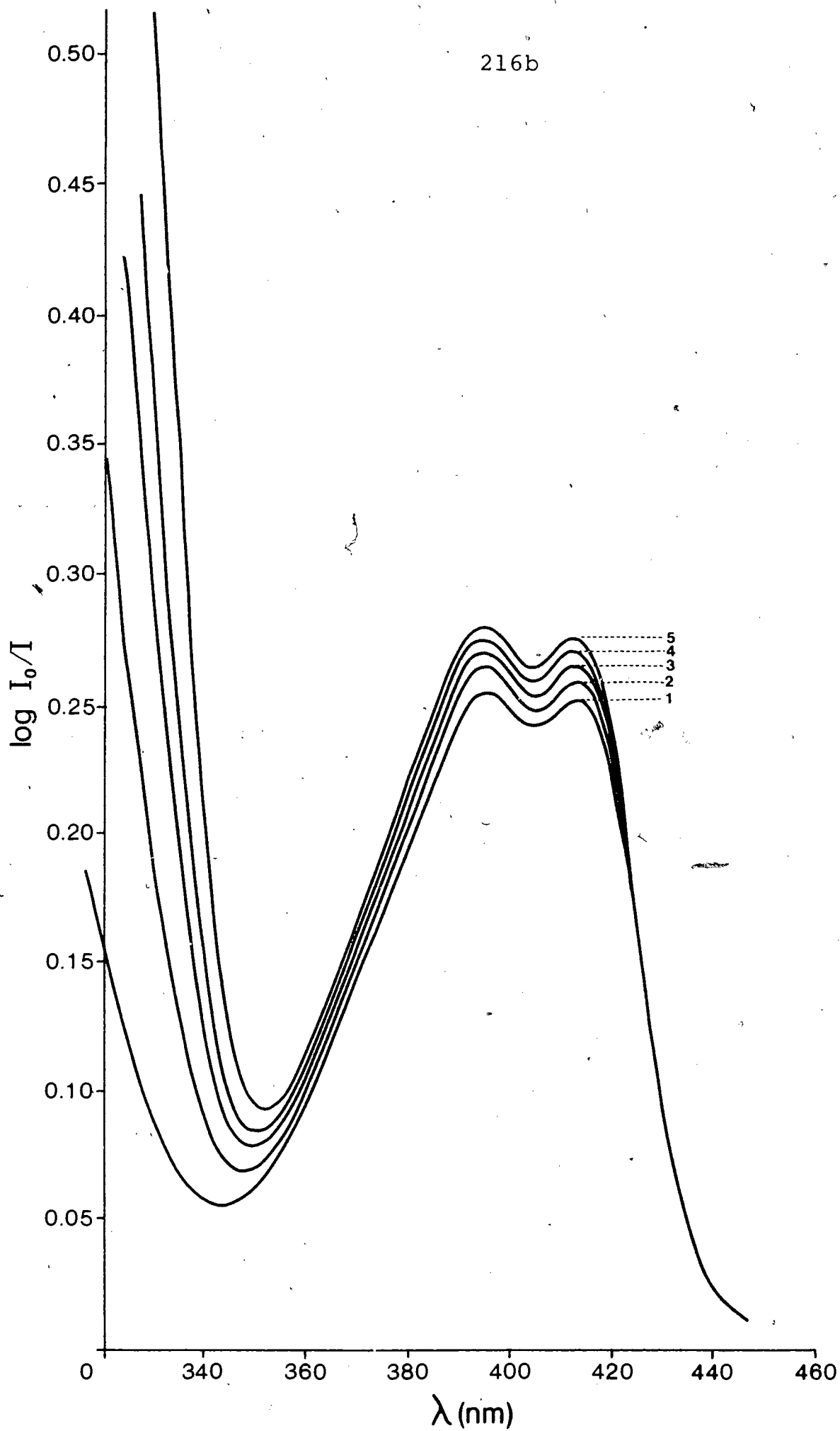
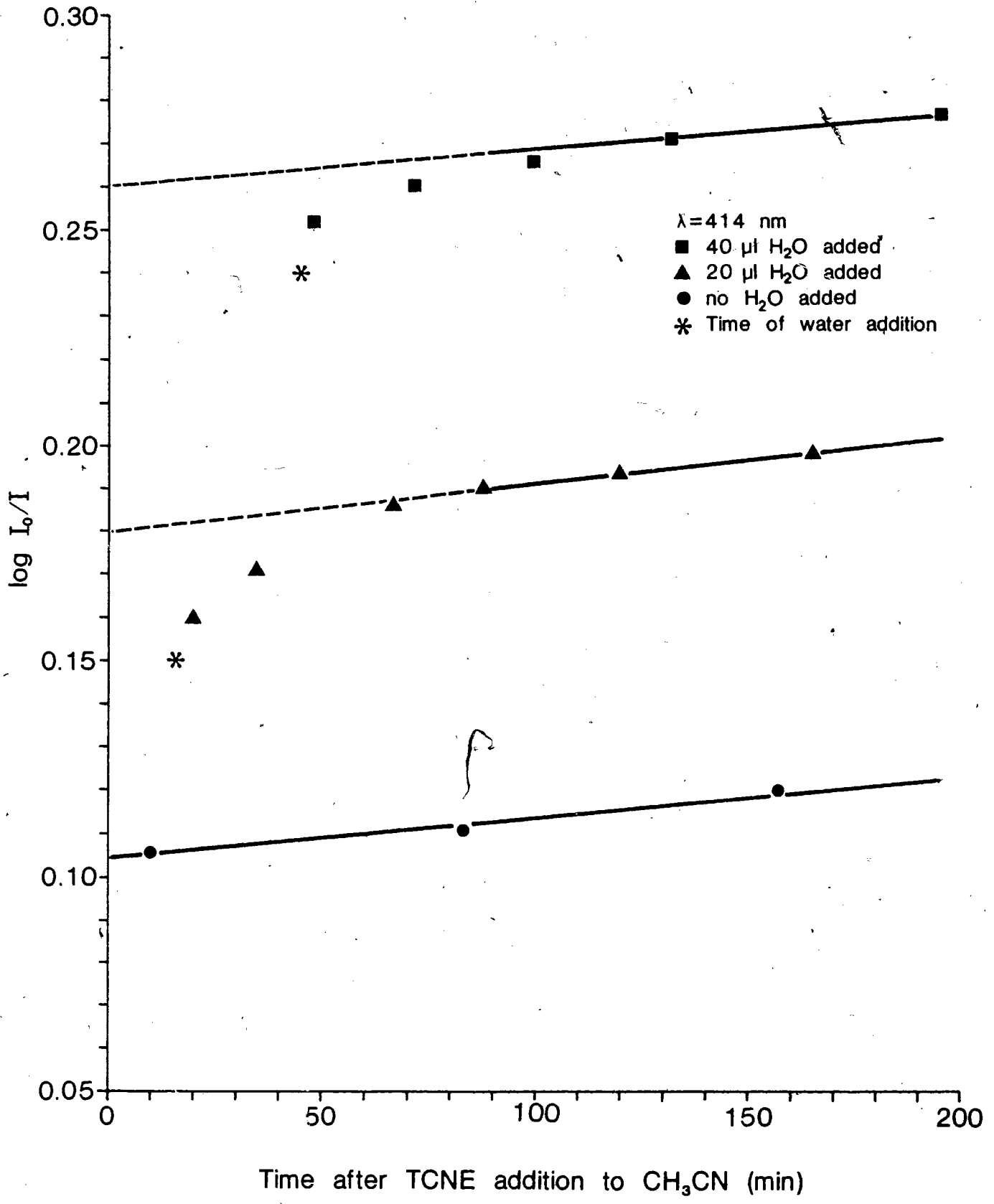


FIGURE 6.8 - LOG I_0/I VS. TIME AFTER WATER ADDITION**Sample: 0.04 M TCNE/DCE** $\lambda = 414 \text{ nm.}$



a slower increase of $[\text{PCP}^-]$ which is independent of $[\text{H}_2\text{O}]$. In Figure 6.9, a graph of $[\text{PCP}^-]$ versus added $[\text{H}_2\text{O}]$ demonstrates a linear relationship between the two. The slope of the line is independent of the time after sample preparation. The starting amount of water in the acetonitrile sample can be estimated at 0.5 M.

Figure 6.10 shows the effect of water addition on the growth of PCP^- concentration in a 0.013 M TCNE/DCE solution. A plot of $[\text{PCP}^-]$ versus added H_2O concentration demonstrates a linear relationship. Two sets of data are plotted for different times after sample preparation. The slope of the lines are the same within the experimental uncertainty. In this case the starting concentration of water in DCE (0.008 M) is much less than that observed in the CH_3CN sample.

The concentration ratio $[\text{PCP}^-]/[\text{TCNE}][\text{H}_2\text{O}]$ corresponds to a possible equilibrium constant for the systems just considered. Values of this ratio are calculated in Table 6.3 for DCE and CH_3CN . The ratios for the two solvents are of the same order of magnitude. Further studies would be required to measure the equilibrium constant governing $[\text{PCP}^-]$, $[\text{TCNE}]$ and $[\text{H}_2\text{O}]$ in solution.

The slow rate of PCP^- growth in DCE and CH_3CN is tabulated in Table 6.4. Rates were independent of water concentration in both solvents. The

AS
FIGURE 6.9 - $[PCP^-]$ vs. $[H_2O]$

Sample: 0.04 M TCNE/CH₃CN

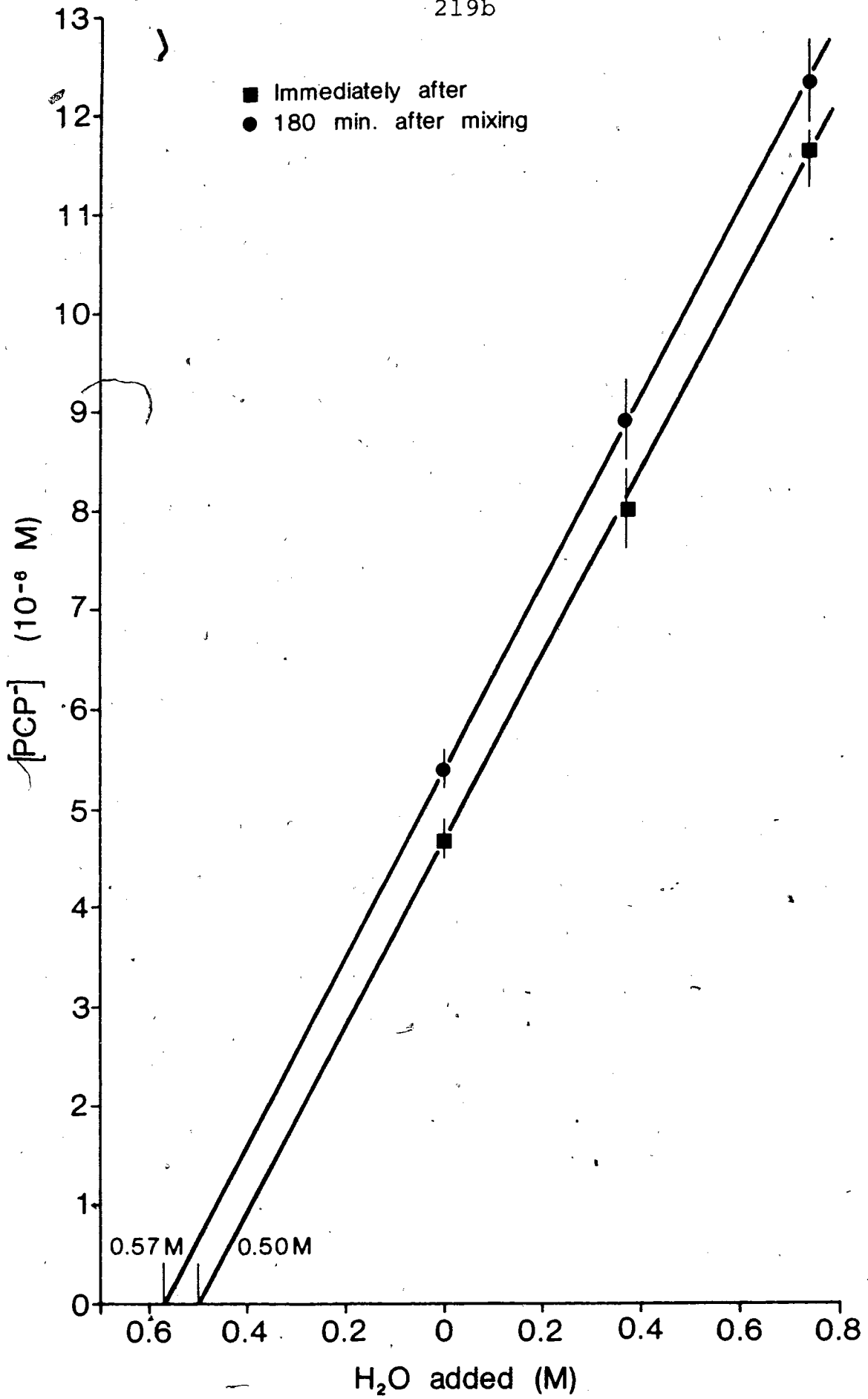


FIGURE 6.10 - $[PCP^-]$ vs. $[H_2O]$

Sample: 0.013 M. TCNE/DCE

$[H_2O] = 0.11$ M. in saturated DCE

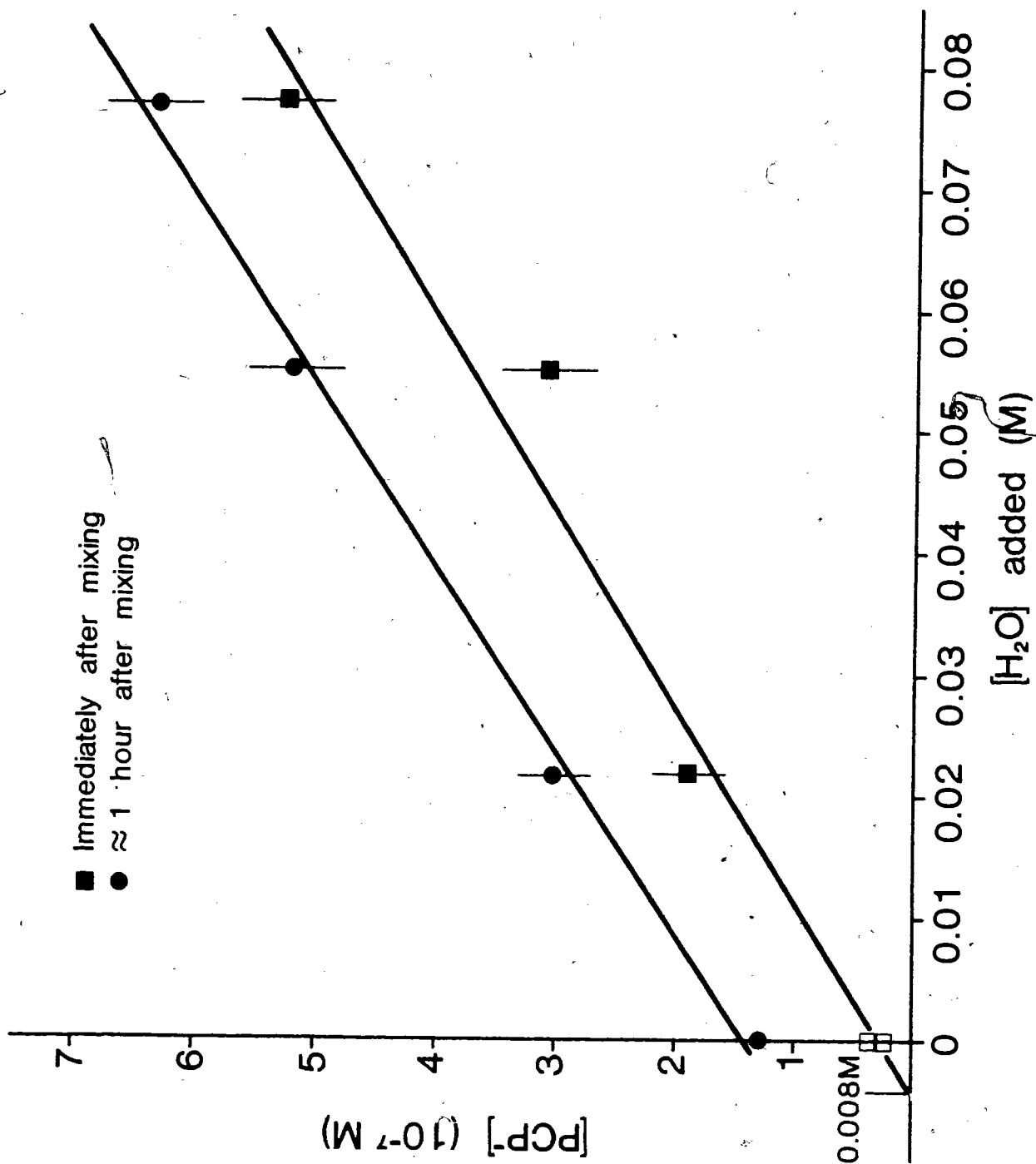


TABLE 6.3

FORMATION OF PCP^- FROM $\text{TCNE} + \text{H}_2\text{O}$
IN DICHLOROETHANE AND ACETONITRILE

SOLVENT	[TCNE]	$[\text{PCP}^-]/[\text{H}_2\text{O}]$	$[\text{PCP}^-]/[\text{TCNE}][\text{H}_2\text{O}]$
DCE	0.013 M	$(6.8 \pm 0.3) \times 10^{-6}$	$(5.2 \pm 0.4) \times 10^{-4} \text{ M}^{-1}$
CH_3CN	0.040 M	$(9.5 \pm 0.3) \times 10^{-6}$	$(2.4 \pm 0.2) \times 10^{-4} \text{ M}^{-1}$

TABLE 6.4

SLOW FORMATION OF PCP^- IN $\text{TCNE}/\text{SOLVENT}$
(INDEPENDENT OF WATER CONCENTRATION)

SOLVENT	[TCNE]	$d[\text{PCP}^-]/dt$ (M/hr)	$(d[\text{PCP}^-]/dt)/$ [TCNE] (1/hr)
DCE	0.013 M	$(1.5 \pm 0.3) \times 10^{-7}$	$(1.1 \pm 0.2) \times 10^{-5}$
CH_3CN	0.040 M	$(2.5 \pm 0.2) \times 10^{-7}$	$(6.3 \pm 0.6) \times 10^{-6}$

reactant producing this increase in $[PCP^-]$ is probably present in the atmosphere. The preliminary data are insufficient to establish the chemical identity of the reactant. Reaction rate constants (normalized to TCNE concentration) are of the same order of magnitude in DCE and CH_3CN . The equilibrium ratios and normalized rate constants in DCE samples are about twice as large as in CH_3CN .

The addition of water to TCNE/ CH_3CN solutions also increases the spectral absorbance at shorter wavelengths and this is probably the result of TCV^- produced in solution. Again, the presence of the intense TCNE band made it difficult to make detailed measurements in the region of the TCV^- peak (295 nm.). Figure 6.11 shows the growth in absorbance at 332 nm as a function of time. The rate of growth increases with water concentration.

Determining the factors influencing the balance of PCP^- and TCV^- ions in DCE requires more experimental work than is presented in this preliminary study. In aqueous solution, pH, or the presence of Lewis bases, dramatically influences whether PCP^- rather than TCV^- is a favoured product of the reaction of TCNE with water. Similar considerations need to be applied to DCE and CH_3CN solutions.

Exposure to water and air can influence charge carriers in solution at different stages of the TCNE/DCE sample preparation. The effect of solvent distillation on a TCNE/DCE spectrum is shown in Figure 6.12. The effect of

FIGURE 6.11 - LOG I₀/I VS. TIME (λ = 332 nm.)

Sample: 3 ml. of 0.04 M TCNE/CH₃CN

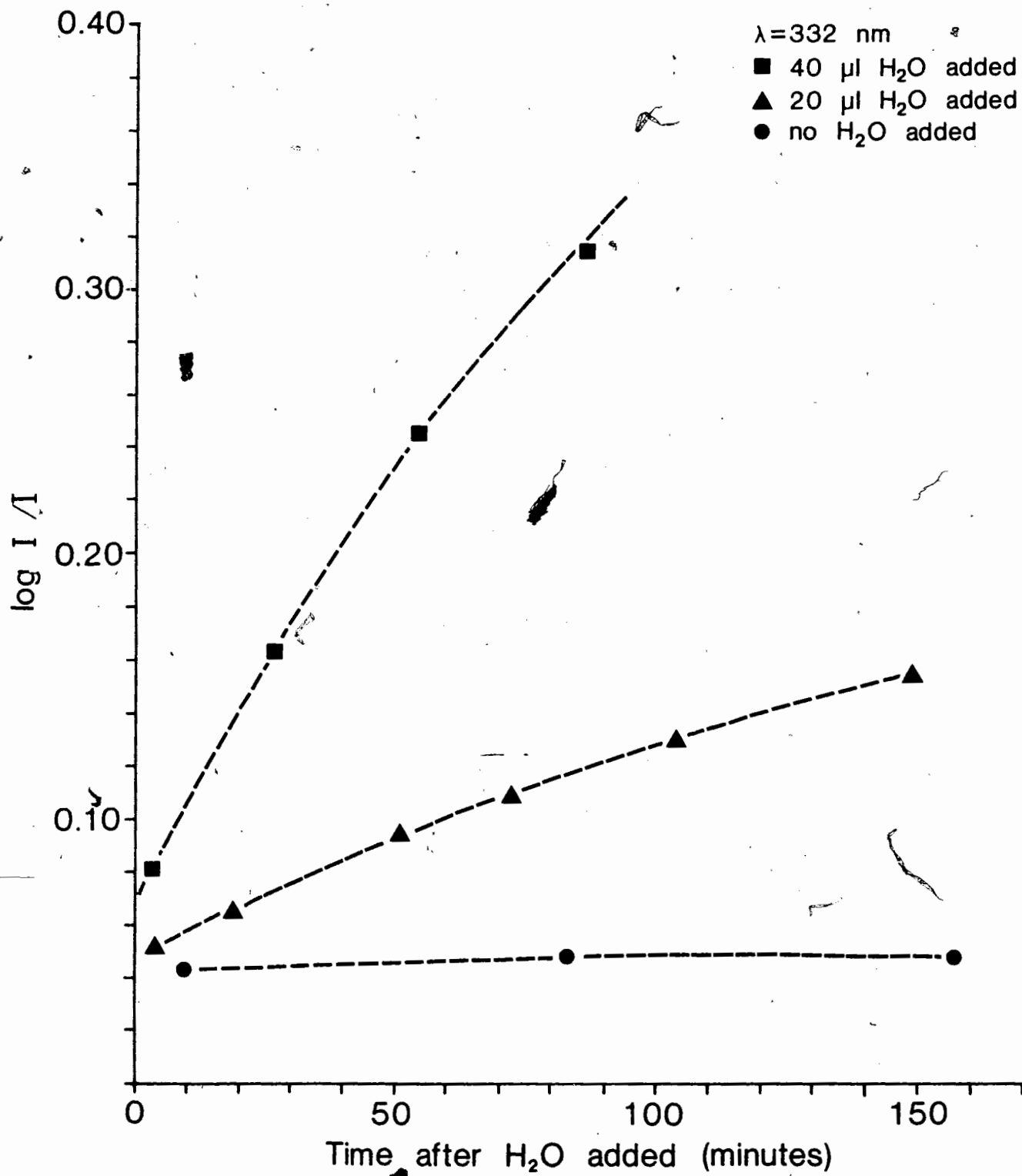
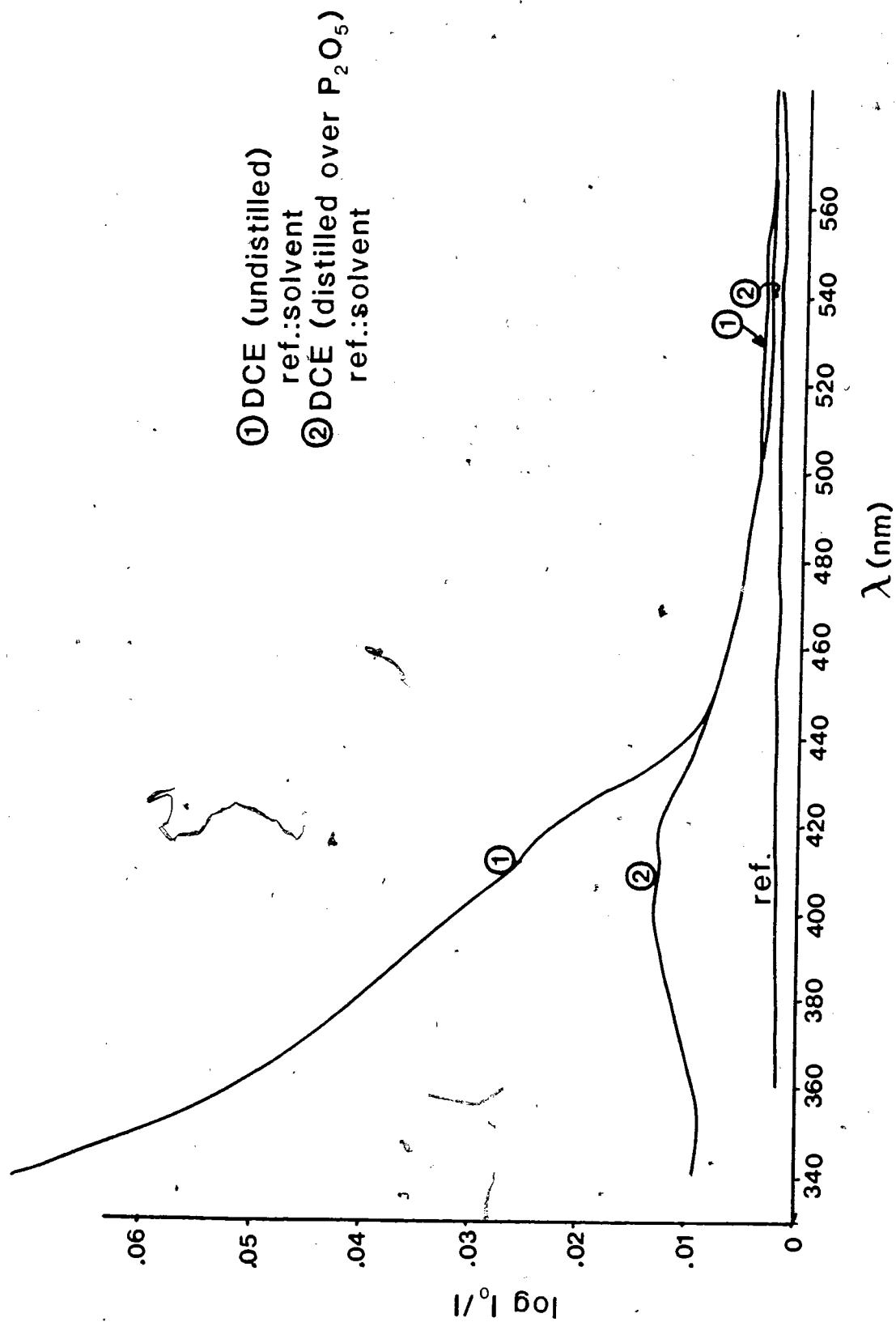


FIGURE 6.12 - TCNE/DCE SPECTRA WITH
AND WITHOUT DISTILLED SOLVENT

Sample: [TCNE] = 0.04 M.



successive sublimations of TCNE crystals on the PCP^- peak intensity in 0.04 M. TCNE in DCE samples is shown in Figure 6.13. The first sublimation dramatically reduces the PCP^- concentration observed in solution. The residual PCP^- concentration observed after the first sublimation could be the result of water in the solvent, water absorbed during 3 days of sample agitation to dissolve TCNE, water absorbed during refrigerator storage of solutions, or water introduced from the surface of pipettes used to transfer solutions. The elimination of water from the samples would have required that all spectroscopic and electrical measurements, as well as sample preparation procedures be carried out in a dry box.

The effect of water on TCNE/DCE solutions turns out to be useful since the production of PCP^- allows direct correlation of ion concentration and current characteristics. The PCP^- ion concentration in extremely pure TCNE/DCE samples would have been too low to monitor using the CARY 210 or CARY 17 spectrophotometers.

6.1.2 - $TCNE^-$ INJECTION IN $TCNE/CH_3CN$ AND $TCNE/DCE$

$TCNE^-$ is easily produced in $TCNE/CH_3CN$ by passing a DC current through the sample. The cell arrangement used to prepare $TCNE^-$ in acetonitrile solutions is shown in Figure 6.1.

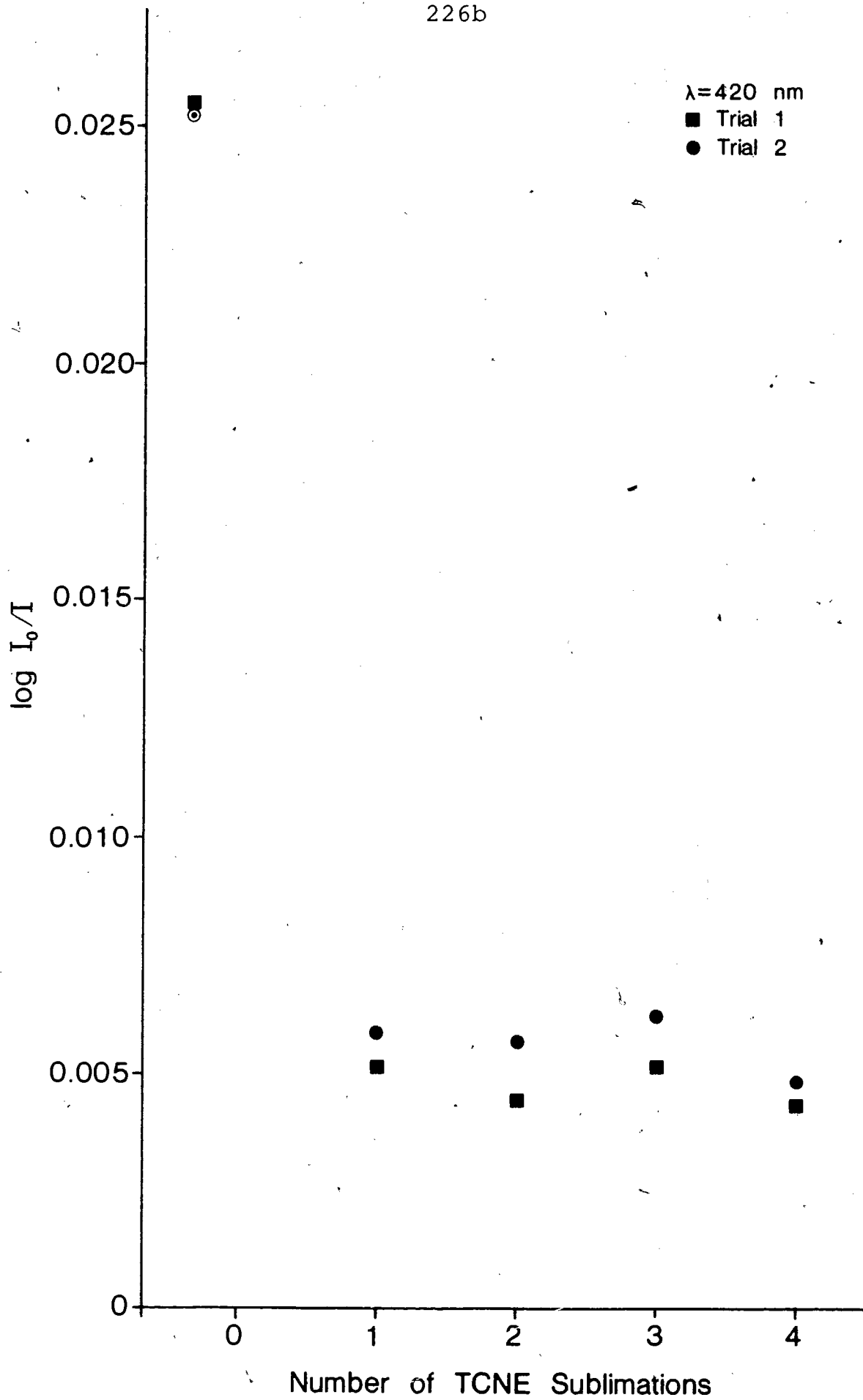
A spectrum of $TCNE/CH_3CN$ before voltage application is shown in Figure

FIGURE 6.13 - LOG I/I (420 nm) VS. *TCNE SUBLIMATIONS

Sample: [TCNE] = 0.04 M. in DCE

Trial 1 and Trial 2 were carried out on two consecutive days.

[TCNE] $\approx 2 \times 10^{-7}$ M after one sublimation.



6.14 (scan 1). The resulting profile arises from superimposed spectra of TCNE^- and PCP^- in CH_3CN . Note the TCNE^- peaks at 457 and 468 nm. During voltage application, the PCP^- peak disappears and is replaced by TCNE^- (Figure 6.14 scan 2). The generation of TCNE^- in solution is accompanied by the sample turning yellow near the cathode. The yellow colour results from the absorption band of TCNE^- (Figure 6.2). After a few minutes of voltage application, the yellow colour of the $\text{TCNE}/\text{CH}_3\text{CN}$ solution appears to be fairly evenly distributed across the cell. About 30 minutes is required for the current and optical absorption to settle to steady state values. The data in Table 6.5 include the concentrations of TCNE^- produced at different voltages and TCNE concentrations. The amount of TCNE^- generated increases with $[\text{TCNE}]$. The ratio of $[\text{TCNE}^-]/(V) [\text{TCNE}]$ for a few different trials agree within the experimental uncertainty and give an average value of $2.1 \times 10^{-5} \text{ V}^{-1}$.

In CH_3CN the conversion from TCNE^- to PCP^- can be observed spectroscopically after setting the voltage to zero. TCNE^- converted back to PCP^- over 3 to 4 hours. Figure 6.15 shows a series of spectra demonstrating the conversion of TCNE^- to PCP^- . Note the isobestic point at 428 nm. resulting from one to one conversion of TCNE^- to PCP^- . The decrease in TCNE^- concentration is equal to the increase in PCP^- concentration ($(6.8 \pm 0.5) \times 10^{-6} \text{ M}$). Probably oxygen, rather than water, in solution reacted with TCNE^- to produce the observed conversion⁵. Not only is TCNE^- more likely to react with oxygen than water, but the reaction with

**FIGURE 6.14 - TCNE/CH₃CN BEFORE AND AFTER
VOLTAGE TREATMENT**

Sample: 0.04 TCNE/CH₃CN

Scan 1: prior to voltage application

Scan 2: after 27 minutes of voltage application

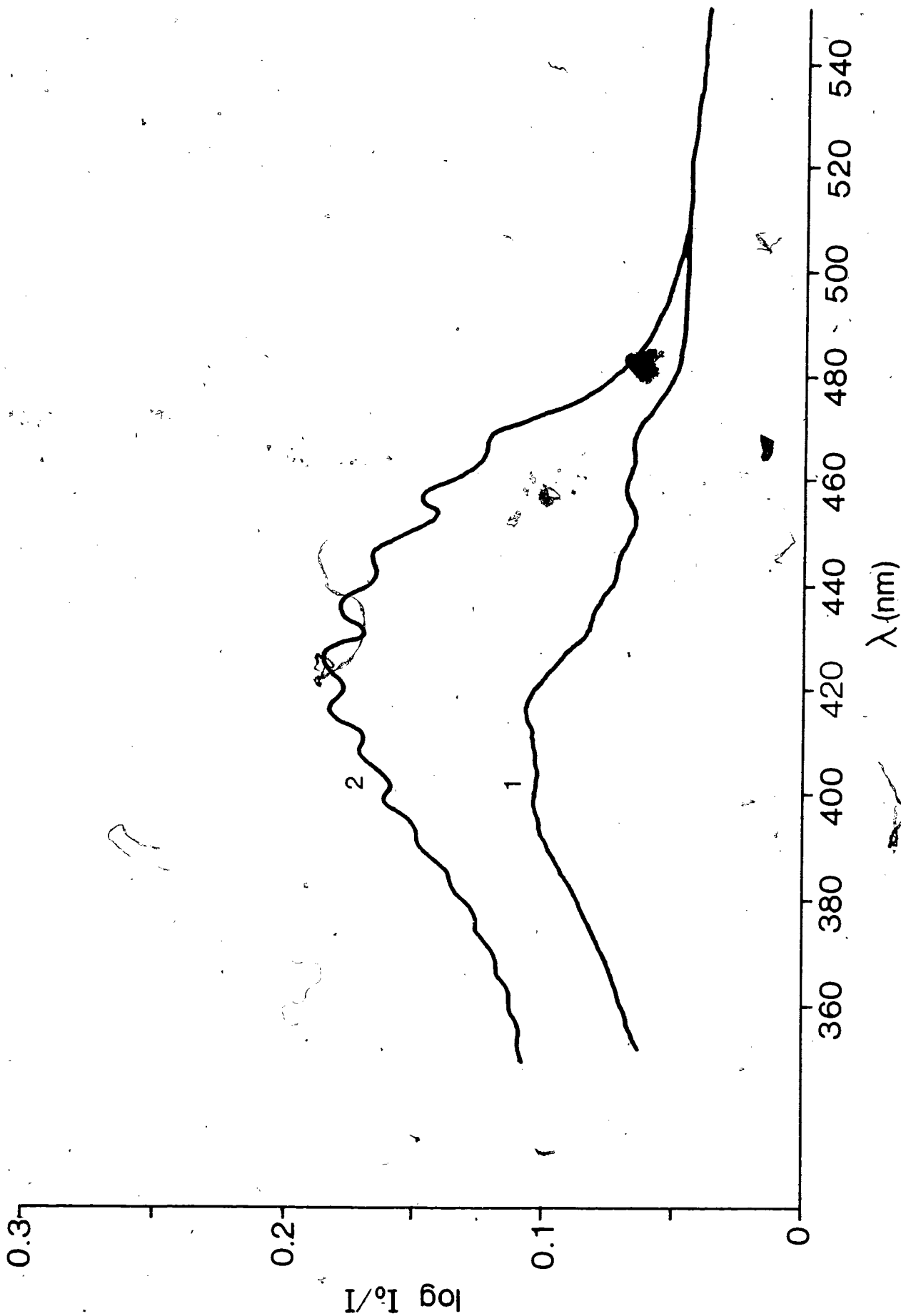


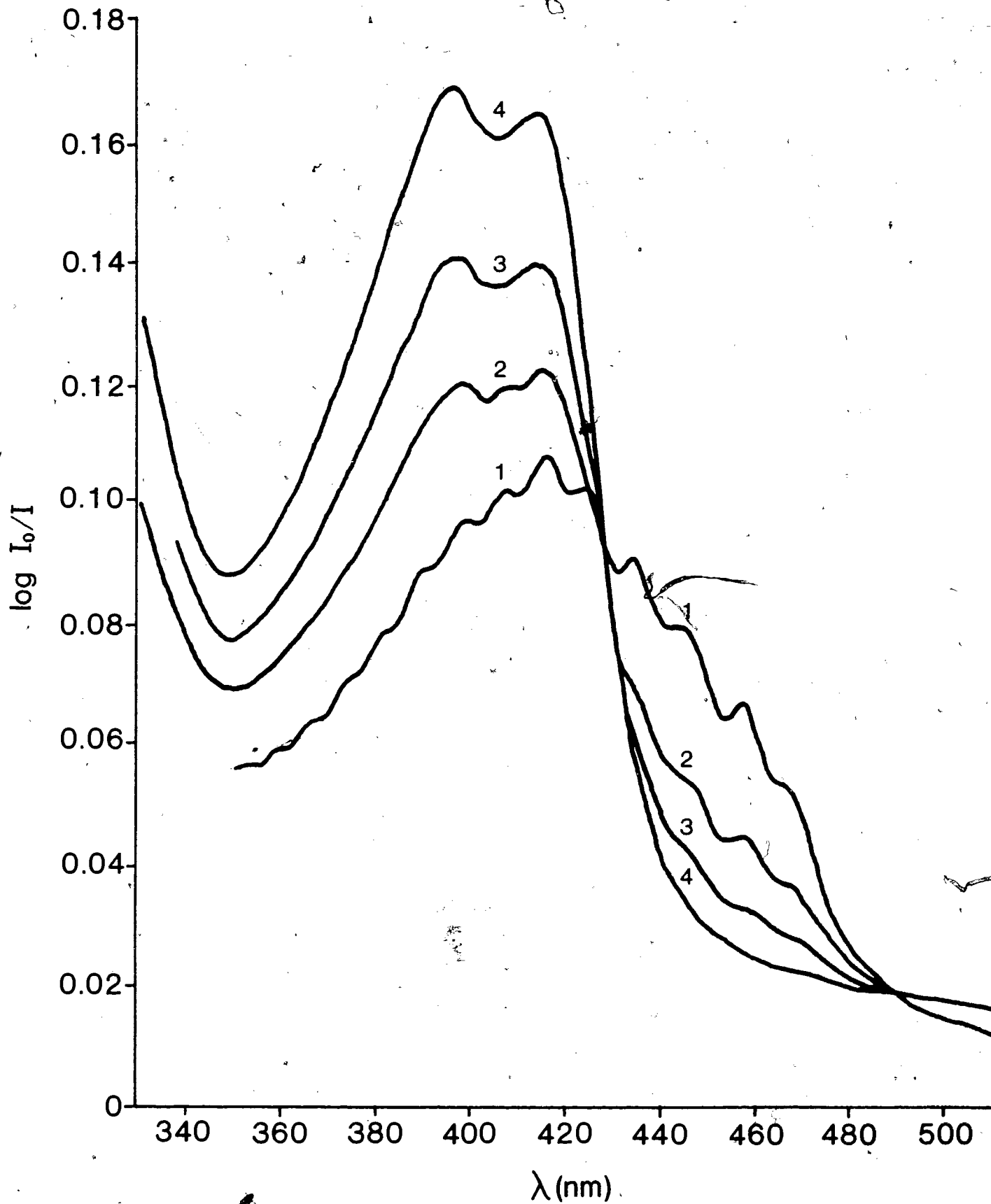
TABLE 6.5

[TCNE⁻] INJECTED INTO ACETONITRILE

[TCNE ⁻] (M)	VOLTAGE (V)	[TCNE ⁻] (M)	$\frac{[TCNE^-]}{(V)[TCNE]}$ (1/V)
0.008	20	$(3.9 \pm 0.2) \times 10^{-6}$	$(2.4 \pm 0.3) \times 10^{-5}$
0.040	10	$(7.5 \pm 0.5) \times 10^{-6}$	$(1.9 \pm 0.2) \times 10^{-5}$
0.040	10	$(8.0 \pm 0.5) \times 10^{-6}$	$(2.0 \pm 0.2) \times 10^{-5}$
0.040	10	$(8.4 \pm 0.5) \times 10^{-6}$	$(2.1 \pm 0.2) \times 10^{-5}$
0.10	10	$(2.16 \pm 0.05) \times 10^{-6}$	$(2.1 \pm 0.2) \times 10^{-5}$

FIGURE 6.15 - CONVERSION OF TCNE⁻ TO PCP⁻**Sample: 0.04 M TCNE/CH₃CN****Time after voltage removal**

Scan 1:	10 min.
Scan 2:	1 hr.
Scan 3:	1 hr. 50 min.
Scan 4:	3 hr. 40 min.



water produces TCV^- and PCP^- . Conversion of TCNE^- to both TCV^- and PCP^- would undermine the 1:1 conversion supported by the data.

The TCNE^- absorbance decayed exponentially in time (Figure 6.16).

$$\text{Log } I_0/I = [\text{TCNE}^-]_t / (\beta l)$$

$$\ln ([\text{TCNE}^-]_t / \beta l) = -k_r t + \ln ([\text{TCNE}^-]_0 / \beta l)$$

where β = molar absorption coefficient ($\text{M}^{-1} \text{cm}^{-1}$)

l = optical path length (cm)

k_r = rate constant (s^{-1})

therefore

$$[\text{TCNE}^-]_t = [\text{TCNE}^-]_0 e^{-k_r t}$$

Measured rate constants are in the range $(0.5-7) \times 10^{-4} \text{ s}^{-1}$ for 0.008 to 0.1M TCNE/DCE solutions. The rate constant is very sensitive to solvent or solution aging.

The growth of a spectral peak at about 520 nm is also observed in the $\text{TCNE}/\text{CH}_3\text{CN}$ sample with the lowest initial TCNE^- concentration (Figure 6.17). This peak remains unidentified although its location is comparable

FIGURE 6.16 - $\ln ([TCNE^-]_t / BI)$ vs. Time

Sample: 0.04 M. TCNE/ CH_3CN

k_r is the rate constant of the reaction.

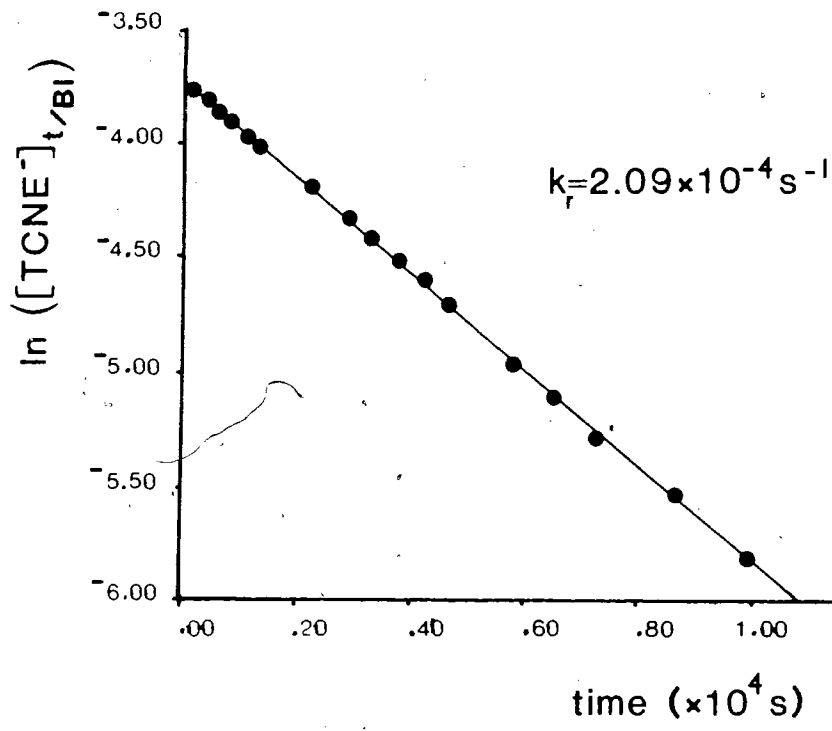
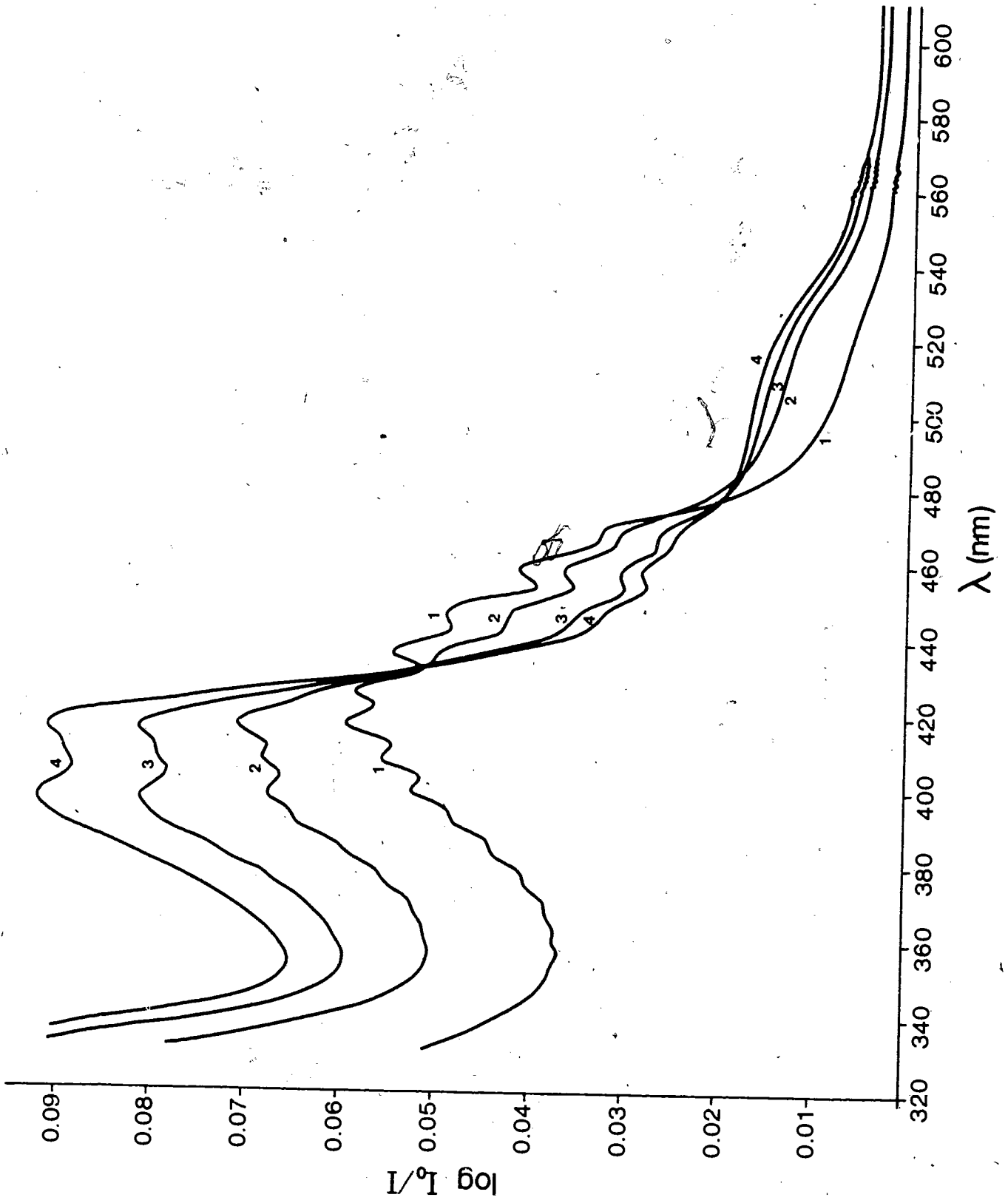


FIGURE 6.17 - CONVERSION OF TCNE⁻ TO PCP⁻ AND ANOTHER SPECIES WITH $\lambda = 320$ nm.

Sample: 0.008 M. TCNE/CH₃CN

Time after voltage removal

Scan 1:	10 min.
Scan 2:	1 hr. 20 min.
Scan 3:	2 hr. 55 min.
Scan 4:	4 hr. 35 min.



with that of the $(\text{TCNE}^-)_2$ dimer at 77 K in MTHF⁹ (Figure 6.18). The appearance of a dimer peak at low TCNE^- concentrations and at room temperature is unlikely.

The chemistry observed in $\text{TCNE}/\text{CH}_3\text{CN}$ solutions is different from that in TCNE/DCE solutions. The injection of TCNE^- into solution was favoured in CH_3CN rather than DCE. A comparison of two spectra of voltage treated TCNE/DCE and $\text{TCNE}/\text{CH}_3\text{CN}$ demonstrates this. The 520 nm. peak observed in some $\text{TCNE}/\text{CH}_3\text{CN}$ solutions is not observed in DCE solutions. The two ions common to both acetonitrile and DCE solutions were TCV^- and PCP^- , and TCV^- was present in TCNE/DCE solutions only with special sample preparation (See next section).

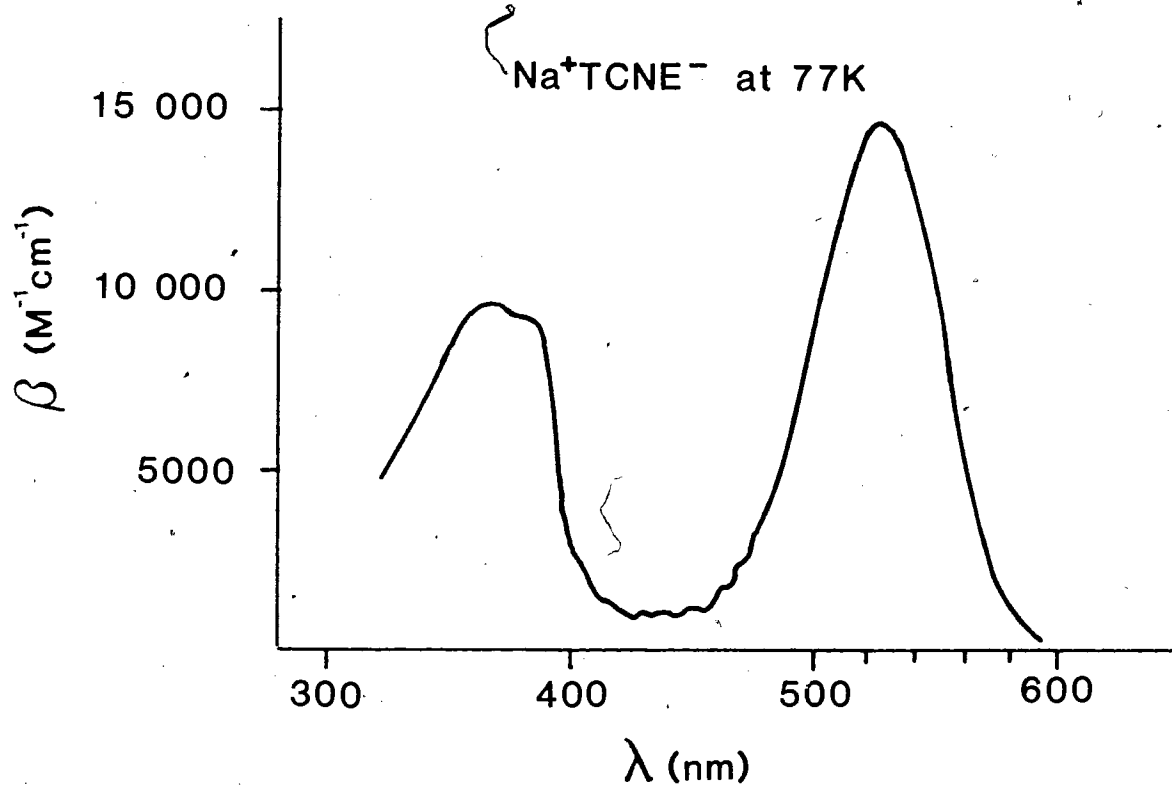
6.1.3 - IONS IN CONDUCTIVITY STUDIES

The ion of greatest importance in the TCNE/DCE conductivity studies is PCP^- . PCP^- is produced in TCNE/DCE solutions by the reaction of TCNE with water. The presence or absence of TCV^- could not be spectroscopically monitored in these samples because of the strong TCNE absorption in the ultraviolet. There was, however, no evidence of any contribution of TCV^- to conduction in TCNE/DCE samples prepared using the standard procedures outlined in Chapter 1.

A DCE solution with a mixture of PCP^- and TCV^- ions was prepared by first

FIGURE 6.18 - SPECTRUM OF $\text{Na}^+(\text{TCNE}^-)$ IN MTHF AT 77 K ⁹





reacting TCNE with deionized water (15 M Ω /cm) and then introducing the aqueous solution into DCE. The spectrum of this sample is shown in Figure 5.11 and the TCV⁻ peak is not hidden by the absorption band of TCNE in the ultraviolet. The conduction of this sample could be accounted for by summing the effects of TCV⁻ and PCP⁻ in solution (Section 5.1.4).

TEA⁺ PCP⁻ dissolves easily in DCE to produce TEA⁺ and PCP⁻ ions. No trace of TCV⁻ is observed in DCE samples containing the tetraethylammonium salt of PCP⁻ (i.e. PCP⁻ did not decompose into TCV⁻ with time) The conduction of this sample could be accounted for strictly on the basis of PCP⁻ concentration.

REFERENCES:

1. W.J. Middleton, E.L. Little, D.D. Coffman, V.A. Engelhardt, "Cyanocarbon Acids and their Salts", Journal of the American Chemical Society 1958, 80, 2795-2806.
2. I. Mellan, "Industrial Solvents Handbook"; Noyes Data Corporation: Park Ridge, N.J, 1970; pp 78-79.
3. M. Itoh, "Formation and Spectrum of Tetracyanoethylene Dimer Anion (TCNE)₂⁻", Journal of the American Chemical Society 1970, 92, 886-889.
4. R. Boyd, "The Solution Conductance of Cyanocarbon Salts", Journal of Physical Chemistry 1961, 65, 1834-1843.
5. O.W. Webster, W. Mahler, R.E. Benson, "Chemistry of Tetracyanoethylene Anion Radical", Journal of the American Chemical Society 1962, 84, 3678-3684.
6. R. Boyd, "The Ionization Behaviour of Cyanocarbon Acids", Journal of Physical Chemistry 1963, 67, 737-744.
7. R.H. Boyd, "The Strengths of Cyanocarbon Acids and an H-Acidity Scale for Concentrated Acid Solutions", Journal of the American Chemical Society 1961, 83, 4288- 4290.
8. C.L Dickinson, D.W. Wiley, B.C. McKusick, "Tricyanoethylene and Tricyanovinyl Chloride", Journal of the American Chemical Society 1960, 82, 6132-6136.
9. M. Itoh, "Dimerization and Electronic Absorption Spectra of Tetracyanoethylene Anion in Solution and in Solid", Bulletin of the Chemical Society of Japan 1972, 45, 1947-1950.

CHAPTER 7 - CONCLUSIONS

This chapter includes a summary of the main conclusions of the thesis as well as suggestions for further work

7.1 - SUMMARY OF THESIS RESEARCH

In the previous chapters a variety of data have been presented on conduction in organic solutions of TCNE/DCE and $\text{TEA}^+\text{PCP}^-/\text{DCE}$. Photoconduction effects in solutions of TCNE/Mesitylene/DCE were also reported.

The photocurrent response of TCNE CT solutions had been interpreted previously in terms of a model of photoionic dissociation of CT complexes. An alternative interpretation of the photosignal as resulting from the interruption of convective patterns in solution by absorption of light was proposed to account for the observations reported in this thesis.

Further work on the current characteristics of TCNE/DCE solutions demonstrated the importance of convective transitions, electrical boundary layers, and spatial and temporal ion concentration changes. The dominant negative charge carrier in TCNE/DCE and $\text{TEA}^+\text{PCP}^-/\text{DCE}$ solutions was identified as PCP^- . TCNE- $\text{H}_2\text{O}/\text{DCE}$ solutions contained both PCP^- and TCV^- . Ion concentrations were typically in the range of 10^{-7} - 10^{-6} M.

✓ The initial current response of these solutions to a step voltage V across a

distance d between the electrodes was accounted for by terms proportional to ion concentration and velocity, cv (with $v = \mu V/d$ where μ is an effective mobility). The effective mobilities of ions in TCNE/DCE, TCNE-H₂O/DCE and TEA⁻ PCP⁻/DCE were $(3 \pm 1) \times 10^{-8} \text{ m}^2 \text{ V}^{-1} \text{ s}^{-1}$, $(4 \pm 1) \times 10^{-8} \text{ m}^2 \text{ V}^{-1} \text{ s}^{-1}$, and $(4.0 \pm 0.9) \times 10^{-8} \text{ m}^2 \text{ V}^{-1} \text{ s}^{-1}$ respectively. Transient current behaviour followed changes in the ion concentration with time. The transient drift velocities differed from $\mu V/d$ because of electrical boundary layer potentials and convective flow in the solution.

An investigation of the time evolution of spatial ion concentration profiles demonstrated the presence of hydrodynamic instabilities in solution. Instability in fluid flow was associated with a concentration gradient of about $6 \times 10^{-7} \text{ M/mm}$. This gradient was sufficient to generate a diffusion drag force in the liquid which was 12 % of the weight of the fluid DCE.

A model describing the contributions of the diffusion drag force (F_d) and the space charge drag force (F_e) in electrolyte solutions was presented. Both forces were shown to increase with the magnitude of concentration gradients. The relative contribution of F_d and F_e was related to the ion concentration and electric field:

$$\frac{F_e}{F_d} = \frac{(\epsilon \epsilon_0) E^2}{2kT c}$$

The contribution of diffusion drag forces should be considered over a wide range of ion concentrations and electric fields, but it has been largely ignored in studies of conduction in dielectric liquids. This study is the first to examine the importance of diffusion generated convection in solutions in the absence of gravitationally driven fluid flow.

7.2 - SUGGESTIONS FOR FURTHER WORK

The study of conduction and convection in organic solutions with cyanocarbon anions should be extended to include a wider range of ion concentrations and applied electric fields. The effects of different solvents, electrode materials and electrolytes also warrant further study.

Diffusion driven convection is a general mechanism for generating fluid flow and should be considered in corrosion studies, and electrochemical work. Electrohydrodynamics and diffusion driven convection are likely to be of importance in biological systems too. The concentration gradients and electric fields existing near cell membranes may be sufficient to generate fluid flow under some circumstances. Fluid flow could in turn influence the transport of life-supporting substances to and from the cell wall.

Hydrodynamic flow from the presence of concentration gradients is expected to occur in the absence of a gravitational field. This prediction could be tested in low or zero gravity conditions. Understanding the

mechanisms for convection under conditions of zero gravity is of technological importance for materials science in space¹.

REFERENCES:

1. V.I. Polezhaev, "Convective Processes at Low Gravity", Material Sciences in Space, Proceedings of the Third European Symposium, Grenoble 24-27 April 1979, 25-31.